The Variability of the Void Ratio of Sand and its Effect on Settlement and Infinite Slope Stability

Dissertation

zur Erlangung des akademischen Grades

Doktor-Ingenieur

an der Fakultät Bauingenieurwesen

der

Bauhaus-Universität Weimar

vorgelegt von

M.Sc. Pengtao Zhu

aus Henan (China)

Gutachter:

1. **Prof. Dr. -Ing. Karl Josef Witt**
2. **Prof. Dr. Ren. Nat. Tom Lahmer**
3. **Prof. Dr. -Ing. Habil. Ivo Herle**

Tag der Disputation: 05 März 2018

Vorwort des Betreuers

Die Zusammensetzung von Boden ist hochgradig stochastischer Natur. Kein Korn gleicht dem andern, keine zwei Bodenproben sind wirklich identisch. Dennoch gibt es Bodengruppen und Bodenarten, denen eine kollektive Identität zugesprochen werden kann. Zuschreibungskriterien können die Korngrößenverteilung, die plastischen Eigenschaften, die Wasserempfindlichkeit, die Steifigkeit, die Scherfestigkeit, die Wasserdurchlässigkeit, die Frostempfindlichkeit oder auch andere bodenmechanische Eigenschaften sein. Aber je nach Betrachtungsmaßstab findet man anstatt vermeintlicher Homogenität eine streuende Zusammensetzung des Bodens vor und damit eine gewisse räumliche Streuung der betrachteten physikalischen Eigenschaft. Das macht den Boden so interessant und bietet selbst dem Experten immer wieder Überraschungen.

Geht man tiefer in die Materie, zeigt sich, dass das mechanische Verhalten des i. A. aus mineralischer Masse, Wasser und Luft zusammengesetzten Materials »Boden« maßgeblich durch die Packung der Körner, die Struktur des Bodens sowie durch deren Komplement, die Struktur des Porenraums bestimmt wird. Neben der Korngröße, Kornform und Mineralogie bestimmt die Porosität das mechanische Verhalten der Packung. Möchte man die Streuung der mechanischen Eigenschaften verstehen, sollte man bei der Streuung der die Eigenschaften bestimmenden Grundlagen beginnen, der räumlichen Streuung der Struktur des Bodens. Einer physikalischen Kenngröße dieser Grundlagen hat sich Pengtao Zhu im Detail gewidmet. Als Stipendiat an unserer Professur hat er die Analyse und physikalische Beschreibung der räumlichen Streuung der Porenziffer zum Thema seiner Dissertation gemacht. Dabei hat er sich auf Sand beschränkt.

Herr Zhu hat eine klar formulierte wissenschaftliche Frage bearbeitet: Ob und wenn ja, wie die statistischen und geostatistischen Kenngrößen einer streuenden Porenziffer eines Sandes tiefenabhängig sind. Und er hat nach der Analyse untersucht, welchen Einfluss dies auf zwei konkrete makroskopische Eigenschaften hat, auf das Setzungsverhalten und auf die Standsicherheit einer Böschung bei einem ebenen, böschungsparallelen Versagensmechanismus. Der Lösung hat er sich baukastenmäßig angenähert. Randbedingungen und Gesetzmäßigkeiten hat er teilweise aus wissenschaftlichen Publikationen übernommen um darauf aufbauend mit einem selbst kreierten Zufallsfeld Simulationen durchzuführen. Er konnte zeigen, dass die Tiefenabhängigkeit der Variabilität durch den Spannungszustand beeinflusst wird. Einige Detailergebnisse sind erwartungsgemäß, andere überraschen und sind noch weiter auf Praxisrelevanz zu analysieren.

Bei der Entstehung der Arbeit und bei vielen Verzweigungen gab es immer wieder Anregung, Kritik, Diskussion und wissenschaftlichen Input von Herrn Dr. Maximilian Huber, der während der Initialphase dieser Promotion Postdoktorand am DFG-Graduiertenkolleg 1462 »Modellqualitäten« war. Hierfür meinen herzlichsten Dank. Die anregenden Diskussionen waren nicht nur für das wissenschaftliche Weiterkommen von Herrn Zhu wichtig, sondern auch für mich stets bereichernd. Schließlich möchte ich auch den beiden Ko-Referenten und meinem Nachfolger an der Professur, den Professoren Ivo Herle, Tom Lahmer und Torsten Wichtmann für die Begutachtung, Prüfung und Kritik an der finalen Dissertation danken. Der differenzierte Blick aus unterschiedlichen Richtungen eröffnet doch immer wieder Horizonte und gibt wertvolle Anregungen zur weiteren Forschung.

Weimar, März 2018 Karl Josef Witt

Acknowledgments

Thanks are due to many people who provided me with an enormous help and encouragement. This acknowledgment is a small appreciation for their priceless support.

First and foremost, I would like to express my sincere appreciation to my supervisor and mentor Professor Karl-Josef Witt for his continuous encouragement, guidance, valuable advice, and patience throughout the whole PhD period. I feel so privileged to be able to have his support in these years. Working with him has been rewarding and enjoyable, though certainly not easy. Through many pleasant conversations with him, I have also learned many things beyond academic matters.

I greatly appreciate my co-supervisor Dr. Maximilian Huber. It is the first step that is troublesome. He taught me how to bring my idea into practice step by step using an appropriate method. His encouragement and kindness help me through this toughest period.

I want to express my sincere gratitude to Prof. David Mašín in Charles University in Prague for giving me such a precious opportunity to visit him, and for helping me revise the program using hypoplastic model. Many thanks to my friends Haiquan Suan and Qijie Ma for their advice on hypoplastic model.

My warm gratitude also goes to my colleagues at Bauhaus Universität Weimar. Special thanks to my friends and colleagues: Maria Noack, Mingming Fang, Mohamad Reza Sadaghiani, Paul Winkler, Robert-Balthasar Wudtke, and Mojtaba Shahraki for their advice and discussion. With them by my side, my life in Weimar is full of joy.

I am thankful to China Scholarship Council (CSC) for the financial support.

Finally, I am very appreciated to my family for their continuous unconditional love and endless support I always got to achieve this work. I dedicate this work to my beloved parents, my beautiful wife, and my dearest daughter. I believe my greatest asset in life is my family and for that I feel so blessed and am so thankful.

Abstract

The uncertainty of a soil property can significantly affect the physical behavior of soil, so as to influence geotechnical practice. The uncertainty can be expressed by its stochastic parameters, including the mean, the standard deviation, and the spatial correlation length. These stochastic parameters are regarded as constant value in most of the former studies. The main aim of this thesis is to prove whether they are depth-dependent, and to evaluate the effect of this depth-dependent character on both the settlement and the infinite slope stability during rainwater infiltration.

A stochastic one-dimensional settlement simulation is carried out using random finite element method with the von Wolffersdorff hypoplastic model, so as to evaluate the effect of stress level on the stochastic parameters of void ratio related parameters of sand. It is found that these stochastic parameters are both stress-dependent and depth-dependent.

The non-stationary random field, considering the depth-dependent character of these stochastic parameters, can be generated through the distortion of the stationary random field.

The one-dimensional settlement analysis is carried out to evaluation the effect of the depth-dependent character of the stochastic parameters of void ratio on the strain. It is found that the depth-dependent character has low effect on the strain.

The deterministic analysis of infinite slope stability during rainwater infiltration is simulated. The transient seepage is carried out using finite difference method, while the steady state seepage is simulated using the analytical solution. The saturated hydraulic conductivity (ks) is taken as the only variable. The results show that the depth-dependent ks has a significant influence on the stability of the slope when the negative flux is high. Without considering the depth-dependent character, can overestimate the factor of safety of the slope. A slope can fail if the depth-dependent character is considered, while it is stable if the depth-dependent character is neglected. The failure time of the slope with a greater depth-dependent ks is earlier during transient infiltration.

Meanwhile, the stochastic infinite slope stability analysis during infiltration, is also carried out to highlight the effect of the depth-dependent character of the stochastic parameters of ks. The results show that: the probability of failure is significantly increased if the depth-dependent character of mean is considered, while, it is moderately reduced if the depth-dependent character of the standard deviation is accounted. If the depth-dependent character of both the mean and standard deviation of ks is considered, the depth-dependent mean value plays a dominant influence on the results. Furthermore, the depth-dependent character of the spatial correlation length can slightly reduce the probability of failure.

Kurzfassung

Problemstellung und Zielsetzung der Arbeit

Die Variabilität von unsicheren, räumlich streuenden Bodeneigenschaft kann durch die statistischen Größen Mittelwert, Standardabweichung, Variationskoeffizient und durch deren räumliche Korrelation beschrieben werden. Die Streuung der Bodeneigenschaften beeinflusst eine geotechnische Analyse der Baugrundeigenschaften wie auch die geotechnischen Nachweise wesentlich. Die geotechnische Nachweise gehen jedoch von deterministischen Gesetzmäßigkeiten und meist nicht von unsicheren Einwirkungen und Widerständen aus.

In der Ingenieurpraxis wird die Variabilität der Bodenkenngrößen dahingehend berücksichtigt, dass der Baugrund in subjektiv definierte Homogenbereiche mit sicheren, bekannten Eigenschaften unterteilt wird. Während bisher gelegentlich Trends hinsichtlich der Variation des Mittelwertes im Baugrundmodell und in den darauf aufbauenden Nachweisen eingeführt wurden, blieb eine tiefenabhängige Streuung der Standardabweichung und der Korrelationslänge sowohl in der Wissenschaft, als auch in praktischen Anwendungen vollkommen unberücksichtigt. Da sich der Spannungszustand im Boden bereits unabhängig von externen Einwirkungen durch den Überlagerungsdruck mit der Tiefe ändert, liegt nahe, dass auch hinsichtlich der Variabilität der Kenngrößen ein Tiefeneinfluss besteht.

Die vorliegende Dissertation setzt sich wissenschaftlich mit dem Phänomen der räumlichen und spannungsabhängigen Streuung der Porosität in Sand und mit deren Folge auseinander. Die Hauptziele sind die Klärung der Fragen:

- sind die stochastischen Größen der porenzahlbezogenen Kenngrößen von Sand spannungs- und damit tiefenabhängig?
- wie lässt sich ein realitätsnahes Zufallsfeld der Tiefenabhängigkeit der streuenden Kenngrößen modellieren und stochastisch beschreiben?
- Welchen Einfluss hat eine tiefenabhängige Streuung der porositätsbezogenen Kenngrößen auf die exemplarisch ausgewählten geotechnischen Nachweise der eindimensionalen Kompression und der Stabilität einer unendlich langen Böschung bei einer Infiltration von Niederschlag?

Stand der Wissenschaft

Die Variabilität von Bodeneigenschaften, deren Beschreibung und der Einfluss auf die Sicherheit von Bauwerken war in den letzten Dekaden immer wieder ein relevantes Forschungsthema. In den Analysen und bei der Modellierung des Tiefeneinflusses der streuenden Kenngrößen wurden der Mittelwert und die Standardabweichung entweder als konstant oder als trendbehaftet linear tiefenabhängig angenommen. Die Tiefenabhängigkeit des Variationskoeffizienten wurde meinst nicht untersucht, die räumliche Korrelationslänge der Kenngröße wurde bisher immer als konstant angenommen.

Bei stochastischen Analysen zur Bewertung der Auswirkung der Variabilität einer Bodeneigenschaft in geotechnischen Nachweisen, wurden bisher die statistischen Kenngrößen wie auch die räumliche Korrelationslänge der Bodeneigenschaft innerhalb eines Homogenbereiches als konstant oder rein zufällig streuend betrachtet. Der Einfluss des Spannungszustandes und die daraus zu erwartenden Effekte auf spezifische geotechnische Nachweise wurden bisher nicht untersucht.

Eingesetzte Methoden

Die Beziehung zwischen dem Spannungsniveau und der Änderung der statistischen Größen der porenzahlbezogenen Kenngrößen eines Sandes wurde mit einer stochastischen Analyse anhand der der eindimensionalen Kompression untersucht. Dabei wurde ein Zufalls-Finite-Elemente-Modell entwickelt. Dem Sand wurde ein hypoplastisches Stoffgesetzt zugeordnet. Mit diesen Methoden konnte ein Zufallsfeld entwickelt werden, das den Einfluss des Spannungszustandes und damit den der Tiefenabhängigkeit abbildet. Die tiefenabhängigen Phänomene wurden anhand der Dehnung bewertet, was einer Setzungsanalyse gleichkommt.

Der Einfluss einer tiefenabhängigen Streuung der bodenmechanischen Kenngrößen und deren Korrelationslängen wurde exemplarisch für eine unendlich lange Böschungen (ebene Gleitfuge) analysiert wobei auch die Infiltration von Niederschlagswasser als Einwirkung betrachtet wurde. Die stationäre Infiltration wurde mit Hilfe der deterministischen Lösung simuliert, die instationäre mit dem Finite-Differenzen-Verfahren nach dem Crank-Nicolson-Schema. Die globale Standsicherheit der Böschung mit unsicheren Kenngrößen wird während der Infiltration von Niederschlagswasser maßgeblich durch die ungesättigte Wasserdurchlässigkeit des Bodens bestimmt und hängt damit wesentlich von der Matrix-Spannung ab. Die Variabilität der gesättigten Wasserdurchlässigkeit bei variablen Bodeneigenschaften konnte über empirische Korrelationen berücksichtigt werden. Für die Änderung der in der ungesättigten Zone wesentlichen Einflussgröße Saugspannung wurde auf bekannte Modellierungen und Gesetzmäßigkeiten zurückgegriffen, bei denen jedoch keine Variabilität der räumlichen Strukturen berücksichtigt werden konnte.

Wesentliche Ergebnisse

Mit der systematischen Analyse zur Wirkung des Spannungsniveaus auf die stochastischen Größen der porenzahlbezogenen Kenngrößen des Sandes konnte gezeigt werden, dass

- die statistischen Kennwerte der Porosität von Sand signifikant vom Spannungszustand beeinflusst werden,
- der Mittelwert und die Standardabweichung der porenzahlbezogenen Kenngrößen von Sand damit ebenfalls spannungsabhängig sind und sich auch die räumliche Korrelationslänge mit einer Zunahme des Spannungsniveaus reduziert,
- damit auch die statistischen Kennwerte der porenzahlbezogenen bodenmechanischen Kenngrößen von Sand tiefenabhängig sind.

Das nichtstationäre Zufallsfeld mit tiefenabhängigem Mittelwert und/oder tiefenabhängiger Standardabweichung kann durch eine Verzerrung des stationären Zufallsfeldes erzeugt werden. Das nichtstationäre Zufallsfeld mit einer tiefenabhängigen räumlichen Korrelationslänge kann auf zwei verschiedene Weisen erzeugt werden: (i) durch eine Verzerrung des stationären zufälligen Feldes oder (ii) vereinfacht durch ein geschichtetes zufälliges Feld mit unterschiedlichen räumlichen Korrelationslängen in verschiedenen Schichten.

Durch die stochastische Analyse der eindimensionalen Kompression wurde gezeigt, dass die tiefenabhängigen Phänomene der statistischen Parameter der Porenzahl einen geringen Einfluss auf die Dehnung ausüben.

Bei der deterministischen Analyse der Standsicherheit einer Böschung wurde für die Infiltration von Niederschlag ein konstanter Fluss angenommen. Die Ergebnisse zeigen, dass die tiefenabhängige Wasserdurchlässigkeit einen wesentlichen Einfluss hat. Die Vernachlässigung der tiefenabhängige Variabilität und der damit verbundenen Phänomene ist nicht konservativ. Weiterhin wurde festgestellt, dass die Böschung bei einer tiefenabhängigen Wasserdurchlässigkeit früher versagt und die kritische Gleitfläche näher an der Oberfläche verläuft.

Bei der numerischen Analyse der Standsicherheit und mit der Simulation der Infiltration wurde ebenso ein konstanter Fluss betrachtet, jedoch wurde die Wasserdurchlässigkeit der Böschung als log-normalverteilt angenommen. Die Ergebnisse zeigen, dass unter diesen Bedingungen

- die tiefenabhängigen Phänomene des streuenden Mittelwertes der Wasserdurchlässigkeit einen signifikanten Einfluss auf die Stabilität der Böschung haben,
- bei einem mit der Tiefe linear abnehmenden Mittelwert eine stationäre Infiltration zu einer signifikanten Erhöhung der Versagenswahrscheinlichkeit der Böschung führt, bei einer instationären Infiltration die Effekte dagegen von der Dauer der Infiltration abhängen,
- die Phänomene der streuenden Standardabweichung der Wasserdurchlässigkeit mit der Tiefe abnehmen und sich die Versagenswahrscheinlichkeit der Böschung bei stationärer Infiltration nur wenig reduziert,
- bei einer instationären Infiltration die Versagenswahrscheinlichkeit im frühen Stadium der Infiltration unterschätzt, bei langer Infiltration jedoch überschätzt wird,
- bei gleichzeitiger Berücksichtigung der Tiefenabhängkeit von Mittelwert und Standardabweichung der Wasserdurchlässigkeit der Mittelwert den dominanten Einfluss besitzt,
- eine tiefenabhängig streuende räumliche Korrelationslänge der Wasserdurchlässigkeit nur einen sehr geringen Einfluss auf die Versagenswahrscheinlichkeit hat und für praktische Anwendungen vernachlässigt werden kann.

Der Einfluss einer streuenden Durchlässigkeitsanisotropie wurde im Rahmen dieser Arbeit nicht untersucht. Jedoch lassen sich aus den Ergebnissen mögliche Effekte als Diskussionsgrundlage ableiten.

Contents

List of Figures

List of Tables

Notation

Symbol	Unit	Description
$1d$	[-]	one-dimensional
$2d$	[-]	two-dimensional
$3d$	[-]	three-dimensional
a	[-]	weighting factor
a_1	[-]	constant
a_2	[-]	constant
AIC	[-]	AKAIKE information criterion
ANN	[-]	artificial neural network
ASM	[-]	advanced second moment
b_1	[-]	constant
b_2	[-]	constant
$\mathbf{b}$	[-]	vector of the parameters of the variogram
c'	$[kN/m^2]$	effective cohesion
C	$[1/m]$	specific water capacity
C_i^j	$[1/m]$	specific water capacity a space i and time j
$Cov(.)$	[-]	covariance function
cot	[-]	cotangent
CPT	[-]	cone penetration test
CV	[-]	coefficient of variation
CV_{ks}	[-]	coefficient of variation of saturated hydraulic conductivity
dz	[m]	discretization of the slope
$d\phi$	[°]	the range of variation of friction angle within the weathering zone
e	[-]	soil void ratio
e_i	[-]	void ratio of i^{th} element
e_{c0}	[-]	critical void ratio for zero inter-granular stress
e_{d0}	[-]	void ratio of minimum densification for zero inter-granular stress
e_{i0}	[-]	void ratio of maximum densification for zero inter-granular stress
err	[-]	residual error ratio
$E[.]$	[-]	expected value of the quantity in the square brackets
$FOSM$	[-]	first order second moment
FS	[-]	factor of safety
FS_{min}	[]	minimum factor of safety
h	[m]	(pore-water) pressure head
h_0	[m]	pressure head at z=0
h_i	[m]	pressure head at elevation z_i
h_{i-1}	[m]	pressure head at elevation z_{i-1}
h_s	[kPa]	granulate hardness
H	[m]	total head
dH	[m]	increment of total head
k	[m/s]	hydraulic conductivity
k_0	[-]	number of parameters in the statistical model
$k_1; k_2$	[-]	the portion of each individual random field to the whole random field
kk	[-]	slope of vertical influence
ks	[m/s]	saturated hydraulic conductivity
ks_i	[m/s]	saturated hydraulic conductivity of layer i
L	[m]	slope depth above the groundwater table
L_0	[-]	maximum value of the likelihood function for the estimated model

L_1;L_2	[m]	length of each individual random field
L	[-]	lower triangular matrix from LU decomposition
$LRFD$	[-]	load and resistance factor design
m	[-]	porosity
m_0	[-]	porosity at the ground surface
m_w	[-]	slope of the SWCC
min	[-]	minimum
n	[-]	number or parameter
N	[-]	number of pairs
$NSCL$	[-]	normalized spatial correlation length
OLS	[-]	ordinary least square
$PCEM$	[-]	polynomial chaos expansion method
PDF	[-]	probability density function
PEM	[-]	point estimating method
Pf	[-]	probability of failure
q	[m/s]	preset infiltration flux
q_c	[MPa]	cone resistance
Q	[kPa]	all loads
R	[- or kPa]	reliability or total resistance
$RFEM$	[-]	random finite element method
RF	[-]	random field
RSM	[-]	response surface method
RSS	[-]	residual sum of squares
SLS	[-]	serviceability limit state
SCL	[m]	spatial correlation length
SCL_{lower}	[m]	spatial correlation length in the lower layer
SCL_{upper}	[m]	spatial correlation length in the upper layer
SPT	[-]	standard penetration test
SSE	[-]	sum of squared errors of prediction
SSR	[-]	sum of squared residuals
STD	[-]	standard deviation
STD_e	[-]	standard deviation of void ratio
STD_{ks}	[-]	standard deviation of saturated hydraulic conductivity
SVM	[-]	support vector machine
$SFEM$	[-]	stochastic finite element method
$SWCC$	[-]	soil water characteristic curve
t	[s]	time
T	[m]	averaging domain
$T(.)$	[-]	trend function
tan	[-]	tangent
U	[-]	final Gaussian random field
U1	[-]	normalized Gaussian random field
U2	[-]	normalized spatially correlated Gaussian random field
$Var[.]$	[-]	variance of the quantity in the square brackets
VR	[-]	variance reduction
w_i	[-]	weight given to the i^{th} observation
WLS	[-]	weighted least square
X	[-]	final random field
x_i	[-]	the i^{th} sample
x	[-]	a set of random variables
Y	[-]	soil property
z	[m]	depth or elevation
z_w	[m]	depth of the weathered zone
$Z1$	[-]	stationary random field
$Z2$, $Z3$	[-]	non-stationary random fields
α	[kPa^{-1} or -]	SWCC parameter or VW hypoplastic model parameter

α_1	[°]	slope angle measured from vertical
β	[° or -]	slope angle measured from horizontal or VW hypoplastic model parameter
$\gamma(.)$	[-]	theoretical (semi)variogram
$\hat{\gamma}(.)$	[-]	sample variogram
γ_s	$[kN/m^3]$	soil unit weight
γ_w	$[kN/m^3]$	unit weight of water
Γ	[-]	variance reduction factor
δ	[m]	spatial correlation length
δ_C	[m]	calculated spatial correlation length
δ_h	[m]	horizontal spatial correlation length
δ_v	[m]	vertical spatial correlation length
δ_{v_down}	[m]	downside spatial correlation length
δ_{v_up}	[m]	upside spatial correlation length
δ_T	[m]	true spatial correlation length from GSTAT
Δ	[-]	dimensionless spatial correlation length
Δm	[-]	range of variation in porosity
$\Delta\phi$	[°]	range of variation in friction angle
$\epsilon(.)$	[-]	residual to the trend
θ	[-]	volumetric water content
θ_r	[-]	residual water content
θ_s	[-]	saturated water content
μ	[-]	mean value
μ_e	[-]	mean of void ratio
μ_z	[-]	mean value at depth z
ξ	[-]	distorting ratio
$\rho(\tau)$	[-]	theoretical autocorrelation function
$\hat{\rho}(.)$	[-]	evaluated autocorrelation function
σ	[-]	standard deviation
σ^2	[-]	variance
σ_t	$[kPa]$	total stress
σ_T^2	[-]	variance of a soil property after local averaging of an element
τ	[m]	distance between any two point
$\boldsymbol{\tau}$	[m]	lag vector
τ_f	$[kPa]$	shear strength of soil
τ_x	[m]	distance between any two point in the x coordinate
τ_y	[m]	distance between any two point in the y coordinate
ϕ	[°]	effective friction angle
ϕ_0	[°]	effective friction angle at ground surface
ϕ_c	[°]	critical friction angle used in VW hypoplastic model
χ	[-]	degree of effective saturation

1. Introduction

1.1. Background

It is inevitable to confront and handle with uncertainties in geotechnical engineering because soil properties are highly variable. Catastrophic disasters can be found in geotechnical engineering because of the underestimation of uncertainty. The uncertainties of soil properties have long been appreciated in geotechnical engineering, and have never been ignored since the establishment of soil mechanics. Studies about uncertainties can be categorized into two parts: (i) having a better understanding of the uncertainty through field explorations and experiments, (ii) incorporating the uncertainty into geotechnical design wisely, so as to make a geotechnical structure in a good balance of both economics and safety.

The methods used in the geotechnical design can be classified into three generations, through how to deal with uncertainties:

- The deterministic methods are used in the first generation through idealizing a soil layer homogeneous, using the mean value only. A factor of safety and partial safety factors higher than one are adopted to implicitly considerate uncertainties. These methods are commonly adopted in national standards.
- In the second generation, the probabilistic methods are employed to highlight the effect of uncertainties on geotechnical practice. Besides mean value, the standard deviation is also taken into consideration. Some classical methods, e.g. First Order Second Moment (FOSM) method, are in this generation.
- The probabilistic methods are improved in the third generation, in order to honor the importance of the spatial variation of soil properties, through considering the spatial correlation structure using a correlation function together with a spatial correlation length. Some well-known methods, like random finite element method and stochastic finite element method, are in this generation.

Right now, the methods of the third generation are most popular to be employed, to evaluate the effect of the uncertainty of a soil property on geotechnical practice. All the stochastic parameters, including the mean, the standard deviation, and the spatial correlation length are considered to be significant.

1.2. Motivation

It is a common sense that the stress level can significantly influence soil properties. Some works have been carried out to find the relation between the stress level and the mean value of a soil property. For example, using the odeometer test to find the relation between the change in stress level and the mean void ratio. However, as mentioned before, the mean value is not enough to conclude a rational decision. The standard deviation and the spatial correlation length are also greatly required nowadays. However, little work can be found in how a change in stress level affects the standard deviation and spatial correlation length of a soil property. So some questions come up:

- Can the change in stress level affect the standard deviation and the spatial correlation length of a soil property?
- How does the change in stress level affect both the standard deviation and the spatial correlation length?

Since soil suffers different stress of self-weight at different soil depth, the value of a soil property (e.g. porosity) might be depth-dependent due to the mechanical compaction and consolidation. Some of the former studies have confirmed that, the mean value of some soil properties is depth-dependent. For example, the porosity and friction angle of sand (Lu and Godt, 2008), and the cohesion of marine clay (Lumb, 1966). However, this depth-dependent mean trend is seldom considered during the stochastic analysis. It is worth to question:

- If this depth-dependent character of the mean trend affects the results?
- Is this effect significant enough to be considered?

When the standard deviation and the spatial correlation length are under consideration, some questions also rise up:

- Are the standard deviation and spatial correlation length depth-dependent?
- If yes, how does the depth-dependent character of these stochastic parameters affect geotechnical practice? and is the influence significant enough to be considered?

Field exploration, like the cone penetration tests, supplies a lot of data to help us understand the variation of some soil properties. When dealing with these data, we are too eager to obtain the mean trend, the standard deviation and the spatial correlation length of a soil property, so we directly assume both the standard deviation and the spatial correlation length are all constant (or depth-independent). The assumption is taken for granted because it is not easy to find if the standard deviation and the spatial correlation length are depth-dependent, unless there is a clear difference in a soil property profile at a different depth. In this case, we normally assume the soil is in different types (e.g. layered soil). In reality, the progressive change of stress level with soil depth might cover the true relation between the stress level and both the standard deviation and the spatial correlation length, makes us believe they are depth-independent. It is necessary to find a way to uncover if the assumption is right.

This thesis gives some attempts to answer the questions mentioned above.

1.3. Study aim

The main aim of this research is to evaluate the effect of stress level on the variation of soil properties, and its effect on geotechnical practice, within the framework of both deterministic and stochastic methods. To accomplish this aim, three main topics are carried out step by step:

Firstly, the stochastic simulation of one-dimensional compression test is carried out to evaluate the effect of stress level on the uncertainty of void ratio related properties of sand, to find out if the change in stress affects the mean, the standard deviation, and the spatial correlation length of void ratio related properties of sand, and if these stochastic parameters are depth-dependent.

Then, some explorations are conducted to generate the related random fields, taking the depth-dependent character of each stochastic parameter into consideration.

Finally, its consequences to geotechnical practice are discussed, including to the one-dimensional settlement analysis, infiltration, and infinite slope stability analysis during infiltration.

All the analysis carried out in this thesis consider only one-dimensional effect.

1.4. Thesis scope

Seven further chapters are arranged:

Chapter 2 describes the background information related to the present work, including (a) a short description of the mathematical framework, (b) an extensive literature review of the soil uncertainty, especially the inherent spatial variability, its quantification, and its effect on geotechnical practice.

Chapter 3 focuses on the effect of stress level on the uncertainty of void ratio using the random finite element method, with a hypoplastic model through the one-dimensional compression simulation. The effect of stress level on the stochastic parameters, including the mean, the standard deviation, and the spatial correlation length, is analyzed in detail. Then this effect is extended into the other void ratio related parameters of sand. Moreover, if these stochastic parameters depth-dependent is also discussed.

Chapter 4 concentrates on the random field generation considering the depth-dependent character of each stochastic parameter. The mean spatial correlation length of layered random field with different spatial correlation length in different layer is also calculated.

Chapter 5 is the stochastic one-dimensional settlement analysis. The effect of the depth-dependent character of of the stochastic parameters of void ratio on the strain is analyzed.

Chapter 6 is the deterministic analysis of infinite slope stability with and without considering the effect of the infiltration. Both steady and transient state infiltration are considered. The depth-dependent character of saturated hydraulic conductivity is highlighted. Furthermore, some important parametric studies are also carried out.

Chapter 7 presents the stochastic analysis of infinite slope stability during rainwater infiltration. The effect of the coefficient of variation of ks and the spatial correlation length of ln(ks) are carried out. Moreover, the depth-dependent character of the mean and standard deviation of ks, and the spatial correlation length of ln(ks) are highlighted during both steady state and transient state infiltration.

Chapter 8 summarizes all major findings of this research, draws conclusions, and recommends possible further researches.

2. Literature review on soil variability and its effect on geotechnical practice

2.1. Background of soil variability

Soil is a complex geotechnical material. Its properties vary from one location to another, because it experienced complex and varied natural geological processes, such as weathering and erosion processes, transportation, different kinds of sedimentation, various stress history, etc. (Chiasson et al., 1995; Dasaka and Zhang, 2012; Huber, 2013; Jaksa, 1995; Kim et al., 1978; Lloret-Cabot et al., 2014; Soga and Mitchell, 2005). The variation of soil properties can cause the uncertainty during parameter estimation. Some parameters are directly related to the stiffness and strength, which control the safety and performance of geotechnical structures (Srivastava and Babu, 2009). Therefore, it is really important to consider the soil variation and uncertainty in geotechnical practice. The uncertainty has long been appreciated. The past experience and judgements from experts are taken into account in order to consider the soil uncertainties in conventional approaches. A factor of safety (FS) higher than one is chosen in the safety design of a geotechnical structure in order to implicitly consider the uncertainty. For example, Terzaghi et al. (1996) recommended the FS should be between 1.5 and 3.0, so as to guarantee the stabilization of a structure in a long term. However, this experience-based way in selecting representative parameters highly depends on personal preference (Schweiger et al., 2001), and it is not explicit and rational. As a result, the uncertainty-based approaches are developed and widely used to take uncertainties into consideration in a more rational way. Uzielli et al. (2006) summarized the following advantages of the uncertainty-based approaches:

(i) The approaches take the uncertainties of input parameters into consideration.

(ii) The approaches can provide complete and realistic information, which is related to the level of safety of design.

(iii) The approaches can provide more rational results by explicitly declaring the uncertainty, and this can help the designer make a better decision on a desired or required performance level of a structure.

Since soil uncertainty is so important, it is very useful for us to understand soil uncertainty and its effect on geotechnical engineering. Within this chapter, the author summarized the basic information about soil variability, including, its sources, its quantification, its simulation, and its effect on geotechnical practice.

2.2. Sources and scales of soil variability

The parameters used in both conventional approaches and reliability-based approaches during geotechnical analysis come from in-situ and experimental tests. The estimation of these parameters is inevitably related to uncertainties. The uncertainty of an estimated soil property comes from different sources: the inherent variability, the measurement errors, and the transformation uncertainty (Phoon and Kulhawy, 1999*a*), as illustrated in Figure 2.1.

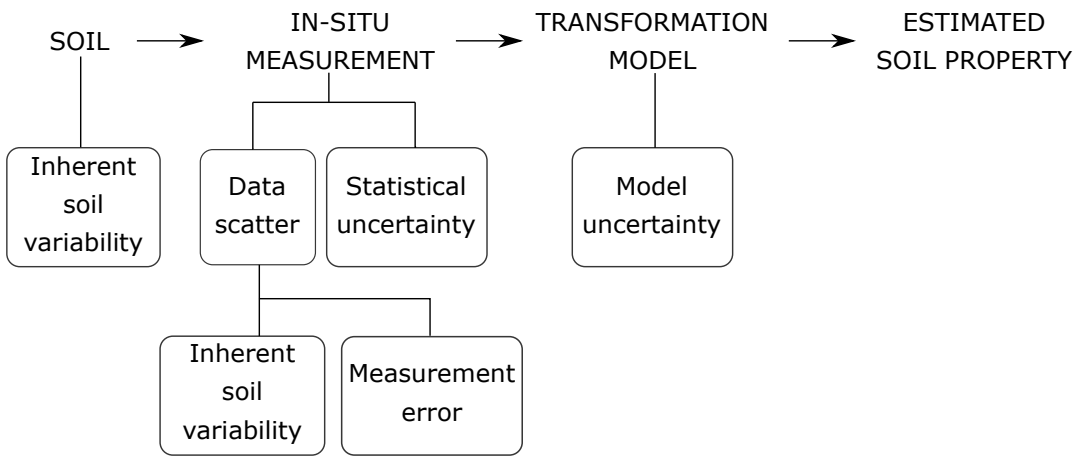

Figure 2.1.: Uncertainty in soil property estimation (source: Phoon and Kulhawy 1999*a*, p. 613)

(i) The inherent soil variability (or inherent uncertainty): it is the primary source of geotechnical uncertainty (Phoon and Kulhawy, 1999*a*). It originates from the mineral composition, the environmental conditions during deposition, past stress history, and variations in moisture content (Tang, 1984), which produce and continually modify the soil mass.

(ii) The measurement errors: it is caused by equipment, procedural-operators, and random testing effects (Nobahar, 2003).

(iii) The transformation uncertainty: this uncertainty comes from the transformation between the field or laboratory measurements and the design soil properties using empirical or other models (Nobahar, 2003).

The inherent uncertainty is a natural character of soil. It is independent from the knowledge of experts, and it cannot be decreased by more data. It is the physical uncertainty which is usually categorized as **aleatory uncertainty**, while the other uncertainties, such as the measurement uncertainty and the model uncertainty are categorized as **episdemic uncertainty**. The episdemic uncertainty is related to incomplete knowledge, and it can be reduced by more data, better instruments, better models, and so on.

Many scientists have investigated the variability of soil properties in different fields, ranging from hydrology, soil science, reservoir engineering, up to geotechnical engineering. Koltermann and Gorelick (1996) pointed out that the variability of a soil property needs to be treated separately at different scales. The variation of a soil property exists in all kinds of scales from the grain size scale to the geological scale, and the variation differs from one scale to another, as is shown in Figure 2.2. Therefore, it is important to be clear in the scale of our target before the evaluation of soil variability. Herein, we focus on the variability in the geotechnical scale, which lies between the specimen scale and the geological scale.

2.3. Quantification of soil variability

2.3.1. Description of soil variability

As is shown in Figure 2.3, the variation of a soil property can be presented as a sum of the trend and residual (Phoon and Kulhawy, 1999*a*) by:

$$Y(z) = T(z) + \epsilon(z) \tag{2.1}$$

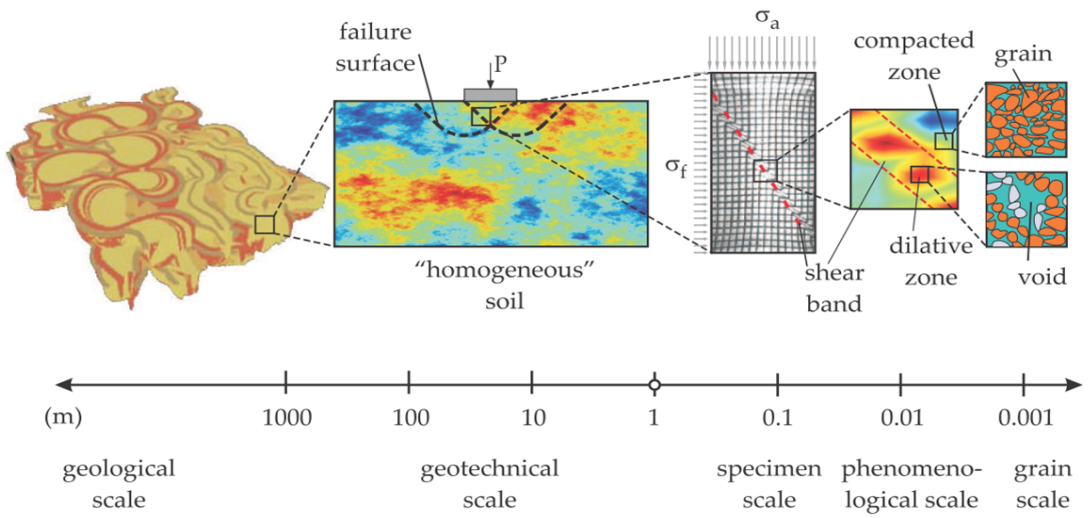

Figure 2.2.: Illustration of the multi-scale nature of soil variation (source: Huber 2013, p. 10)

where Y(z) is the soil property, T(z) is the trend function giving the mean value of the soil property at location z, and ϵ(z) is the residual off the trend.

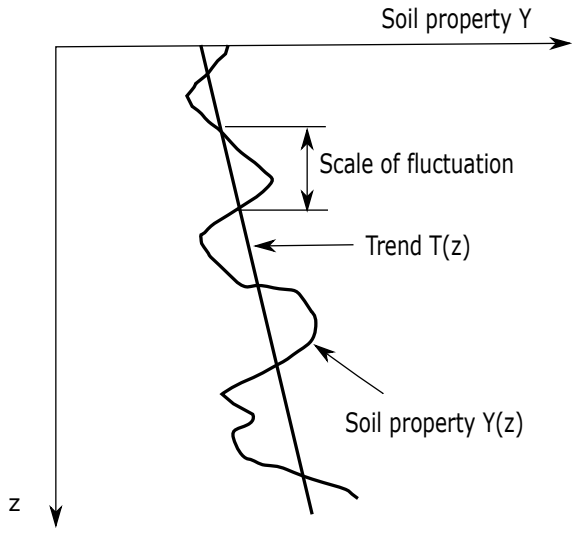

Figure 2.3.: Illustration of the variability of a soil property with depth

Herein, z is the vertical depth of the location under the ground surface. T(z) could be either depth-dependent or depth-independent, and it is usually estimated by a regression analysis. The residual ϵ(z) is usually spatial correlated, which can be expressed by the scale of fluctuation (or range, spatial correlation length). The residual includes the inherent uncertainty and measurement error. It is really difficult to separate them (Phoon and Kulhawy, 1999*a*,*b*). Since the key uncertainty comes from inherent uncertainty, only inherent uncertainty is considered in this thesis.

The mean value μ at depth z can be obtained by,

$$\mu_z = \frac{1}{n}\sum_{i=1}^{n} x_i \tag{2.2}$$

x_i is the i^{th} sample in the same depth, n is the total number of samples in the same depth.

The residual $\epsilon(z)$ is usually expressed by the variance (or coefficient of variation), and a correlation structure. The variance is a measure of the dispersion of data to the mean value, and it can be evaluated by,

$$\sigma_z^2 = \frac{1}{n-1}\sum_{i=1}^{n}(x_i - \mu_z)^2 \tag{2.3}$$

Detail information about the correlation structure will be elaborated later.

2.3.2. Mathematical description of inherent spatial correlation

As pointed out before, the physical properties of natural soil vary from place to place. In classical statistics, the residual is usually assumed to be uncorrelated, and only the mean and variance are chosen to depict the uncertainty. However, site exploration shows that observations made at different locations may not be independent. For example, measurements made at nearby locations may be closer in value than measurements made at locations farther apart. This phenomenon is called spatial correlation. It can be positive or negative. A positive spatial correlation means similar values occur near one another, while a negative spatial correlation means dissimilar values occur near one another. Therefore, the spatial correlation also needs to be included, besides the mean and the variance.

The degree of spatial correlation of residuals can be expressed by (auto)covariance function Cov as,

$$Cov(\boldsymbol{\tau}) = E[Y(x+\boldsymbol{\tau}) - \mu(x+\boldsymbol{\tau})][Y(x) - \mu(x)] \tag{2.4}$$

where $\boldsymbol{\tau}$ is the separation distance or lag. E[] is the expected value of the quantity in the square brackets. The covariance is high at a small lag, and it decays to zero as the lag increases. Besides the lag $\boldsymbol{\tau}$, the covariance is also related to its direction. The domain is **isotropic** when the covariance depends only on the lag, and it is **anisotropic** when the covariance depends on both the lag and the direction. The soil domain is **stationary** when both the mean and the variance are constant, meanwhile, the covariance function only depends on the separation distance. Otherwise, the soil domain is **non-stationary**.

Besides the covariance function, the theoretical variogram is also used in geostatistics in quantifying spatial variability. For a second-order stationary case, the theoretical variogram can be expressed as,

$$\gamma(\boldsymbol{\tau}) = \frac{1}{2}Var[Y(x+\boldsymbol{\tau}) - Y(x)] \tag{2.5}$$

where Var[] means the variance of the quantity in the square brackets. The variogram shows the dissimilarity between Y(x) and Y(x+$\boldsymbol{\tau}$) related to the separation distance. $\gamma(\boldsymbol{\tau})$ is also called ' **semivariogram**', however, the term '**variogram**' is usually adopted because of its simplicity and some theoretical arguments (Chiles and Delfiner, 2009). Empirically speaking, the variogram is zero at lag=0, and it increases asymptotically to the variance, as the increase of lag $\boldsymbol{\tau}$.

For a second-order stationary case, the relation between the covariance function and the theoretical variogram is expressed as,

$$\gamma(\boldsymbol{\tau}) = Cov(0) - Cov(\boldsymbol{\tau}) \tag{2.6}$$

For the stationary random field, it is equivalent to know $\gamma(\boldsymbol{\tau})$ or Cov($\boldsymbol{\tau}$), as is shown in Figure 2.4, where the variance is one.

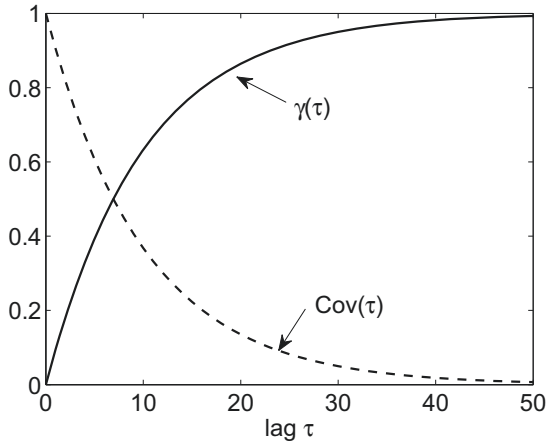

Figure 2.4.: Relation between the covariance function and the variogram for the stationary random field

2.3.3. Estimation of the correlation structure

When dealing with real data, the underling variogram (or correlation function) and the variance are unknown, estimators of these variables need to be used. The estimators of the variogram and variance are sample variogram and sample variance, respectively. After the collection of data, e.g. Cone Penetration Test (CPT) or Standard Penetration Test (SPT), the estimators will be evaluated. The key to evaluate the correlation structure of a soil property is to estimate the trend and the correlation function of the residuals (DeGroot and Baecher, 1993).

There are many methods to evaluate the correlation structure, such as method of moments, maximum likelihood approach, amongst other approaches (DeGroot and Baecher, 1993). Here the variogram approach and autocorrelation function approach in the moment of methods category are elaborated since they are commonly used in geotechnical engineering.

(a) The variogram approach

The sample (also known as empirical or experimental) variogram $\hat{\gamma}(\boldsymbol{\tau})$ is a moment estimator of the variogram function. For one-dimensional stationary random domain measured at uniform intervals of unit distance, the sample variogram of a soil property Y(x) can be calculated by,

$$\hat{\gamma}(\boldsymbol{\tau}) = \frac{1}{2n(\boldsymbol{\tau})} \sum_{i=1}^{n(\boldsymbol{\tau})} [Y(x_i + \boldsymbol{\tau}) - Y(x_i)]^2 \tag{2.7}$$

in which, n($\boldsymbol{\tau}$) denotes the count pairs of points separated by the mutual distance $\boldsymbol{\tau}$ between the property values $z(x_i)$ at location x_i. The maximum $\boldsymbol{\tau}$ of the measurement should be at least less than 1/5 or 1/4 of the correlation length. If the sampling distance is longer, the estimated spatial correlation length is not right since not enough data are available to support a proper spatial correlation length; if the sampling distance is very small, the correlation length may be at a smaller scale level.

The sample variogram will be fitted by theoretical variogram models. We need to make a distinction between the sample variogram and the variogram model. The sample variogram is an empirical estimate of the theoretical variogram of a Gaussian process. It is a visualization of a possible spatial correlation, and is not directly usable in kriging without constraints or further processing, while the variogram model is further used to define the weights of the kriging function.

Theoretical variogram models

The sample variogram cannot be computed at any value of the distance, due to the constraint of data exploration. However, it is necessary to obtain the variogram at all distance in geostatistical simulation or interpolation. Detail processes of fulfilling the continuity of sample variogram are elaborated in Chiles and Delfiner (2009). The sample variogram is used in the first step of spatial prediction as tools that provide insight into the spatial continuity and structure of a random process. However, the sample variogram cannot be used directly to describe the correlation structure, because firstly, it may violate the required property of conditional negative definiteness; secondly, for various purposes, i.e. kriging, we may require an estimate of the variogram at a lag not represented in the data; finally, the sample variogram may be quite bumpy. A smoothed version may be helpful for understanding the nature of the spatial dependence. It is critical to note that the sample variogram provides an estimate of the theoretical variogram only when the random field is stationary. When the sample variogram is calculated, it is then necessary to choose a proper theoretical variogram model based on the estimation so as to evaluate the correlation structure.

The shape of commonly used theoretical variograms rise monotonically as a function of distance. It is typically characterized in terms of particular parameters. These parameters are the range, the sill, and the nugget effect, as is shown in Figure 2.5. The **sill** is the upper bound of the variogram. It is the summation of the nugget effect and the partial sill. The **range** (or the range of influence) is defined as the distance at which samples become independent of one another. The range denotes the distance at which the variogram reaches the sill. The **nugget effect** represents a discontinuity of the variogram that can be present at the origin. It is typically attributed to microscale effects, sampling or statistical errors, or measurement error (Jaksa, 1995). The variogram is always zero at distance τ=0; hence, the nugget effect demonstrates itself as a jump in the variogram as soon as τ>0.

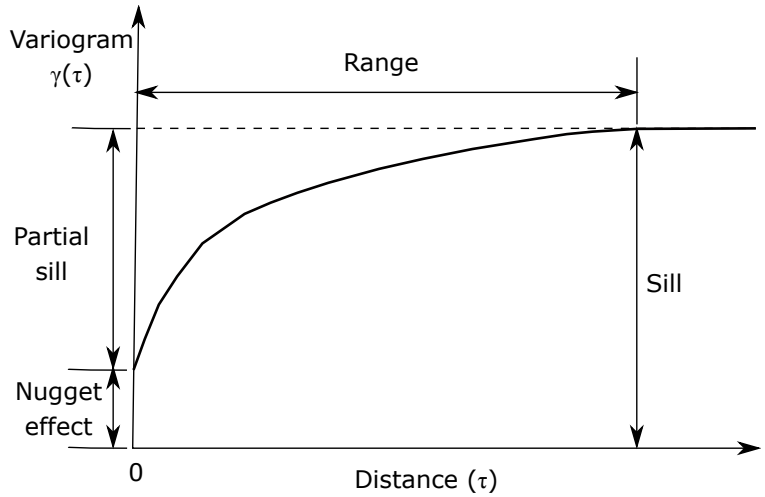

Figure 2.5.: Illustration of the variogram

The theoretical variogram models are employed to describe the spatial structure of random processes. A lot of information can be provided by the shape and characteristics of the theoretical variogram model. The normally used theoretical models are spherical variogram model, exponential variogram model, and Gaussian variogram model, which are listed in Table 2.1. The shapes of these three models are plotted in Figure 2.6. Figure 2.6a shows these three theoretical variogram models with a_0 =1 and sill c_0=4. The range of spherical model is 1 because the variogram reaches to the sill when the lag τ reaches to 1, then the variogram stops increasing as the increase of τ. However, for the exponential and Gaussian variogram models, the variogram keeps approaching to the sill asymptotically as the increase of τ, but never reaches to the sill. In these cases, the 'effective range' is used. It is defined as the lag where the variogram is approximately 95% of its sill,

or where the covariance is approximately 5% of its value at zero. Here in Figure 2.6a the effective ranges are $\sqrt{3}$ and 3 for Gaussian and spherical models, respectively, and the effective range of the spherical model can be regarded as the range. The shapes of these theoretical models with the same sill and (effective) range are shown in Figure 2.6b. One should note that although the range is defined as the distance at which the variogram reaches the sill, a_0 is used in reality as the range, and the effective range can truly denote as the distance of which the variogram reaches the sill.

Table 2.1.: Normally used theoretical variogram models

Model	Theoretical variogram fuction
Spherical	$\gamma(\tau) = \begin{cases} c_0[\frac{3}{2}\frac{\tau}{a_0} - \frac{1}{2}(\frac{\tau}{a_0})^3], & \text{if } \tau \leq a_0 \\ c_0, & \text{if } \tau > a_0 \end{cases}$
Exponential	$\gamma(\tau) = c_0[1 - exp(-\frac{\tau}{a_0})]$
Gaussian	$\gamma(\tau) = c_0[1 - exp(-\frac{\tau^2}{a_0^2})]$

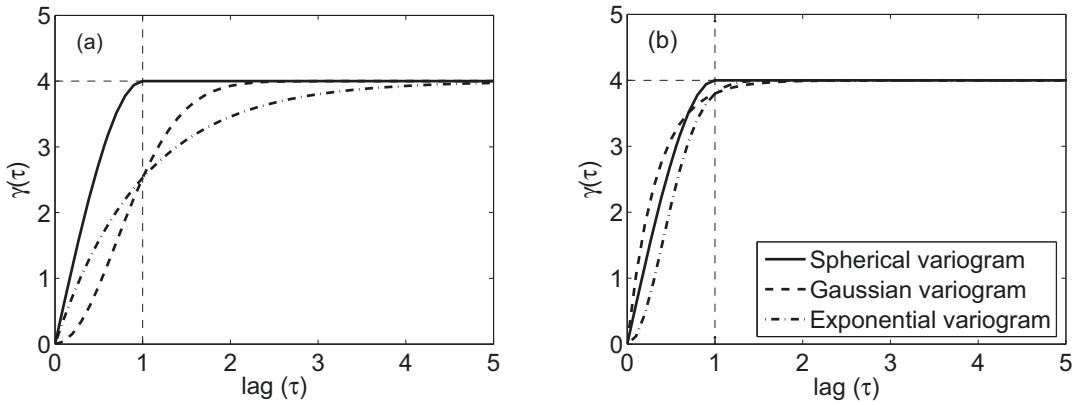

Figure 2.6.: Theoretical variogram model comparison with c_0=4 and (a) a_0=1, (b) (effective) range=1

Variance and sill

One question needs to ask is if the variance and sill are same. If the separation distance is so large that Z(x) and Z(x+$\boldsymbol{\tau}$) in Eq. 2.5 are uncorrelated (i.e. $\boldsymbol{\tau} \geq$ range), the variogram equals to the population variance. That is, the sill of the underlying variogram equals to the variance of the underlying population (Barnes, 1991), which means,

$$\gamma(\boldsymbol{\tau}|\boldsymbol{\tau} > range) = \sigma^2 \tag{2.8}$$

When dealing with real data, the underling variogram and the true population variance are unknown. In this situation, Eq. 2.8 is not always useful. Some researchers in geostatistics suggested using the sample variance, which is a good estimator of the population variance, to estimate the sill of the variogram (David, 2012; Journel and Huijbregts, 1978), however, this suggestion has been proved to be valid only if the N sample values are collected evenly distributed over a domain many times larger than the variogram range (Barnes, 1991).

Variogram model fitting

There are many methods of fitting, such as, by visual assessment, ordinary least square (OLS) methods, generalized least square methods (GLS), weighted least square (WLS) methods, maximum likelihood method, and so on. For OLS, GLS, WLS, the key is to calculted the residual sum

of squares. Only the calculation of the residual sum of squares for OLS and WLS methods are summarized here.

Residual Sum of Squares

The Residual Sum of Squares (RSS) is used in variogram model fitting. RSS is also known as the Sum of Squared Residuals (SSR) or the Sum of Squared Errors of prediction (SSE). It is a measure of the discrepancy between the data and an estimation model. A small RSS indicates a tight fit of the model to the data. For ordinary least squares method, the RSS can be calculated as,

$$RRS = \sum_{i=1}^{n} \epsilon_i^2 = \sum_{i=1}^{n} [\hat{\gamma}(\tau_i) - \gamma(\tau_i; \mathbf{b})]^2 \tag{2.9}$$

in which, $\hat{\gamma}(\tau_i)$ is the sample variogram at distance τ_i, $\gamma(\tau_i; \mathbf{b})$ is the theoretical variogram at τ_i, and $\mathbf{b}$ is a vector of the parameters of the variogram, such as the range, sill, nugget effect and so on.

For ordinary least square method, the estimated coefficients provide the regression equation that minimizes RSS=$\sum_{i=1}^{n} \epsilon_i^2$. One of the common assumptions underlying most process modeling methods, including linear and nonlinear least squares regression, is that each data point provides equally precise information about the deterministic part of the total process variation. In other words, the standard deviation of the error term is constant over all values of the predictor or explanatory variables. This assumption, however, clearly does not hold, even approximately, in every modeling application. When it may not be reasonable to assume that every observation should be treated equally, weighted least squares is often used to maximize the efficiency of parameter estimation. This is done by attempting to give each data point its proper amount of influence over the parameter estimates. A procedure that treats all of the data equally, would give less precisely measured points more influence than they should have and would give highly precise points too little influence.

For weighted least squares method , the estimated equation minimizes RSS=$\sum_{i=1}^{n} w_i \epsilon_i^2$, where w_i is a weight given to the i^{th} observation. Weighted least squares can be used in the presence of nonconstant variance, and be used as the basis for doing 'robust' regression in which outliers are given less weight than points that are not outliers.

The main advantage of the weighted least squares is the ability to handle regression situations in which the data points are of varying quality, and it can also make good use of small data sets. The biggest disadvantage of it, is probably the fact that the theory behind this method is based on the assumption that the weights are known exactly. This is almost never the case in real applications, so estimated weights must be used instead. The effect of using estimated weights is difficult to assess, but experience indicates that small variations in the weights due to estimation do not usually affect a regression analysis or its interpretation. However, when the weights are estimated from small numbers of replicated observations, the results of an analysis can be very badly and unpredictably affected. This is especially likely to be the case when the weights for extreme values of the predictor or explanatory variables are estimated using only a few observations. It is important to remain aware of this potential problem and to only use weighted least squares when the weights can be estimated precisely relative to one another (Carroll et al., 1998).

Weighted least squares regression, like the other least squares method, is also sensitive to the effects of outliers. If potential outliers are not investigated and dealt with appropriately, they will likely have a negative impact on the parameter estimation and other aspects of a weighted least squares analysis. If a weighted least squares regression actually increases the influence of an outlier, the results of the analysis may be far inferior to an unweighted least squares analysis. The

normally used weights are, N, $N/(\gamma(\tau))^2$, and N/τ^2, where N is the number of pairs, γ is the variogram, and τ is the distance.

(b) Autocorrelation function approach

Another way to evaluate the spatial structure is the autocorrelation function, besides the variogram method. The autocorrelation function approach, which comes from mathematicians, is also adopted by engineers to evaluate the spatial variation of a soil property. For stationary random function, it can be expressed as,

$$\hat{\rho}(\boldsymbol{\tau}) = \frac{\sum_{i=1}^{n(\boldsymbol{\tau})} [Y(x_i) - \mu][Y(x_i + \boldsymbol{\tau}) - \mu]}{[n(\boldsymbol{\tau}) - 1]\hat{\sigma}^2} \tag{2.10}$$

in which n is the number of pairs separated by the distance $\boldsymbol{\tau}$.

Like variogram, the number of pairs reduces for calculating $\hat{\rho}(\tau)$ as τ increases. Generally, the number of pairs are regarded as insufficient to calculate $\hat{\rho}(\tau)$ when τ exceeds a quarter of the sampling space domain (Box et al., 2015; Lumb, 1975). For the random field with a depth-dependent trend, a detrending process needs to be carried out so as to make sure the random field is stationary. The sample variogram (no-nugget effect) and sample autocorrelation function follows the relation of Eq. 2.11 (Huber, 2013), as is shown in Figure 2.7, where the $Var[z(x)]$=1.

$$\hat{\rho}(\boldsymbol{\tau}) = Var[z(x)][1 - \hat{\rho}(\boldsymbol{\tau})] \tag{2.11}$$

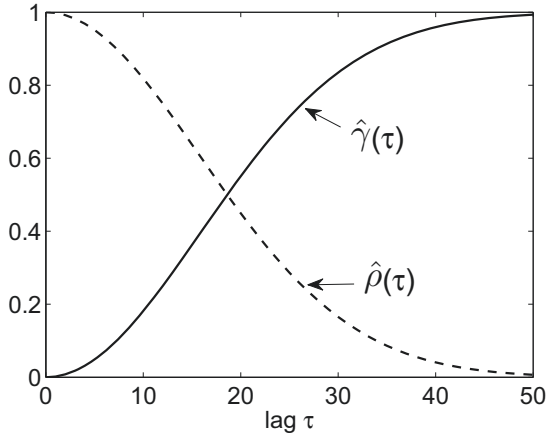

Figure 2.7.: Relation between the variogram and the autocorrelation function with $Var[z(x)]$=1

Theoretical autocorrelation models

The theoretical autocorrelation models are needed in the sample autocorrelation fitting, so as to find some essential properties during the evaluation of the spatial correlation. Here the only property is the spatial correlation length. Two definitions need to be clarified, the **scale of fluctuation** and the **spatial correlation length**. According to Fenton and Griffiths (2008): " *The correlation length, also sometimes referred to as the scale of fluctuation. Loosely speaking the correlation length is the distance within which points are significantly correlated (i.e., by more than about 10%). Conversely, two points separated by a distance more than the correlation length will be largely uncorrelated.*" This means the scale of fluctuation and the spatial correlation length are the same. Some other researchers also regarded them as the same thing (Phoon and Kulhawy, 2005). In this thesis, they are considered the same. Here some normally used theoretical autocorrelation models are listed in Table 2.2 (Nie

et al., 2015; Vanmarcke, 2010, 1977). The autocorrelation fitting methods are similar to the variogram fitting approaches. A detail procedure of fitting the best theoretical correlation model to the sample correlation function is elaborated in Lloret-Cabot et al. (2014).

Table 2.2.: Some commonly used theoretical autocorrelation models

Model	Autocorrelation models
Spherical	$\rho(\tau) = \begin{cases} c_0 - c_0[\frac{3}{2}\frac{\tau}{\delta} - \frac{1}{2}(\frac{\tau}{\delta})^3], & \text{if } \tau \leq \delta \\ 0, & \text{if } \tau > \delta \end{cases}$
Exponential	$\rho(\tau) = c_0 exp(-\frac{2\lvert\tau\rvert}{\delta})$
Gaussian	$\rho(\tau) = c_0 exp(-\pi\frac{\lvert\tau\rvert^2}{\delta})$

Notes: τ is the separation distance and δ is the spatial correlation length.

Range VS. Scale of fluctuation

Two difference procedures are described above to evaluate the spatial dependency, the variogram approach and the autocorrelation approach. They result in the range and the scale of fluctuation, respectively. Both of them are indications of distance within which the property values show relatively strong correlation. Then one question comes up, are they the same or not? Eq. 2.11, as well as Figure 2.7, shows that the sample variogram and the sample autocorrelation follow a linear relation for the stationary random field situation. Comparing the theoretical variogram models with the autocorrelation models, we can conclude that, as long as the theoretical variogram model and the theoretical autocorrelation model follow Eq. 2.11, the range (a_0) and the scale of fluctuation (δ) should be the same. Jaksa (1995) compared the scale of fluctuation and the range using in-situ CPT test data, and find they are positively correlated, but not the same. This might be because the CPT data is a non-stationary random field and the existence of the nugget effect.

Fitting the best variogram model

A number of methods for variogram fitting have been suggested, from statistical techniques such as maximum likelihood and least squares (Huber, 2013), to techniques such as visual assessment (Remy et al., 2009). During fitting the best variogram model to the sample variogram function, there are some keynotes need to be aware:

(i) There is no best variogram model. The goodness character of a fitted model is elusive and cannot be measured by rigorous tests. A combination of visual assessment and statistical methods is suggested.

(ii) One should avoid overfitting the sample variogram (Goovaerts, 1997). The objective is to capture major spatial features of the attributes, rather than to model any details of sample variogram. When different models provide similar fits, one should select the simplest one. The more complicated model usually does not lead to more accurate estimates. It is also important to realize that the sample variogram is in itself just an estimate. Therefore, fitting a theoretical variogram model as closely as possible to the sample variogram is also not always reasonable. The key is to model the general spatial structure of the sample variogram. It makes sense that the simplest theoretical variogram model that adequately captures the spatial structure of the sample variogram should be used, and more complicated theoretical variogram models would only be considered if simpler models cannot capture the major spatial structure of the sample variogram to a satisfactory level.

(iii) "*the most important aspect of the fitted variogram model is the nugget-effect and the slope near the origin*" (Morgan, 2005). Armstrong (1998) also stated that the behavior of the variogram at and near the origin has a significant influence on kriging results, as well as their stability.

(iv) In the majority of cases, the sample variance and sample variogram sill should be approximately equal. When the experimental sill and sample variance of the spatial attribute do not coincide, the number of samples used to calculate the sample variance and the number of data pairs used to calculate the sample variogram lags might be the reason. A small number of samples or data pairs often imply poor sample variance and variogram lag estimates. Generally, if certain lags of the sample variogram start behaving strangely, it is because the number of samples used in calculating these lags is small. When the experimental variogram sill and the sample variance are not coincided, one opinion is to force the modeled sill to equal the sample variance, but Goovaerts (1997) disagrees. In general, the variogram sill is from the fit to the sample variogram sill rather than to the sample variance, because the sample variance is calculated assuming random, independent samples.

AKAIKE information criterion

In this thesis, the most appropriate model is selected via the AKAIKE information criterion (AIC), which is defined for a finite sample set n:

$$AIC = 2k_0 - 2ln(L_0) \tag{2.12}$$

where k_0 is the number of parameters in the statistical model, and L_0 is the maximum value of the likelihood function for the estimated model. The first term is a penalty factor for the introduction of additional parameters into the model, and it discourages overfitting. The second term is a measure of the quality of fit of a model. AIC not only rewards goodness of fit, but also includes a penalty that is an increasing function of the number of estimated parameters. AIC is a measure of the loss of information incurred by fitting an incorrect model to the data. Therefore, given a set of different models for the data, the preferred model is the one with the minimum AIC value. Assuming that the model errors are normally and independently distributed, the AIC can be rewritten for a fitting by least squares.

$$AIC = 2k_0 - n[ln(2\pi\frac{RSS}{n}) + 1] \tag{2.13}$$

$$RSS = \begin{cases} \sum_{i=1}^{n} e_i^2, & \text{for } OLS \\ \sum_{i=1}^{n} w_i e_i^2, & \text{for } WLS \end{cases} \tag{2.14}$$

Alternative criterions are described in detail in other literature (Akaike, 1998; Webster and Oliver, 2007).

An example of fitting the best variogram model

Take the q_c (cone resistance) of the CPT data as an example, the basic steps of how to obtain the best theoretical variogram model and to estimate the scale of fluctuation is:

(i) Find the trend of q_c in each CPT test, and remove it from data.

(ii) Calculate the sample variogram using the residual data of each CPT.

(iii) Choose some possible theoretical variogram models and weights and fit them to the sample variogram function

(iv) Calculate the mean AIC of each theoretical variogram model and weight, the best model and weight are likely the case with the smallest mean AIC.

(v) Once the best theoretical variogram model is chosen, the scale of fluctuation can be obtained.

2.3.4. Literature review of soil variability quantification

The importance of the soil variability is a big inspiration for researchers to quantify the variability of soil properties using all kinds of experiments. In order to obtain maximum information at the least expense, the site exploration usually follows some sampling schemes, such as systematic, nested, stratified and random schemes, details of these methods can be found in DeGroot (1996). The aim is to obtain the trend (or mean), the variance (or standard deviation), the distribution and the correlation structure of a soil property.

Trend and standard deviation

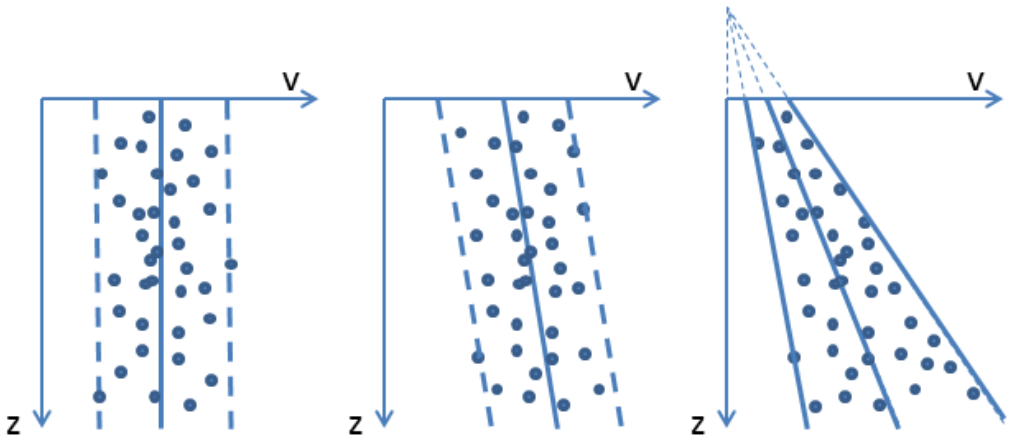

Figure 2.8.: Types of soil variability

Lumb (1966) summarized three types of variation of a soil property as is shown in Figure 2.8, where v is the variable, z is the depth. These three types are:

(i) Both the mean and standard deviation of the property v are depth-independent (i.e. $\tan(\phi)$ of silty sand).

(ii) The mean increases with soil depth linear while the standard deviation is depth-independent (i.e. compression index of sandy clay),

(iii) The mean is linearly depth-dependent, while the standard deviation linearly increases with depth (i.e. cohesion of marine clay).

The other trend, besides constant and linearly depth-dependent, can also be found: e.g. both the cone tip resistance and the Sleeve Friction of Keswick Clay follow quadratic trends (Jaksa, 1995).

Coefficient of variation

The coefficient of variation (CV), which is the ratio of the sample standard deviation over the sample mean. It is very commonly employed in quantifying the geotechnical uncertainty as a replacement of variance, because it is dimensionless and can provide a meaningful way to evaluate the relative dispersion of data around the sample mean. Generally speaking, the CV of a soil property is highly dependent on soil types, locations, and their geological environment. The strength parameters have high variability, in terms of a high CV. The CV of undrained shear strength is higher than the CV of (un)drained friction angle. Some selected CV of undrained shear strength and void ratio are listed in Table 2.3 and Table 2.4, respectively; the CV of some other selected geotechnical parameters are summarized in Table 2.5.

Table 2.3.: Some selected CV of undrained shear strength

CV% range	Sources	Notes
12 -45	Cherubini et al. (1995)	Medium to stiff soil
22	Soulie et al. (1990)	clay deposit in James Bay area
28-96	Ejezie and Harrop-Williams (1984)	-
13-40	Duncan (2000)	base on the data from Kulhawy (1993), Lacasse and Nadim (1997)
20-60	Meyerhof (1995)	-
60-85	Lumb (1971)	extremely variable clay
6-80	Phoon and Kulhawy (1999*a*), Phoon and Kulhawy (1999*b*)	Clay, fine-grained soil

Table 2.4.: Some selected CV of void ratio (e)

CV% range	Sources	Notes
13-42	Baecher and Christian (2005)	Data compiling from various sources
7-30	Lacasse and Nadim (1997)	-
15-30	Lumb (1975)	-
5-26	Deodatis et al. (2014)	Various soil including glacial clays, sands, and chalks

Table 2.5.: CV for selected geotechnical parameters

Property	CV% range	Sources
Dry unit weight	2-13	(Srivastava and Babu, 2009)
Elastic modulus	15-70	(Srivastava and Babu, 2009)
Effective friction angle for clay	10-50	(Cherubini, 2000)
Effective friction angle for silt	5-25	(Cherubini, 2000)
Effective friction angle for sand	5-15	(Cherubini, 2000)
Coefficient of permeability	60-90	(Srivastava et al., 2010)
Unconfined compression strength of clay	30 -50	(Fredlund and Dahlman, 1972; Lumb, 1971; Matsuo and Kuroda, 1974; Morse, 1971)

Distribution

Besides the mean and the standard deviation (or coefficient of variation), the distribution is very necessary to be chosen so as to analyze the data and to simulate the uncertainty. This part still has a big controversy. Popescu et al. (1998*b*) concluded that most soil properties exhibit skewed, non-Gaussian distribution, and different soil properties follow different distributions (Harr, 1977; Popescu et al., 1998*b*); El-Ramly et al. (2003) pointed out that no general distribution is available for soil properties, and the distribution is site and parameter specific. However, the normally used distributions are Gaussian (normal), lognormal, and beta distribution. The Gaussian distribution is widely used (Hicks and Samy, 2002) because of its simplicity. However, its shortcoming is that the variable contains negative value, which is unacceptable since most of the soil properties are non-negative, e.g. porosity and friction angle. Another one commonly used is the log-normal distribution (Fenton and Griffiths, 2003; Griffiths and Fenton, 2004), to compensate the disadvantage of the Gaussian distribution. Phoon and Kulhawy (1999*b*) recommended the Gaussian distribution for small CV situation, while the log-normal distribution is used when the CV is large. For soil shear strength, some researchers (Ejezie and Harrop-Williams, 1984; Duncan, 2000; Al-Bittar and Soubra, 2013; Harr, 1977), recommended a Beta distribution; the distribution of the permeabil-

ity is usually assumed to follow a lognormal distribution (Fenton and Griffiths, 1994; Hoeksema and Kitanidis, 1985; Sudicky, 1986).

Sometimes, a random variable follows a Gaussian distribution, but it is limited to a certain range (e.g. the initial void ratio in Hypoplasticity). The truncated Gaussian distribution is used in this situation. The truncated Gaussian probability density function is defined by a general Gaussian probability density function by specifying parameters μ (mean) and σ (standard deviation), as well as a truncation range [a, b]. The key is how to deal with the value outside the range. Two normally used ways to deal with it are: (i) The probability density function (PDF) associated with the general Gaussian distribution is modified by setting values outside the range to zero, and uniformly scaling the values inside the range so that the total integral is 1 (Burkardt, 2014). (ii) Numbers outside that range is cut-off to the minimum or maximum value (Roddeman, 2016). The truncated Gaussian distribution with the second way to deal with the value outside the range is chosen in Chapter 3 and 5 to simulate the random field of the void ratio.

Correlation structure and spatial correlation length

The correlation structure is required to describe the spatial variation of a soil property. It is typically described by a correlation function, which expresses the relation between the variogram (or the correlation function) and the distance. The correlation length is regarded as a parameter in the variogram model (or correlation function). Vanmarcke (1977) published a classic work to introduce the spatial correlation concept into the geotechnical profession, and this concept is further utilized and summarized by some researchers, including DeGroot (1996), Fenton and Griffiths (1996), Lacasse and Nadim (1997), Phoon and Kulhawy (1996), Uzielli et al. (2006).

The inherent spatial variability of a soil property is often characterized by a correlation model in geotechnical practice, e.g.(Jaksa, 1995; Kim and Sitar, 2013; Li and Lumb, 1987; Lloret-Cabot et al., 2014; Phoon et al., 2003; Uzielli et al., 2005). Theoretical correlation models such as exponential, spherical, and Gaussian correlation functions are often adopted to fit the correlation structure of soil properties, as pointed out by Kasama et al. (2012), Li and Lumb (1987). The exponential and Gaussian models are usually adopted to describe the correlation of soil properties (Baecher and Keeney, 1982; Vanmarcke, 1977); based on the CPT data, a nested spherical model is adopted by Jaksa (1995) for the undrained shear strength of Keswick Clay.

The spatial correlation length is a stochastic parameter, which is the mean value of a number of spatial correlation lengths calculated in the same domain. Take the CPT test as an example, a lot of CPT tests need to be carried out in one domain, and the spatial correlation length of each CPT test is calculated, then the final spatial correlation length of the domain is the mean of all these spatial correlation lengths. Therefore, if we want to carry out a study about the spatial correlation length, the stochastic method is required. The uncertainty of the spatial correlation length evaluation may come from many sources, like the inherent uncertainty of the soil, the measure and transformation error of the data, the detrending processes, the theoretical model chosen, and the modeling error and so on.

As mentioned before, the correlation length describes the similarity of a soil property between two points. If the distance between these two points is less than the correlation length, the two points are strongly correlated, and the correlation needs to be considered, otherwise, if the distance is longer than the correlation length, the two points are considered to have no correlation or have very weak correlation which could be neglected. The normally used correlation length is spatial correlation length (or range, or the scale of fluctuation). The spatial correlation length (δ) of soil properties has been evaluated by many researchers, etc. (Jaksa et al., 1999; Li and Lee, 1991; Phoon and Kulhawy, 1996) through both laboratory and field tests.

The vertical spatial correlation length (δ_v) is usually smaller than the horizontal spatial correlation length (δ_h), and δ_h is more difficult to be obtained because it needs a larger area and more

example points. Dasaka (2005) found that the variability of a design parameter in a 2d situation could be underestimated, if the field is assumed to be isotropically correlated based on δ_v, similar results can be found in the other works (Hicks and Samy, 2002). Li and Lee (1991) found that the vertical correlation distance of clay is in the range of 0.13-8.6m. For undrained shear strength, Phoon and Kulhawy (1999*b*) summarized that the δ_v is between 0.5m and 6m, mostly in the range of 1m-2m, and the δ_h is between 40m and 60m. Base on the cone penetration records from many researcher's works, Lacasse and Nadim (1997) believed that the δ_v and δ_h should be in the range of 1m-3m and 5m-38m respectively. Popescu (1995) found that the δ_h is 12m for a sandy soil deposit, while Soulie et al. (1990) found the δ of 7m-30m and 3m in horizontal and vertical directions respectively. Chiasson et al. (1995) found the δ_v is 2m for a clay deposit, and the δ_h found by PrzewLócki (2000) is 5m for another clayey soil deposit. Pyrcz and Deutsch (2014) concluded that the horizontal range of fluvial and eolian deposits is 10 to 100 times longer than its vertical range. Huber (2013) summarized the correlation lengths after an extensive literature review.

Some researchers (DeGroot and Baecher, 1993; Fenton, 1999*b*) found that δ is related to the domain size and the sampling interval. Fenton (Fenton, 1999*a*,*b*) found that natural soil properties are fractal through analyzing the in-situ data. He concluded that the correlation length is dependent on the domain size. When the domain size is increased, the correlation length might be increased too.

2.4. Fluctuation of the generated random field

2.4.1. Local averaging and variance reduction

The spatial variability of a soil property is usually simulated using random field theory (Vanmarcke, 1977). Three parameters are needed so as to generate the random field, (i) mean, (ii) variance (or standard deviation or coefficient of variation) and (iii) the spatial correlation length. It is known that the inherent spatial variability of a soil property is different in different random fields, even all these three parameters in these random fields are the same, respectively. Therefore, the Monte Carlo simulation is usually adopted to generate enough realizations of random fields. Detail information about random field generation is elaborated in chapter 4. The fluctuation of the random field is controlled by the variance and the spatial correlation length.

The given variance σ^2 of inherent spatial variability is at the point level, while what we needs in the random field generation is the variance of an element size (σ_T^2). The σ_T^2 can be obtained through a local averaging process so as to take the sample size into account (Fenton and Griffiths, 2008). It can be expressed as (Shen and Fu, 2011):

$$\sigma_T^2 = \sigma^2 \Gamma(T) \tag{2.15}$$

where T is the averaging domain and $\Gamma(T)$ is the variance reduction factor. $\Gamma(T)$ measures the reduction of the point variance σ^2 under local averaging. It is related to both the correlation function $\rho(\tau)$ and the element size, the 1d form with the Markovian spatial correlation function which is commonly used (Fenton and Griffiths, 2008; Shen and Fu, 2011) are as follows,

$$\rho(\tau) = e^{(-\frac{2}{\delta}|\tau|)} \tag{2.16}$$

$$\Gamma(T) = \frac{2}{T^2} \int_0^T (T - \tau)\rho(\tau) d\tau \tag{2.17}$$

where τ is the difference between any two points.

the 2d form with the squared finite element is,

$$\rho = e^{(-\frac{2}{\delta}\sqrt{\tau_x^2+\tau_y^2})} \tag{2.18}$$

$$\Gamma(T) = \frac{4}{T^4}\int_0^T \int_0^T (T-\tau_x)(T-\tau_y)\rho d\tau_x d\tau_y \tag{2.19}$$

where τ_x and τ_y are the differences between any two points in the x and y coordinates respectively.

The variance reduction function with other correlation functions can be found in Vanmarcke (2010).

Sometimes, a dimensionless spatial correlation length Δ is used,

$$\Delta = \frac{\delta}{T} \tag{2.20}$$

Numerical integration of the function as represented by Eq.2.17 leads to the variance reduction values plotted in Figure 2.9. It can be seen that $\Gamma(T)$ increases with the increase of the dimensionless correlation length.

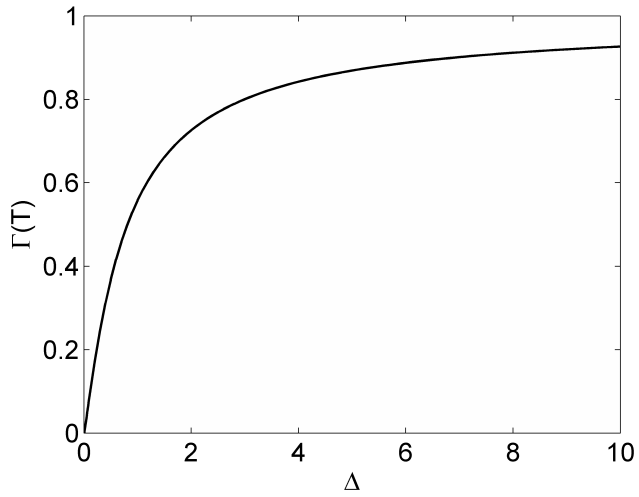

Figure 2.9.: Variance reduction factor VS Δ with a Markov correlation function

2.4.2. Effect of the dimensionless spatial correlation length on the fluctuation of a random field

Taking the Gaussian random field generation using covariance matrix decomposition as an example, the generated random field can be expressed as,

$$\mathbf{U} = \mu + \sigma_T \cdot \mathbf{U2} \tag{2.21}$$

where **U2** is the normalized spatially correlated Gaussian random field. It can be given as,

$$\mathbf{U2} = \mathbf{L} \cdot \mathbf{U1} \tag{2.22}$$

where **L** is the lower triangular of the covariance matrix decomposition; **U1** is the normalized Gaussian random field with zero mean, unit standard deviation.

Substituting Eq.2.22 and Eq.2.15 into Eq.2.21 yields:

$$\mathbf{U} = \mu + \sigma\sqrt{\Gamma} \cdot \mathbf{L} \cdot \mathbf{U1} \tag{2.23}$$

The dimensionless spatial correlation length is related to both the variance reduction factor (Γ) and the correlation matrix (**L**) of the LU decomposition through the correlation function. Therefore, the dimensionless spatial correlation length can influence the fluctuation of a random field in two different ways:

(i) The dimensionless spatial correlation length influences the fluctuation of a random field through the variance reduction factor. As it is shown in Figure 2.9, a decrease of the dimensionless spatial correlation length can reduce the variance reduction factor, which can decrease the variance of an element size (σ_T^2), so as to reduce the fluctuation of a random field using Eq.2.15. If the dimensionless spatial correlation length is zero, the value of each element in a generated random field equals to the mean value (μ).

(ii) The dimensionless spatial correlation length influences the fluctuation of a random field through the correlation matrix (**L**). Comparing with a large dimensionless spatial correlation length case, a small dimensionless spatial correlation length can make the normalized spatially correlated Gaussian random field **U2** in Eq.2.22 has a relatively large fluctuation. Therefore, the final random field can have a big fluctuation. As is shown in Figure2.10, the fluctuation of a random field decreases as the increase of the normalized spatial correlation length. When the normalized spatial correlation length approaches to the definite infinity, the random field has no fluctuation. However, the value of this random field may not equal to the mean value.

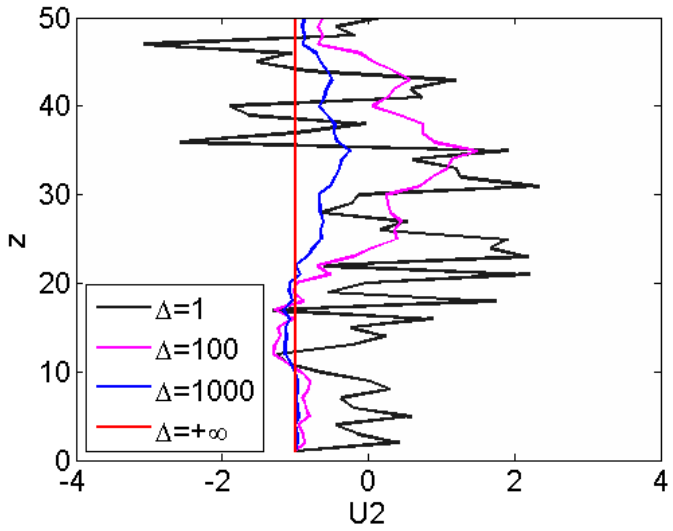

Figure 2.10.: Effect of normalized spatial correlation length on a random field (μ=0, σ=1) through **L** matrix

Therefore, the dimensionless spatial correlation length has two opposite ways to affect the fluctuation of a random field. As the increase of the dimensionless spatial correlation length, the fluctuation is reduced by the correlation matrix, meanwhile, it is increased by the variance reduction. An example of the random field is shown in Figure 2.11 considering the effect of both the correlation matrix and the variance reduction. It can be seen that the fluctuation of the random field is the highest when the dimensionless spatial correlation length is at a moderate level. A higher or lower dimensionless spatial correlation length can reduce the fluctuation of the random field.

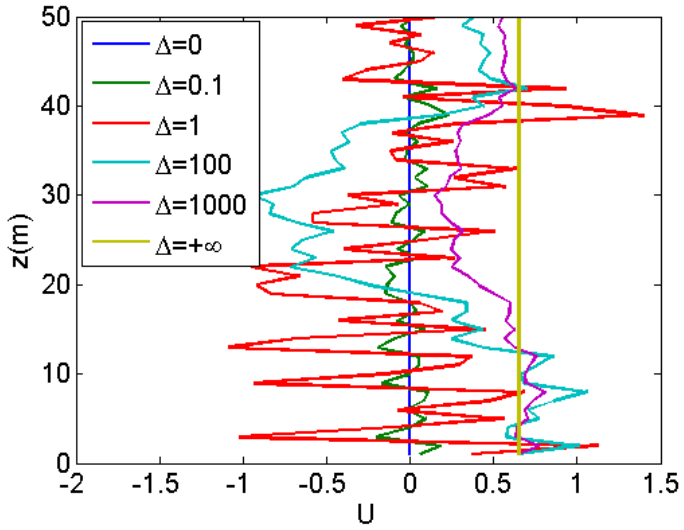

Figure 2.11.: Effect of normalized spatial correlation length on a random field (μ=0, σ=1) considering both the **L** matrix and the variance reduction

2.5. Methods of reliability analysis

The reliability of an engineering system is defined as its ability to fulfill its design purpose for some time period and environmental conditions. The reliability of a component or system can be assessed in the form of a probability of meeting satisfactory performance requirements according to some performance functions under specific service and extreme conditions within a stated time period. **Reliability** (R) is the probability that unsatisfactory performance or failure will not occur.

$$R = 1 - Pf \tag{2.24}$$

where Pf is the probability of failure.

The **state variables** are the basic load and resistance parameters used to formulate the performance function. If all loads (or load effects) are represented by the variable Q and total resistance (or capacity) by R, then the space of the state variables is a 2d space as shown in Figure 2.12. Within this space, we can separate the 'safe domain' from the 'failure domain'; the boundary between the two domains is described by the limit state function g(R, Q)=R-Q=0 (Nowak and Collins, 2012).

The structural reliability methods is usually categorized according to **Levels** (Madsen, 1992):

- **Level I methods** are deterministic reliability methods that use only one 'characteristic' value to describe each uncertain variable. The uncertainties of the problem are taken into account by introducing the safety analysis suitable 'characteristic value' of the random variables, associated with partial safety factors that should be deduced from probabilistic considerations so as to ensure appropriate levels of reliability in the design. Level I methods correspond to standard deterministic design methods used in the standards, e.g. Load and Resistance Factor Design (LRFD) method.

- **Level II methods** are probabilistic reliability methods that use two values (i.e. mean and variance) to describe each uncertain variable, supplemented with a measure of correlation between variables, usually the covariance. The First Order Second Moment (FOSM) (Tylor series) method and Point Estimating Method (PEM) are at this level.

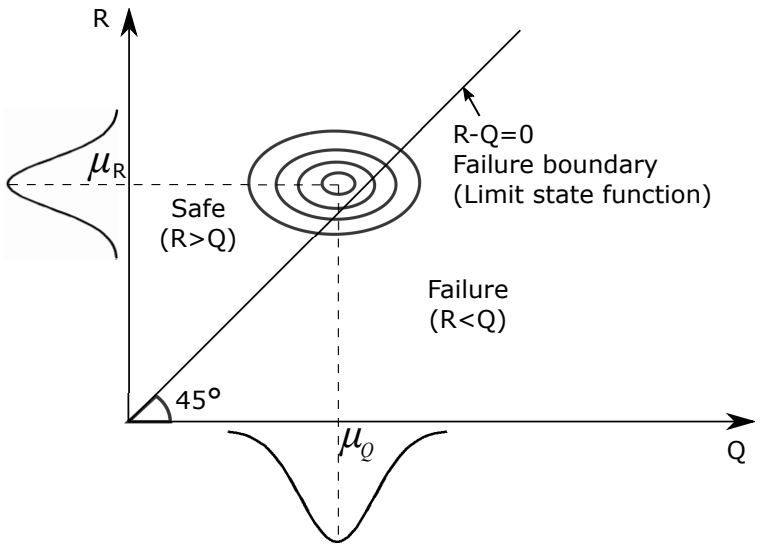

Figure 2.12.: Safe domain and failure domain in 2d state spaces (Source: Nowak and Collins 2012, p. 115)

- **Level III methods** are probabilistic reliability methods that encompass complete analysis of the problem, and use the multidimensional joint probability distribution of all the uncertain variables to describe each uncertain variable. The reliability in this level is expressed in terms of suitable safety indices, e.g. reliability index and the probability of failure (Pf). The methods includes: (a) Advanced Second Moment (Hasofer-Lind index) Methods (ASM); (b) Direct integration method (e.g. standardized integral region, Joint probability density function, Multivariate integration, advanced method of integration); (c) simulation methods (e.g. Random Finite Element Method (RFEM), Stochastic Finite Element Method (SFEM)); (d) Response Surface Methods (RSM) (i.e. Support Vector Machine (SVM), Artificial Neural Network (ANN), Polynomial Chaos Expansion Method (PCEM)).

- **Level IV methods** are the reliability methods that compare a structural prospect with a reference prospect, according to the principles of engineering economic analysis under uncertainty. They are appropriate for a structure that is of major economic importance, and consider costs and benefits of construction, maintenance, repair, consequences of failure, and interest on capital, etc. Foundations for sensitive projects like nuclear power projects, transmission towers, highway bridges, are suitable objects of level IV design.

2.6. Effect of soil variability on geotechnical practice

2.6.1. Settlement

The modern methods to study the effect of uncertainty on the foundation settlement started in the early 1980s. Beacher and Ingra (1981) carried out a 2d stochastic finite element analysis so as to evaluate the uncertain of total and differential settlements. They took the soil elastic modulus as the random variable with a Gaussian distribution using the exponential spatial correlation model. They found that the total and differential settlements are normally distributed. Meanwhile, they concluded that the CV of the total settlement increases with the increase of the autocorrelation distance, they also pointed out that the maximum differential settlement happens when the ratio between the autocorrelation distance and the footing width is 0.75 to 1. Moreover, the type of the correlation structure has little effect on both the total and the differential settlement.

Zeitoun and Baker (1992) evaluated the total and differential settlement of shallow foundations using a modified Stochastic Finite Element Method (SFEM) proposed by themselves, taking soil shear modulus as a random variable with a Gaussian distribution. The soil was assumed to be linear elastic under both axial-symmetrical and plane strain situation. They found that the CV of both the total and the differential settlements increase with the increase of the autocorrelation distance of shear modulus. Meanwhile, they also found that the ratio of CV between the total settlement and the shear modulus increase gradually till approaching an asymptotic value which is smaller than 1. The results mean that the variability of the surface settlement is normally smaller than that of the shear modulus.

Paice et al. (1994) investigated how the random soil stiffness affects the foundation settlement, considering the elastic modulus as a spatially random variable with a lognormal distribution. The CV of elastic modulus was assumed between 0.02 and 0.42, and the random field owns an exponentially correlated structure. They used the influence coefficient ($I = \frac{\rho \pi E}{ph}$) which is proposed by Poulos and Davis (1974). A moderate increase of both the mean and the CV of influence coefficient can be found when the CV of elastic modulus is increased in the range of 0.02-0.42, for the unlikely case where the CV of elastic modulus is larger than 0.42, the increase of both the mean and the CV of the influence coefficient is dramatic. The scale of fluctuation of elastic modulus has little effect on both the mean and the CV of influence coefficient when the CV of elastic modulus is smaller than 0.42, and a high scale of fluctuation can considerably increase the expected settlement if the CV of elastic modulus is above 0.42.

Fenton and Griffiths (2002) studied both the total settlement (s) and the differential settlement of strip foundations in a probabilistic framework using random finite element method (RFEM). The elastic modulus (E) was taken as a variable with a lognormal distribution, the soil is considered to be isotropically correlated. They found that the total settlement can be represented by a lognormal distribution for a single foot. The mean value of ln(s) is determined by both the mean and the variance of ln(E), and the variance of ln(s) can be approximately estimated by the variance of ln(E). For the two footings case, the distribution of differential settlement is complex, because the histogram is quite erratic, although it can be conservatively estimated by a Gaussian distribution. They concluded that the scale of fluctuation can significantly influence the distribution of the differential settlement, and recommended the scale of fluctuation is 10 times smaller than the distance between footings so as to avoid a big mechanical interaction. In their another paper, Fenton and Griffiths (2005) extended the work into the 3d situation, so as to estimate the uncertainty of settlements of shallow foundations against the limit state. As the former work, they used RFEM to simulate the foundation settlement taking the elastic modulus as a lognormally distributed random field with an isotropic correlation structure. Similar results were found for the one-foot situation, furthermore, they found that: the footing settlement, for one footing case, could be approximated very well through the geometric average of the elastic modulus field in the volume under the footing. For the two footings case, they found the bivariate lognormal model is better than the Gaussian distribution, which is recommended by the former paper, and the bivariate lognormal distribution could closely predict the differential settlement of the two footings when they are away from each other, however, when the footings are close to each other, this model could overestimate the joint settlement. Later, they (Griffiths and Fenton, 2009) compared the 2d probabilistic settlement analysis results of stochastic finite element method (SFEM) and RFEM, and found the RFEM is better than SFEM since SFEM had several shortcomings such as, it could neither simulate the influence of soil spatial variability nor model the nonsymmetrical lognormal distribution, these drawbacks could cause an unconservative result of the probability of failure.

Kuo et al. (2004) extended the work of Fenton and Griffiths (2005) into the multi-layered soil. A three-dimensional two-layered soil was regarded as random soil field with Young's modulus a variable, and the probabilistic settlement of a square pad was investigated. It is found that the

CV of settlement of the pad resting on a layered soil had a modest decrease comparing with the settlement of a uniform single layered soil case, and the CV of footing settlement is affected by the depth of the interface between soil layers, furthermore, the variation of soil near the foundation has the most significant effect on the settlement.

Using Monte Carlo simulations combined with deterministic finite element method, Nour et al. (2002) analyzed the variation of the settlement and differential settlement of a pair of foundations on random heterogeneous medium, taking the elastic modulus, and the Poisson ratio as random soil properties with lognormal and Beta distribution respectively. It is found that (a) for the elastic modulus, the increase of its CV can significantly increase the settlement statistics (the mean, the standard deviation, and the differential settlement); for isotropic correlation length case, as the increase of the normalized correlation length (δ/L, where L is the foundation width), the settlement statistics increase quickly to the maximum when δ/L is about 1 to 1.5, then the settlement statistics decrease till they reach some constant levels; for the anisotropic correlation case, when the normalized horizontal correlation length (δ_h/L) is large, both the mean and the CV of settlement are independent to the horizontal correlation length δ_h; the differential settlement reduces to zero as δ_h increases; when the normalized vertical correlation length (δ_v/L) is considered, the mean settlement decrease quickly till it reaches to a certain value as the δ_v/L increases; both the standard deviation of settlement and the differential settlement increase quickly as the δ_v/L increases from zero to a certain level. (b) For the Poisson ratio, the increase of CV can moderately reduce both the mean and the standard deviation of the settlement, and the reduction becomes more obviously when the CV of elastic modulus is high; the variability the Poisson ratio has little influence on the differential settlement. (c) Positive correlation between the elastic modulus and the Poisson ratio can moderately increase the settlement statistics, while the negative correlation, on the other side, can moderately decrease the settlement statistics.

Popescu et al. (2002) found that the CV and distribution of soil shear strength are the most significant factors to the variation of the settlement, and increasing the soil variability can increase the number of loose pockets in soil mass, which can strongly increase the differential settlement of soil foundations.

Youssef Abdel Massih and Soubra (2008) carried out a reliability-based analysis of a strip foundation subjected to a central vertical load. The footing displacement was evaluated using the response surface methodology taking the elastic properties (Young's modulus and Poisson ratio) as random variables. They found that the partial safety factors of both elastic modulus and Poisson ratio decrease with the increase of the load for the uncorrelated soil case, till they approach one when the load caused a maximal prescribed settlement. However, the partial safety factor of Poisson ratio is always smaller than 1 for the soil with a negatively correlated elastic properties. Furthermore, the probability of failure is found to be highly affected by the uncertainty of Young's modulus, which is in agreement with Nour et al. (2002).

Jimenez and Sitar (2009) studied the probabilistic settlement of a shallow foundation using RFEM, considering the elastic modulus as a random variable. The effect of different distributions (lognormal distribution, gamma distribution, and beta distribution) were investigated. It is found that the type of distribution can significantly influence the settlement results, especially in the case that the CV of elastic modulus is high, and the scale of fluctuation of Young's modulus is large.

Al-Bittar and Soubra (2013) carried out a probabilistic analysis of both vertical and horizontal displacements of strip footings founded on a spatially varying soil. Both isotropic and anisotropic random fields were taking into account for the elastic properties. They found that a larger autocorrelation distance can cause a bigger variability of the displacement of the footing for the vertical load situation, and both the mean and the CV of footing displacement are higher when the CV of elastic modulus is high.

In summary, the elastic modulus is the most popular spatial correlated variable used to carry out the effect of soil variability on the settlement. It is found that (a) both the CV and the spatial correlation length of the elastic modulus can significantly affect both the mean and the CV of differential settlement; (b) the distribution may have a big influence when both the CV and the spatial correlation length are high; (c) the settlement follows a lognormal distribution, while the differential settlement is quite erratic. The settlement is more sensitive to the elastic modulus than to the Poisson ratio.

2.6.2. Bearing capacity

Early attempts combining the probabilistic analysis to the bearing capacity starts in the late 1960's. Wu and Kraft (1967) studied the uncertainty in soil bearing capacity taking the applied load and soil strength as random variables without fully considering the spatially correlated structure. The studies using modern probabilistic methods to evaluate the bearing capacity of shallow foundations have been made over the past 3 decades (Al-Bittar and Soubra, 2013; Cherubini, 2000; Easa, 1992; Griffiths and Fenton, 2001; Jamshidi Chenari and Mahigir, 2014; Kasama and Whittle, 2011; Popescu et al., 2005).

Easa (1992) evaluated the bearing capacity of a shallow strip foundation resting on cohesionless soil using a probabilistic method. The effective friction angle and soil unit weight were considered as random variables. It is found that the uncertainty of soil unit weight has a considerable effect on the bearing capacity of the foundation.

Cherubini (2000) evaluated the reliability of shallow foundations considering their bearing capacity using a probabilistic method with reliability index. The soil shear strength parameters were regarded as cross-correlated variables. An unconservative result is found without considering the negative correlation between shear strength parameters. Also, the vertical spatial correlation length is found to have a significant effect on the reliability of shallow foundations. Meanwhile, the variance reduction has a remarkably strong effect on the reliability of the shallow foundation. Furthermore, the reliability of shallow foundations is found to be high when the cross-correlation between the shear strength parameters are negative and the fluctuation scale is small.

Nobahar and Popescu (2000) evaluated the bearing capacity of shallow foundations resting on an over-consolidated clayey soil. It is found that the inherent spatial variability of soil strength can significantly affect the shallow foundations with regard to both the mean and the CV of bearing capacity. Comparing to the deterministic analysis results, the mean ultimate bearing capacity is 25% lower in the case. In their another paper, Nobahar and Popescu (2001) pointed out that the inherent spatial variability of soil strength affects soil behavior through changing the failure mechanism. Then, Nobahar and Popescu (2002) found that the vertical scale of fluctuation has a significant influence on the bearing capacity comparing to the effect of the horizontal scale of fluctuation, which is in agreement with Cherubini (2000). Furthermore, It is found a longer horizontal correlation distance can reduce the effect of local averaging, and so as to increase the variabilities of the ultimate bearing capacity. Meanwhile, Popescu et al. (2002) studied the effect of soil heterogeneity on the bearing capacity of shallow strip foundations standing on an overconsolidated clay layer under undrained conditions with a depth-independent shear strength. The nonlinear finite element analysis with stochastic input generated by Monte Carlo simulation was used, and the random field was two-dimensional non-Gaussian with an exponential decaying correlation structure in a certain range of the spatial correlation length. They found that the CV of shear strength and the left tail of the probability distribution of the cohesion can significantly affect the bearing capacity, because these two factors are the key in formulating the loose zones, which can cause unsymmetrical displacement and soil failure. Nobahar (2003) evaluated how the soil heterogeneity affected the bearing capacity of strip foundations under undrained conditions. It is found that both the CV and the distribution of soil shear strength are the most significant factors. Increasing

the soil variability can increase the number of loose pockets in soil mass, which can strongly reduce the bearing capacity of soil. This result is in compliance with their former studies. Popescu et al. (2005) pointed out that there is no average failure surface, because different random fields have different weak paths. Meanwhile, the footing rotation is observed which is impossible in the corresponding deterministic analysis of homogeneous soil. Homogeneous soil here means the soil is uniform throughout in composition or properties.

Fenton and Griffiths did a lot of works in this part using RFEM. They (Fenton and Griffiths, 2003) studied the bearing capacity of smooth rigid strip footing resting on the isotropic spatially correlated random soil. The cohesion and friction angle were considered as stochastic variables with a lognormal and a bounded distribution respectively. It is found that the mean value of bearing capacity increases to Prandtl solution when the CV of soil shear strength decreases to zero. The mean value is reduced quickly with the increase of CV, especially for a small spatial correlation length case. Furthermore, the CV of bearing capacity can be increased if the spatial correlation length is increased. They also found that the CV is a major factor to influence the bearing capacity, while the influence of the spatial correlation length is little, in the considered range. They concluded that, in the isotropic case, a spatial correlation length equals to the footing width could result in the lowest value for the foundation bearing capacity, and this phenomenon is confirmed by other studies (Al-Bittar and Soubra, 2013; Soubra et al., 2008). In their another paper (Griffiths and Fenton, 2001), the bearing capacity of the undrained clay was simulated with spatially varying strength. Similar results are found. Meanwhile, they pointed out that the soil heterogeneity could cause the asymmetric behavior of foundations which is in agreement with Popescu et al. (2005). Furthermore, it is found that the mean value of bearing capacity becomes the minimum when the width of the footing is about 1.5 times as long as the spatial correlation length. They also compared both rigid and smooth footing results. Despite little differences is found, the smooth footing causes marginally higher probability of failure. Griffiths et al. (2002) studied the bearing capacity of a rough rigid strip footing resting on a cohesive soil. Three parameters: Young's modulus, Poisson ratio, and undrained shear strength were considered as random variables. It is found that the mean bearing capacity is always lower for the heterogeneous soil than for the homogenous soil, and the weak element dominates the mean bearing capacity. Griffiths et al. (2006) evaluated the case of two-strip footings. The undrained shear strength was regarded as the variale with a lognormal distribution. The mean absolute difference of the settlements between two footings is influenced by both the CV and the normalized spatial correlation length of the undrained shear strength; a moderate normalized spatial correlation length (approximate one) could be seen to result in a minimum bearing capacity. The bearing capacity is increased for lower or higher normalized spatial correlation length due to the effect of local averaging or the more uniform random field of the undrained shear strength. The footing interference was highlighted and it could increase the mean bearing capacity when the footings were regarded to support separate structure. However, the interface could decrease the mean bearing capacity when the footings support a single structure, because the failure of either footing is the failure of the whole structure. The interference between footings is not so great for frictionless material.

Zekkos et al. (2004) studied the reliability of a shallow foundation using the standard penetration test results considering all sources of uncertainties. It is found that the factor of safety approach could cause conservative results, and the foundations with small factors of safety could have small probabilities of failure in some cases.

Przewłócki (2005) studied the ultimate bearing capacity of a strip footing resting on the purely cohesive random field using stochastic finite difference method. He found that the ultimate bearing capacity is significantly effect by the spatial correlation length of the soil. Furthermore, he also pointed out the CV of cohesion is extremely important.

Dasaka (2005) compared the results of both deterministic and probabilistic analysis of bearing

capacities in both sand and cohesive soil. He found that, for sand, the allowable pressure is lower in the probabilistic analysis result than in the deterministic analysis for the same reliability index. Meanwhile, for cohesive soil in his case, the net ultimate bearing pressure needs to be reduced by a factor of 2.7 so as to result in the target reliability index of 3.

Soubra et al. (2008) evaluated the ultimate bearing capacity of a shallow strip footing resting on a spatially variable clayey soil. The shear strength parameters were considered as random variables. It is found that the mean value of the ultimate bearing capacity is lower in the spatially random field than in the homogeneous soil. The minimum value is found when the autocorrelation length equals to the footing breadth, and the mean value of ultimate bearing capacity is easier effected by the horizontal spatial correlation length than the vertical spatial correlation length. Youssef Abdel Massih and Soubra (2008) carried out a reliability-based analysis of the ultimate bearing capacity of a strip foundation subjected to a central vertical load considering the shear strength parameters as variables using response surface method with Hasofer-Lind reliability index. They found that the reliability of the foundation can be highly increased if the negative correlation between the cohesion and the friction angle are taken into consideration. Meanwhile, the probability of failure can be significantly increased as the increase of the CV of friction angle. The Pf is slightly increased when the CV of cohesion is increased. The serviceability limit state was investigated in another paper (Youssef Abdel Massih and Soubra, 2008) using the same method, the soil elastic properties are taken as variables. They found that increasing the CV of elastic modulus can significantly increase the Pf, while increasing the CV of Poisson ratio can only slightly increase the Pf.

Sivakumar Babu et al. (2006) evaluated the bearing capacity of a shallow foundation. The undrained shear strength was taken as the variable with a lognormal distribution. Its mean and variance are calculated from the cone tip resistance results from Static Cone Penetration Test (SCPT). A conservative value of allowable bearing capacity is found with reliability-based approaches, comparing with the results from factor of safety approach. Meanwhile, a decreasing trend of the reliability index is found with the increase of both the applied pressure and the CV of undrained shear strength. They also found that the point variance of undrained shear strength could cause a low reliability index. A further study was carried out by Srivastava and Babu (2009) using finite difference code FLAC 5.0 with Monte Carlo simulation. They compared the situations with and without the linear trend of soil parameters, and found that the linear trend could improve the reliability of the shallow foundation.

Cho and Park (2010) studied the bearing capacity of a rough strip footing resting on the spatially variable soil considering the cross-correlated shear strength parameters as variable. They combined the commercial finite difference method with random field theory to generate the anisotropic random field. They found that, a decrease of vertical autocorrelation length could reduce the CV of bearing capacity, and an increase of the negative correlation coefficient could decrease the failure probability. They concluded that the horizontal autocorrelation range has insignificant effect on the stochastic behavior of bearing capacity while the vertical autocorrelation length is found to have a big influence on the statistical response, especially when the negative cross-correlation of shear strength parameters are considered, and ignoring the negative cross-correlation could cause unconservative results.

Kasama and Whittle (2011) carried out a probabilistic analysis of bearing capacity of a strip footing suffering the vertical load. The Cholesky decomposition technique with midpoint method was used to generate the isotropic random field. The undrained shear strength (c_u) was taken as a random variable with a lognormal distribution. They found that the spatial variability of undrained shear strength could reduce the bearing capacity of the strip footing, comparing with the homogeneous soil situation, and this reduction is found to be maximum when the CV is high and the correlation length ratio (the correlation length of $\ln(c_u)$ over the footing width) is low.

Meanwhile, the results were compared with the former works of Griffiths et al. (2002). They found that, both results has a good agreement, however, the method (Local Average Subdivision) could overestimate the probability of failure when the correlation lengths are large.

Al-Bittar and Soubra (2013) presented a study of the ultimate bearing capacity of a strip footing found on a spatially varying soil. They took the soil cohesion and friction angle as cross-correlated variables, and the random field was anisotropic and non-Gaussian. It is found that the variability of the ultimate bearing capacity is mainly effect by the soil cohesion. The Pf increases when the increase of CV of the variable. Also, a smaller variation of the ultimate bearing capacity is found when the autocorrelation length is smaller, which is in agreement with the results from Cho and Park (2010). Furthermore, they found that the ultimate bearing capacity becomes the minimum when the autocorrelation length and the footing breadth are nearly same for the isotropic case, which is consistent with Griffiths' results (Fenton and Griffiths, 2003). However, this minimum is found to be related to the ratio between the horizontal and vertical spatial correlation lengths for the anisotropic case.

In summary, the variability of the ultimate bearing capacity is usually evaluated taking the shear strength as a variable with different reliability methods. The CV, left tail of the probability distribution, vertical spatial correlation length, together with the variance reduction can have significant effect on the reliability of a foundation. When the cohesion and friction angle are treated separately as variables, the variability of cohesion is far more important than the variability of the friction angle in the effect on the reliability of a foundation. Meanwhile, the negative cross-correlation between the cohesion and the friction angle can increase the reliability of a shallow foundation. For the serviceability bearing capacity case, the variability of elastic modulus is far more important than the variability of Poisson ratio in the reliability analysis.

2.6.3. Slope stability

As an important branch of geotechnical practice, slope stability analysis is highly valuable to be probabilistic treatment and it has caught great attention.

i. One-dimensional case

The infinite slope stability analysis is an oldest and simplest slope stability method used to evaluate the shallow landslides. The shallow landslides are usually induced by rainfall, because the rainwater infiltration (both transient of steady state infiltration) can reduce the matric suction and increase the groundwater table, so as to reduce the stability of a shallow slope.

Griffiths et al. (2011) carried out a probabilistic infinite slope stability analysis using both the first order reliability method and the RFEM. In the case that the undrained shear strength (c_u) is considered as the variable with a lognormal distribution, the probability of failure decreases with the increase of the spatial correlation length of $\ln(c_u)$ and the failure surface is very likely at the bottom of the slope, especially when the spatial correlation length is large. When both the cohesion and the friction angle are considered as variables, it is found that the negative cross-correlation could decrease the probability of failure. They concluded that the probability of failure could be underestimated if the spatial variability of undrained shear strength of the cohesion is ignored.

The effect of soil variability on the unsaturated slope during infiltration was studied by Santoso et al. (2011), taking the saturated hydraulic conductivity (ks) as a stationary lognormal random variable. The groundwater table is kept constant during the infiltration. They found that the Pf decrease as the increase of the spatial correlation length during steady state infiltration.

Cho (2014) carried out a probabilistic slope stability analysis during rainfall infiltration. The

shallow slope locates on the top of an impermeable bedrock in his case. RFEM is adopted and the ks is a regarded as a variable with a lognormal distribution. It is found that the portion of the critical failure surface located at the impermeable interface could be significantly increased as the increase of the effect the CV of ks, especially in the early stage of the infiltration. The effect of the spatial correlation length of ln(ks) is smaller than the CV of ks. In the early stage of the infiltration, the portion is reduced as the increase of the spatial correlation length because the infiltration at the upper part of the slope causes the positive pressure head in this area, and this positive pressure head can increases the probability of the slope failure above the interface. As the infiltration duration keeps increasing, the portion is increased as the increase of the spatial correlation length, because the wetting front reaches the interface, and the positive pressure head is generated at the interface.

Li et al. (2014) studied the reliability of an infinite slope considering the spatial variation of shear strength parameters, their mean trend is assumed to increase linearly with depth. The random field theory is employed to simulate the spatial variation of the shear strength parameters. It is found that the reliability of a clayey slope could be significant effect by the mean trend of the shear strength parameters, and ignoring this trend could overestimate the probability of slope failure, which is against the results from Hicks and Samy (2002). Furthermore, the slip surface at the slope bottom had a considerable reduction when the mean trend is included, which coincides with the results from Hicks and Samy (2002). Meanwhile, the results show that the probability of failure has a moderate reduction as the increase of the mean friction angle, and it is significantly reduced with the increase of the spatial correlation length of friction angle. They also found that the linearly increased mean trend of friction angle could considerably influence the distribution of critical failure depths of sandy slopes.

ii. Two-dimensional cases

The two-dimensional (2d) slope model is widely used in slope stability analysis, and extensive studies have been carried out. Two main type can be categorized in probabilistic slope stability analysis: with and without the infiltration.

Case without the infiltration

Matsuo and Kuroda (1974) found that, if the variability of soil properties was taking into consideration, the probability of slide failure of the embankment could suffer an unexpectedly high value (15%-20%) when the design factor of safety is 1-1.5. He also recommended the Gaussian distributions for both the moisture content and the strength parameters.

Using first-order probability analysis, Alonso (1976) evaluated the slope stability considering soil heterogeneities. He found that the variability of the relevant parameters of soil, such as cohesion, pore-pressure could strongly affect the uncertainty of slope safety.

El-Ramly et al. (2002) developed a simple spreadsheet way combining Microsoft Excel with @Risk software based on Monte Carlo simulation technique to study the probabilistic slope stability. The approach is applied to handling several real slope problems (El-Ramly et al., 2002, 2003, 2005, 2006). The results show that the soil variability could have a substantial effect the reliability of the slope design, and ignoring it could cause erroneous, misleading, or a big overestimate of the probability of failure.

Griffiths and Fenton (2004) carried out a probabilistic slope stability analysis of an undrained soil slope using RFEM. The undrained shear strength was considered as the variable, in a dimensionless form C, where $C = c_u/\gamma_{sat}H$, with H the slope height, and a range of both the CV (or V_c) and the the spatial correlation length were performed. They also compared their results with the results from the simplified probabilistic approach in which the spatial variability is neglected. They found that the simplified probabilistic approach could cause an unconservative estimate of

the probability of failure, especially when the CV is relatively high. The results from RFEM show that the CV has a significant effect on the probability of failure slope (Figure 2.13a). As the CV increases, the probability of slope failure increases quickly. The effect of the spatial correlation length on the probability of slope failure is more complicated. Two branches are shown (Figure 2.13b). When the CV is smaller than 1, an increase of the spatial correlation length could increase the probability of slope failure, while increasing the correlation length could decrease the probability of slope failure when the CV is larger than 1. In a later work, Griffiths et al. (2009*a*) investigated the probability of slope failure using both FEM combined with FORM without spatial variation and RFEM so as to honor the effect of spatial variation. They found that, when the CV of shear strength parameters are beyond a critical value, the probability of slope failure would be nonconservatively estimated if the spatial variation is ignored. However, the probability of slope failure would be conservatively estimate ignoring the spatial variation for normal soil variability ranges, especially when the CV is lower than the critical value.

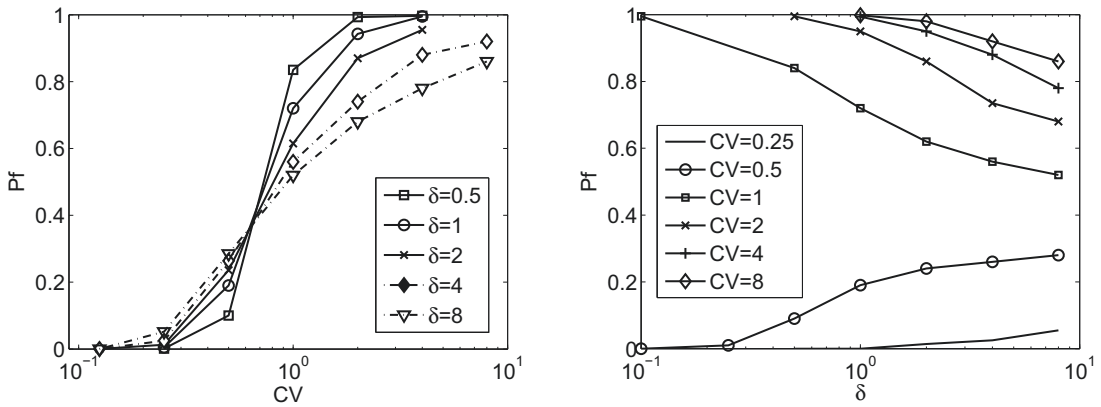

Figure 2.13.: Effect of the (a) CV and (b) spatial correlation length, of C on the probability of slope failure using RFEM. The mean=0.25 (Source: Griffiths and Fenton 2004)

Hicks and Samy (2002) studied the influence of soil heterogeneity on an undrained clay slope using RFEM, highlighting the effect of the anisotropic random field. He took the undrained shear strength a variable with a Gaussian distribution, and divided the spatial correlation length into vertical and horizontal spatial correlation length. Meanwhile the linearly depth-dependent mean of undrained shear strength was considered. They found that, for a given factor of safety, the reliability is the highest when the undrained shear strength is depth-independent, and the rupture surfaces are usually originated from the slope toe (sometimes near the toe). When undrained shear strength increases linearly with depth, the reliability is smaller, and a greater range of possible rupture surface originated from the top to the toe of the slope can be found. Furthermore, a modest change of reliability is found when the anisotropy phenomenon is considered, which differs from results from Hicks and Onisiphorou (2005), in which case, they concluded that the soil anisotropy can sometimes have a significant effect on the slope stability. Later, Hicks and Samy (2004) continued their research by comparing the results with the simple probabilistic analysis results. They found that the results from the simple probabilistic model gives an over-conservative estimation of the failure probability because of ignoring the spatial variation, which is in agreement with the results from Griffiths and Fenton (2004). Furthermore, they recommended an infinite horizontal spatial correlation length for many cases.

Dasaka (2005) found that the stability of a slope is increased with the decrease of the cross-correlation between the cohesion and the angle of internal friction. He also pointed out that an increase of CV of strength parameters would decrease the optimum slope angle.

Cho (2007) developed a numerical method for a probabilistic slope stability analysis using the Monte Carlo simulation considering the spatial variability of soil properties. The approach combining Spencer's limit equilibrium method with FORM so as to seek the reliability index, the results confirmed the importance of the spatial variability of soil properties. Later, Cho (2009) reinvestigated the effect of spatial variability of shear strength parameters considering the cross-correlation between cohesion and friction angle. The procedure used in random field generation is a Karhunen-Loève expansion with MCS. It is shown the probability of failure can be reduced with the reduction of the negative correlation between cohesion and friction angle, which in consistency with the former studies (Dasaka, 2005).

Bakhtiari (2011) carried out a stability analysis using stochastic finite element method with a Monte Carlo simulation. It was found that the range of structural responses increases as the increase of the degree of anisotropy; this range is smaller for isotropic case. He also found that the increase of the vertical scale of fluctuation could increase the range of possible structural responses and increase the probability of slope failure. Furthermore, he concluded that considering the soil heterogeneity could closely predict the failed zones of the excavation project in his research.

Shen and Fu (2011) analyzed the slope reliability of layered slope considering the spatial variability of soil cohesion using elastoplastic finite difference method with random field theory. They considered both stationary and non-stationary situations, as well as the local averaging domain (T). In the stationary case, they found that the Pf reduces modestly as the T increases, and the increase of spatial correlation length can greatly increase the Pf (case with a small CV of cohesion). In the non-stationary case, they concluded that the Pf increased as the increase of the spatial correlation length, when the mean cohesion was considered to increase linearly with depth.

Ji and Low (2012) carried out a slope reliability analysis considering the spatial variation using stratified response surface method. It was found that the spatial variation has a big influence on the slope stability, and the reliability index could be more vulnerable to vertical autocorrelation length than to horizontal autocorrelation length, which is in agreement with the results from Bakhtiari (2011). They concluded that the Pf could be significantly overestimated if the spatial variation is neglected.

Calamak et al. (2014) carried out a probabilistic slope stability analysis for earth-fill dams considering the spatial variability of saturated hydraulic conductivity, unit weight, and soil strength parameters. The Monte-Carlo simulation method with five different limit equilibrium methods (Ordinary, Bishop, Janbu, Morgenstern-Price, Spencer) was used so as to compare the results. They found that Janbu method is the most conservative one resulting in the lowest reliability indices, while the Morgenstern-Price method is the most unconservative method since it giving highest reliability indices. Furthermore, they found that the CV of FS varied in the range of 19%-25%, and this needed to be seriously considered in order to avoid a high slope failure probability.

Case with infiltration

Bergado and Anderson (1985) developed a probabilistic slope stability analysis model considering the shear strength and pore pressure as random variables. It was found that the variabilities of both the soil strength and the soil permeability have significant effects on the results of the probabilistic analysis, and the pore pressure can strongly influence the probability of failure.

Gui et al. (2000) studied the effect of soil heterogeneity on the stability of an earth slope with an undergoing internal water flow using FOSM analysis. The saturated hydraulic conductivity (ks) was considered as a spatially correlated variable with a lognormal distribution. It was found that the standard deviation (σ) of the factor of safety (FS) increases with the increase of the standard deviation of the ln(ks) ($\sigma_{ln(ks)}$). They also found that the slope reliability is negatively correlated with $\sigma_{ln(ks)}$, meanwhile, the FS follows a Gaussian or lognormal distribution when $\sigma_{ln(ks)}$ is less than 0.5.

Through simulating the transient infiltration processes, Sivakumar Babu and Murthy (2005) found that the variability of ks can significantly affect the slope reliability. Meanwhile, the reliability of the unsaturated slope above the wetting front reduces with the increase of the CV of ks, which coincides with the results from Zhang et al. (2005). They also pointed out that the failure zone can be better captured by the reliability index than by the factor of safety.

Srivastava et al. (2010) investigated the slope stability on steady state seepage condition, taking the permeability parameter as a random variable with a lognormal distribution. They found that the mean FS reduces gradually with either the increase of the CV or the decrease of the correlation length of the permeability parameter.

Le et al. (2015) investigated the stability and the failure size of an unsaturated slope suffered from the rainfall with a constant intensity. The void ratio was taken a random variable. The random finite element method was used to evaluate both the factor of safety and the size of the sliding mass. It was found that both the spatial correlation length and the CV of the void ratio could significantly affect both the mean value and the variability of these two quantities. This effect is more significant during the transient regime comparing with that during steady state situation. Interestingly, it was found that the relevant sliding mass might be relatively small when the FS is small in some case, while the corresponding sliding mass is rather big when the FS is large in some other cases.

iii. Three-dimensional case

In three dimension situation, most works are about the comparison of the factor of safety between the two dimension situation and three dimension situation.

Several studies (Cavoundis, 1987; Duncan, 1996; Stark and Eid, 1998) have been carried out on this issue, and it was found that in most cases, the factor of safety in three dimension situation is larger than that in two dimension situation for rather uniform slopes. Some researchers (Hungr, 1987; Chen and Chameau, 1983) even concluded that the factor of safety in three-dimensional situation is always larger than that in two-dimensional situation. However, it is not reasonable that the FS in three dimension slope is always larger, since some unusual combination of geometry and soil properties might happen. Jardine et al. (2004) found that the three-dimensional slope is more critical when some slope has highly variable cross-sections. Some other researchers also found the most critical factors of safety in the 3d slopes (Chen and Chameau, 1983; Seed et al., 1990). Moreover, a 'high' factor of safety cannot guarantee a low probability of failure (Chowdhury and Xu, 1995; Christian et al., 1994; Duncan, 2000).

Griffiths et al. (2009*b*) carried a 3d slope stability simulation using RFEM, and concluded that: the probability of 2d slope failure might be underestimated if the spatial correlation length in the out-of-plane direction is infinite. They also found that, the ratio between the length in the out-of-plane direction and the height of the slope is equal to or approximately equal to 3 as a boundary between the conservative and unconservative results, and, generally speaking, the failure probability of the 2d slope would be underestimated if the length of the slope in the out-of-plane is longer.

Spencer and Hicks (2007) performed a 3d slope stability analysis of a cohesive soil using RFEM, and compared the results with that in the 2d situation. The undrained shear strength was considered as the random variable with a Gaussian distribution. In order to reduce the computational time of the big slope, the parallel computation was adopted. They focused on the effect of the slope length, the scale of fluctuation, and the degree of anisotropy on the slope stability. They found three distinct failure mechanisms in the 3d slope stability analysis: one at single or multiple discrete points along the length of the slope and two along the whole length of the slope. Comparing with the 2d situation, the mean and variance of failure probability are increased and reduced respectively in 3d slope stability analysis. Furthermore, they also concluded that the horizontal

scale of fluctuation has a big effect on the failure mode. This work was continued by their another paper (Hicks and Spencer, 2010). They found that three failure modes could be observed, when the ratio between the horizontal scale of fluctuation and the slope size is changed: Mode 1: the failure path is through many high and low zones When the ratio is small (the horizontal spatial correlation length is smaller than the slope height(H)), mode 2: through semi-continuous weak zones when the horizontal spatial correlation length is between the slope height and slope length, and mode 3: through continuous weak zones when the horizontal spatial correlation length is longer than slope length, as is shown in Figure 2.14. Hicks et al. (2014) continued the work, they concluded that the intermediated spatial correlation length is likely to cause the discrete 3d slope failure. Furthermore, they also found that the potential slides might be in small volumes, when the probability of failure is low.

(a) Mode 1 (b) Mode 2 (c) Mode 3

Figure 2.14.: Failure modes in 3d soil slope considering the variability of soil properties (Source: Hicks and Spencer 2010)

In summary, the undrained shear strength is commonly used as the spatially correlated variable to analyze its effect on the slope stability analysis. The probability of failure increases significantly with the increase of CV of undrained shear strength; increasing the spatial correlation length could increase the probability of failure when the CV of undrained shear strength is small, however, the probability of failure reduces with the increase of spatial correlation length when CV of undrained shear strength is larger than a certain value. For the anisotropic structure case, it is found that reliability index could be more vulnerable to the vertical autocorrelation length than to the horizontal autocorrelation length. The slip surface follows the weakest path through the material when the variability is considered, rather than of a simple circular failure surface used in the deterministic analysis. The negative correlation between the cohesion and friction angle can reduce the probability of failure. When the infiltration (or seepage) is taken into consideration: the ks is mainly regarded to be the spatial correlated variable, which could significantly affect the slope stability during both steady state and transient state infiltration. For steady state seepage, the slope reliability reduces greatly with the increase of the CV of ks. Meanwhile, the mean FS reduces gradually with both the increase of the CV and the decrease of the spatial correlation length. For transient seepage case, the mean of FS reduces significantly, and the CV of FS increase slightly as the increase of the infiltration duration of the 3d slope in the wetting zone.

2.6.4. Seepage

Studies on probabilistic analysis of seepage have been carried out in fifty years. In the first three decades, the effect of the variability of hydrogeologic parameters (hydraulic conductivity, compressibility and porosity) on the seepage was usually evaluated using the mean, and variance, without considering the effect of spatial correlation (Bakr et al., 1978; Freeze, 1975; Smith and

Freeze, 1979; Warren et al., 1961). The spatial correlation has been taken into consideration since the mid-90s.

Fenton and Griffiths (1994) carried out a probabilistic analysis of flow through earth dams considering the permeability as a lognormally distributed variable. It is simulated by the spatially correlated random field with an isotropic structure. The random finite element method was adopted with a gradually increasing element size as the decrease of the elevation of the dam. They found that (a) the mean flow rate is smaller than the flow rate (q) in the deterministic analysis. This mean flow rate reduces significantly as the increase of the standard deviation of permeability. This reduction is more pronounced at a small spatial correlation length situation. Meanwhile, the mean flow rate increases with the increase of the spatial correlation length. (b) the standard deviation of the flow rate increases dramatically with the increase of the variance of ks when the spatial correlation is large, and it increases slightly with the increase of the variance of ks when the spatial correlation is small. While, the increase of the spatial correlation length can increase the standard deviation of the flow rate. Similar results were found by Srivastava et al. (2010). (c) the mean elevation of the downstream exit point reduces considerably as the increase of the standard deviation of ln(ks) when the spatial correlation length is small, and it reduces at first and then increases as the increase of the standard deviation of ln(ks) when the spatial correlation length is large; the standard deviation of the downstream exit point elevation increases significantly with the increase of both the spatial correlation length and the variance of the ln(ks). Variable geometry of an earth dam was considered in another paper (Fenton and Griffiths, 1996). For a given dam shape and type of random field, they found that the stochastic seepage response of a dam depends on the ratio between the spatial correlation length and the dam dimensions. Meanwhile, they found that the mean of ln(q) is negatively correlated with the variance of ln(ks), and the standard deviation of ln(q) is positively correlated with the variance of ln(ks).

Ahmed (2009) studied the unconfined flow through dams. The hydraulic conductivity was considered as the variable with a lognormal distribution. They found that (a) the free surface line of the steady state seepage is ragged and the exit point was lower, comparing with that in the deterministic seepage situation; (b) the flow through the dam is larger when the ratio between the horizontal and vertical spatial correlation length is larger; (c) the smaller ks core inside a dam might not be necessary when the CV_{ks} is large, because the flow is relatively small in this situation.

Cho (2012) carried out a probabilistic analysis of the steady state seepage through both one- and two-layered embankment, taking the ks as a spatially correlated variable with a lognormal distribution. They found that the mean normalized flow rate (mean flow rate over the deterministic flow rate) is smaller than one if the variability of the ks is taken into account. The normalized mean flow rate is found to reduce significantly as the increase of CV_{ks}, and it has a moderate increase as the increase of the horizontal spatial correlation length. They pointed out that the horizontal spatial correlation length, is more important than the vertical spatial correlation length because the dominant flow is horizontal in their case. The standard deviation of the normalized flow rate increases, with the increase of both the CV and the spatial correlation lengths (both vertical and horizontal). The mean normalized flow rate is not affected by one layer or two layers, however, the two-layer case resulted in a slightly smaller standard deviation of the normalized flow rate. In the case of a two-layered embankment, the variation of flow rate is smaller than the variation of ks when the field is completely correlated, because the variation of ks through the whole flow domain is decreased.

Calamak et al. (2012) focused on the variability of ks to the heads along the free surface of a two-dimensional earth-fill dam. They found that the uncertainty of heads of free surface is increased as the increase of the variability of ks, and the distribution of the head may not follow the Gaussian distribution.

In summary, the variability of ks is usually taken as a spatially correlated variable with a log-normal distribution to evaluate its effect on the seepage. The main outputs are: (a) the mean flow rate of ks is smaller than the deterministic flow rate when the variability of ks is considered; (b) the mean flow rate reduces significantly with the increase of the variance of ks and it increases remarkably with the increase of the spatial correlation length of ln(ks); (c) the standard deviation of the flow rate increased dramatically with the increase of the variance of ks when the spatial correlation length is large, and it increased slightly with the increase of the variance when the spatial correlation length is small. Meanwhile, the increase of the spatial correlation length can increase the standard deviation of the flow rate; (d) the mean elevation of the downstream exit point reduces considerably as the increase of the standard deviation of ks when the spatial correlation length is small.

2.6.5. Other geotechnical practice

Other studies are carried out about how the soil heterogeneity affecting the liquefaction (Baker and Faber, 2008; Fenton and Vanmarcke, 1991; Hicks and Onisiphorou, 2005; Popescu et al., 1996, 1998*a*, 1997; Yegian and Whitman, 1978), the seismic response and wave propagation (Assimaki et al., 2003; Dasaka, 2005; Elkateb, 2003; Popescu et al., 2004; Tantalla et al., 2001; Youssef Abdel Massih and Soubra, 2008) , the lateral loading of buried pipelines (Elachachi et al., 2012; Nobahar, 2003), the bearing capacity of piles (Kwak et al., 2010; Phoon et al., 1990; Robert, 1997; Zhang and Chen, 2012) , the pile settlement (Phoon et al., 1990) and the diffusion (Nishimura et al., 2002; Schiffman and Gibson, 1963).

3. Effect of stress level on the variability of void ratio related properties of sand

3.1. Background and objective

Former studies have shown that some properties of sediments vary with soil depth because of the influence of earth stress and self-weight. For example, soil porosity at the ground surface is typically greater than the porosity at a deeper location (Lu and Godt, 2008). Another example is that the friction angle for a given sand is inversely linearly proportional to its porosity (Cornforth, 1973, 2005; Marachi, 1969; Rowe, 1969). This means some soil properties are stress-dependent. The effect of stress level on the properties of sediments is mostly carried out by laboratory tests or deterministic simulations, so as to result in the relation between the mean trend and the stress level. The effect of the stress level on the standard deviation and the spatial correlation length are usually neglected, since only the trend is used during the deterministic analysis.

The uncertainty and its importance in geotechnical practice have long been appreciated. The stochastic analysis (or probabilistic analysis) is usually carried out to evaluate the effect of the uncertainty of a soil property on geotechnical practice. During the stochastic analysis, all stochastic parameters, including the mean, the standard deviation, and the spatial correlation length, are required. This gives us enough excuses to study how the stress level affects all the stochastic parameters of a soil property.

To the knowledge of the author, all the stochastic analyses in geotechnical engineering are carried out assuming both the standard deviation and the spatial correlation length constant. This means that the standard deviation and the spatial correlation length are assumed to be stress-independent. However, this assumption is not validated by proof. The mean trend is assumed to be constant for most of these studies, e.g. Griffiths and Fenton (2004), while only a few researches are carried out assuming the mean trend of some soil properties are linearly depth-dependent, e.g. the study from Shen and Fu (2011). Here the question comes up: If the mean, the standard deviation, and the spatial correlation length of soil properties are all depth-dependent? Therefore, it is necessary to carry out a research about how the stress level affects the stochastic parameters of soil properties.

The void ratio (e) is one of the key parameters, and it is related to some of the other important parameters, such as the friction angle (Cornforth, 1973, 2005; Marachi, 1969; Rowe, 1969) , saturated hydraulic conductivity (Fredlund and Rahardjo, 1993), unit weight (Terzaghi et al., 1996), and others. This parameter is chosen as a representative parameter to study the effect of stress level on stochastic parameters (mean, standard deviation and spatial correlation length) using stochastic methods. With knowledge of the variability of this key parameter, the results can be extended to the other related parameters.

3.2. Methodology

The effect of stress level on the soil heterogeneities is carried out through one-dimensional settlement simulation with vertical uniform load. The one-dimensional settlement simulation is similar to the oedometer test, and the differences are (a) the sample used here considered the variability

of the void ratio, rather than homogeneous soil, (b) the sample size used here is far larger. The overall steps are:

Firstly, generate one-dimensional stationary random fields of initial void ratio with constant mean, standard deviation, and spatial correlation length. Then, carry out the one-dimensional settlement analysis with samples from the random fields. Finally, calculate the mean, the standard deviation, and the spatial correlation length of the void ratio at each stress level, then compare them with the original mean, standard deviation, and spatial correlation length, respectively.

Since the mean, the standard deviation, and the spatial correlation length are stochastic parameters, the stochastic method is adopted. Here different random fields are generated using Monte Carlo simulation with LU decomposition, which is summarized in chapter 2 and 4.

The hypoplastic constitutive model from von Wolffersdorf (VW model) (von Wolffersdorff, 1996) is employed to simulate the one-dimensional settlement process. Because, on the one hand, the non-linearity behavior of sand can be simulated by the VW model, and on the other hand, the void ratio is one of the state variables in hypoplastic model, makes it easier for us to analyze the results.

3.3. Simulation of the variability of void ratio

3.3.1. Model description

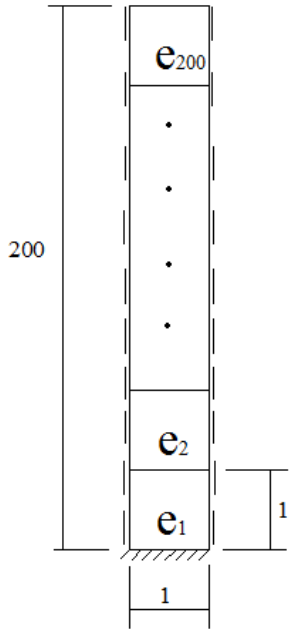

Figure 3.1.: Discretization of the one-dimensional FEM soil model

The physical model is a 200m deep weightless sand slice with a width of 1m as is shown in Figure 3.1. It is equally divided into 200 square elements with a length of 1m; every square will be assigned a void ratio (from e_1 to e_{200}) which is from a generated random field sequentially. Then a uniform vertical load will be put on the top of the sand slice, and the VW hypoplastic model is used to simulate the loading process. The parameters used in hypoplastic model are listed in Table 3.1.

Table 3.1.: Input parameters of the hypoplastic model

$\phi_c(^\circ)$	$h_s(kPa)$	n	α	β	e_{i0}	e_{d0}	e_{c0}
35	8000	0.27	0.06	1.3	1.30	0.30	0.80

The stationary random field of void ratio is generated with the mean, the standard deviation and the spatial correlation length 0.8, 0.1, 10m, respectively. The void ratio is assumed to follow the truncated Gaussian distribution, because it is limited in a certain range between e_{d0} and e_{i0}, due to the requirement of initial void ratio of the hypoplastic model. If the generated void ratio is larger than e_{i0}, it is replaced by e_{i0}. If the generated void ratio is smaller than e_{d0}, it is replaced by e_{d0}.

3.3.2. Selected best variogram model and weight

Both the mean and the standard deviation of void ratio at each stress level can be easily calculated. Here only the evaluation of the spatial correlation length is elaborated. Before the spatial correlation length is calcualted, the best variogram model and weight need to be selected.

Before the evaluation of the spatial correlation length, we need to calculate the sample variogram, and then fit theoretical variogram models to the sample variogram in order to find the most appropriate theoretical model. The weighted least square, instead of the ordinary least square, is chosen to fit different theoretical variogram models to the sample variogram. Because the values of the sample variogram near the origin provide more important information than the other values, and the precision of the variogram decreases with an increase of the distance (Armstrong, 1998; Cressie, 2015). The commonly used weights in the variogram fitting are N, N/τ^2, $N/(\gamma(\tau))^2$ with N the number of point pairs, τ the distance and $\gamma(\tau)$ the variogram. The nugget is set to be zero in the variogram fitting, in order to make sure the fittings are in the same initial situation.

The Akaike Information Criterion (AIC) (Akaike, 1998) and visualized assessment are used here to find out the best weight and the most appropriate theoretical variogram model. 3000 original void ratio data sets are used here in order to get the mean value of AIC. Table 3.2 is the result of the mean AIC from different weights and theoretical variogram models.

Table 3.2.: Mean AIC values from different models and weights

	Spherical	Exponential	Gaussian
N	-147.7	-155.6	-137.9
$N/(\gamma(\tau))^2$	808.6	780.4	1043.8
N/τ^2	**-556.9**	**-560.7**	-480.0

As it is shown in Table 3.2, the N/τ^2 is the best weight, because the AIC value is the minimum for each theoretical model. Meanwhile, Figure 3.2a also shows that this weight is the best since it fits the slope near the origin the best. Both the spherical model and the exponential model can be chosen, since both of the AIC value are very low. However, the spherical model with N/τ^2 is adopted in this research because it fits the slope near the origin better as is shown in Figure 3.2b. Meanwhile, the AIC value from the spherical model with N/τ^2 does not differ too much, comparing with the least value which is from the exponential model with N/τ^2.

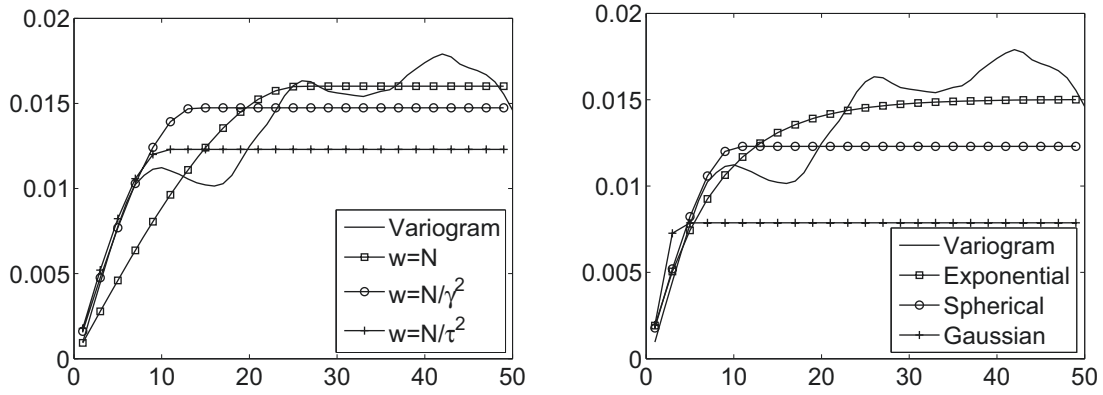

(a) Weights comparison in spherical model (b) Variogram model comparison

Figure 3.2.: Best weight and model chosen

3.3.3. Selected parameters in spatial correlation length calculation

The Gstat package in R language (Pebesma, 2001; Venables et al., 2004) is used here to calculate the sample variogram and to fit the sample variogram automatically. The maximum distance of data pairs, the initial sill, and the initial range need to be chosen in advance. Figure 3.3 shows the effect of the maximum distance on the range. 20 random fields with a predefined range of 10m are used. The true range of each random field is obtained using Gstat with different maximum distances is shown in Figure 3.3. It can be seen that a smaller or larger maximum distance might cause a higher fluctuation of the range (or the spatial correlation length). Although no principle is set in the maximum distance selection, there is one restrict in sample variogram calculation: the sample variogram is considered to be insufficient for the estimation of the range, if the distance between data pairs is more than the length of a quarter of the sampling space domain (Box et al., 2015; Lumb, 1975). The total sample space domain here is 200m, so 50m is chosen to be the maximum distance. The simulation indicates that the initial sill and range have little influence on the variogram fitting, and the values are set to be 0.01m and 10m respectively here.

Since the results of this chapter are the foundation of the following chapters, it is necessary to keep the results in a high level of accuracy. Only the accuracy of the spatial correlation length is considered here. In order to achieve the high accuracy, we hope the error of the spatial correlation length is less than 0.02m, which means that the sample mean value of the spatial correlation length is in the interval of [9.98 10.02]. Since the true spatial correlation length and the preset spatial correlation length might be different, the true spatial correlation length will be calculated, and the random field is accepted only if the true spatial correlation length in the range of [9.9 10.1]. Normally speaking, if the 95% of the mean value is in the interval of [9.98 10.02], the sample size is credible, and the result from mathematical calculation shows that, the sample size should be more than 2401. 3000 are chosen here as the sample size. 5 different sample sets are used to verify the sample size in Figure 3.4. Each of these colored lines represents one sample set to express the relation between the mean spatial correlation length and the sample size. It can be seen that when the sample size reaches to 3000, the spatial correlation lengths of all these 5 sets are in the range of [9.98 10.02]. Therefore, 3000 random fields can make sure the mean spatial correlation length of the void ratio in a high accuracy level.

In summary, the parameters used in variogram calculation and fitting are summarized in Table 3.3.

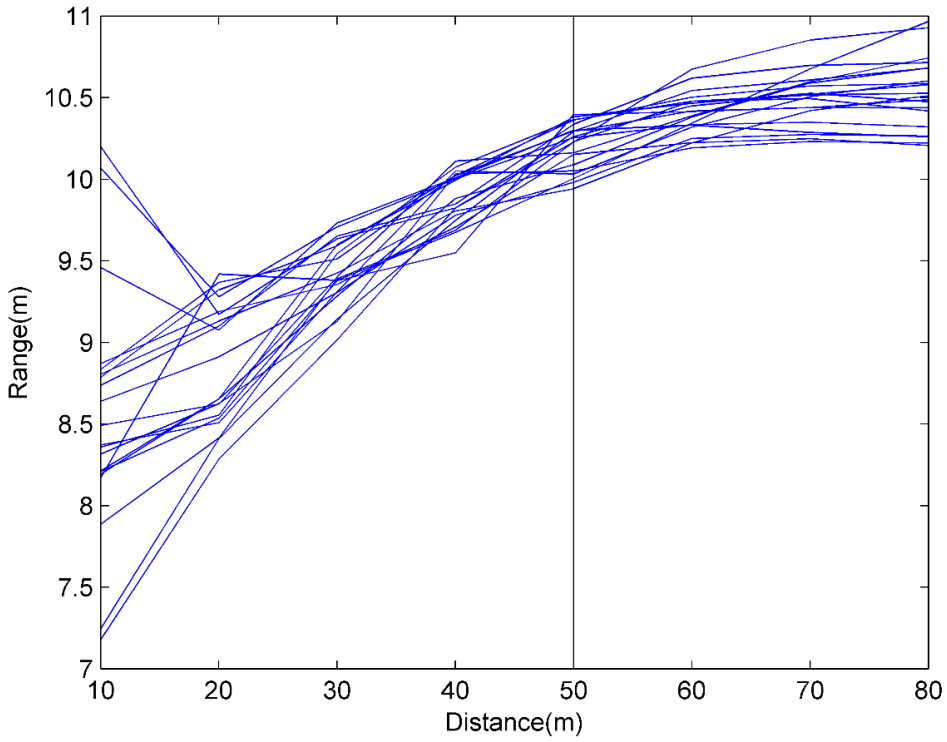

Figure 3.3.: Effect of the maximum distance on the range of the random field

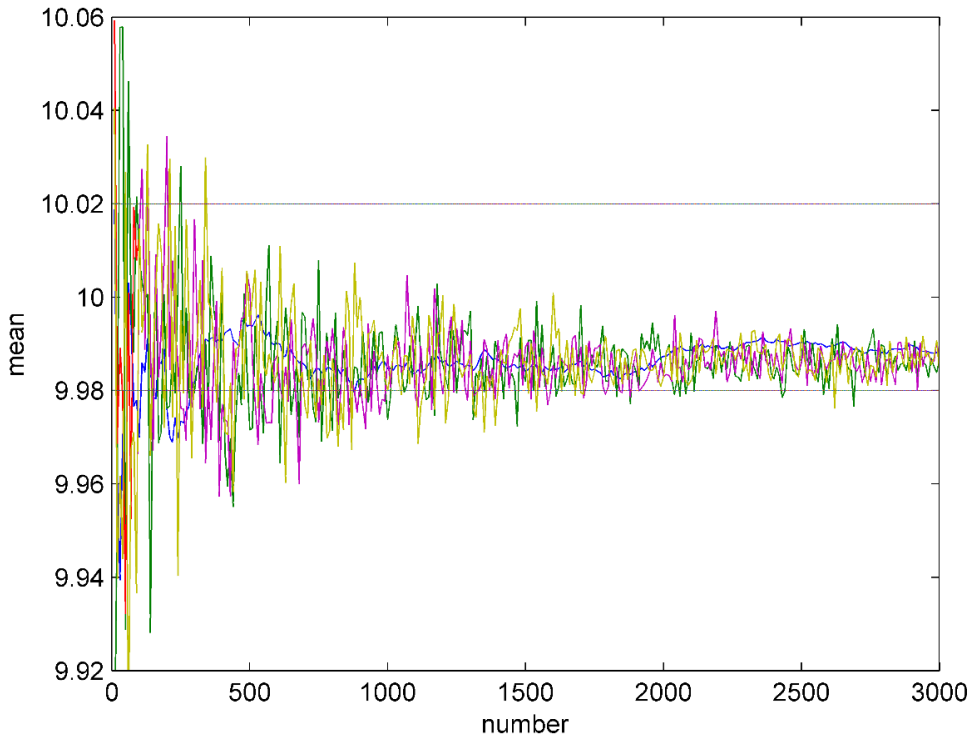

Figure 3.4.: Sample size chosen of the random field

Table 3.3.: Parameters used in the variogram fitting and calculation

Intial sill(m)	Intial range(m)	Distance (m)	model	Weight	Sample size
0.01	10	50	spherical	N/τ^2	3000

3.3.4. Results and discussion

Each of these 3000 random fields of void ratio can generate one mean void ratio (μ_e), one standard deviation of void ratio (STD_e), and one spatial correlation length (SCL) at each stress level. Here μ_e means the mean void ratio of one random field. The mean, the standard deviation and the distribution of μ_e, STD_e and SCL can be finally obtained. The effect of stress level on the soil heterogeneities can be evaluated through studying the changes of these parameters. The mean of μ_e is the mean void ratio of the 3000 μ_e.

Effect of stress level on the mean and standard deviation of μ_e

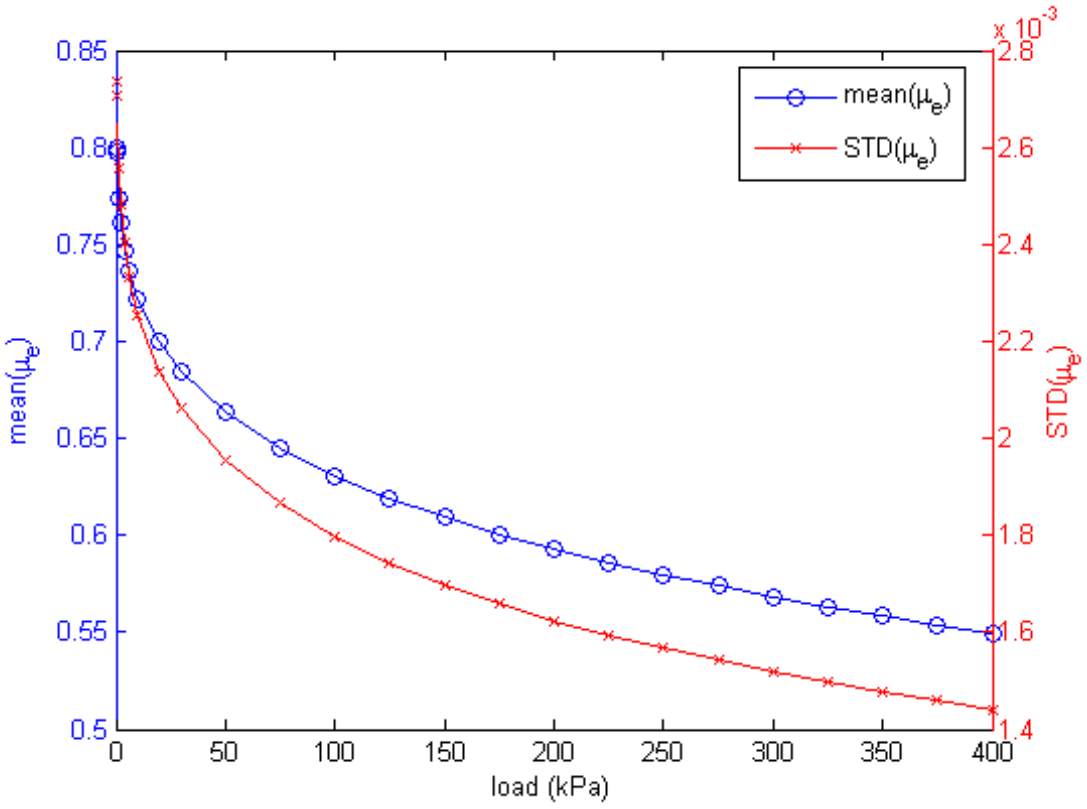

Figure 3.5.: Effect of stress level on both the mean and the standard deviation of mean void ratio

The effect of stress level on the mean of μ_e is depicted in Figure 3.5 (solid line with circles). It shows clearly that the mean of μ_e reduces with the increase of stress level, and the reduction ratio keeps reducing. This result can prove that the mean void ratio is stress-dependent. Meanwhile, the standard deviation of μ_e (solid line with crosses in Figure 3.5) also reduces with the increase of the stress level. This means the range of μ_e is narrowed down as the increase of the stress level, which can be seen through the histograms in Figure 3.6. It can be seen that the histogram moves towards left and the span is reduced, as the increase of the stress level. The histogram and its fitted Gaussian distribution at three selected stress levels in Figure 3.6 show that the Gaussian distribution fits the μ_e very well at different stress levels.

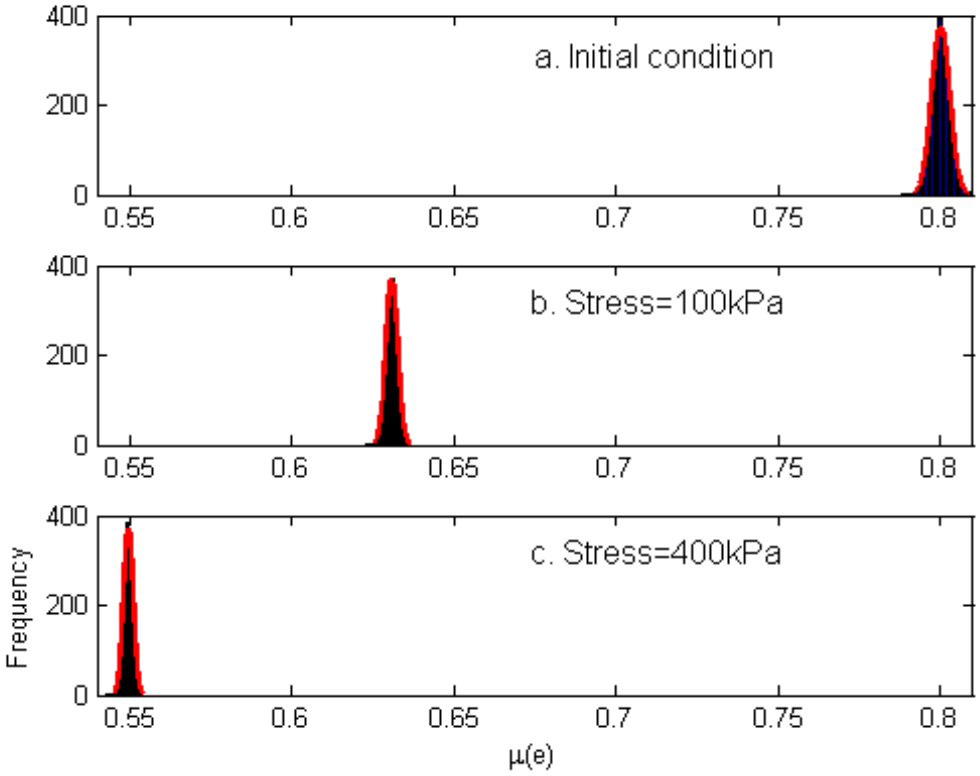

Figure 3.6.: Histogram and fitted Gaussian distribution of mean void ratio at different stress levels

The stress-dependent character of the mean void ratio results in the depth-dependent void ratio, when the self-weight of soil is considered. This depth-dependent character of void ratio is neglected in most of the studies, and the arithmetic mean is usually adopted to carry out the deterministic analysis. In order to evaluate if it is the right choice to use the arithmetic mean of void ratio, a simple comparison is carried out with two cases using one-dimensional compression simulation: case A: the void ratio of the sample in a loose state is 0.8, Case B: the mean void ratio is 0.8, however, the sample is equally divided into two part, the void ratio of the top half is 1.2 (very loose) while the other half is 0.4 (very dense). The results are shown in Figure 3.7. It can be seen that the mean void ratio from Case B (blue solid line with crosses) is slightly lower than the void ratio from Case A (red solid line with circles). In order to explain the difference, each part in case B is used to carry out the one-dimensional compression simulation separately and the changes of the void ratio with stress level are also shown in Figure 3.7 (dash lines). It can be seen that, as the increase of the stress level, the black dash line (initial void ratio is 1.2) approaches to the red solid line (results of Case A) quickly, while the blue dash line (initial void ratio is 0.4) is further away from the red solid line slowly. This is because the void ratio has a larger reduction at the same stress level, when the initial void ratio is higher due to the non-linearity nature of the hypoplastic model. When both results are combined together, the mean void ratio from Case B is lower than the void ratio from Case A. It implies that the arithmetic mean void ratio might not be a good choice to carry out a deterministic simulation. For example, the reduction of the void ratio can be underestimated if the depth-dependent character is neglected in the one-dimensional compression analysis. Furthermore, this difference might have a high influence on the results if a soil parameter is highly sensitive to the void ratio. In reality, the depth-dependent character of the mean trend of void ratio does not change so sharply, and the difference is far smaller than the results generated here. Therefore, whether the depth-dependent character is considered depends

on the case. If the result is very sensitive to the void ratio, this depth-dependent character should be considered, otherwise, it can be neglected.

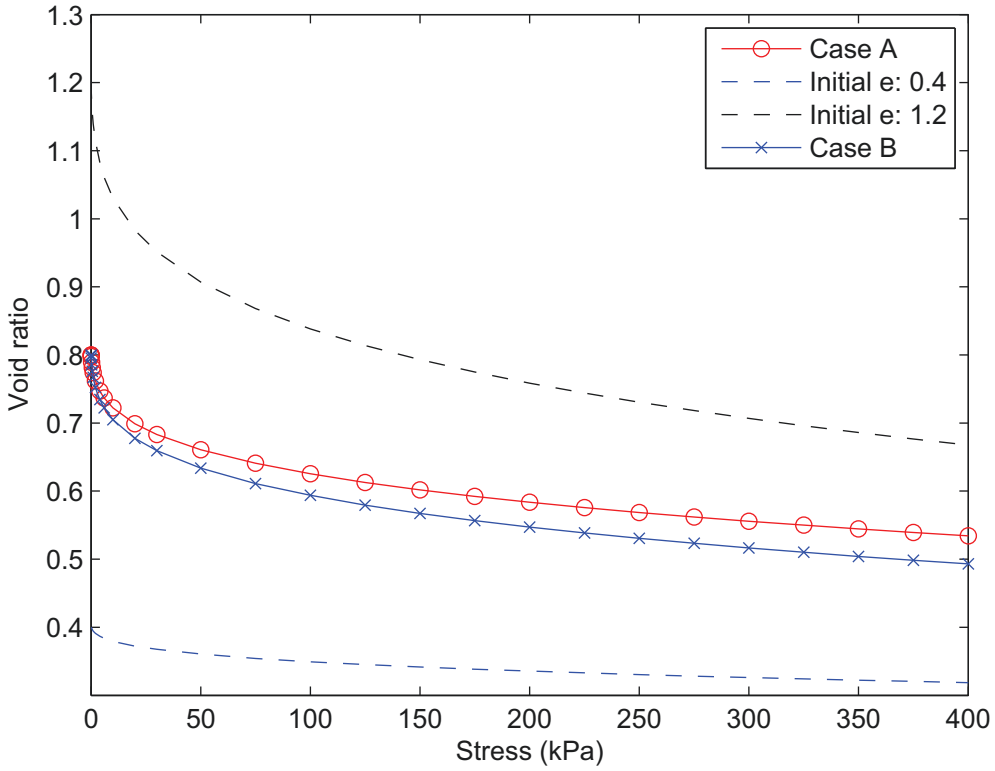

Figure 3.7.: Results comparison with constant and depth-dependent initial void ratio

As shown in Figure 3.8, both the mean (solid line with circles) and the standard deviation (dot line with crosses) of STD_e reduce with the increase of the stress level, and the reduction ratio decreases with the increase of stress level. This is reasonable because an increase of the stress level could reduction the fluctuation of the void ratio. It can be clearly explained by the histogram of the STD_e at different stress levels in Figure 3.9. As the stress increases, the histogram of the STD_e shifts to the left side, and the width of the histogram becomes smaller and smaller. Meanwhile, Figure 3.9 also shows that the STD_e follows a Gaussian distribution at all stress levels.

Furthermore, since the self-weight of soil increases with depth, the results above can prove both the mean and standard deviation of void ratio reduce with soil depth. Lumb (1966) summarized 3 cases of the relation between soil properties and depth. The standard deviation in each case is constant or increases with soil depth, as is shown in chapter 2 (Figure 2.8). Our case can be regarded as the fourth case or as one part of the case three, where both the mean and the standard deviation of a soil property might decrease with depth. Moreover, the void ratio is either directly or indirectly related to most of the other important soil parameters, such as the unit weight, saturated hydraulic conductivity, friction angle and so on. Therefore, it is reasonable to conclude that, both the mean and the standard deviation of these void ratio related parameters should be both stress-dependent and depth-dependent. However, this does not mean the mean and standard deviation of these parameters reduce with soil depth too, because some of these parameters are inversely proportional to the void ratio (e.g. the friction angle).

Effect of stress level on the spatial correlation length of void ratio

It has been widely recognized that the stress level can affect the spatial correlation length (SCL).

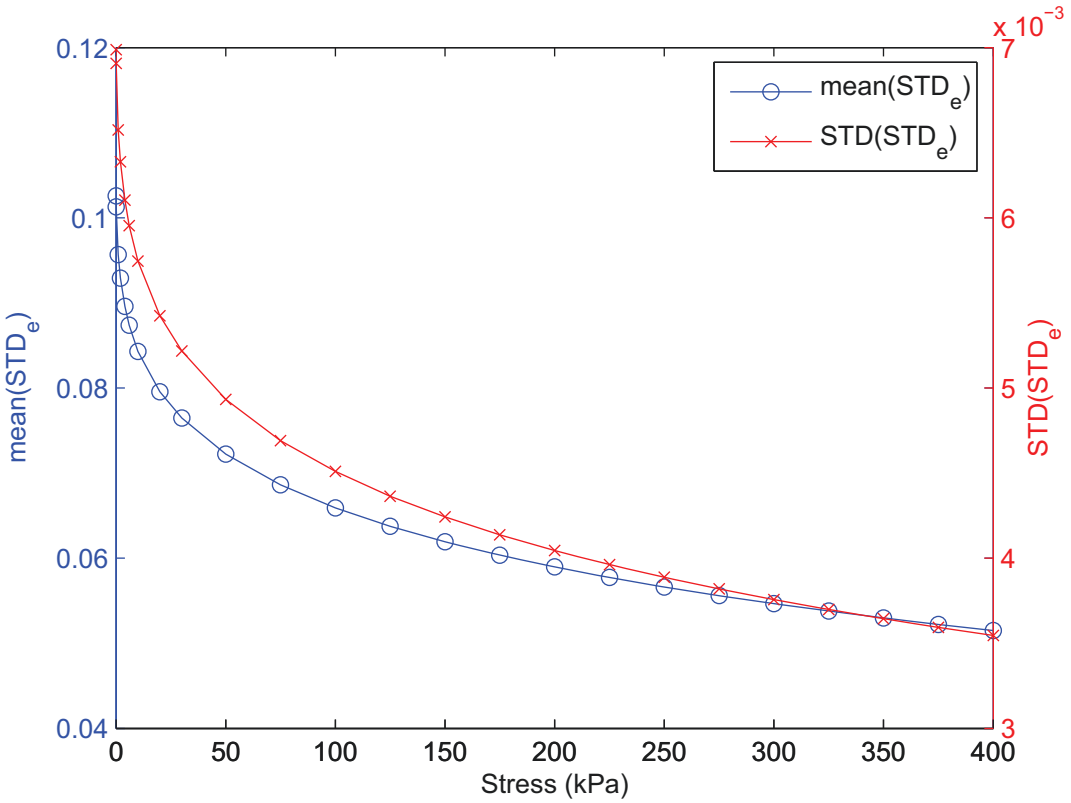

Figure 3.8.: Effect of stress level on both the mean and the standard deviation of STD_e

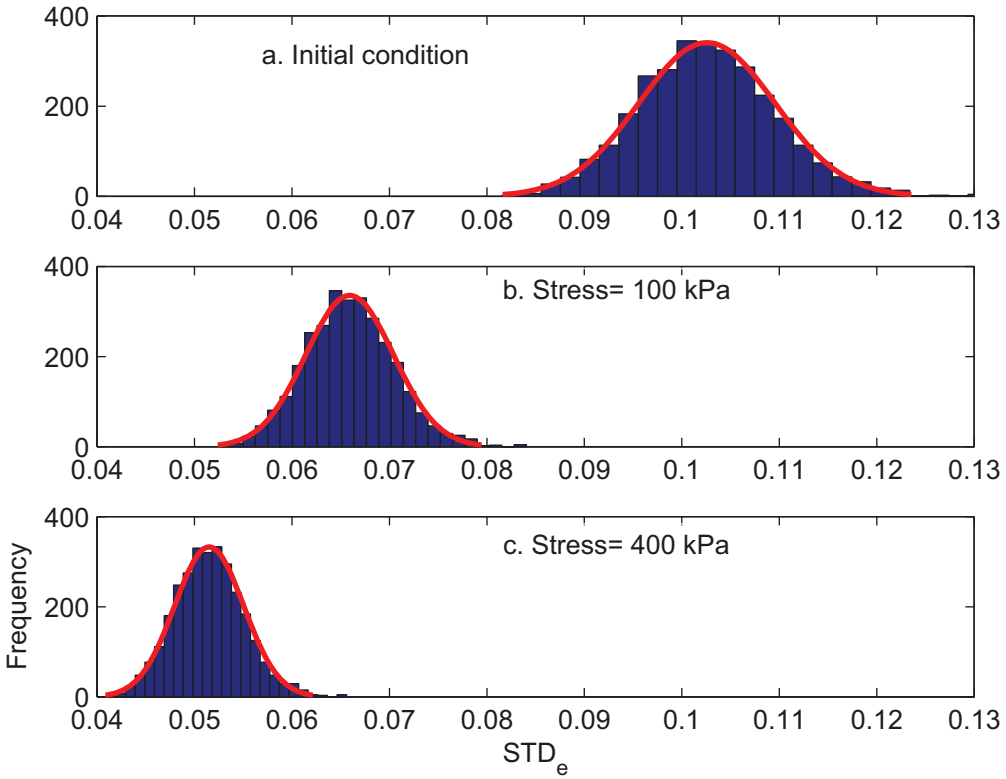

Figure 3.9.: Histogram and fitted Gaussian distribution of STD_e at different stress level

However, to the knowledge of the authors, there is no study about the relation between the stress level and the spatial correlation length of a soil property. In this part, taking the void ratio as an example, the effect of stress level on the SCL of void ratio related properties of sand is evaluated using stochastic one-dimensional compression test.

In order to acquire a general result, the SCL is normalized through dividing the SCL at a stress level by the original SCL before any load is applied, as is shown in Eq. 3.1.

$$NSCL = \frac{SCL\ at\ a\ stress\ level}{Original\ SCL} \tag{3.1}$$

Figure 3.10 shows the changes of both the mean and the standard deviation of the normalized spatial correlation length (NSCL) of void ratio during the one-dimensional compression process. It shows clearly that the mean NSCL of void ratio (solid line with circles) decreases with the increase of the stress level, and the reduction ratio becomes smaller and smaller. The standard deviation of NSCL (dot line with crosses) increases monotonically from 0 to 0.02 when the stress level increases from zero to 400kPa. The development of both the mean and the standard deviation of the NSCL with the increase of the stress level can be better explained using Figure 3.11. They are the histograms of the NSCL of void ratio at several selected stress levels. It shows clearly that the mean NSCL decreases with the increase of load, because the histogram shift to the left with the increase of the stress level, and the standard deviation becomes larger because the span of the NSCL becomes larger as the increase of the stress level. Figure 3.11 also shows that the Gaussian distribution can fit the histogram of NSCL very well at all stress levels. It worth noting that some of the NSCLs reduce quickly from 1 at 0kPa to less than 0.8 at 400kPa while some decrease slowly from 1 to 0.94. This difference is caused by the unique inherent spatial structure of each random

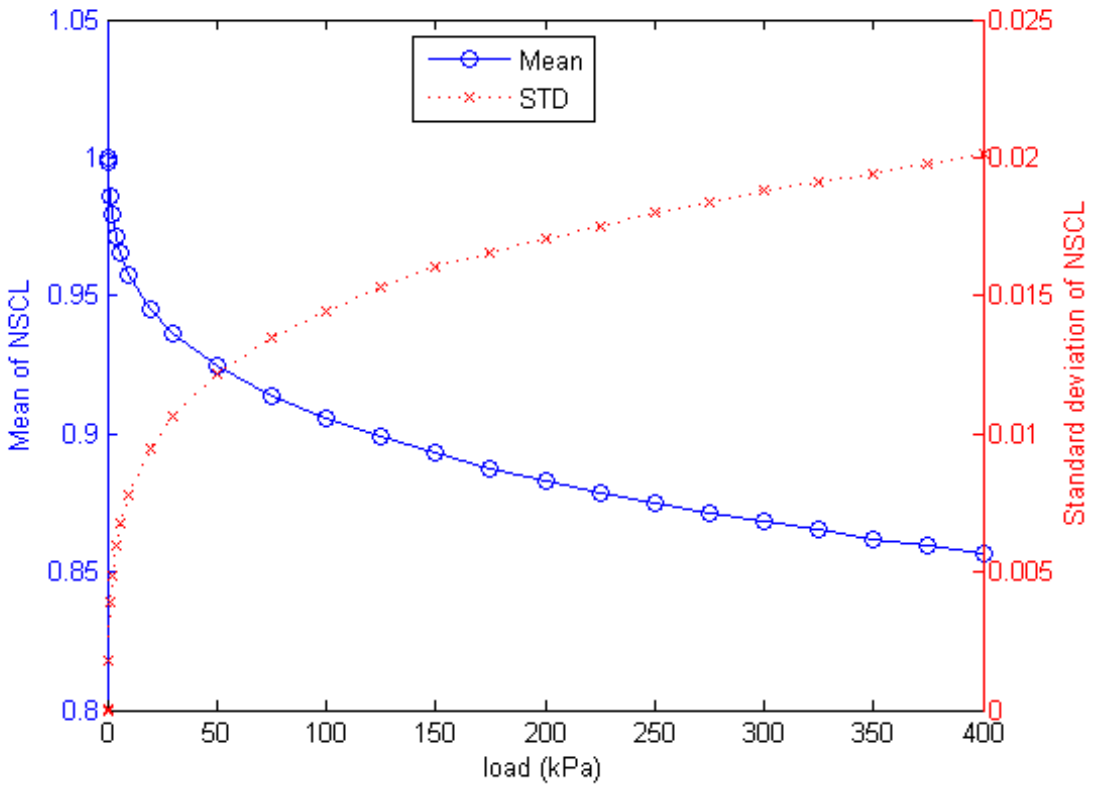

Figure 3.10.: Effect of load on the mean and standard deviation of normalized spatial correlation length (NSCL) of void ratio

field. Some spatial correlation lengths are stress-sensitive, while some are not.

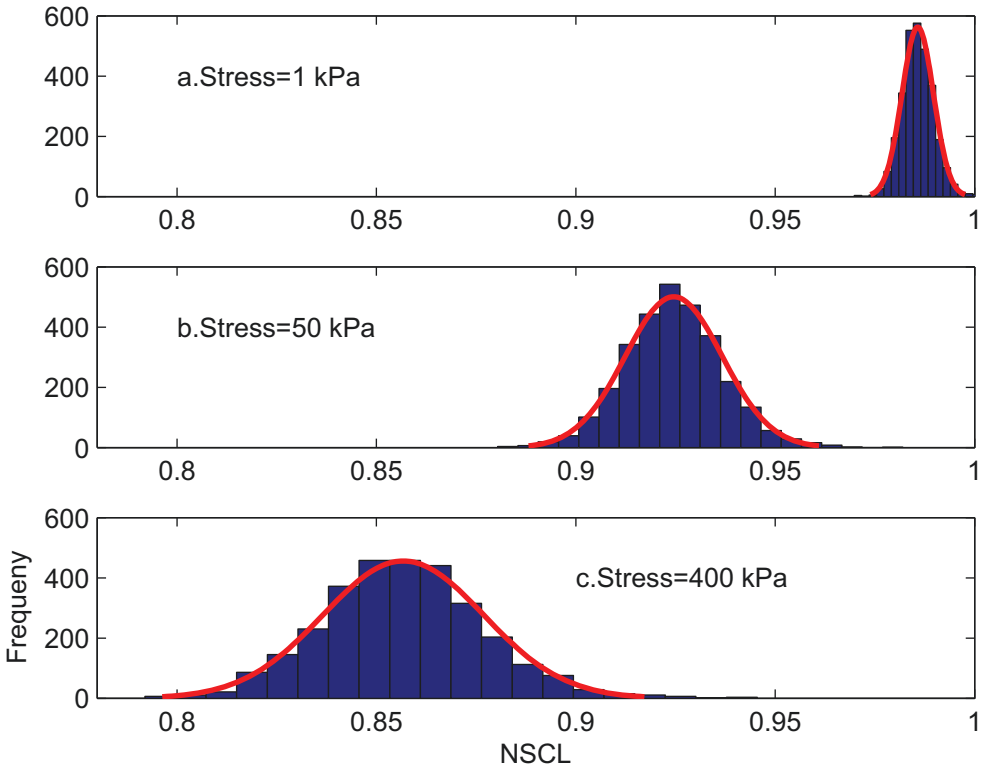

Figure 3.11.: Histogram development and the fitted Gaussian distribution of NSCL of void ratio at selected stress levels

In order to explain why the vertical spatial correlation length reduces with the increase of stress level in a rather simple way, it is necessary to explain the evaluation of the vertical spatial correlation length. The vertical spatial correlation length above, is calculated by fitting the best theoretical variogram model to the sample variogram. However, the vertical spatial correlation length δ_v (or the vertical scale of fluctuation) can also be approximated using a simple method given by Vanmarcke (1977) as,

$$\delta_v \approx 0.8\overline{d} \tag{3.2}$$

The detail explanation about Eq. 3.2 can be seen in Figure 3.12. The mean void ratio is assumed to be depth-independent here. Before the compression, the real void ratio crosses with the mean void ratio at point A, B, C, D, E, F and G, which separate the real void ratio into six segments, the original δ_v can be calculated directly. After the compression, the mean void ratio is reduced, and the cross-points shift to A', B', C', D', E', F', and G', respectively, and each segment is reduced. Therefore the δ_v is reduced too.

Moreover, considering the effect of self-weight of sand, the vertical spatial correlation length of void ratio should reduce with soil depth, since soil at a lower depth subjects to a higher stress. The distance, within which the void ratio have a relatively strong correlation of a point (point A in 3.13), should be different in its upside and downside parts. Meanwhile, it is known that the horizontal spatial correlation length is longer than the vertical spatial correlation length. If all of them are taken into consideration, the distance with a relatively strong correlation around the point should form a pseudo ellipsoidal, where the upside vertical correlation length (δ_{v_up}) is larger than the downside vertical correlation length (δ_{v_down}), and smaller than the horizontal correlation length

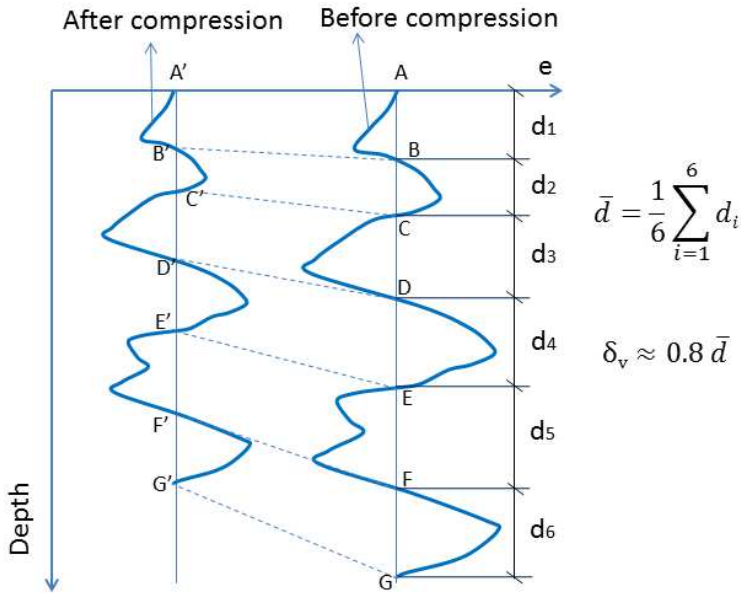

Figure 3.12.: Estimation of the vertical spatial correlation length (δ_v)

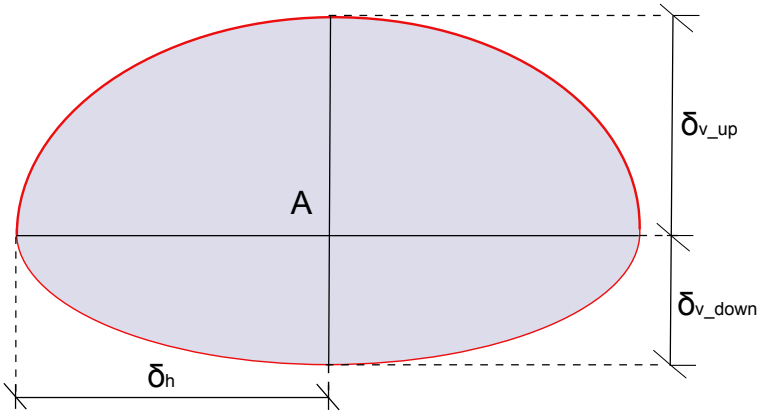

Figure 3.13.: Strongly correlated distance of void ratio in one point

(δ_h), as is shown in Figure 3.13. The horizontal spatial correlation length is kept constant in the left and right side because the stress level is the same.

What is more, the void ratio is directly related to some other important soil parameters such as the unit weight, the saturated hydraulic conductivity, the friction angle and so on. Therefore, it is reasonable to conclude that the vertical spatial correlation lengths of these parameters reduce with the increase of both the stress level and the soil depth.

3.4. Conclusion from this chapter

The effect of stress level on the stochastic parameters of void ratio related properties of sand is studied in this chapter, and the following conclusions can be obtained:

- Both the mean and the standard deviation of void ratio reduce with the increase of the stress level, and the reduction ratio becomes smaller and smaller. Both the mean and the standard deviation of void ratio reduce with soil depth because of the self-weight.
- The spatial correlation length of void ratio is affected by the stress level. The mean spatial correlation length reduces with the increase of stress, and this reduction becomes smaller and smaller as the development of the loading process. The standard deviation of the normalized spatial correlation length increases as the increase of load. The normalized spatial correlation length at different load level follows a Gaussian distribution.
- As far as the geotechnical properties of natural layers are considered, the vertical spatial correlation length of void ratio decreases with the level of overburden stress, i. e. with the depth under the surface, which means it is depth-dependent.
- Since the void ratio is related to most of the important parameters used in geotechnical practice, the mean and standard deviation of these void ratio related parameters of sand should be both stress-dependent and depth-dependent. Meanwhile, their vertical spatial correlation lengths should reduce with the increase of both the stress level and the soil depth.
- The reduction of the void ratio could be underestimated if, the arithmetic mean void ratio is chosen to carry out the deterministic one-dimensional compression analysis.

It is widely recognized that the stochastic parameters, including the mean, the standard deviation, and the spatial correlation length, of some soil properties, can significantly influence geotechnical practice, i.e. settlement, bearing capacity, and slope stability, and a great number of studies can be found in this part. However, most of the works were carried out without considering the depth-dependent character. Therefore, it is necessary to evaluate the effect of the depth-dependent character of these stochastic parameters on geotechnical practice.

4. Relative random field generation

4.1. Objective

The results from chapter 3 have proved that the stochastic parameters, including the mean, the standard deviation, and the spatial correlation length (SCL), of void ratio related properties of sand are depth-dependent. Therefore, it is necessary to evaluation this depth-dependent character of these stochastic parameters with view to geotechnical practice. Before carrying out the evaluation, it is important to discuss the generation of the random field considering the depth-dependent character.

Besides the mean, the standard deviation, and the spatial correlation length, the distribution is also one important parameter used in the random field generation. During random field generation, the Gaussian and lognormal distributions are most commonly used. For the parameters with a Gaussian distribution, the random field can be easily generated because of its simplicity, however, the limitation is negative value might be generated. This is unacceptable for most parameters because they are non-negative, e.g. the void ratio or the saturated hydraulic conductivity. This can be compensated by replacing the Gaussian distribution with the truncated Gaussian distribution so as to avoid negative value. The lognormal distribution is preferred because of its non-negative character.

In this thesis, only the void ratio and the saturated hydraulic conductivity are regarded as spatially correlated variables. According to Kozeny-Carman equation, the saturated hydraulic conductivity is positively related to the void ratio. So the mean, the standard deviation, and the spatial correlation length of both the void ratio and the saturated hydraulic conductivity reduce with soil depth. For the void ratio, the truncated Gaussian distribution is adopted to generate the random field, because the hypoplastic model requires the initial void ratio in a certain range, and all value in a random field cannot be smaller than the minimum value or larger than the maximum value. For the saturated hydraulic conductivity, the lognormal distribution is used, since it is adopted widely in the former studies.

Two different random fields are discussed separately in this chapter, (a) **stationary random field** in which the mean, the standard deviation and the spatial correlation length are all kept constant (depth-independent), and (b) **non-stationary random field**, in which, at least one of the mean, the standard deviation, and the spatial correlation length is depth-dependent. In order to simplify the non-stationary random field generation, the mean, the standard deviation, and the spatial correlation length are assumed to reduce linearly with soil depth. The mean spatial correlation length is also discussed when the spatial correlation length of the random field is depth-dependent.

Only one-dimensional random field generation is focused on in this chapter, because all random fields used in this thesis are in the one-dimensional level. Some two-dimensional random fields are referred so as to help to understand the non-stationary random field generation. Meanwhile, only the random field with the Gaussian and lognormal distribution are discussed here.

4.2. Stationary random field generation

The stationary random field generation of a variable with either a Gaussian or lognormal distribution is well developed, and it is available in almost all the software used in the geostatistical analysis, such as SGeMS, GSTAT package in R language, Tochnog, Matlab, and so on. The basic steps are summarized as (Remy et al., 2009),

Step 1, transform the mean (μ) and the standard deviation (σ) of a variable (X) in the original space Z(X) into a normal core space Y(U). If it follows the Gaussian distribution, then $\mu_U = \mu_X$, $\sigma_U = \sigma_X$; if it follows a lognormal distribution, the transformed mean and standard deviation in a normal core space are $\mu_U = \mu_{lnX}$ and $\sigma_U = \sigma_{lnX}$, respectively.

If X follows a lognormal distribution, the Coefficient of Variation (CV) needs to be calculated at first,

$$CV_X = \frac{\sigma_X}{\mu_X} \tag{4.1}$$

CV_X might be constant or change with soil depth, depending on σ_X, μ_X.

Then,

$$\sigma_U = \sigma_{lnX} = \sqrt{ln(1 + CV_X^2)} \tag{4.2}$$

$$\mu_U = \mu_{lnX} = ln(\mu_X) - \frac{1}{2}\sigma_{lnX}^2 \tag{4.3}$$

Step 2, generate a normalized random field (**U1**) with zero mean, unit standard deviation and a Gaussian distribution. This normalized random field generation does not have a spatially correlated structure.

Step 3, transform the normalized random field into normalized spatially correlated random field (**U2**). In this step, the correlation length is introduced into the normalized random field, while the mean, the standard deviation, and the distribution are same as in step 2. For example, if the LU decomposition is adopted, then,

$$\mathbf{U2} = \mathbf{L} \cdot \mathbf{U1} \tag{4.4}$$

where **U2** is the normalized spatially correlated random field, **L** is the Lower triangular matrix of a covariance matrix after LU decomposition.

Step 4, transform the normalized spatially correlated random field (**U2**) into a final Gaussian random field using,

$$\mathbf{U} = \mu_U + \sigma_{U,T} \cdot \mathbf{U2} \tag{4.5}$$

where $\sigma_{U,T}$ is the standard deviation after variance reduction. Both μ_U and $\sigma_{U,T}$ are constant for the stationary random field situation.

Step 5, back transform the Gaussian random field into the original random field. If the original random field is a Gaussian random field, then $\mathbf{X} = \mathbf{U}$, if it follows a lognormal random field, then $\mathbf{X} = exp(\mathbf{U})$.

Examples of the whole processes of the random field generation are shown in Figure 4.1a where the random field follows a Gaussian distribution, and in Figure 4.1b where the random field follows a lognormal distribution.

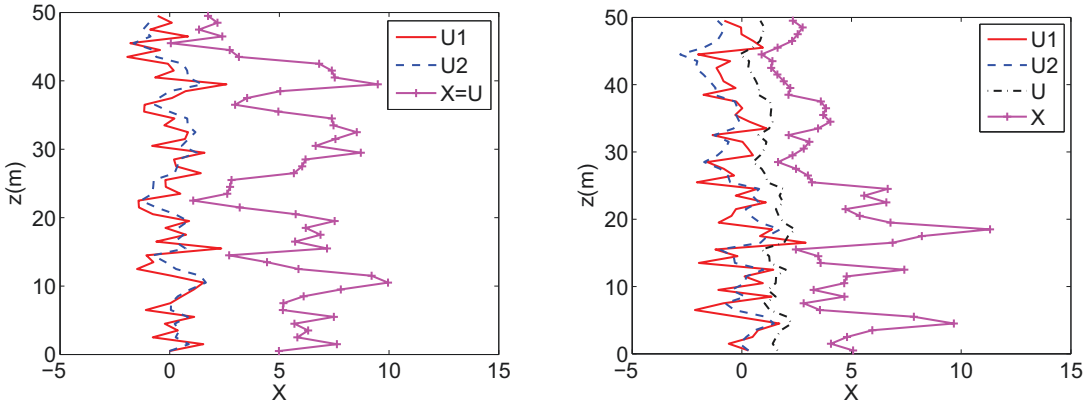

(a) (b)

Figure 4.1.: Illustration of the processes of the random field generation with (a) a Gaussian distribution ($\mu(x)$=5, σ(X)=3, δ_X=10m) and (b) a lognormal distribution ($\mu(x)$=5, σ(X)=3, δ_{lnX}=10m)

4.3. Non-stationary random field generation

The non-stationary random field is regarded as a simple distortion of the stationary random field. All the distortion can be carried out in the final step of random field generation.

4.3.1. With depth-dependent mean and/or standard deviation

Let's assume the soil property is X. The random field generation of X is with constant spatial correlation length, and at least one of the mean and standard deviation is/are linearly depth-dependent. They are given as,

$$\mu_X = a_1 + b_1 z \tag{4.6}$$

$$\sigma_X = a_2 + b_2 z \tag{4.7}$$

where a_1, b_1, a_2, b_2 are constants that control the linearly changes of the depth-dependent property of the mean and standard deviation; z is the elevation.

In this situation, a detrending process is usually firstly carried out so as to get rid of the trend, and then the residual will be analyzed separately. The residual is usually regarded as a Gaussian distributed random field, because it contains both positive and negative value. This kind of random field can be generated similar to the process of stationary random field generation. The difference is in step 4, where the mean and standard deviation are no longer constant.

For example, the random fields with depth-dependent mean and/or standard deviation are compared in Figure 4.2. The original normalized spatially correlated random field in Figure 4.2a is the same. It follows a Gaussian distribution. Based on this random filed, the generated random field Z1 is the stationary random field with μ_X=4, σ_X=2, δ_X=10m; Z2 is the non-stationary random field with μ_X=1+0.06Z, σ_X=2, δ_X=10m; Z3 is the non-stationary random field with μ_X=1+0.12*Z, σ_X=1+0.04*Z, δ_X=10m. If the final random field follows a truncated Gaussian distribution, the values smaller than the minimum value and the values larger than the maximum value will be replaced by the the minimum and maximum value, respectively.

When the random field is assigned to follow a lognormal distribution with depth-dependent mean and/or standard deviation, the non-stationary random field generation is similar to the sta-

tionary random field generation, the differences are (a) the CV_X, μ_{lnX}, σ_{lnX} calculated from Step 1 are vectors, instead of constant values. (b) μ_{lnX}, σ_{lnX} used in step 4 are depth-dependent. This kind of random field is chosen in chapter 5 and chapter 7 for the non-stationary random field with depth-dependent mean and/or standard deviation.

Figure 4.2b shows an example of the non-stationary random field generation with a lognormal distribution and depth-dependent mean and/or standard deviation. The original normalized spatial correlated random field is the same. The spatial correlation length of ln(X) is 10m. The generated random field Z1 is the stationary random field with μ_X=4, σ_X=2, δ_{lnX}=10m; Z2 is the random field with μ_X=1+0.06Z, σ_X=2, δ_{lnX}=10m; Z3 is the random field with μ_X=1+0.12*Z, σ_X=1+0.04*Z, δ_{lnX}=10m.

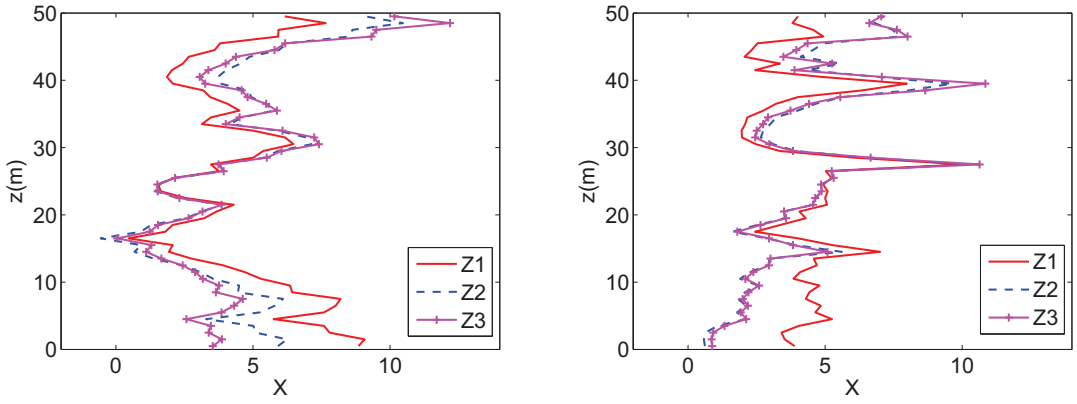

Figure 4.2.: Random field comparison with (a) a Gaussian distribution, (b) a lognormal distribution

4.3.2. With depth-dependent SCL

In order to evaluate the effect of the depth-dependent spatial correlation length of a soil property on geotechnical practice, the random field with a depth-dependent spatial correlation length needs to be generated, while both the mean and the standard deviation are kept constant. Here two methods are given. One is based on the distortion used by Hicks and Samy (2002), the other one is using conditional random field generation.

Hicks and Samy (2002) provided a distortion to generate an anisotropic random field with both vertical spatial correlation length (δ_v) and horizontal spatial correlation length (δ_h) are constant, and $\delta_v \neq \delta_h$. The detail steps, its validation, and shortcoming are shown in A. Appendix. The distortion can be further developed to generate the random field with depth-dependent spatial correlation length. If the vertical spatial correlation length is depth-dependent, the value can be distorted as is shown in Figure 4.3. The general step is similar to the distortion used by Prof. Hicks. The differences are in step 2 and 3, where the depth-dependent ξ, rather than constant ξ, is adopted during the distortion since the vertical spatial correlation length is depth-dependent, makes the size of the averaging cells different at different soil depth.

Figure 4.4 includes two figures: (a) the δ_v is constant and (b) the δ_v decreases with soil depth. All these two random fields are from one isotropic random field with its size 64*2048 (midpoint method), and δ_h =100m. Comparing with δ_v=5m in Figure 4.4a, the δ_v reduces from 100 to about 2 from the top to the bottom in Figure 4.4b.

In this method, the reduction of the standard deviation is also included during the distortion, which is an advantage if it is used properly. However, the size of the original isotropic random

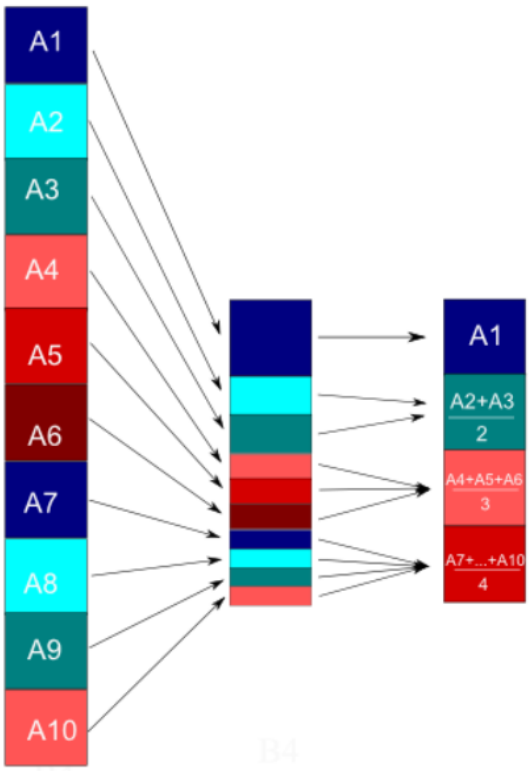

Figure 4.3.: Schematic diagram of normalized spatially correlated random field generation with depth-dependent vertical spatial correlation length (δ_v)

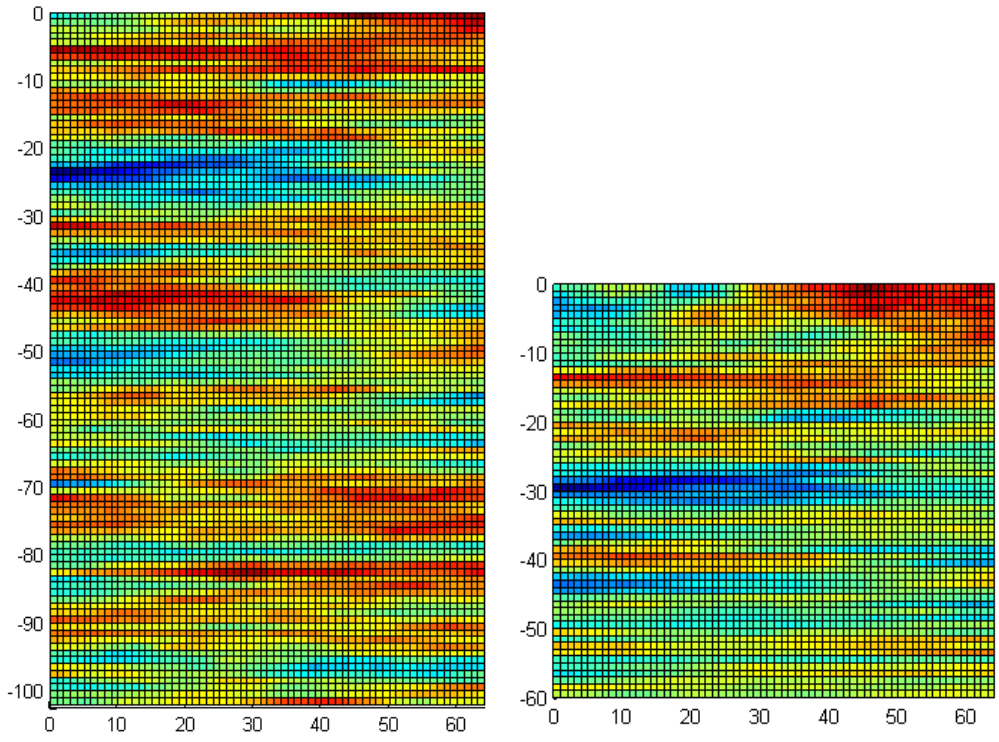

(a) $\delta_v = 5(m)$ (b) $\delta_v = \frac{100}{depth}(m)$

Figure 4.4.: Comparison of random field generation with (a) constant and (b) depth-dependent vertical spatial correlation length

field must be far larger than the final random field. The other methods, e.g. local average subdivision method, can be used in this situation, instead of covariance matrix decomposition method. Because the covariance matrix decomposition method is not suitable for such a large random field generation. Meanwhile, this method is valid only if the distortion ratio of each separated part is an integer. If not, we can round the ratio to the nearest integer.

An alternative way, to generate the anisotropic random field with depth-dependent spatial correlation length, is to divide the whole random field into several segments. Each segment can be regarded as an stationary random field. The individual random field of each segment can be generated, then put them together segment by segment, as is shown in Figure 4.5. The random field of Figure 4.5c is the combination of Figure 4.5a and Figure 4.5b. However, the shortcoming of this method is the discontinuity of the interface between adjacent layers, as is shown in Figure 4.5c where a clear boundary can be found in x=20, and the elements near to this line might affect the correlation length and the other properties of the whole random field.

If the discontinuity does not affect the results, this method can be used; if it does affect the results, we need to generate the layered random field with a smooth connection at the interface. The **layered random field** is specifically defined here as the random field with at least two different spatial correlation lengths. Generally speaking, two random fields layered together cannot be considered as a unit, because the interface causes some chaos. For example: if the SCL=10m, then the last 10m of the first random field, and the first 10m of the second random field at the interface is the chaos area. Normally speaking, if the SCL is 10m, the random field should be at least 40m, because if the length of the random field is too small, the SCL cannot be calculated correctly. In this case, if two 40m random fields with 10m SCL are layered together, the chaos is about 25% of the whole area. The calculation results show that the SCL of the whole area does not have a big difference. Meanwhile, it is not so easy to evaluate the effect of the boundary on the SCL, since the chaos area cannot be taken out separately to evaluate the SCL and the area is too small.

The discontinuous interface between two adjacent random fields could affect the consistency of the whole random field, so as to affect the final results. There are plenty of software can be used to fix the discontinuity of layered random field, such as SGeMS, GSTAT. The SGeMS software is chosen here to illustrate the layered random field generation. The first half random field is generated by unconditional random field generation, then the second half random field is generated by conditional random field generation taking the data of the first half random field as the hard data. Detail information refers to SGeMS. The comparison of these two kinds of random fields generated by SGeMS are shown in Figure 4.6. As we can see from Figure 4.6b, conditional random field generation can smooth the boundary of two adjacent random fields, while two random fields layered together in Figure 4.6a have a clear boundary between the top half and the bottom half of the layered random field. The SGeMS will be adopted to generate the layered random field in chapter 5 and chapter 7, so as to evaluate the effect of the depth-dependent spatial correlation length on geotechnical practice.

4.4. Mean SCL evaluation of layered random field

In order to evaluation the effect of the depth-dependent spatial correlation length on the results, both the stationary and non-stationary random field need to be used. In order to make the results comparable, besides the mean and the standard deviation, the mean spatial correlation length of the layered random field should equal to the spatial correlation length of the stationary random field.

The consistency of the mean and the standard deviation of these two random fields can be easily reached in the case that the mean and standard deviation of the random field are linearly related

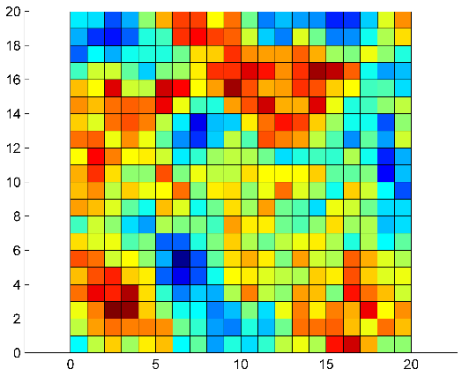

(a) Random field A

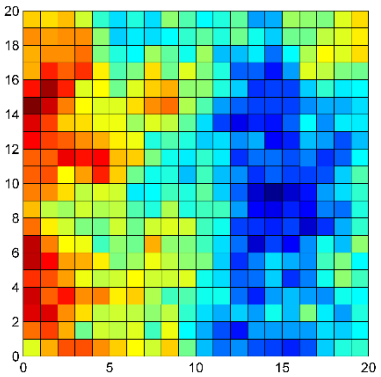

(b) Random field B

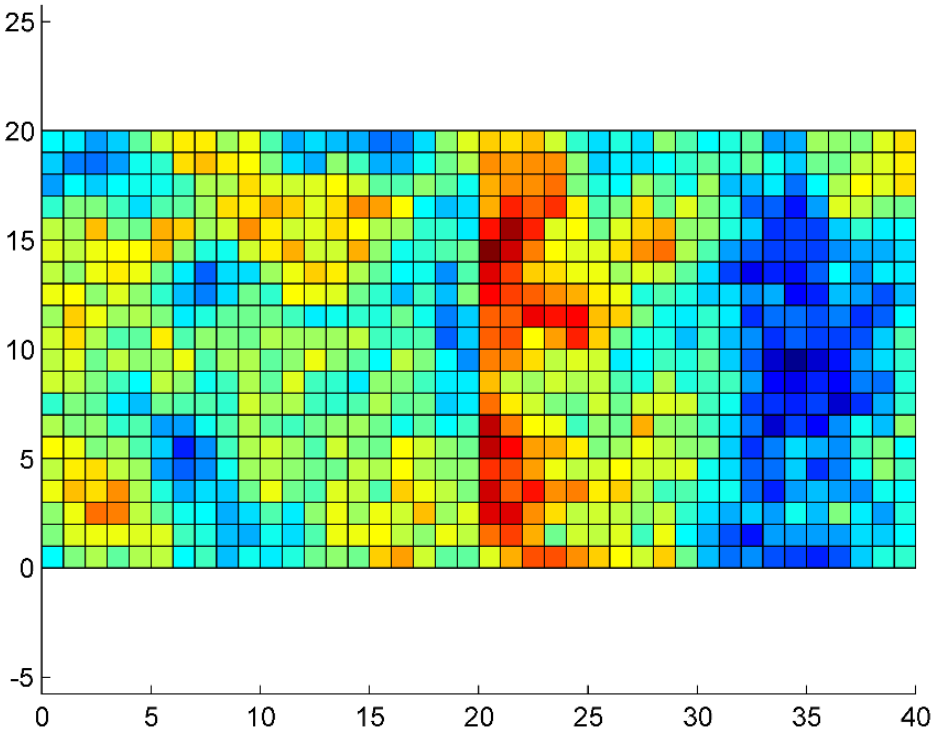

(c) Random field A+B

Figure 4.5.: Visualization of layered random field

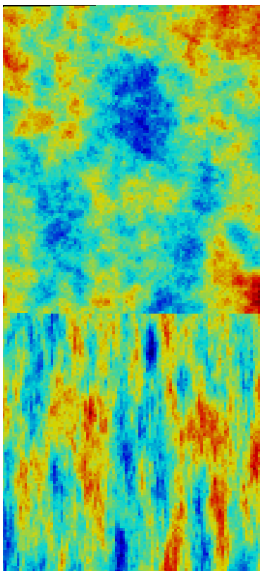

(a) Unconditional layered random field

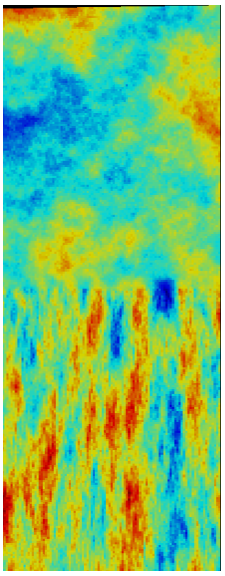

(b) Conditional layered random field

Figure 4.6.: Comparison of layered random fields generated by SGeMS

to the depth, all we need to do is to make sure the mean and standard deviation at the middle point of the random field equal to the mean and standard deviation of the stationary random field, respectively. The only problem left is to make sure the mean spatial correlation length of a layered random field equals to the spatial correlation length of the stationary random field.

If the random field has a depth-dependent spatial correlation length, two important questions come up: what is the mean spatial correlation length of the random field? What factors would affect the mean spatial correlation length? In order to find the answers of these questions, the layered random fields are generated and analyzed.

4.4.1. Effect of the individual SCL on the mean SCL of the whole random field

Two sets of 2000 random fields with zero-mean, unit-variance, the spatial correlation length δ=10m and 15m are generated respectively. The length of each one-dimensional random field is 150m, it is equally divided into 150 elements. Then one random field with δ=10m is layered under the bottom of the random field with δ=15m, so as to formulate a layered random field with a total length of 300m; Then the mean spatial correlation length of the whole random field is calculated. The results is shown in Table 4.1. The mean spatial correlation lengths of some other kinds of layered random fields are listed in Table 4.2, where 10-20-30 in the each δ column means the random field has three layers with the correlation length of 10m, 20m, and 30m respectively. On the condition that each individual random field has the same length, some conclusions can be made based on Table 4.1 and Table 4.2:

(i) the mean spatial correlation length of layered random field is between the highest and lowest individual spatial correlation length,

(ii) the mean spatial correlation length increases as the increase of the individual correlation length,

(iii) the mean spatial correlation length is not equal to the arithmetic mean of individual spatial correlation length.

Table 4.1.: The stochastic parameters of the spatial correlation length (δ) of the layered random field (RF)

	Mean(δ)	STD(δ)	CV(δ)
RF A	9.99	0.12	0.012
RF B	14.99	0.21	0.014
Layered RF (A+B)	11.92	1.014	0.085

Table 4.2.: Mean spatial correlation length calculation for layered random field with different individual spatial correlation length (δ)

Mean(δ)	CV(δ)	Each δ	Length of each layer
16.98	0.14	10-20-30	200
13.43	0.12	10-20	200
15.94	0.18	10-30	200
23.74	0.10	20-30	200

4.4.2. Effect of the length of individual random field on the mean SCL of the whole random field

Three groups of data in Table 4.3 are listed in order to evaluate the effect of the length of each individual random field (RF) on the mean spatial correlation length of the whole random field. For example, in group 1, 10-15 in each δ column means the random field has two layers with the spatial correlation length of 10m and 15m respectively, while 100-200 in the column of the length of each layer means the length of each random field is 100m and 200m, corresponding to the correlation lengths. The mean spatial correlation length of each group shows a reduction pattern, when the length of the random field with a smaller spatial correlation length increases, while the length of the random field with a greater spatial correlation length is fixed. This means the length of each individual random field can affect the mean spatial correlation length of the whole random field.

Table 4.3.: Effect of the length of each individual random field on the mean spatial correlation length of the whole random field

	Mean(δ)	Each δ	Length of each layer
Group 1	12.62	10-15	100-200
	12.30		150-200
	12.00		200-200
Group 2	14.92	10-20	100-200
	13.95		150-200
	13.43		200-200
Group 3	19.00	10-20	100-200
	17.25		150-200
	15.94		200-200

4.4.3. Relation between the mean SCL of the whole random field and both the SCL and the length of individual random field

The results above show that, both the spatial correlation length and length of the individual random field have essential influence on the mean spatial correlation length of the whole random field for one-dimensional layered random field simulation.

The mean spatial correlation length of the layered random field can be calculated by,

$$\mu_\delta = \frac{L_1 + L_2}{\frac{L_1}{\delta_1} + \frac{L_2}{\delta_2}} \tag{4.8}$$

where the L_1 and L_2 are the lengths of each individual random field, while δ_1 and δ_2 are the corresponding spatial correlation length of each random field.

Eq. 4.8 can be rewritten as,

$$\mu_\delta = \frac{1}{\frac{k_1}{\delta_1} + \frac{k_2}{\delta_2}} \tag{4.9}$$

where, k_1 and k_2 represent the portion of each individual random field to the whole random field, with $k_1 = \frac{L_1}{L_1+L_2}$, $k_2 = \frac{L_2}{L_1+L_2}$.

Eq. 4.9 shows that the mean spatial correlation length of the whole random field can be represented by the harmonic mean of the spatial correlation length of each individual random field.

4.4.4. Validation of the relation

In order to testify the accuracy of Eq. 4.9, the layered random field with different spatial correlation length and different length of the random field are generated. The calculated results δ_C from Eq. 4.9, and the true value δ_T calculated using GSTAT package, of the mean spatial correlation length, together with the residual error ratio (err) are listed in Table 4.4.

Residual error ratio is defined here as,

$$err = \frac{|\delta_C - \delta_T|}{\delta_T} \tag{4.10}$$

Table 4.4.: Comparison of the calculated and true means of spatial correlation length (δ)

	Each(δ)	Length of each layer	δ_T	δ_C	err
Group 1	10-15	100-200	12.62	12.88	0.020
		150-200	12.30	12.37	0.006
		200-200	12.62	12.88	0.001
Group 2	10-20	100-200	14.92	15.00	0.005
		150-200	13.95	14.00	0.004
		200-200	13.43	13.33	0.007
Group 3	10-30	100-200	19.00	17.96	0.055
		150-200	17.25	16.13	0.065
		200-200	15.94	14.98	0.060

Table 4.4 shows that the residual error ratio is very small (less than 6.5%), so Eq. 4.9 can be used to calculate the mean spatial correlation length of the layered random field. The error is larger if the difference of the individual spatial correlation length is larger.

5. 1d compression analysis considering the depth-dependent variation of void ratio

Since the stochastic parameters of void ratio, including the mean, the standard deviation, and the spatial correlation length (SCL), have been proved to reduce with soil depth in chapter 3, it is necessary to evaluate how the depth-dependent character affects the results. In this chapter, the one-dimensional (1d) compression analysis is carried out, so as to find out the effect of the depth-dependent character on the strain at different stress level. Like in chapter 3, the void ratio is considered as the only variable, and the von Wolffersdorff (VW) hypoplastic model is used. In order to simplify the problem, the stochastic parameters of void ratio are all considered to reduce linearly with soil depth.

5.1. Deterministic compression analysis

5.1.1. Deterministic model description

Although the void ratio is depth-dependent, it is assumed to be constant, and the arithmetic mean value is adopted in many cases. It is necessary to check if the results have a big difference. A two-layered soil model is adopted here to evaluate the effect of the linearly depth-dependent void ratio on the one-dimensional compression test results in this section, as is shown in Figure 5.1. The size of both layers is the same. Three cases with different initial void ratio in each layer are assigned, while keeping the arithmetic mean of the whole soil the same. The values of these three cases are also shown in Figure 5.1. The parameters in VW hypoplastic model are listed in Table 5.1.

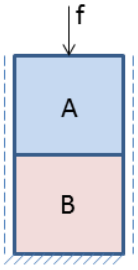

Void ratio in each case

	Case 1	Case 2	Case 3
A	0.8	1.0	1.2
B	0.8	0.6	0.4

Figure 5.1.: Schematic figure and void ratio chosen in the deterministic 1d compression analysis

Table 5.1.: Parameters used in VW hypoplastic model

$\phi_c(^\circ)$	$h_s(kPa)$	n	α	β	e_{i0}	e_{d0}	e_{c0}
35	8000	0.27	0.06	1.3	1.30	0.3	0.85

5.1.2. Results analysis

Figure 5.2 is the comparison of 1d compression test results with both constant and depth-dependent void ratio. The stress-strain relation is adopted here to neglect the effect of the sample size. Case

1 is the constant void ratio case, while case 2 and 3 are the cases with the depth-dependent void ratio. The mean void ratio of these three cases is the same while the difference between the two layers is 0, 0.4 and 0.8 in Case 1, 2 and 3, respectively. It can be seen that the strain is smaller in the depth-dependent void ratio case. Meanwhile, the strain becomes smaller as the difference of the void ratio between the two layers increases. It is caused by the non-linearity nature of the settlement simulated by the hypoplastic model. Therefore, the negative strain (or settlement) is underestimated if the depth-dependent void ratio is simplified by the arithmetic mean void ratio. However, normally speaking, the void ratio reduces with soil depth far slower than the ratio used in case 2, therefore the effect of the depth-dependent character on the strain is far lower.

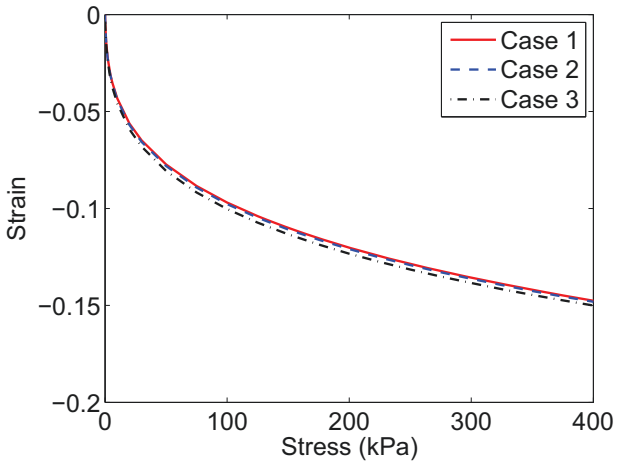

Figure 5.2.: Deterministic strain-stress relation comparison with both constant and depth-dependent void ratio

5.2. Stochastic compression analysis

5.2.1. Stochastic model description

In this section, the variability of void ratio is taken into consideration. The depth-dependent character of the mean, the standard deviation, and the spatial correlation length of void ratio is considered separately during the stochastic one-dimensional compression analysis, so as to study the effect of this depth-dependent character on the strain.

The one-dimensional physical model used here is similar to the model used in chapter 3. The only difference is the size used here is a soil column of 60m, which is equally divided into 60 elements. The mean void ratio of the whole column is 0.8. The depth-dependent behavior of void ratio is control by kk, which is the slope of vertical influence. As is shown in Figure 5.3, kk=0 means the void ratio is constant, while kk$\neq$0 represents the depth-dependent void ratio. A high kk means the void ratio is highly depth-dependent. 1500 realizations are simulated in each case.

5.2.2. Effect of the variance reduction

The variance reduction (VR) plays an important role in the random field generation, and it is necessary to evaluation the effect of the variance reduction of void ratio on the results of the 1d compression test. The generated random field of void ratio is stationary, without considering its depth-dependent character in this section. The values of the parameters in Table 5.1 are adopted here. The stochastic parameters of the initial void ratio are listed in Table 5.2.

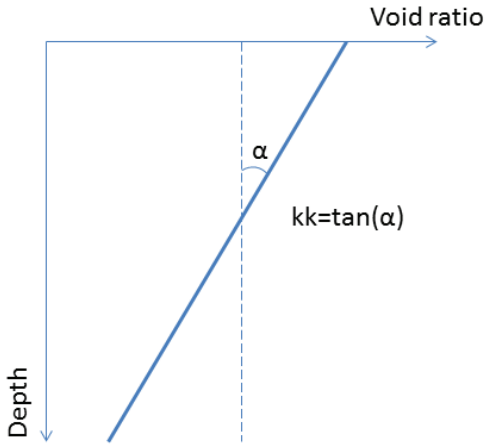

Figure 5.3.: Schematic diagram of the depth-dependent void ratio

Table 5.2.: Stochastic parameters of void ratio for the effect of variance reduction

μ	σ	max	min	$\delta(m)$	Distribution
0.8	0.1	1.3	0.3	10	Truncated Gaussian

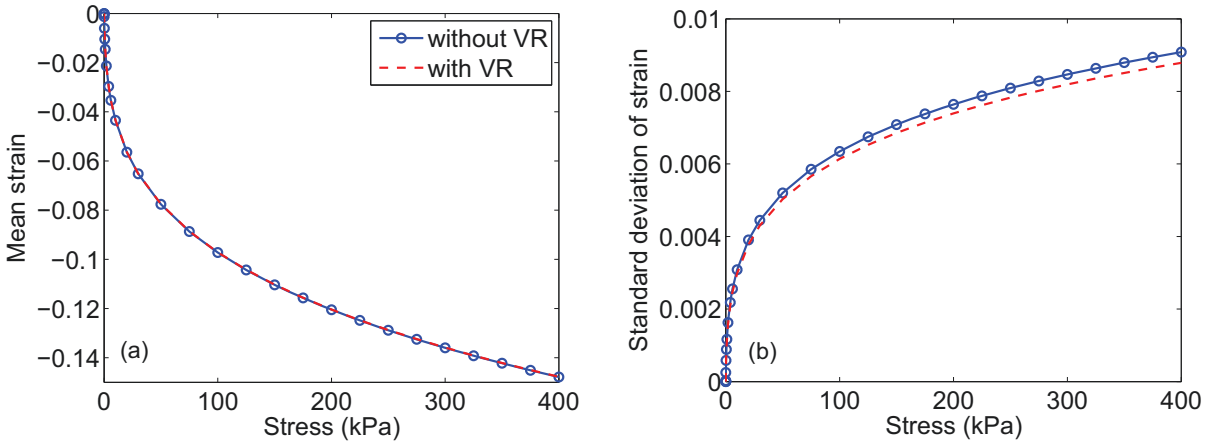

Figure 5.4.: Effect of variance reduction (VR) on the (a) mean, (b) standard deviation of strain

Figure 5.4 shows the effect of the variance reduction on the mean and standard deviation of strain. As shown in Figure 5.4a, the lines with and without considering the variance reduction coincide with each other. This means the variance reduction has little effect on the mean strain, this is reasonable because, (a) the depth-dependent character is not so great, and (b) the variance reduction does not affect the mean value of the void ratio with a truncated Gaussian distribution in this case. However, the variance reduction can reduce the fluctuation of the void ratio, this is why the standard deviation of the strain is smaller in Figure 5.4b when the variance reduction is taken into consideration. A larger standard deviation does not always mean that the foundation has a higher probability of failure. What we are interested in is the foundation which can have a large settlement, because this kind of foundation is the failed part during the probabilistic settlement analysis. The empirical PDF (Probability Density Function) of the strain at 400 kPa is shown in Figure 5.5. Geotechnical limit state design for footings requires limiting excessive displacement to meet serviceability limit state (SLS). If the displacement is over a prescribed value, the footing

fails. In the reliability analysis of the footing, the performance function, defined with respect to a prescribed admissible footing displacement at the SLS, is usually given to evaluate the reliability of the footing. The Pf is the probability that the displacement is over the prescribed value. It is not so proper to evaluate the reliability of the footing here, since it is the 1d compression simulation carried out in this chapter, rather than 2d or 3d simulation, and our aim is about the strain. However, the left tail of the empirical PDF of the strain at a certain stress level can imply the Pf of the footing. It can be seen in Figure 5.5 that the left tail of the empirical PDF is slightly lower when the variance reduction is considered. This means the Pf is lower when the variance reduction is taken into consideration during the reliability analysis of the footings with the SLS as a performance function. However, the difference is very small and can be neglected in this case.

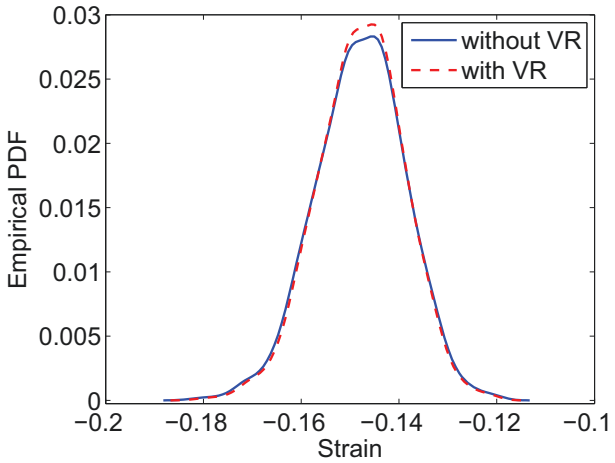

Figure 5.5.: Effect of the variance reduction (VR) on the empirical PDF of strain (stress=400kPa)

5.2.3. Effect of the depth-dependent mean

In order to evaluate the effect of the depth-dependent mean void ratio on the stochastic analysis of 1d settlement, the random field with depth-dependent mean void ratio is generated while both the standard deviation and the spatial correlation length of void ratio are kept constant. The basic parameters used in random field generation are listed in Table 5.3. 1500 realizations of the random field are used. The mean void ratio can be expressed using,

$$\mu_e = e_i * (1 - kk * (L/2 - z)) \tag{5.1}$$

where e_i is the initial void ratio, here it equals to 0.8; L is the total depth of the soil, z is the depth of the center of each element in the soil column. kk controls the depth-dependent character, which is already explained in Figure 5.3.

Table 5.3.: Parameters used in random field generation of void ratio with depth-dependent mean

σ	Distribution	max	min	kk	L(m)	Dz(m)	z
0.1	Truncated Gaussian	1.3	0.3	0, 0.005, 0.01	60	1	0.5:Dz:L

Figure 5.6 illustrates one realization of the random field with different kk. The original normalized spatially correlated random field is the same in all three cases. Comparing with the constant void ratio case (the solid line where kk=0 in Figure 5.6), the void ratio with a higher kk is smaller in the bottom half of the slope, and larger in the top half of the slope.

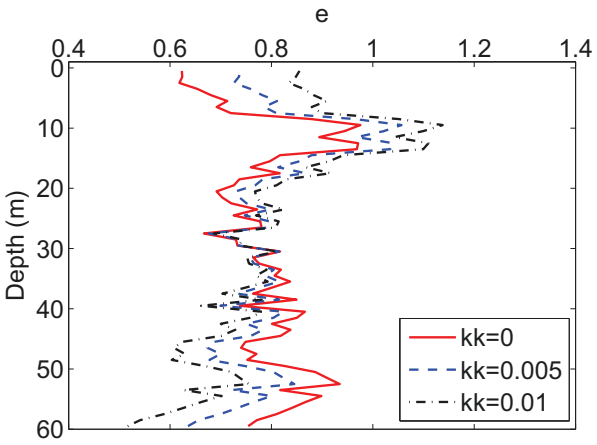

Figure 5.6.: Representative random field of void ratio with depth-dependent mean

Figure 5.7 shows the effect of the depth-dependent mean of void ratio on the mean, and standard deviation of the strain at different stress levels. Figure 5.7a shows that a highly depth-dependent mean of the void ratio can slightly increase the mean of the negative strain, this result is in accordance with the results from the deterministic analysis. Figure 5.7b is the effect of the depth-dependent mean void ratio on the standard deviation of the strain. It can be seen that the standard deviation of strain is slightly decreased as the increase of kk. Figure 5.8 shows that the left tail of the empirical PDF is slightly higher for the random field with a higher kk. This means the probability of failure is slightly higher, when the depth-dependent character of the mean void ratio is taken into consideration, during the reliability analysis of the footing with the SLS as a performance function.

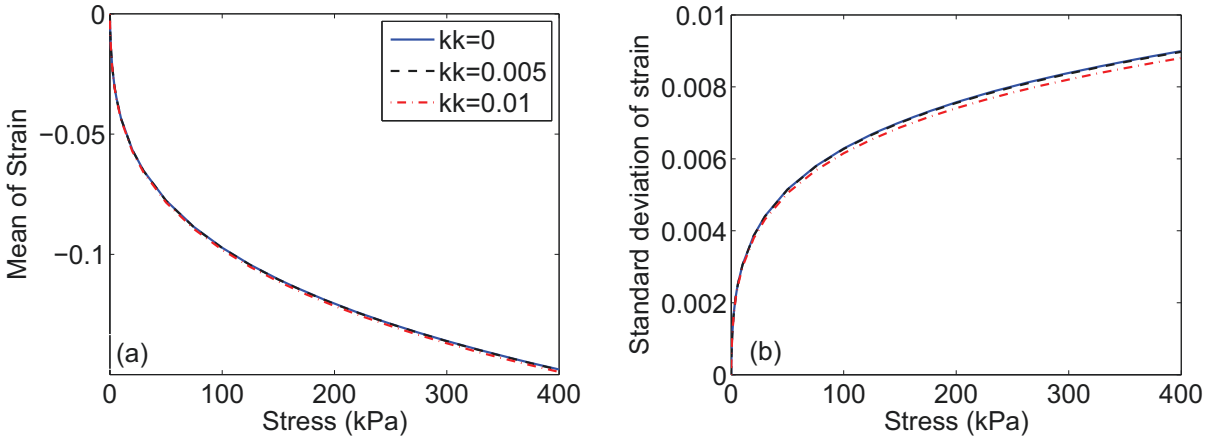

Figure 5.7.: Effect of the depth-dependent mean void ratio on the (a) mean, (b) standard deviation of the strain

5.2.4. Effect of the depth-dependent standard deviation

In order to evaluate the effect of the depth-dependent standard deviation of void ratio on the 1d compression test results, the random fields are generated with and without considering the depth-dependent character of standard deviation while the other stochastic parameters (the mean and the spatial correlation length of the void ratio) are kept constant. Then the random fields are used

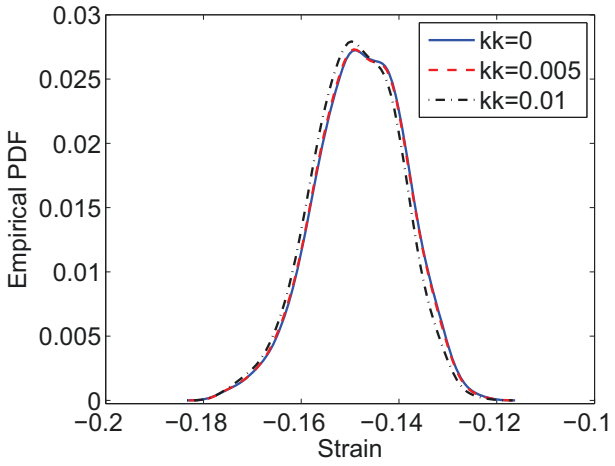

Figure 5.8.: Effect of the depth-dependent mean void ratio on the empirical PDF of one-dimensional strain (stress=400kPa)

to carried out the 1d compression simulation. At last, the stress-strain relation is compared. In this case, the standard deviation is assumed to reduce linearly as the increase of the soil depth. It can be expressed using,

$$\sigma_e = \sigma * (1 - kk * (L/2 - z)) \tag{5.2}$$

where σ_e is the depth-dependent standard deviation of void ratio; σ is the original standard deviation of void ratio, here it equals to 0.1. L is the total length of the soil column; kk controls the depth-dependent trend of the standard deviation. The other parameters used in the random field generation here are listed in Table 5.4. Three different kk are used: kk=0 means the standard deviation is constant, while kk=0.005 and 0.01 mean the standard deviations are lowly and highly depth-dependent, respectively.

Table 5.4.: Parameters used in random field generation of void ratio with depth-dependent standard deviation

μ	Distribution	max	min	kk	L(m)	Dz(m)	z
0.8	Truncated Gaussian	1.3	0.3	0, 0.005, 0.01	60	1	0.5:Dz:L

One realization of the random field is illustrated in Figure 5.9. Since the top half of the random field has a larger standard deviation for the case with a higher kk, the value is further away from the mean of void ratio, comparing with the stationary random field (solid line). The bottom half shows an opposite trend. These three random field profiles do not have too much difference, because the standard deviation is small, and the initial void ratio is limited to a certain range.

Figure 5.10 shows the effect of the depth-dependent standard deviation of void ratio on the stress-strain relation. It can be seen in Figure 5.10a that, the depth-dependent character of the standard deviation of void ratio has little effect on the mean strain. However, the standard deviation of strain can be slightly increased if the depth-dependent character of the standard deviation of the void ratio is taken into consideration. It is interesting to see that the case with a higher kk (kk=0.01) has a smaller standard deviation of strain, comparing to the case with kk=0.005. Figure 5.11 shows that the left tail of the empirical PDF is slightly higher when kk is larger. This means the probability of failure is higher when the depth-dependent character of the standard deviation of void ratio is taken into consideration, during the reliability analysis of the footing with the SLS

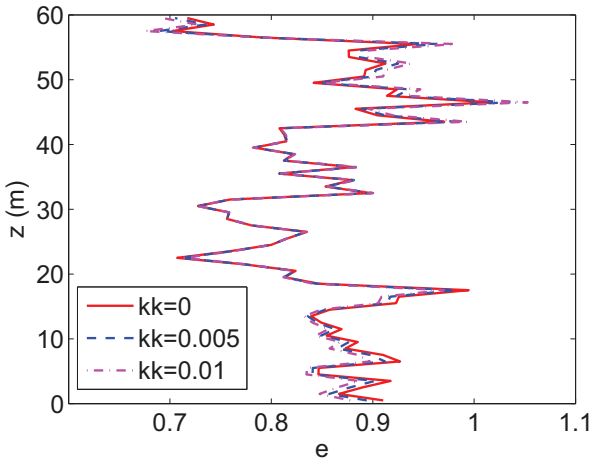

Figure 5.9.: One random field of the void ratio with depth-dependent standard deviation

as a performance function. The difference is small and can be neglected. It can also prove that a higher standard deviation does not always mean a high Pf through the comparison of both the standard deviation and the empirical PDF.

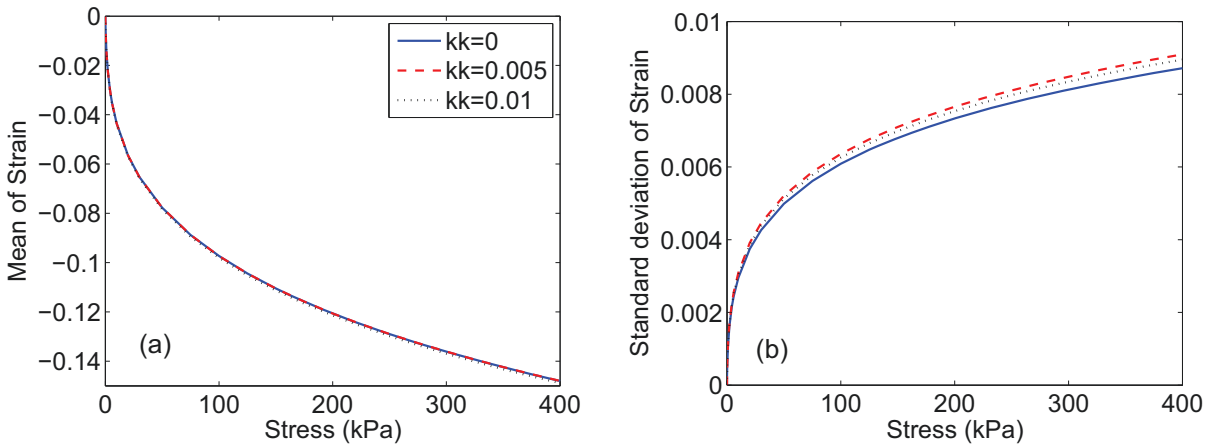

Figure 5.10.: Effect of the depth-dependent standard deviation of void ratio on the (a) mean, (b) standard deviation of strain

5.2.5. Effect of the depth-dependent spatial correlation length

In order to evaluate the effect of the depth-dependent spatial correlation length of void ratio on the one-dimensional settlement, the layered random fields are generated using SGeMS. The spatial correlation length in the top and bottom layers are 15m and 5m, respectively. The length of the top and bottom layers are 75m and 25m, respectively, so as to make sure the mean spatial correlation length of the layered random field is 10m. The generation of the layered random field has been elaborated in chapter 4. Stationary random fields with a constant spatial correlation length of 10m are also generated in order to compare the results. Both the mean and the standard deviation of void ratio are kept constant, so as to present the effect of depth-dependent spatial correlation length clearly. The truncated Gaussian distribution is adopted, and the element size is 1 m. The parameters of void ratio used in random field generation are summarized in Table 5.5.

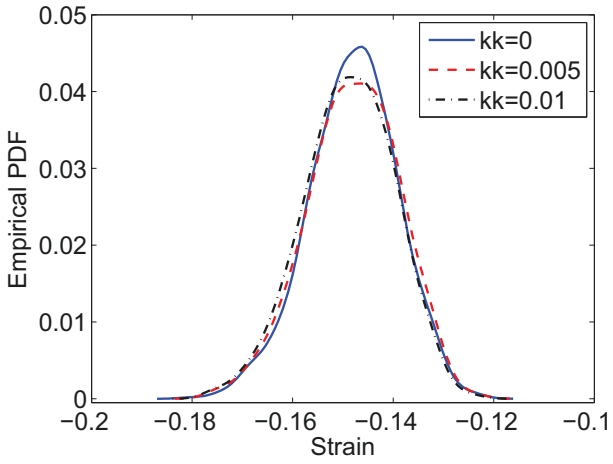

Figure 5.11.: Effect of the depth-dependent standard deviation of void ratio on the empirical PDF of one-dimensional strain (stress=400kPa)

Table 5.5.: Parameter comparison of void ratio between random field with layered and constant spatial correlation length (δ)

	RF with layered δ		RF with constant δ
	Top layer	Bottom layer	
μ	0.8	0.8	0.8
σ	0.1	0.1	0.1
δ(m)	15	5	10
L(m)	75	25	100
dL(m)	1	1	1
Distribution	Truncated Gaussian		Truncated Gaussian

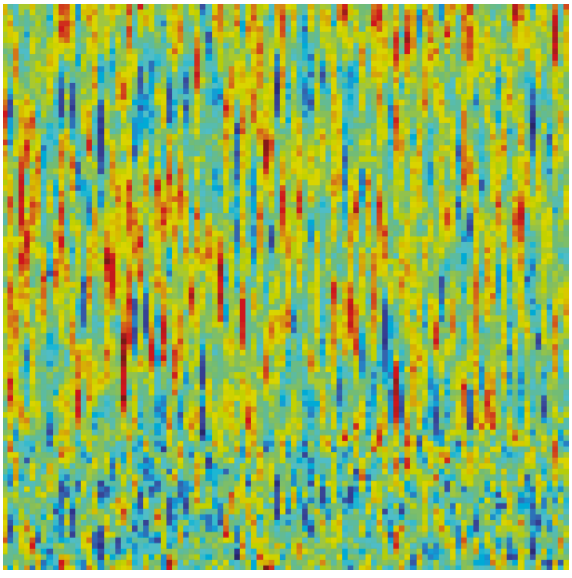

Figure 5.12.: Illustration of the random field generation of void ratio with depth-dependent spatial correlation length

Figure 5.12 illustrates 100 independent columns of the one-dimensional layered random field of

void ratio. In each column, the spatial correlation length of the top 75 elements is 15m, and it is 5m in the last 25 elements.

As is shown in Figure 5.13, the depth-dependent SCL has little effect on the mean strain of the one-dimensional compression test (Figure 5.13a), since both lines coincides with each other with and without considering the depth-dependent character of SCL. This is expected because the depth-dependent SCL does not affect the mean of a normally distributed random field. Figure 5.13b shows that, comparing with the constant SCL case, the depth-dependent character of the SCL can slightly reduce the standard deviation of strain. From the empirical PDF of the strain at 400kPa, Figure 5.14 shows that, the depth-dependent character of the SCL has little effect on the left tail of the empirical PDF. This means the depth-dependent character of SCL has little effect on the probability of failure.

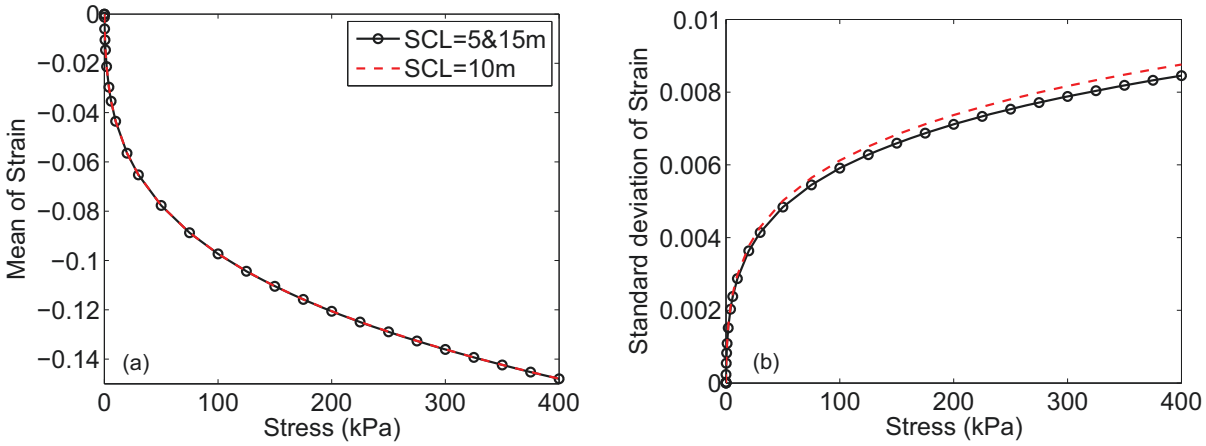

Figure 5.13.: Effect of the depth-dependent spatial correlation length of void ratio on the (a) mean, and (b) standard deviation, of strain

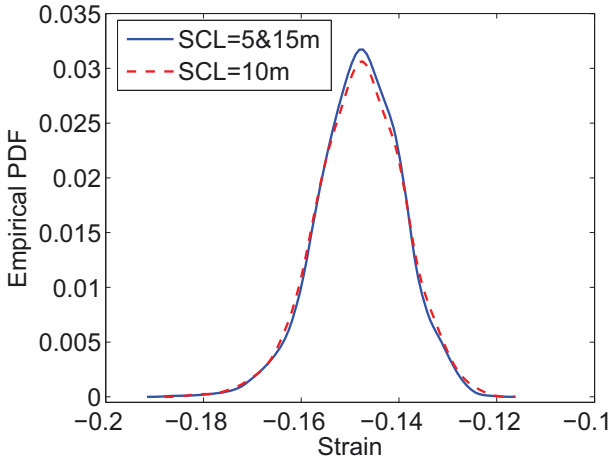

Figure 5.14.: Effect of the depth-dependent SCL of void ratio on the empirical PDF of one-dimensional strain (stress=400kPa)

5.3. Concluding remarks

In this chapter, the effect of the depth-dependent character of the stochastic parameters of void ratio on the strain is analyzed through the one-dimensional settlement analysis. The following results can be concluded,

- The strain is slightly underestimated if the arithmetic mean void ratio is adopted in the one-dimensional settlement analysis.
- Comparing with constant void ratio case, the depth-dependent mean, standard deviation, and spatial correlation length of void ratio have little effect on the mean strain.
- When the mean void ratio is highly depth-dependent, the probability of failure can be slightly increased, during the reliability analysis of the footing with the SLS as a performance function. The depth-dependent character of the standard deviation of void ratio can slightly increase the probability of failure, and the depth-dependent character of the spatial correlation length has little effect on the probability of failure.

In reality, the hs (granular hardness) is far larger, so the strain should be far smaller than the results obtained in this chapter. Therefore, the effect of this depth-dependent character on the mean and standard deviation of strain could be neglected. It is known that the weakest area of a random field plays a key role on the probability of failure, and the area with high void ratios is very important to the variation of the strain. However, the initial void ratio of sand can only fluctuate in a certain range, because of the requirement of the hypoplastic model. Therefore, it is not surprising that the depth-dependent character of the stochastic parameters has no effect on the mean strain and has little effect on both the standard deviation of the strain and the probability of failure.

6. Deterministic analysis of infinite slope stability during infiltration

6.1. Background of infinite slope stability and objective

The failure of natural or engineered earth slope can be induced by many factors, such as weathering, vegetation, topography, geological features. Researches (Lim et al., 1996; Gasmo et al., 2000; Collins and Znidarcic, 2004; Rahardjo et al., 2007) have shown that the shallow slope failure is usually induced by rainwater infiltration. In classical slope stability analysis, the shear strength is calculated using Terzaghi's effective stress principle, and the water pressure is calculated using saturated seepage theory, in which the negative pore-water pressure does not exist. However, field cases have shown that the shallow slope failure might occur in the area above groundwater level under partially saturated soil condition (Wolle and Hachich, 1989; De Campos et al., 1991; Godt et al., 2007), makes the assumption of saturated condition invalid during slope stability analysis. Nowadays, it has been commonly recognized that the negative pore-water pressure, which is also called as matric suction, is one part of the shear strength, and it helps to stabilize the slope (Fredlund and Rahardjo, 1993). As the rainwater infiltrates into a soil slope, the negative pore-water pressure becomes smaller, or even becomes zero when the rain intensity is large enough and the rain lasts long enough. The reduction of negative pore-water pressure can reduce the shear strength, so as to decrease the stability of a slope, then the slope might fails.

As one of the oldest and simplest slope stability model, the infinite slope model is usually adopted to study the stability of a shallow slope, in which the length of the slope is significantly larger than the thickness of the slope (Lu and Godt, 2008; Griffiths et al., 2011; Santoso et al., 2011; Cho, 2014).

It has been proved that the stochastic parameters (mean, standard deviation and spatial correlation length) of void ratio reduce with soil depth. The relation between the void ratio and saturated hydraulic conductivity (ks) can be expressed using Kozeny-Carman equation (Taylor, 1948; Carrier III, 2003), in which the ks is positively related to the void ratio. So it is reasonable to conclude that the stochastic parameters of ks are depth-dependent, and the stochastic parameters including the mean, the standard deviation, and the spatial correlation length, reduce with soil depth too. Somerton et al. (1975) has confirmed that the permeability of coal reduces with the increase of stress. Some parametric studies are carried out in this chapter. However, the prime aim is to figure out how the depth-dependent trend of ks affects the infiltration and the slope stability. In order to make it simple, the ks is assumed to reduce linearly with soil depth when the effect of the depth-dependent character is evaluated. The infinite slope stability model is used here to study the one-dimensional slope stability during infiltration. Both steady state and transient state infiltration are considered.

6.2. Relevant theory

6.2.1. One-dimensional unsaturated seepage

The fluid flow, which is assumed to follow Darcy's law, can be expressed as:

$$q = -k\frac{dH}{dz} \tag{6.1}$$

where q is the flow flux (negative q indicates infiltration), k is the hydraulic conductivity (or coefficient of permeability) in the direction of the flow, H is the total head, which is the summation of pore-water pressure head h and the gravitational head, z is the elevation.

Combining Darcy's law with the mass conservation law results in the governing equation of one-dimensional flow of water through an unsaturated soil (Fredlund and Rahardjo, 1993) above the groundwater level:

$$\frac{\partial}{\partial z}(k\frac{\partial H}{\partial z}) = m_w\gamma_w\frac{\partial H}{\partial t} \tag{6.2}$$

where m_w is the slope of the soil-water characteristic curve (SWCC), γ_w is the unit weight of water, and t is the time.

6.2.2. Hydraulic characteristics

The hydraulic conductivity (k) depends on the effective saturation (χ) or the pore-water pressure in unsaturated soil, which is different to the saturated seepage. Several empirical and semi-empirical functions have been proposed to express the hydraulic conductivity function, however, here in this study, the van Genuchten SWCC equation (Van Genuchten, 1980), which is commonly used in infinite slope stability analysis, is adopted:

$$\frac{\theta - \theta_r}{\theta_s - \theta_r} = (1 + |\alpha(u_a - u_w)|^n)^{1/n-1} \tag{6.3}$$

where θ is the volumetric water content, θ_r and θ_s denote the residual and saturated volumetric water contents, respectively, α is the curve-fitting parameter inversely related to the air-entry value (kPa^{-1}), n is the curve-fitting parameter related to the pore size distribution, u_a and u_w are the pore-air pressure and pore-water pressure respectively, $(u_a - u_w)$ represents the matric suction.

The (pore-water) pressure head (h) of unsaturated soil is expressed as,

$$h = \frac{u_w - u_a}{\gamma_w} \tag{6.4}$$

A number of functions have been proposed to express the relation between the hydraulic conductivity and the matric suction, the function adopted here is:

$$k = \begin{cases} ks \cdot exp[-\alpha(u_a - u_w)], & \text{if } u_a - u_w \geq 0 \\ ks, & \text{if } u_a - u_w < 0 \end{cases} \tag{6.5}$$

herein Gardner's model (Gardner, 1958) is adopted for the unsaturated seepage where the matric suction is positive, and k equals to the ks when the pressure head is positive.

In steady state seepage, the flux q is kept constant, and the storage does not change with time, so the right-hand side of Eq. 6.2 becomes zero. For unsaturated seepage, substituting Gardner's model into Eq. 6.2, the analytical solution of the pressure head in the steady state seepage for homogeneous soil can be derived (Yeh, 1989; Lu and Griffiths, 2004) as,

$$h = \frac{1}{\alpha\gamma_w} ln\{exp(-\alpha\gamma_w z)[exp(\alpha\gamma_w h_0) + q/ks] - q/ks\}, \qquad -q \leq ks \tag{6.6}$$

in which z is the elevation, h_0 is the prescribed pressure head at z=0, and h_0 is non-positive.

If the negative flow flux is larger than ks, the infiltration domain is regarded as saturated area. Therefore, the pressure head can be calculated by,

$$h = h_0 - z(1 + q/ks), \qquad -q \geq ks \tag{6.7}$$

Eq. 6.6 is proved to be applicable to the multi-layered soil (Yeh 1989). The pressure head in the steady state seepage for multi-layered soil can be expressed as:

$$h_i = \frac{1}{\alpha\gamma_w} ln\{exp(-\alpha\gamma_w dz)[exp(\alpha\gamma_w h_{i-1}) + q/ks_i] - q/ks_i\}, \qquad -q \leq ks \tag{6.8}$$

where, h_{i-1} and h_i are the pressure head at elevation z_{i-1} and z_i respectively, and the pressure head should not be positive; ks_i is the saturated hydraulic conductivity of layer i. The constrain of this equation is that the negative downward infiltration flux -q cannot be larger than the saturated hydraulic conductivity (Lu and Griffiths, 2004).

For layered soil profile, the pressure head can be calculated using Eq. 6.8 recursively, starting from the bottom layer of the soil profile. The physical constrain of Eq. 6.8 is that the pressure head is not positive. However, it is possible that the positive pressure head is generated under layered soil profile, and this case will be discussed in detail in section **6.4.1**.

For transient infiltration, the analytical solution is available only for a few special cases with simple initial and boundary conditions, for example, in the cases with homogeneous soil profile and two-layered soil profile (Srivastava and Yeh, 1991). Numerical approximation with finite element method (Cheng, 2008) or finite difference method is commonly adopted for general unsaturated seepage analysis, and some programs are already available for the transient infiltration: e.g. Seep/W, SWMS-2D, THFELA with finite element method, and Unsat-H with finite difference method. The simulation of infiltration will be elaborated later.

6.2.3. Infinite slope stability analysis

If the matric suction is considered, the shear strength of soil can be expressed as (Lu and Griffiths, 2004):

$$\tau_f = c' + [(\sigma_t - u_a) + \chi(u_a - u_w)]tan\phi' \tag{6.9}$$

where c' is the effective cohesion of the soil, ϕ' is the effective friction angle, σ_t is the total stress, and χ is the coefficient of effective stress or the (degree of) effective saturation, which can be expressed as:

$$\chi = \frac{\theta - \theta_r}{\theta_s - \theta_r} \tag{6.10}$$

The effective friction angle is usually assumed to be constant for a given soil in classical infinite slope stability analysis. However, this assumption is rarely true taking the field condition into consideration, because soil porosity (or void ratio) normally reduces with soil depth due to the mechanical compaction and consolidation under self-weight and/or external loading (Lu and Godt, 2008). The effective friction angle of sand is also proved to be inversely linearly proportional to the porosity by experimental evidence (Marachi et al., 1900; Rowe, 1969; Cornforth, 1973, 2005). The relation between the friction angle and the porosity (m) can be described as:

$$\phi = \phi_0 + \frac{\Delta\phi}{\Delta m}(m_0 - m) \tag{6.11}$$

where ϕ_0 and m_0 are respectively the friction angle and porosity at the ground surface, $\Delta\phi$ and Δm are the range of variation in friction angle and porosity respectively within the weathering zone z_w. The porosity can be expressed as (Lu and Godt, 2008),

$$m = m_0 - \frac{\Delta m}{1 + \frac{z_w}{H_{ss}}} \tag{6.12}$$

Substituting Eq. 6.12 into Eq. 6.11 leads to:

$$\phi = \phi_0 + \frac{\Delta \phi}{1 + \frac{z_w}{H_{ss}}} \tag{6.13}$$

where the soil depth $H_{ss} = L - z$, L is the total thickness of the slope, and z is the elevation from the bottom of the slope, as is shown in Figure 6.1. Therefore, the depth-dependent friction angle can also be expressed as (Santoso et al., 2011):

$$\phi(z) = \phi_0 + \frac{\Delta \phi}{1 + \frac{z_w}{L - z}} \tag{6.14}$$

Using Mohr-Coulomb failure criterion, the safety factor of the infinite slope in Figure 6.1 can be written as:

$$FS(z) = \frac{\tau_f}{\gamma_s (L - z) sin\beta cos\beta} \tag{6.15}$$

where γ_s is the total unit weight of soil, β is the slope angle. Eq. 6.15 can be rearranged as,

$$FS(z) = \frac{2c'}{\gamma_s (L - z) sin2\beta} + \frac{tan\phi'}{tan\beta} + \frac{\chi (u_a - u_w)(tan\beta + cot\beta) tan\phi'}{\gamma_s (L - z)} \tag{6.16}$$

where the three terms on the right side show the resistance from cohesion, friction angle, and matric suction, respectively.

6.3. Infinite slope description

An infinite slope model (Figure 6.1) from Santoso et al. (2011), together with the depth-dependent ks, are adopted to study the effect of depth-dependent ks on the infiltration and infinite slope stability. Like in chapter 5, kk (slope of vertical influence) is used to denote the depth-dependent behavior of mean ks, as it is shown in Figure 6.1. In order to make it simple, the ks is assumed to increase linearly with the elevation of the slope, while the mean of ks in the whole slope keeps constant. During the simulation, it is assumed that: (a) the groundwater level keeps constant, (b) no ponding in the ground surface, extra flux runs off.

6.4. Numerical simulation of infiltration

6.4.1. Numerical simulation of the steady state infiltration

Since the depth-dependent ks of the slope is considered during infiltration, the problems are how to express the depth-dependent ks in the slope, and how to use the depth-dependent ks during simulation. Here we equally divides the slope into several layers, and assumes the ks is constant in each layer. The ks is calculated based on the elevation of the midpoint of each layer.

Given enough time, the infiltration will reach at steady state, where the volumetric water content of the slope does not change with time. It is the lowest bound of a slope stability, since the factor of safety of the slope is the lowest during steady state infiltration. Comparing with the simulation of unsaturated infiltration in the transient state, the simulation of unsaturated infiltration in the steady state is simple, because the right side of Eq. 6.2 becomes zero. In this condition, the pressure

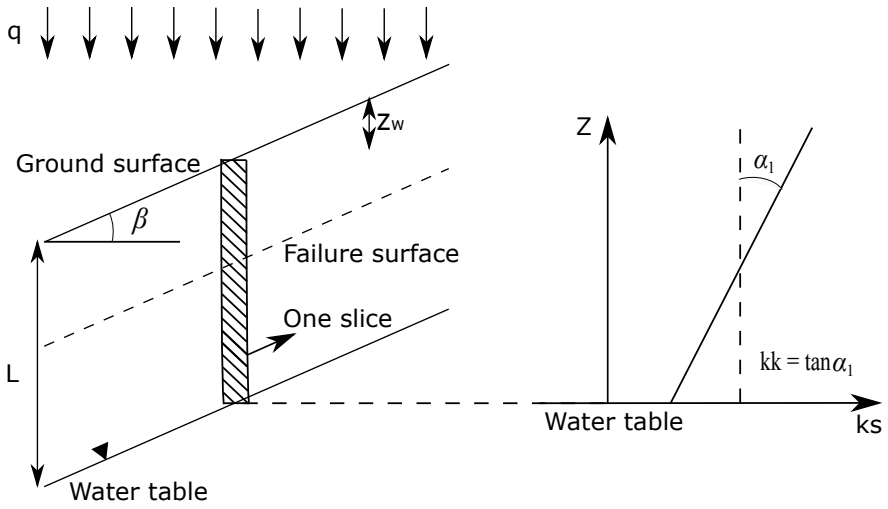

Figure 6.1.: Typical infinite slope model with a weathered mantle

head does not change with time, and only the conductivity function on the left side of the equation is involved. Analytical solution (Eq. 6.8) is available and is commonly used in the steady state infiltration in unsaturated soil. Eq. 6.8 can also be used in the multi-layered situation.

The limitation of Eq. 6.8 is that the pressure head cannot be positive. For homogenous soil, the absolute infiltration flux |q| is kept less than the saturated hydraulic conductivity ks, so as to make sure the pressure head is not positive. Excess flux is easily handled as run-off when the negative flux is larger than ks. However, for layered soil situation, the infiltration becomes more complex. |q| might be larger than the ks in one layer, and the positive pore-water pressure might be generated when the infiltration flows from a high permeable layer to a low permeable layer. This is a thorny problem, because Eq. 6.8 is not valid when the pressure head is positive. Some authors (Cheng, 2008; Santoso et al., 2011) still adopted Eq. 6.8 in layered soil with positive pressure head above the groundwater table, while some authors chose to neglect the positive pressure (Fayer, 2000). Here, an alternative method is proposed. Yeh (1989) has illustrated that Eq. 6.8 can be used when $h_i \leq 0$, including the case that the absolute flux is larger than ks. When h_i>0, Eq. 6.7 can be adopted to calculate the pressure head above. Therefore, this thorny problem can be solved by the switch between Eq. 6.7 and Eq. 6.8. It is inevitable that one layer contains both negative and positive pressure head. In this situation, we can divide this layer into several very small segments, especially when the layer is thick. Eq. 6.8 can be used for each segment from bottom to top, until the positive pressure head is calculated. Since the segment size is very small, the positive pressure head should be small too. This positive pressure head might not be correct, however, it is very small, and the error should be acceptable. Then, this positive pressure head can be regarded as the initial point to carry out the saturated seepage with positive pressure head using,

$$h_i = h_{i-1} - dz(1 + q/ks_i) \tag{6.17}$$

Eq. 6.17 can be used to calculate the positive pressure head till the negative pressure head appears again in a certain segment or layer. Then Eq. 6.8 can be switched back. Finally, if the pressure head is negative at the ground surface, it is all right. However, if the pressure head is positive at the ground surface, the absolute flux will be reduced, and extra flux flows as run-off. Then, the pressure head is recalculated from bottom to top using this new flux, till the pressure head at the surface is about zero.

6.4.2. Numerical simulation of the transient state infiltration

Eq. 6.2 can be rewritten as,

$$\frac{\partial}{\partial z}[k(\frac{\partial h}{\partial z}+1)]=\frac{\partial \theta}{\partial t}=C\frac{\partial h}{\partial t} \tag{6.18}$$

where, k is the unsaturated hydraulic conductivity which is a function of the pressure head h (negative for unsaturated flow), θ is the moisture content. $C=\frac{d\theta}{dh}$, which is the specific water capacity. It can be derived from Eq. 6.3.

As mentioned before, the most common methods to approximate the transient state infiltration are finite element method and finite difference method. The finite difference method is adopted here.

Let the entire flow domain be divided into a grid of equal intervals Δz, and the time domain be similarly divided into intervals Δt, the partial differential equation of Eq. 6.18 can be approximated by a finite difference equation replacing and respectively in the following way,

$$C_i^{j+a}\frac{h_i^{j+1}-h_i^j}{\Delta t}=\frac{1}{\Delta z}[k_{i+1/2}^{j+a}(\frac{h_{i+1}^{j+a}-h_i^{j+a}}{\Delta z}+1)-k_{i-1/2}^{j+a}(\frac{h_i^{j+a}-h_{i-1}^{j+a}}{\Delta z}+1)] \tag{6.19}$$

where i and j are the indices of space and time respectively. a is a weighting factor ($0\leq a\leq 1$) introduced in such a manner that by putting a=0, it is transformed into the explicit scheme, a=0.5 into Crank-Nicolson scheme, and a=1 into the implicit scheme, therefore:

$$\begin{aligned} h_i^{j+a}&=(1-a)h_i^j+ah_i^{j+1}\\ h_{i+1}^{j+a}&=(1-a)h_{i+1}^j+ah_{i+1}^{j+1}\\ h_{i-1}^{j+a}&=(1-a)h_{i-1}^j+ah_{i-1}^{j+1} \end{aligned} \tag{6.20}$$

The value of C_i^{j+a}, $k_{i+1/2}^{j+a}$, $k_{i-1/2}^{j+a}$ can be approximated by:

$$\begin{aligned} C_i^{j+a}&=F_1=(1-a)C_i^j+aC_i^{j+1}\\ k_{i+1/2}^{j+a}&=F_2=(1-a)k_{i+1/2}^j+ak_{i+1/2}^{j+1}=(1-a)\sqrt{k_i^jk_{i+1}^j}+a\sqrt{k_i^{j+1}k_{i+1}^{j+1}}\\ k_{i-1/2}^{j+a}&=F_3=(1-a)k_{i-1/2}^j+ak_{i-1/2}^{j+1}=(1-a)\sqrt{k_i^jk_{i-1}^j}+a\sqrt{k_i^{j+1}k_{i-1}^{j+1}} \end{aligned} \tag{6.21}$$

Substitution of Eq. 6.20 and Eq. 6.21 yields the following linear algebraic equation valid for each nodal point:

$$\begin{aligned} &[-aF_3\tfrac{\Delta t}{(\Delta z)^2}]h_{i-1}^{j+1}+[F_1+aF_2\tfrac{\Delta t}{(\Delta z)^2}+aF_3\tfrac{\Delta t}{(\Delta z)^2}]h_i^{j+1}-[aF_2\tfrac{\Delta t}{(\Delta z)^2}]h_{i+1}^{j+1}=\\ &[(1-a)F_3\tfrac{\Delta t}{(\Delta z)^2}]h_{i-1}^j+[F_1-(1-a)F_2\tfrac{\Delta t}{(\Delta z)^2}-(1-a)F_3\tfrac{\Delta t}{(\Delta z)^2}]h_i^j\\ &+[(1-a)F_2\tfrac{\Delta t}{(\Delta z)^2}]h_{i+1}^j+(F_2-F_3)\tfrac{\Delta t}{\Delta z} \end{aligned} \tag{6.22}$$

When Eq. 6.22 is applied at all nodes, the result is a system of simultaneous linear algebraic equations with a tridiagonal coefficient matrix with zero elements outside the diagonals and unknown value of h. In solving this system of equations, the so-called direct method can be used by applying a tridiagonal algorithm of the kind discussed by Remson et al. (1971).

The major advantage of explicit finite difference method is that, it is relatively simple, and it is computationally fast for each time step. However, the main drawback is that the solution is unstable in some conditions and the time step size cannot be too big. The main advantage of the implicit method is that there is no restrictions on time step, and the fully implicit scheme is unconditionally stable, the disadvantages are, (a) an inaccurate solution might be generated when the time step is large, (b) it is computationally slower for each time step. Both explicit and implicit

scheme are only first order accurate. The main advantages of Crank-Nicolson scheme are, it is unconditionally stable and it is second order accurate. Therefore, it is more accurate than both explicit and implicit schemes. The main drawback is that the calculation is time-consuming for each time step. The Crank-Nicolson scheme is used during the transient seepage in this and next chapters. For the finite difference approximation with Crank-Nicolson scheme, Eq. 6.22 can be rewritten as,

$$\begin{aligned}&[-\tfrac{1}{2}F_3\tfrac{\Delta t}{(\Delta z)^2}]h_{i-1}^{j+1}+[F_1+\tfrac{1}{2}F_2\tfrac{\Delta t}{(\Delta z)^2}+\tfrac{1}{2}F_3\tfrac{\Delta t}{(\Delta z)^2}]h_i^{j+1}-[\tfrac{1}{2}F_2\tfrac{\Delta t}{(\Delta z)^2}]h_{i+1}^{j+1}=\\&[\tfrac{1}{2}F_3\tfrac{\Delta t}{(\Delta z)^2}]h_{i-1}^{j}+[F_1-\tfrac{1}{2}F_2\tfrac{\Delta t}{(\Delta z)^2}-\tfrac{1}{2}F_3\tfrac{\Delta t}{(\Delta z)^2}]h_i^{j}\\&+[\tfrac{1}{2}F_2\tfrac{\Delta t}{(\Delta z)^2}]h_{i+1}^{j}+(F_2-F_3)\tfrac{\Delta t}{\Delta z}\end{aligned} \tag{6.23}$$

6.4.3. Boundary condition

To model the infiltration of rainwater, a fixed flux is set on the slope surface (flux boundary condition). If the negative flux is greater than the infiltration capacity of the slope surface, a fix pressure head (h_1=0) is used at the slope surface (head boundary condition). Extra water runs off. The groundwater table at the bottom of the slope is fixed.

The boundary conditions need to be specially treated. As is shown in Eq. 6.23, in order to obtain the pressure head of point i=1 (the first grid point) at the second time step (Figure 6.2), we need the pressure head at i=0, 1 and 2 at the first time step. However, the point 0 does not exit, so, it is regarded as a fictitious boundary point. For the last grid point (i=n), the pressure head before and after a time step is kept zero, because the last grid point situates at groundwater level, and the groundwater level is assumed to be constant.

Flux boundary condition

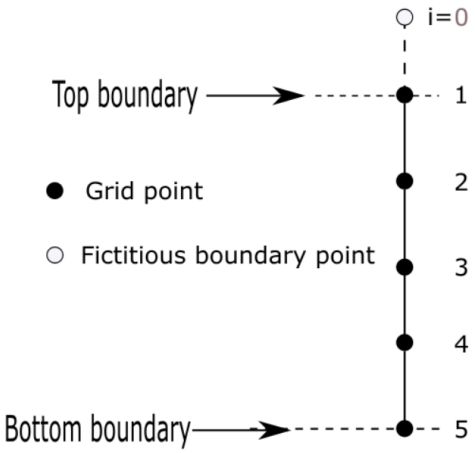

Figure 6.2.: Discretization of the numerical domain with fictitious boundary points, which are employed to set flux boundary conditions

For the grid point 1 at the top of the slope with a flux boundary condition,

$$q_1 = k_1(\frac{\partial h_1}{\partial z}+1) \tag{6.24}$$

It can be approximated using the central finite difference method as,

$$q_1 = k_1(\frac{h_2-h_0}{2\Delta z}+1) \tag{6.25}$$

Since the flux is constant, q_1=q, the pressure head at the fictitious boundary point (i=0) can be calculated through Eq. 6.26 as,

$$h_0 = h_2 - 2\Delta z(\frac{q}{k_1} - 1) \tag{6.26}$$

Head boundary condition

When the absolute flux is larger or equal to the saturated hydraulic conductivity of the top layer, extra water is assumed as run-off. Then the top boundary condition is head boundary condition, and it can be defined as,

$$h(z = L, t) = 0 \tag{6.27}$$

where L is the length of the slope.

The bottom boundary condition is always,

$$h(z = 0, t) = 0 \tag{6.28}$$

6.5. Case study

6.5.1. Deterministic analysis without considering the depth-dependent character

In this section, some parametric studies are carried out using homogeneous soil so as to study the effect of the n, α, and the flux on the effective saturation profile, suction head profile, pressure head profile, and factor of safety profile.

Case 1 description

The infinite slope and its coordinate system is shown in Figure 6.1. Unless pointed out directly, the parameters and their value used in this case are summarized in Table 6.1.

Table 6.1.: Parameters and their value used in Case 1

Parameters	Definition	Value
ks (m/s)	Saturated hydraulic conductivity	10^{-6}
α (kPa^{-1})	SWCC parameter	0.2
n	Empirical fitting parameter	1.35, 3
γ_s (kN/m^3)	Soil unit weight	20
c' (kN/m^2)	Effective cohesion	0
ϕ_0 (°)	Effective friction angle at ground surface	40
$d\phi$ (°)	The range of variation of friction angle within the weathering zone	6
z_w (m)	Depth of the weathered zone	0.5
β (°)	Slope angle measured from horizontal	45
dz (m)	Discretization of the slope	0.05
L (m)	Slope depth above the groundwater table	6

Effect of empirical fitting parameter n on the profiles

Figure 6.3 shows the effect of the empirical fitting parameter n on the effective saturation, pressure head, and the factor of safety profiles under hydrostatic equilibrium (no infiltration). For the case with a large n (n=7), the effective saturation reduces dramatically from fully saturated situation at the groundwater table to the residual state at about 1m above the groundwater table, then it becomes stable. As the decrease of parameter n, the reduction becomes slower (Figure 6.3a), and the location that the effective saturation reaches to residual state becomes higher, until this location disappears. The pressure head profile in Figure 6.3b shows that when the parameter n is

large (n=7), the pressure head reduces quickly from zero at groundwater table to the lowest point (about -0.3m) at about 0.4m above groundwater table, then it increases toward zero again; the point becomes vaguer when the parameter n is smaller; when the parameter n is smaller enough (n=1.35), the pressure head would reduce monotonously from zero at the groundwater table to the final value at the slope surface. Figure 6.3c is the factor of safety profile corresponding to the pressure head profile in Figure 6.3b. The maximum factor of safety is corresponding to the minimum pressure head in the case of n=7, and the factor of safety profile moves towards the right with the decrease of parameter n. In all, parameter n controls the shape of these profiles, since the shape of each profile (the effective saturation profile, the pressure head profile and the factor of safety profile) is different with different n.

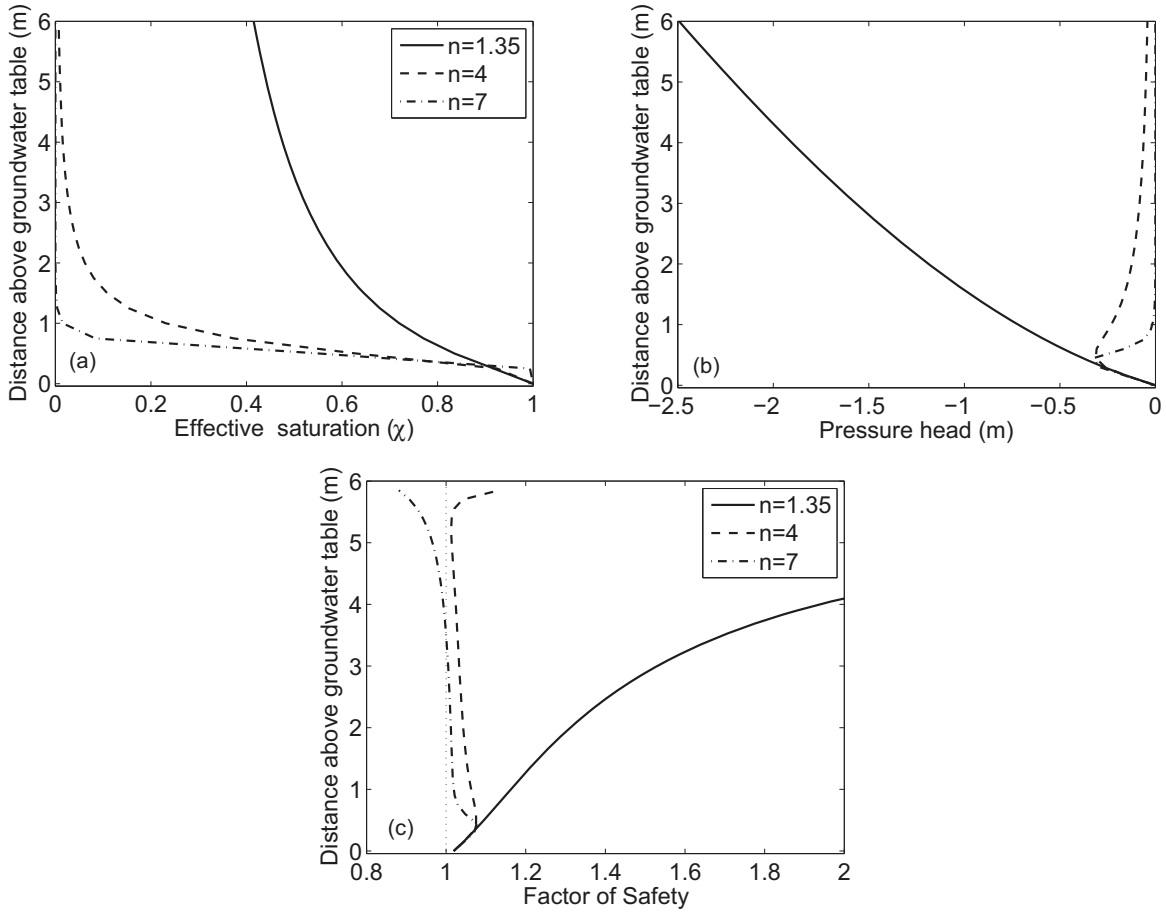

Figure 6.3.: Effect of n on the (a) effective saturation (b) pressure head, and (c) factor of safety profiles of the slope in the hydrostatic state (α=0.2)

Effect of SWCC parameter α on the profiles

Since the profiles show different patterns with small and large parameter n, it is necessary to check the effect of the SWCC parameter α on the profiles with a small and a large parameter n separately, which are depicted in Figure 6.4. It can be seen that, no matter the parameter n is large or small, the parameter α can only affect the magnitude of the profiles, and it does not affect the shape of the profiles. Meanwhile, as the parameter α increases, both the effective saturation profile and the factor of safety profile move towards left, while the pressure head profile moves towards right.

Effect of the flux on the profiles

Both n=1.35 and n=3 are used to study the effect of the infiltration flux on the homogenous soil

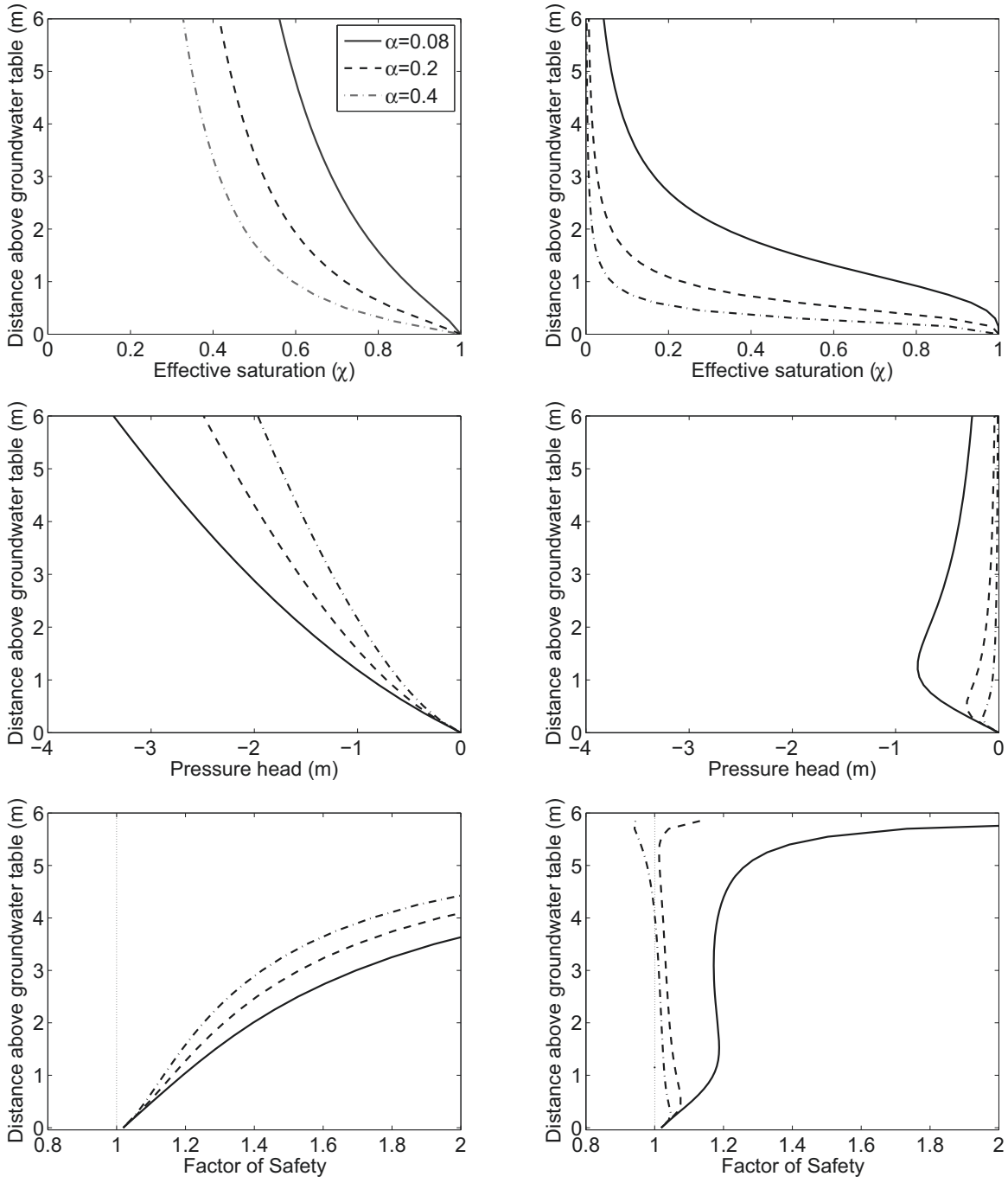

(a) n=1.35 (b) n=3

Figure 6.4.: Effect of α on the effective saturation profile, pressure head profile, and factor of safety profiles of a slope in the hydrostatic state

slope during steady state infiltration. The results are shown in Figure 6.5. As is shown in Figure 6.5 (a1, a2), the effective saturation increases with the increase of the negative flux; Figure 6.5 (b1) shows that the pressure head and the negative flux are positively correlated at the same elevation above the groundwater table when parameter n is small. However, the relation becomes more complex when parameter n is large, as is shown in Figure 6.5 (b2). When the negative flux is low, the pressure head decreases quickly from zero at the groundwater table to a minimum value at the location not far above the groundwater level, then it increases as the increase of the distance above groundwater table. A slight increase of the negative flux could dramatically change the pressure head above the location of the minimum value, and slightly move this location towards the ground surface, while keeping the overall trend of the pressure profile the same. However, as the negative flux increases to a high level (e.g. $5{\cdot}10^{-7}$ m/s, $9.5{\cdot}10^{-7}$ m/s), the pressure head

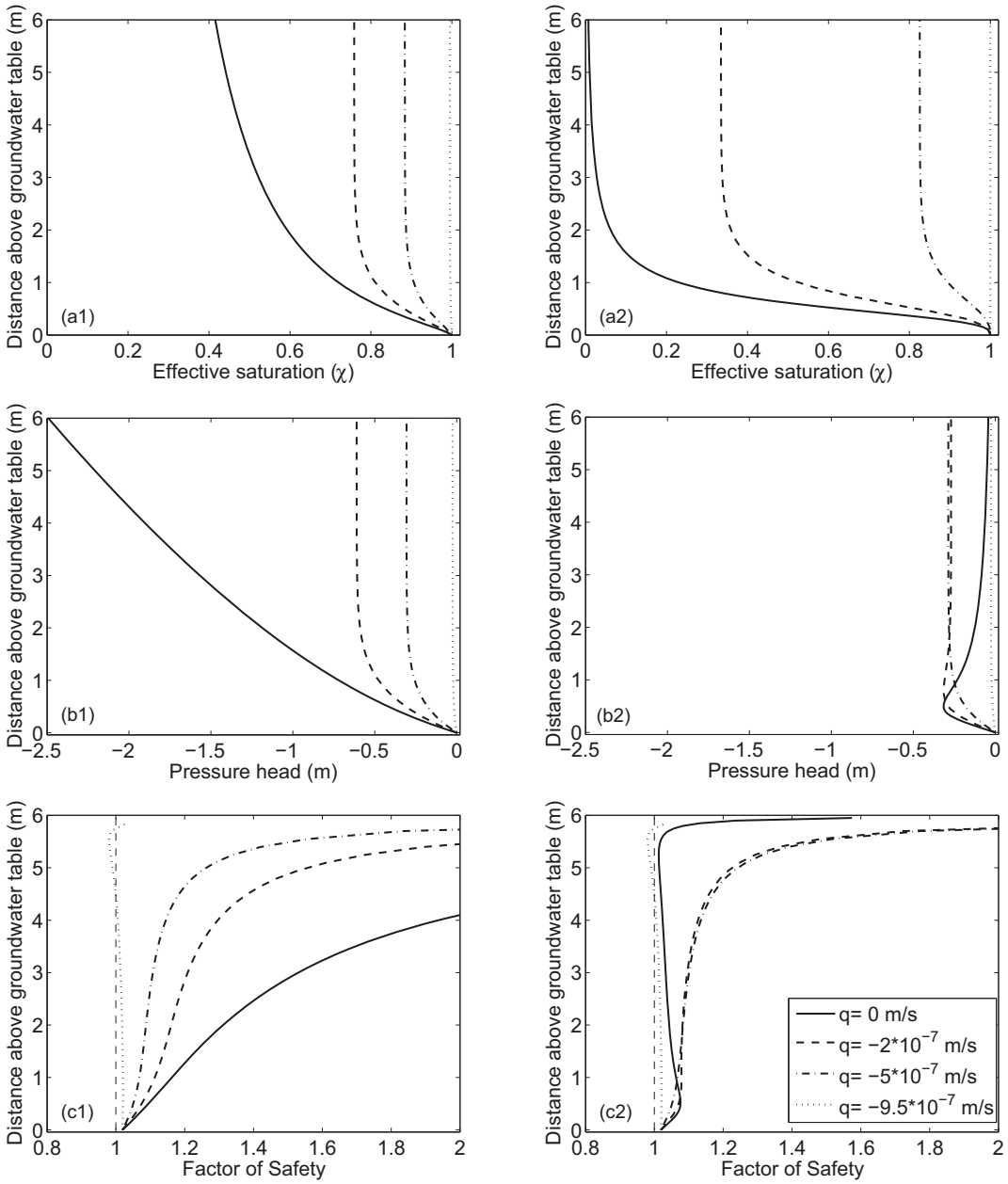

Figure 6.5.: Effect of infiltration flux on the (a1, a2) effective saturation profile, (b1, b2) pressure head profile, (c1, c2) factor of safety profile with different n (n=1.35 in a1-c1, n=3 in a2-c2)

decreases quickly from zero at the groundwater table to a certain value, then it nearly remains constant as the increase of the distance above groundwater table. The corresponding factor of safety profiles are depicted in Figure 6.5 (c1, c2). When n is small, an increase of the negative flux can make the factor of safety profile move towards left, and the weakest location of the slope remains at groundwater table, except for the situation that the negative flux is very large, e.g. q=-$9.5{\cdot}10^{-7}$ m/s, in which case a failed zone can be observed in the zone between 0.1 m and 1.2m under the ground surface, meaning that shallow landslides might be induced under heavy rainfall condition. Figure 6.5 (c2) shows an interesting fact: when the parameter n is large, the factor of safety profile above groundwater level moves towards right with a certain increase of the negative flux, indicating that a proper rainfall can help stabilize the slope above the groundwater table when the parameter n is large. However, as the negative flux keeps increasing, the factor of safety profile moves towards left again. When the negative flux approaches to saturated hydraulic conductivity, the factor of safety profile is similar to the profile with a small parameter n.

6.5.2. Deterministic analysis considering the depth-dependent character

i. Case 2 description

Table 6.2 summarizes the parameters and their value used in case 2. The total thickness of the slope above the groundwater table is 6m, and it is equally divided into 120 layers. The layer is thin enough to produce a reasonable result. The slope with depth-dependent ks is simplified as layered slope with different ks in different layer, however, the ks is constant in each layer. The infinite slope model and the depth-dependent character of ks are shown in Figure 6.1.

Table 6.2.: List of parameters and their value for case 2

Parameters	Definition	Value
ks(m/s)	Saturated hydraulic conductivity	10^{-6}
kk	Slope of vertical influence	0, 0.05, 0.10, 0.15
θ_s	Saturated water content	0.395
θ_r	Residual water content	0
α (kPa^{-1})	SWCC parameter	0.2
n	Empirical fitting parameter	1.35
q (m/s)	Infiltration flux	-5 $\cdot 10^{-7}$
γ_s (kN/m^3)	Soil unit weight	20
c' (kN/m^2)	Effective cohesion	0
ϕ_0 (°)	Effective friction angle at ground surface	29
$d\phi$ (°)	The range of variation of friction angle within the weathering zone	4
z_w (m)	Depth of the weathered zone	0.5
β (°)	Slope angle measured from horizontal	30
dz (m)	Discretization of the slope	0.05
L (m)	Slope depth above the groundwater table	6

ii. Zero pressure head situation

In order to have a basic understanding on the case, the factor of safety profile of the slope with constant ks under saturated condition is plotted in Figure 6.6. The pressure head is zero all over the slope above the groundwater table. Since the cohesion here is zero, the safety factor depends only on the friction angle. It shows that the slope failure can only happen in the top 0.17m of the slope, and the slope underneath is stable at the zero-pressure head situation. However, the slope failure might be induced at a lower location when positive pressure head is generated above the groundwater table, due to the fact that an increase of the pressure head can reduce the effective stress and lead to a reduction of the shear strength. Therefore, two types of failure might exist:

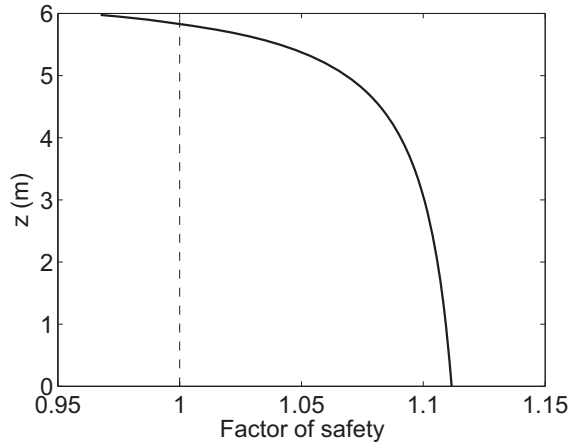

Figure 6.6.: Factor of safety profile of the saturated slope with zero pressure head above the groundwater table

(a) losing matric suction in one layer of the top 0.17m, (b) the generation of positive pressure head beneath the top 0.17m. It is necessary to separate these two types, because the generation of a positive pressure head is crucial to assess the effect of the depth-dependent character of ks on the slope stability analysis. Normally speaking, the top 0.3-0.5m of soil is covered by grass which increases the strength, makes the slope difficult to fail in the top 0.3-0.5m. Therefore, some researchers did not consider the slope failure of the top 0.5m. If we neglect this failure, the slope can always be stable at zero pressure head situation. However, it might fail if the depth-dependent character is considered, because the positive pressure head might be generated.

iii. Steady state infiltration and the infinite slope stability analysis

Effect of the depth-dependent ks on the pressure head profile under steady state infiltration

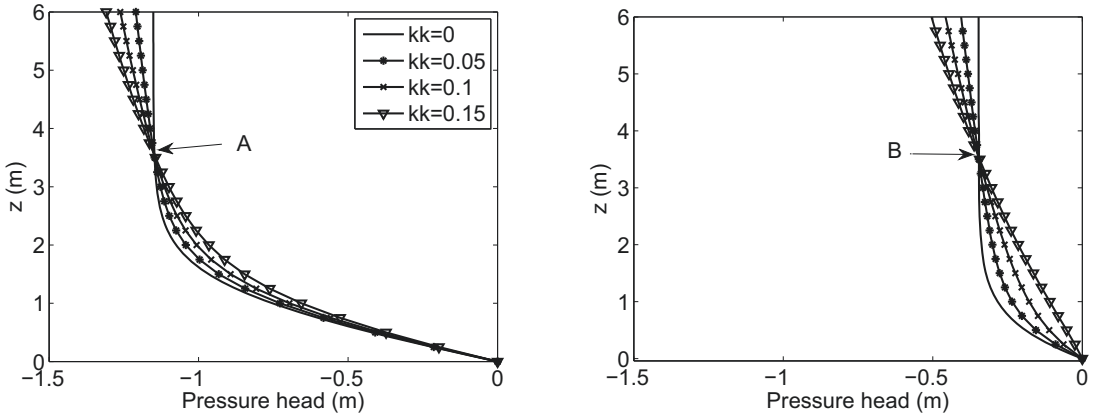

(a) q=-10^{-7} m/s (b) q=-5·10^{-7} m/s

Figure 6.7.: Effect of the depth-dependent ks on the steady-state infiltration with low negative flux

Figure 6.7 shows the effect of the depth-dependent ks on the steady state infiltration at low negative flux cases. It shows that the pressure head with constant ks (kk=0) reduced quickly from zero at groundwater level (z=0m) to a certain value, then it remains constant. For the depth-dependent case (kk≠0), the pressure head keeps reducing with the increase of the elevation. Meanwhile, the pressure head profiles with different kk crossed at a certain depth (at Points A and B in Figure 6.7), divided the profile into the upper and lower segments. In the lower segment, the pressure

head is higher for the slope with a larger kk. This means, comparing with the constant ks case, the pressure head is higher at the same elevation for depth-dependent ks case at the same elevation. In the upper part, the reductions of the pressure heads at all cases are almost linear, and a higher kk can cause a lower pressure head, because the effective saturation is lower for a higher kk case. Comparing these two figures, it can be seen that the amount of fluxes do not affect the overall trend of the pressure head profile, and the differences of the pressure head with different kk at the same elevation does not have a big change. For example, the difference of the pressure head at the surface of the slope is kept to be about 0.15m between case kk=0 and kk=0.15 when the negative flux increases from 10^{-7} m/s to $5{\cdot}10^{-7}$ m/s. It can be concluded that the depth-dependent character of ks has a moderate effect on the pressure head profile, when the negative flux is low.

Since the ks reduces with soil depth when the depth-dependent character is considered, it is inevitable that the positive pressure head is generated when the negative flux is large enough. Some steady state infiltration with high negative fluxes are simulated, as is shown in Figure 6.8. When q=-$7{\cdot}10^{-7}$ m/s, the positive pressure head is firstly generated in the slope with the highest kk (kk=0.15) in the bottom of the slope above the groundwater level, while the pressure head of the slope with a smaller kk is still negative (Figure 6.8a). As the negative flux keeps increasing, the positive pressure head area becomes larger and larger for the slope with the highest kk, and the slope with a lower kk begins to own positive pressure head zone too (Figure 6.8b, c); when the negative flux is large enough, the positive pressure head will be all over the slope for the cases with depth-dependent ks, while the slope with constant ks owns a zero pressure head profile (Figure 6.8d). The positive pressure head can only be generated if the depth-dependent character is considered. Notes that extra flux runs off, so the highest pressure head is zero at the surface of the slope. In all, the depth-dependent ks can significantly affect the pressure head profile when the negative flux is large.

Effect of depth-dependent ks on the factor of safety profile under steady state infiltration

The effect of the depth-dependent character on the factor of safety profile is shown in Figure 6.9 for low negative flux cases. A cross-point (point A or B in Figure 6.9) divides the factor of safety profile into two parts: for the lower part of the slope, a lower factor of safety can be found at the same elevation when the kk of ks is higher. The upper part of the slope shows an opposite trend. A higher negative flux can increase the difference of the factor of safety profiles. Note that, although the factor of safety profile can be affected by the depth-dependent character, the weakest surface is at the bottom of the slope and the factor of safety of the slope is still the same (equals to 1.11) when the negative flux is low.

The factor of safety profile is depicted in Figure 6.10 for the cases with high negative fluxes. When the negative flux is large ($7{\cdot}10^{-7}$ m/s), the weakest surface (point) is no longer at the groundwater table for the case with the largest kk (e.g. at point A for kk=0.15 in Figure 6.10a). However, the slope is still safe because the factor of safety of the slope is still higher than one. As the negative flux increases to $9{\cdot}10^{-7}$ m/s, the slope with the largest kk fails (Figure 6.10b) firstly. Meanwhile, the weakest surface is no longer at the groundwater table in the slope with kk=0.10 (at point B). If the negative flux keeps increasing, the slope with a lower kk would fail too (e.g. kk=0.1 in Figure 6.10c). Finally, all slopes fail when the negative flux is large enough (Figure 6.10d). However, for the constant ks case, the slope failure is induced by losing the negative pressure head, and the failure surface is less than 0.17m under the slope surface, while the slope failure is caused by the positive pressure head with a lower failure surface for the depth-dependent ks case. It should be noted that the failure zone, where the safety factor is smaller than one, is longer for the slope with a higher kk, as is shown in Figure 6.10d. It can be concluded that the depth-dependent character of ks plays a key role on the slope failure, and has a significant influence on the factor of safety of the slope when the negative flux is high.

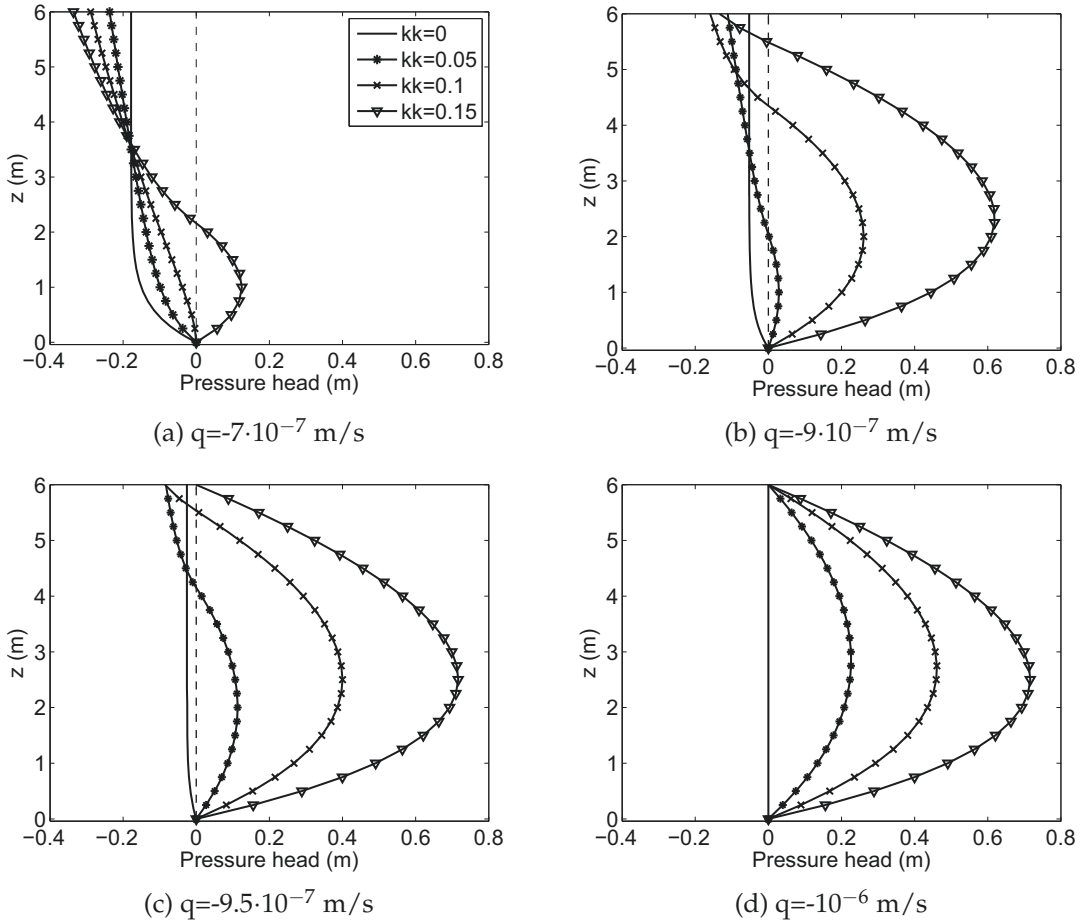

(a) q=-7·10^{-7} m/s (b) q=-9·10^{-7} m/s

(c) q=-9.5·10^{-7} m/s (d) q=-10^{-6} m/s

Figure 6.8.: Effect of depth-dependent ks on the steady-state infiltration with high negative flux

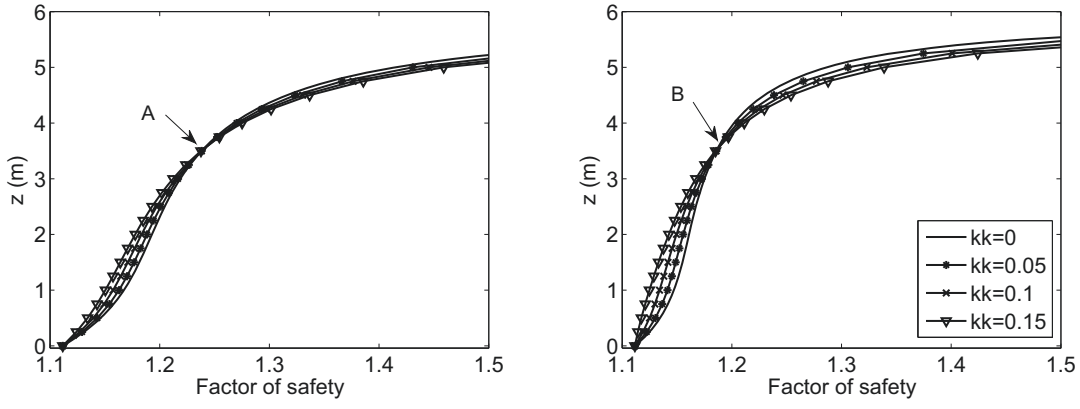

(a) q=-3·10^{-7} m/s (b) q=-5·10^{-7} m/s

Figure 6.9.: Factor of safety of an infinite slope during steady state infiltration with depth-dependent ks and low negative flux

In summary, when the negative flux is low, the depth-dependent character of ks has a moderate effect on the pressure head profile, and has a low influence on the stability of the slope during steady state infiltration. However, when the negative flux is high (near to the mean of ks), the depth-dependent character has significant influences on both the pressure head profile and the stability of the slope, because positive pressure head can be generated in the slope when the depth-dependent character is considered. This positive pressure head can induce the slope failure with a low failure surface. Without considering the depth-dependent character can overestimate the stability of the slope during the steady state infiltration when the negative flux is high.

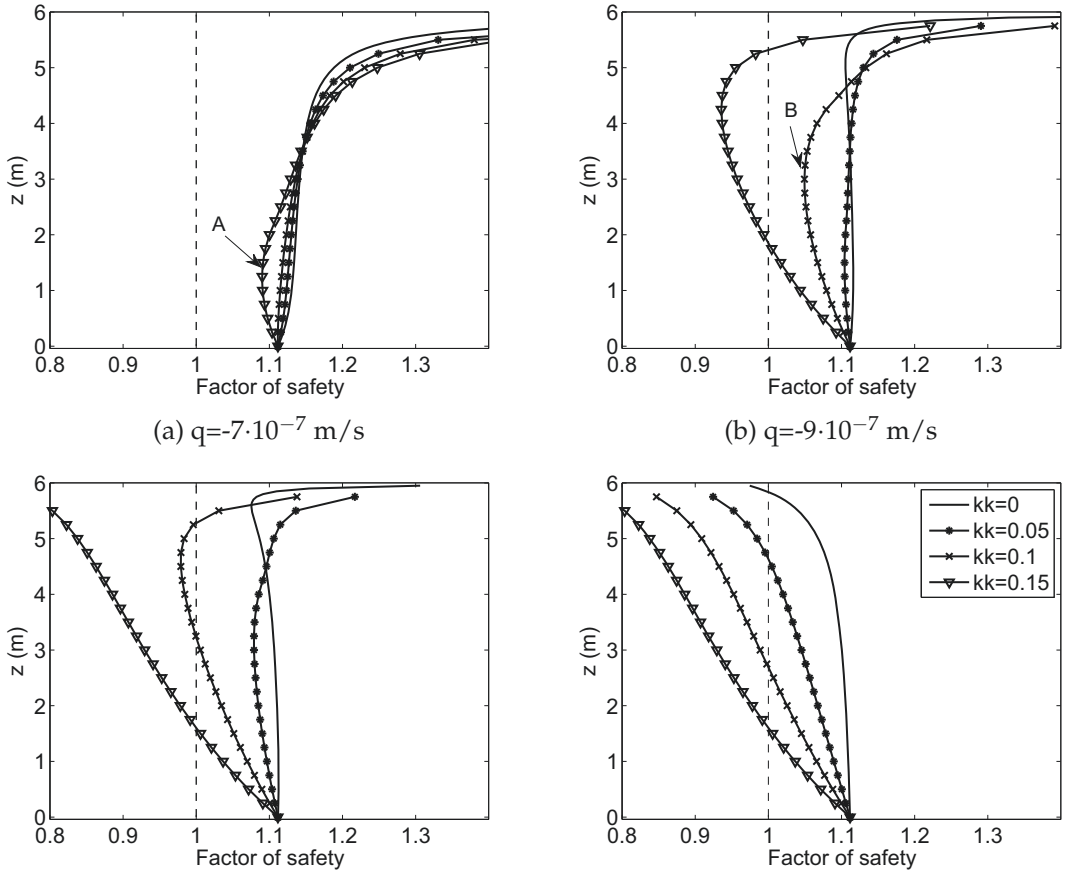

(a) q=-7·10^{-7} m/s (b) q=-9·10^{-7} m/s

(c) q=-9.5·10^{-7} m/s (d) q=-10^{-6} m/s

Figure 6.10.: Factor of safety profile of the infinite slope during steady state infiltration with depth-dependent ks and high negative flux

iv. Transient state infiltration and infinite slope stability analysis

In order to have a basic understanding of the transient infiltration and the corresponding factor of safety profile of the infinite slope during transient infiltration, the changes of the pressure head profile and factor of safety (FS) profile during deterministic transient infiltration with constant ks are simulated (|q|/ks=0.5), and the results are depicted in Figure 6.11. The depth-dependent character is not considered in this case. It can be seen that, as the infiltration continues, the wetting front goes deeper, and the FS decreases in the wetted zone. However, the minimum FS is at the bottom of the slope. It can also be seen that the pressure head at 20 days approaches to the pressure head at steady state. Meanwhile, this negative infiltration flux is not large enough to induce a slope failure.

Effect of the depth-dependent ks on the pressure head profile during transient infiltration

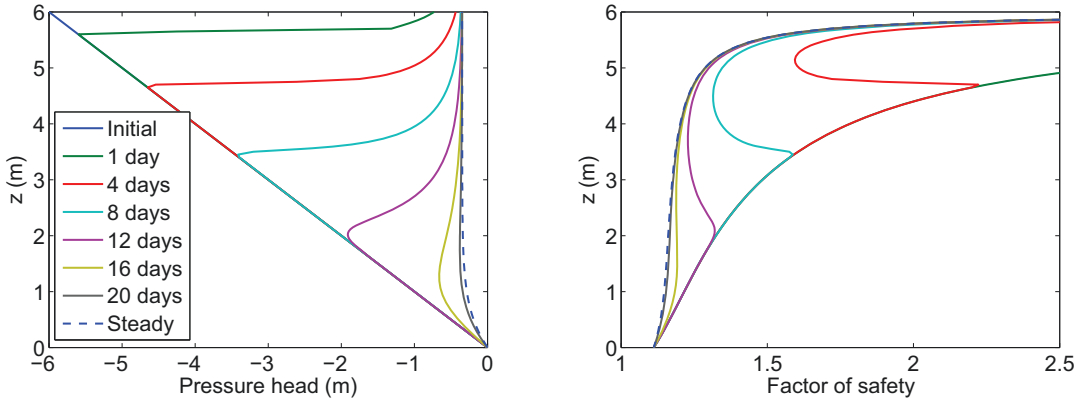

(a) (b)

Figure 6.11.: (a) Pressure head profile and (b) factor of safety profile during transient seepage from deterministic analysis with constant ks

The pressure head profile under transient state infiltration with |q|/ks=0.5 is depicted in Figure 6.12, considering the effect of the depth-dependent character of ks. A cross-point (e.g. Point A) can be found for the pressure head profile in the wetted zone with different kk, dividing the wetted zone into the upper and lower parts. A higher kk can cause a slightly lower pressure head in the upper part, and a higher pressure head in the lower part. Figure 6.12 also shows that the slope with a higher kk has a lower wetting front during transient infiltration. The relative differences of the wetting fronts become larger at the early stage (0-12 days) of the infiltration, and then the difference becomes smaller as the infiltration continues. No positive pressure head is generated because the negative flux is smaller than the minimum ks.

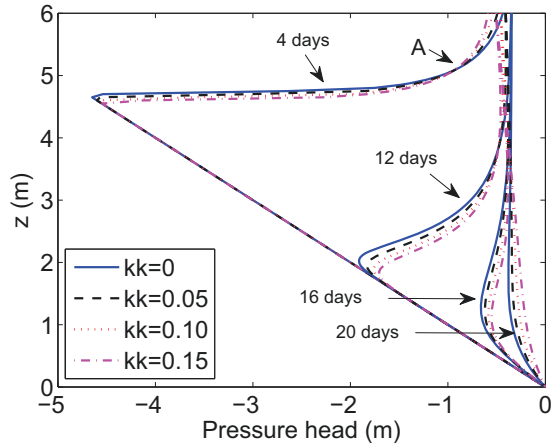

Figure 6.12.: Effect of the depth-dependent ks on the pressure head profile during transient state infiltration

Figure 6.13 is the pressure head profile during transient infiltration with high negative fluxes. It shows that, as the negative flux increases, the wetting front is lower in the same time span. While, the pressure head profile with a high negative flux is similar to the profile with a low negative flux when the pressure head profile is negative. However, as the infiltration duration increase, the positive pressure head begins to be generated for the case with the highest kk (kk=0.15 at 20 days in Figure 6.13a). As the negative flux increases, the positive pressure head begins to be generated for the case with a lower kk, and the pressure head is higher at the same elevation for the case

with a higher kk at the late stage of the transient infiltration. Notes that the wetting front of the slope with kk=0 is the lowest when the negative flux equals to the mean ks (Figure 6.13d), which is different from the other cases, because the initial boundary condition is different. In this situation, the head boundary condition is used, while flux boundary condition is adopted for slopes with kk>0. Moreover, it can be seen that the positive pressure head can only be generated at the late stage of the infiltration. Note that, for the depth-dependent ks case, different depth has different ks, which means the infiltration rates are different. Therefore, if the slope fails, the failure time should be different, this will be discussed in detail later.

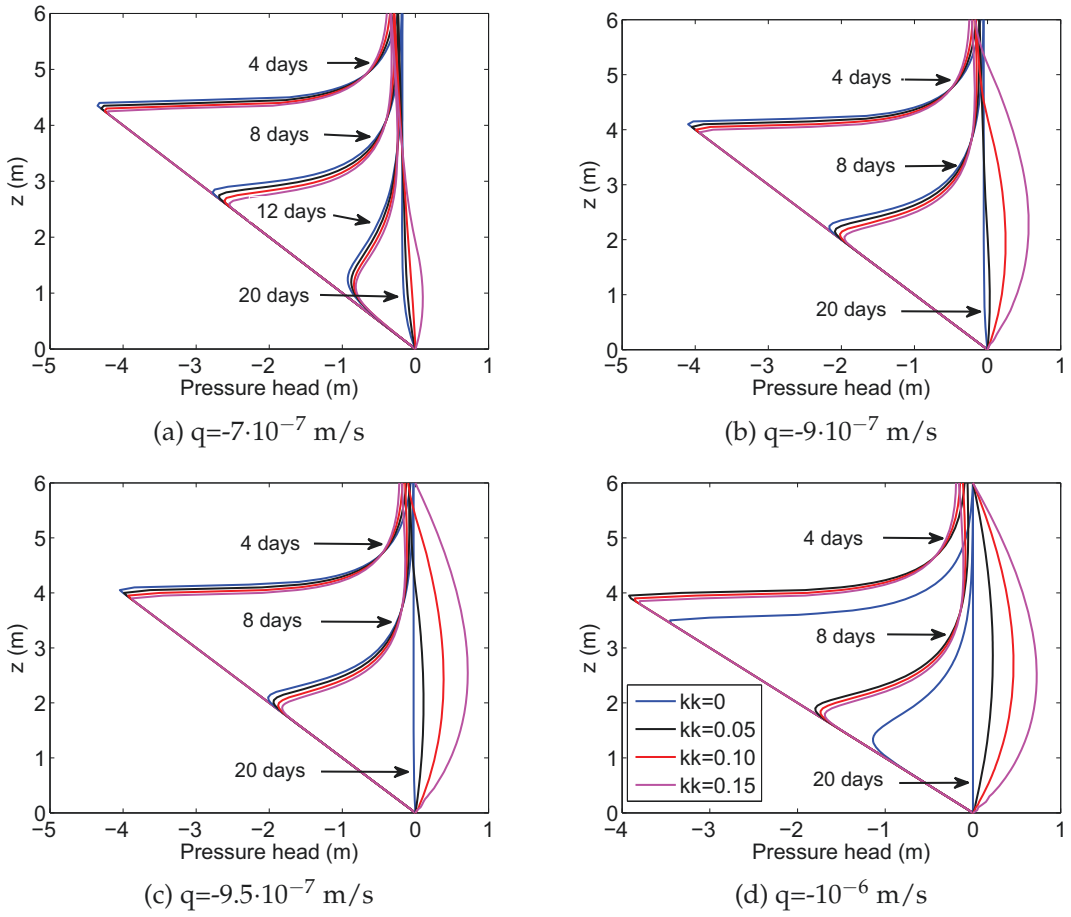

(a) q=-7·10^{-7} m/s (b) q=-9·10^{-7} m/s

(c) q=-9.5·10^{-7} m/s (d) q=-10^{-6} m/s

Figure 6.13.: Pressure head profile at transient infiltration from deterministic analysis

Effect of the depth-dependent character on the factor of safety profile during transient infiltration

The safety factor profiles during transient infiltration with high negative flux are depicted in Figure 6.14. It shows that kk has a small effect on the factor of safety in the wetted zone, if the infiltration duration is not too long (0-12 days), when the positive pressure head is not generated (Figure 6.14a). Meanwhile, the weakest surface is always at the groundwater table. As the infiltration duration reaches to the late stage, the weakest surface rises up from the groundwater table for the slope with the highest kk of ks, because of the effect of the positive pressure head (e.g. kk=0.15 at 20 days in Figure 6.14a). However, the slope is still safe because the safety factor of the slope is larger than one. When the negative flux is high enough (close to the ks), the kk has a significant influence on the factor of safety profile at the late stage of the transient infiltration, in which the slope fails firstly for the case with the highest kk, as is shown in Figure 6.14b (kk=0.15 at 20 days).

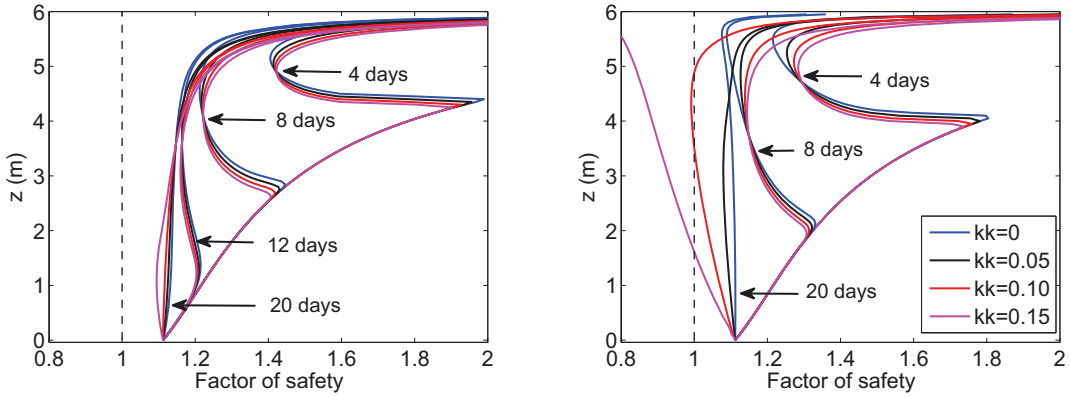

(a) q=-7·10^{-7} m/s (b) q=-9.5·10^{-7} m/s

Figure 6.14.: Safety factor profiles during transient infiltration from deterministic analysis

Failure time discussion of the slope with depth-dependent ks during transient infiltration

Figure 6.15a and b are the pressure head profiles and the factor of safety profiles of the slope at the failure time respectively during transient infiltration with q=-10^{-6} m/s. The failure time here means the duration from the beginning of the infiltration to the time that the slope fails. For depth-dependent ks case (kk≠0), Figure 6.15b shows that the slope with a higher kk fails earlier during transient infiltration, and the failure surface is lower. The reason is shown in Figure 6.15a. When kk is large, the generated positive pressure head in a low elevation is high enough to induce the slope failure. However, when kk is low, the generated positive pressure head is low, so the slope failure needs to be assisted by the reduction of the friction angle. Since the friction angle decreases with the increase of the elevation, the failure surface is higher. For the constant ks case (kk=0), the slope failure is caused by the reduction of the negative pressure head, rather than the generation of the positive pressure head. When the infiltration duration increases to a certain level, the soil near the ground surface reaches to the saturated condition. Therefore, the negative pressure head is reduced, and the slope failure is induced. When the failure of the top 0.5m is neglected, the slope is always stable. However, the slope could be induced if the depth-dependent character is considered. Therefore, the stability of the slope could be overestimated (slope failure in the top 0.5m is not considered) if the depth-dependent character is not taken into account.

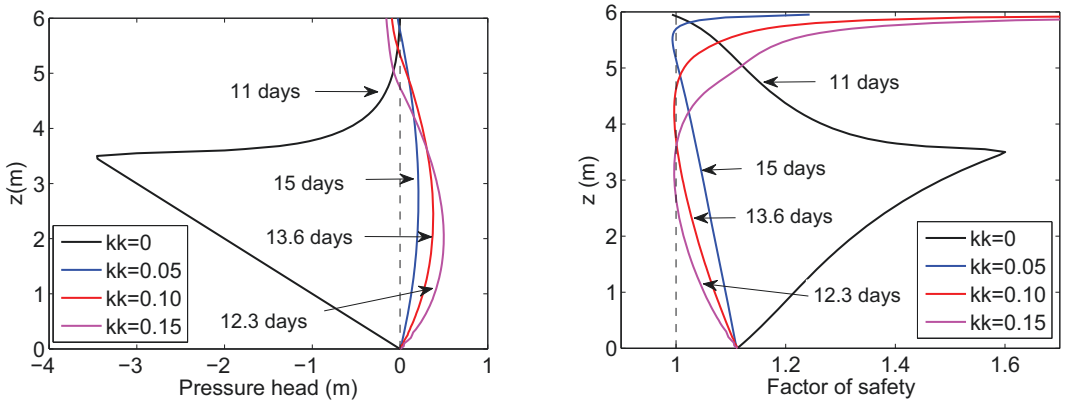

(a) (b)

Figure 6.15.: (a) Pressure head profile, and (b) Factor of safety profile of the slope at the failure time considering depth-dependent ks during transient infiltration (q=-10^{-6} m/s)

6.6. Conclusion of this chapter

In this chapter, some parametric studies are carried out, meanwhile the effect of the depth-dependent ks on the infiltration and the slope stability during the infiltration is highlighted. The key results are:

- Through the parametric study, it is found that the empirical fitting parameter n of the SWCC controls the shape of the effective saturation profile, the pressure head profile, and the factor of safety profile, while the SWCC parameter α controls the magnitude of these profiles. Meanwhile, a low negative flux can help stabilize the slope above the groundwater table in the case with a large n.

- When the negative flux is low, the depth-dependent ks has a moderate effect on the pressure head profile and has a low influence on the stability of the slope during steady state infiltration. However, when the negative flux is high (approaches to the mean of ks), the depth-dependent ks has a significant influence on both the pressure head profile and the stability of the slope. This is because the positive pressure head can be generated in the slope with a depth-dependent ks, which can cause the slope failure with a low failure surface. Neglecting the depth-dependent character of ks can overestimate the factor of safety during the steady state infiltration when the negative flux is high.

- During the transient state infiltration, a cross-point can be found dividing the pressure head profile or factor of safety profile in the wetted zone into two parts. In the upper part, the pressure head is smaller for the case with a higher kk. The lower part shows an opposite trend. The corresponding factor of safety in the wetted zone is higher for a higher kk case in the upper part, and the lower part shows an opposite trend too. If the negative flux is high, the positive pressure head can be generated at the late stage of the transient infiltration when the depth-dependent character is considered. The failure time of the slope is related to the depth-dependent character of ks. For the case with a greater depth-dependent character, the slope fails earlier and the failure surface is lower.

7. Probabilistic infinite slope stability analysis during infiltration considering the variation of ks

In this chapter, the stochastic infinite slope stability analysis is carried out during infiltration, so as to evaluate the effect of the variability of saturated hydraulic conductivity (ks) on the slope stability analysis during both steady state and transient state infiltration. The ks is assumed to be the only stochastic variable. According to former studies (Hydraulic, 2008; Freeze, 1975; Sudicky, 1986), it follows a lognormal distribution. Both stationary and non-stationary random field are considered. The stationary random fields are used to evaluate the effect of the standard deviation of ks and the spatial correlation length (SCL) of ln(ks) on both the infiltration and the slope stability. The non-stationary random fields are adopted to highlight the effect of the depth-dependent character of the stochastic parameters of ks, including the mean and standard deviation of ks, and the spatial correlation length of ln(ks), on both the infiltration and the slope stability. Detail information about the generation of each random field is elaborated in chapter 4. The mean, the standard deviation, and the spatial correlation length are all considered to reduce linearly with depth when the depth-dependent character is considered.

7.1. Reliability estimation

The factor of safety profile FS(z) varies from one realization to another during stochastic infinite slope stability analysis. Since the ks is the only variable, the limit state function can be formulated as,

$$g(\mathbf{x}) = FS_{min}(\mathbf{x}) - 1.0 = \min_{x}(FS(z, \mathbf{x})) - 1.0 \tag{7.1}$$

in which, **x** represents a set of random variables used to simulate the random field of ks, and z is the elevation (distance to the groundwater level) here. Two cases will be used later, $0 \leq z < L$, and $0 \leq z \leq L - 0.5m$ (L is the length of the slope). For most cases, only $0 \leq z \leq$ L-0.5m is considered to calculate the probability of failure of the slope, since the failure unlikely happens within the top 0.5m of the slope, because of the vegetation effect or roots cohesion. $0 \leq z \leq$ L is also used in some cases to compare the results.

7.2. Case description

The physical model of the infinite slope (Figure 7.1) adopted here is the same as is used in Chapter 6. The slope of vertical influence (kk) is also used to express the depth-dependent character. The parameters and their values are listed in Table 7.1. The ks is assumed to be the only stochastic variable. The mean of ks is set to be 10^{-6} m/s, while the preset (deterministic) flux is -5·10^{-7} m/s, where negative value means infiltration. Our interest is to check if the variation of ks has a significant effect on the slope stability during both the steady state infiltration and the transient state infiltration. 5000 realizations of the random field are used in each situation during the steady

state infiltration, because 5000 realizations are enough to produce a stable result. Meanwhile, 1500 realizations are adopted in each situation during the transient infiltration, since the simulation of transient infiltration is time-consuming. These two numbers of the realizations were used by some former researchers (Santoso et al., 2011) to simulate the steady state and transient infiltration, respectively. Remember that a higher negative pressure head leads to a higher shear strength, so as to produce a higher factor of safety and lower probability of failure (Pf). The pressure head profile, the factor of safety profile, the probability of failure, the location of the critical failure surface, and the true flux flowing through the slope during infiltration are studied.

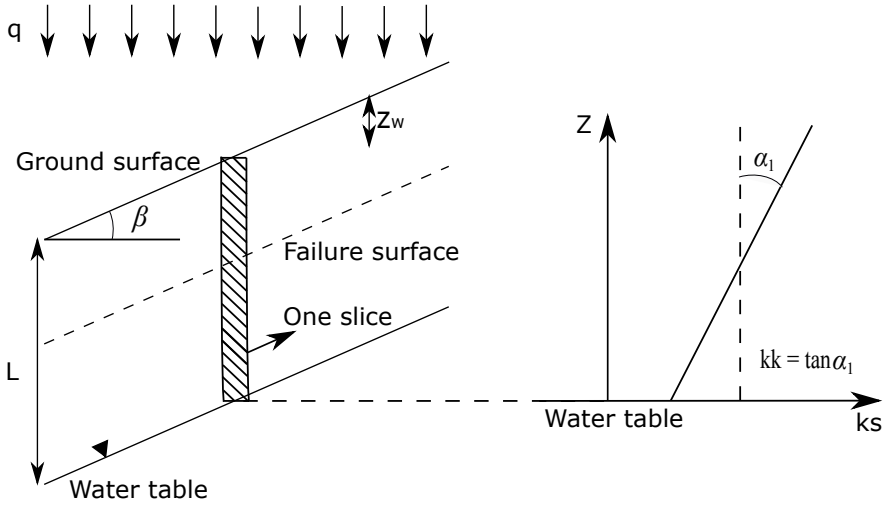

Figure 7.1.: The infinite slope model with a weathered mantle

Table 7.1.: List of parameters and their value used in Chapter 7

Parameters	Definition	Value
ks (m/s)	Saturated hydraulic conductivity	10^{-6}
kk	Slope of vertical influence	0, 0.05, 0.10, 0.15
θ_s	Saturated water content	0.395
θ_r	Residual water content	0
α (kPa^{-1})	SWCC parameter	0.2
n	Empirical fitting parameter	1.35
q (m/s)	Preset infiltration flux	$-5 \cdot 10^{-7}$
γ_s (kN/m^3)	Soil unit weight	20
c' (kN/m^2)	Effective cohesion	0
ϕ_0 (°)	Effective friction angle at ground surface	29
$d\phi$ (°)	The range of variation of friction angle within the weathering zone	4
z_w (m)	Depth of the weathered zone	0.5
β (°)	Slope angle measured from horizontal	30
dz (m)	Discretization of the slope	0.05
L (m)	Slope depth above the groundwater table	6

According to Santoso et al. (2011), it is not sufficient to conclude that the variation of ks which produces a higher mean of pressure head will always produce higher pressure heads. The quantiles or the distribution of the pressure head profile is very helpful to understand the significance of the variation of ks on a rainfall-induced landslide. Therefore, the quantile profiles of both the pressure head and the factor of safety are adopted, rather than using the mean profiles, in the following contents.

7.3. Probabilistic infinite slope stability analysis during infiltration without considering the depth-dependent character

In this section, the stationary random field without considering the depth-dependent character of the stochastic parameters of ks is adopted so as to have a basic understanding of how the variation of ks affects the infinite slope stability during infiltration. The effect of the coefficient of variation (CV) of ks and the SCL of ln(ks) are highlighted.

7.3.1. Effect of the variation of ks on the slope stability under steady state infiltration

In order to have a basic understanding about the effect of the variation of ks, on the infinite slope stability analysis during steady state infiltration, the stochastic infinite slope stability analysis is carried out with mean of ks -10^{-6} m/s, standard deviation of ks 10^{-6}, and spatial correlation length of ln(ks) 1m. The pressure head profile and factor of safety profile are plotted and, compared with the deterministic situation respectively, without considering the variation of ks. The results are shown in Figure 7.2. Q25%, Q50% (median) and Q75% profiles are obtained by taking respectively the 25%, 50% and 75% quantiles of the pressure head profile and factor of safety profile at each elevation. The factor of safety profile here means the relation between the factor of safety at the bottom of each layer and the corresponding elevation. It can be seen that when the variation of ks is taken into consideration, the pressure head profile of the infinite slope varies in a large range, and a certain percentage of the pressure head profile is with positive pressure head. However, for the deterministic case, the pressure head profile is a constant curve without any fluctuation, and the pressure head is negative all over the slope above the groundwater level in this case (Figure 7.2a). Similarly, the factor of safety profile fluctuates in a certain range, and a certain percentage of the factor of safety of the slope (FS_{min}) is lower than one when the variability of ks is taken into consideration, e.g. Q25% factor of safety profile in Figure 7.2b. This means there is at least 25% probability that the slope fails in the stochastic analysis. However, the slope is stable during the deterministic analysis when the variation of ks is not considered under steady state infiltration (Figure 7.2b). Therefore, the variation of ks can significantly affect the slope stability under steady state infiltration.

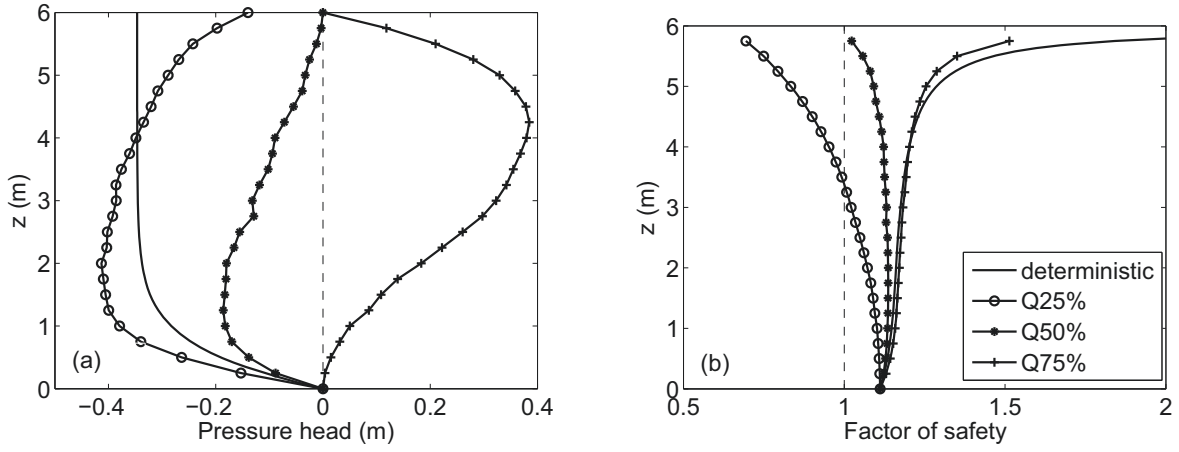

Figure 7.2.: Effect of the variation of ks on the quantiles of the (a) pressure head profile, and (b) factor of safety profile, during steady state infiltration

7.3.2. Effect of the CV of ks on the slope stability under steady state infiltration

The effect of the coefficient of variation (CV) of ks on both the steady state infiltration and slope stability are evaluated in this section. According to Srivastava et al. (2010), the CV of ks is in the range of 60%-90%. Here, it is assumed to be 0.5, 1.0, and 1.5 to represent a low, high, extremely high variation of ks, respectively. The spatial correlation length (SCL) of ln(ks) is kept to be 1m. The values of the other parameters are listed in Table 7.1.

Pressure head profile and factor of safety profile

Figure 7.3a is the quantile estimation of the pressure head profile with different CV of ks. The

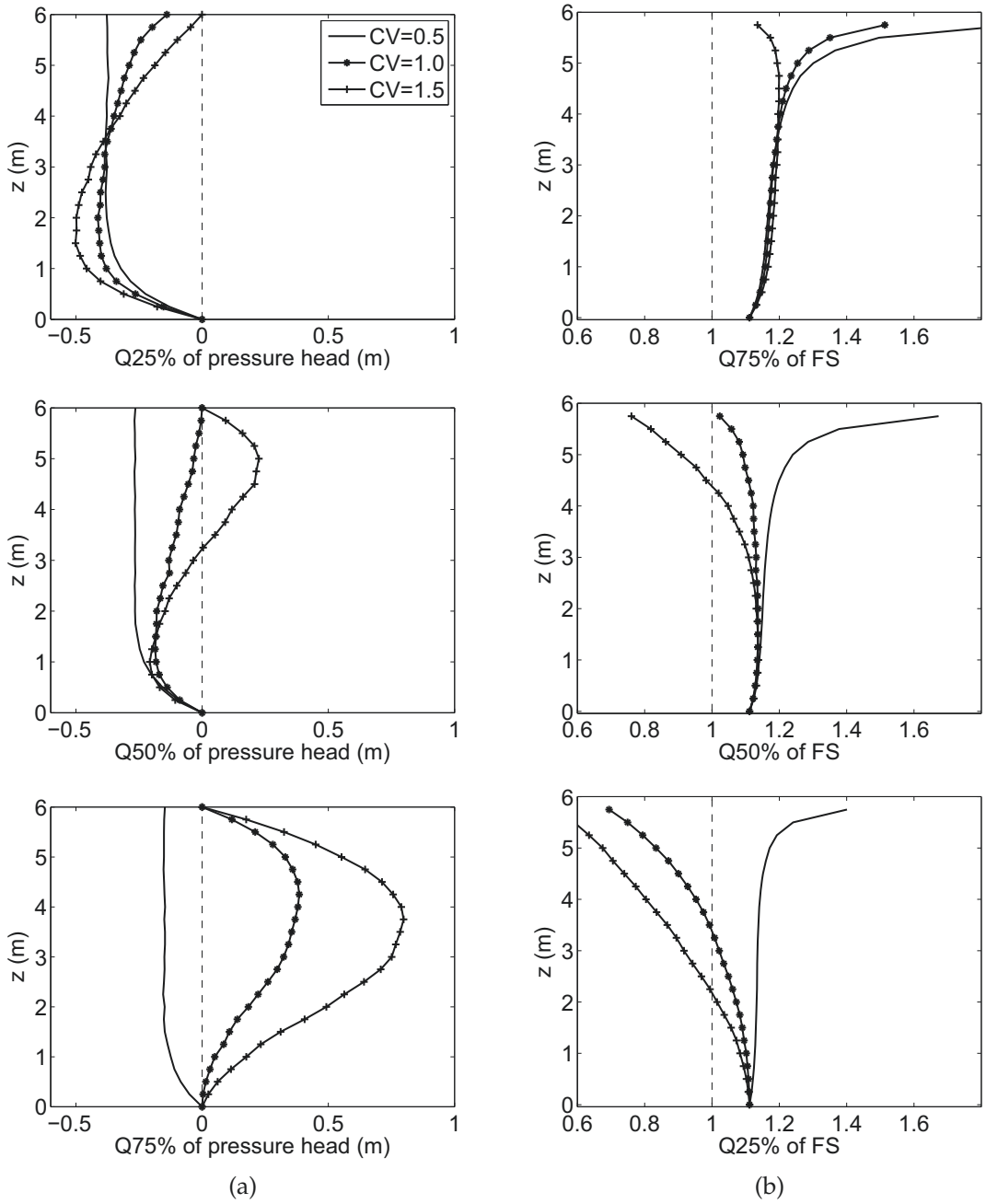

Figure 7.3.: Effect of the CV of ks on the quantiles of (a) pressure head profile and, (b) factor of safety profile, during steady state infiltration

Q25% profile of pressure head in Figure 7.3a shows that a higher CV can cause a higher pressure head in the upper part of the slope, and a lower pressure head in the lower part of the slope. Because a higher CV can cause a more dramatic variation of ks. Therefore, there is more chance that the low permeable layer is generated in the upper part of the slope. These low permeable layers can cause the generation of the positive pressure head at the top part of the slope, so as to reduce water to infiltrating into the lower layer. Therefore, the lower part of Q25% pressure head is smaller, and the upper part is higher for the case with a higher CV. As the quantile increases, the upper part becomes larger and larger, until there is no lower part. Meanwhile, it can be seen at Q50% profile of pressure head from Figure 7.3a that there is more chance that the positive pressure head is generated for the slope with the highest CV (CV=1.5), since the positive pressure head is shown at Q50% pressure head profile. As the quantile reaches to Q75%, all the slope above the groundwater level is the positive pressure head zone for the cases with a high and an extremely high CVs. This is because a higher CV of ks also means more chances that the low ks layers are generated in the lower part of the slope. When the flux reaches to these layers, extra water can perch on the top of the layer, causing the generation of positive pressure head, and the positive pressure head zone can be accumulated. Therefore the positive pressure head zone becomes larger as the quantile increases. However, the slope with a small CV does not have a positive pressure head zone, because there is less chance for the generation of the low permeable layer.

Figure 7.3b is the quantile estimation of the factor of safety profile with different CV of ks. It can be seen that, for Q25% and Q50% (median) profiles, a higher CV of ks can reduce the factor of safety (FS) at all elevations above the groundwater table. For Q75% profile, a higher CV could cause a smaller FS in the upper part of the slope, and a slightly higher FS in the lower part of the slope. The reason can be easily concluded through the pressure head profiles from Figure 7.3a. Meanwhile, it shows clearly in Q25% and Q50% profiles that the failure zone (area where the FS<1) is longer for a higher CV case at the same quantile situation, which means the slope can fail in a wider area. Therefore, there is more chance that the slope with a higher CV fails during the steady state infiltration.

Probability of failure

Figure 7.4 shows the effect of the CV of ks on the probability of failure (Pf) of the slope. The Pf is higher when the critical failure surface at the top 0.5m is taken into consideration, and the difference becomes slightly larger as the increase of CV when the Pf is compared with and without considering the top 0.5m. As mentioned before, the slope failure seldom locates in the top 0.5m of

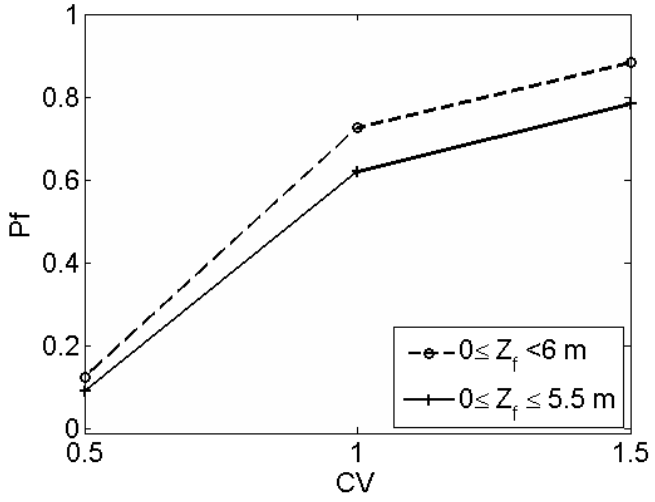

Figure 7.4.: CV of ks VS Pf with and without considering the failure in top 0.5m of the slope

a slope. Therefore, the slope failure without considering the top 0.5m is focused on for most of the following works. It can be seen in Figure 7.4 that the probability of failure increases significantly with the increase of CV of ks. The Pf is only 10% when the CV is 0.5, it increases quickly to about 80% when the CV reaches to 1.5. Therefore, an increase of the CV of ks can significantly increase the probability of failure during steady state infiltration.

Crictical failure surface

Since 5000 realizations of the random field are used to investigate the stability of the infinite slope, some slopes are stable, while some slopes fail. If it fails in one realization, where is the critical failure surface? Does the CV affect the elevation of the critical failure surface? Here the critical failure surface means the location with a minimum factor of safety of each failed slope. The critical failure surface might be in several locations in one realization of the random field. In this situation, the lowest location is taken into consideration. Figure 7.5 shows the effect of the CV on the frequency of the elevation of the critical failure surface. It can be seen that the overall trends are similar. Most of the critical failure surface locates at the top area of the slope (slope failure within the top 0.5m is not considered) no matter the change of CV. However, as the increase of CV, the probability of failure increases dramatically. Meanwhile, the failure zone becomes longer as the increase of CV.

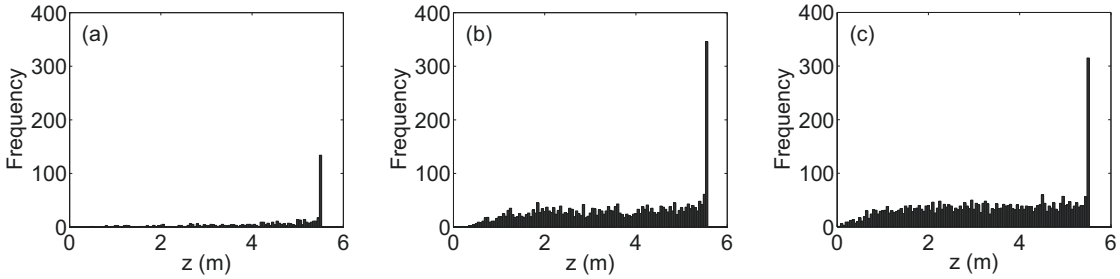

Figure 7.5.: Histograms of the elevation of the critical failure surface at (a) CV=0.5, (b) CV=1.0, (c) CV=1.5

True flux

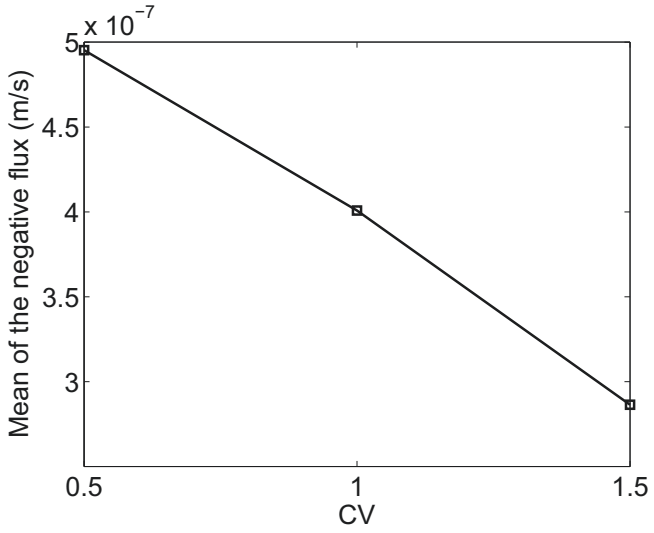

Figure 7.6.: Effect of the CV of ks on the mean of the true negative flux

Figure 7.6 shows the effect of the CV of ks on the true negative flux. Although the preset negative

flux is $5{\cdot}10^{-7}$ m/s, the true negative flux infiltrated into the slope is a little bit smaller when the CV of ks is 0.5. As the CV of ks increases, the mean of the negative flux keeps reducing. This is because, when the CV of ks is larger, there is more chance that the low permeable layers are generated, and more water is blocked, and then runs off from the surface of the slope.

In summary, the CV of ks can significantly affect the steady state infiltration and the slope stability during infiltration. An increase of CV can increase the chance of the low permeable layer generation, so as to: (i) increase the chance of the positive pressure head generation, (ii) reduce the mean negative flux, (iii) increase the probability of failure, and (iv) increase both the failure zone and the chance that the slip surface fails at each elevation.

7.3.3. Effect of the SCL of ln(ks) on the slope stability under steady state infiltration

In this section, the effect of the spatial correlation length (SCL) of ln(ks) on the slope stability analysis under steady state infiltration is evaluated without considering the depth-dependent character. The CV of ks is kept to be 1.0.

Pressure head profile and factor of safety profile

The quantiles of the pressure head profile are depicted in Figure 7.7a, so as to evaluate the effect of the SCL of ln(ks) on the pressure head profile of the slope during steady state infiltration. For the Q25% profile, the pressure head is lower for a higher SCL case, except for the SCL=10000m case, in which the slope in each realization can be regarded as a homogenous slope. For the Q50% profile, the lower part of the pressure head profile follows the trend of Q25% profile, however, for the upper part of the pressure head profile (rectangular area in Figure 7.7a), a moderate SCL (equals to 0.4m here) can cause the highest pressure head, while a higher or lower SCL would cause a lower pressure head. For the Q75% profile, a moderate SCL of 1m can cause the highest pressure head all over the slope. Note that the moderate SCL, which can cause the highest pressure head, is different at different quantile situation.

However, what we are interested in is the situation when the positive pressure head is generated, because this is the key reason that the slope fails. So the generation of the low permeable layers is very important. As described in chapter 2, the SCL can influence the fluctuation of the random field in two opposite ways through both the variance reduction and the correlation matrix. A moderate SCL can make the random field have the greatest fluctuation, so as to help to generate more low permeable layers. This is why a moderate SCL can produce the highest pressure head in Q75% profile.

Figure 7.7b shows that the longest failure zone can be found when the SCL of ln(ks) is moderate (equals to 1.0m here) in the case of Q25% factor of safety profile, and a higher or lower SCL could reduce the size of the failure zone. Meanwhile, the smallest factor of safety can be found when the SCL equals to 0.4m in the case of Q50% factor of safety profile. In the case of Q75% factor of safety profile, the factor of safety is higher for a larger SCL case at the same elevation above the groundwater table, and the weakest surfaces always lie on the groundwater table. This result can be easily conducted through the pressure head profiles from Figure 7.7a.

Probability of failure

Figure 7.8 shows that, if the failure at the top 0.5m of the slope is not taken into consideration, the probability of failure increases from about 0.5 to 0.65 when the SCL of ln(ks) increases from 0.1m to 0.4m, then the Pf keeps reducing as the SCL increases. If the SCL is large enough, the Pf reduces to zero. When the slope failure of the top 0.5m is considered, the Pf increases to its peak and then decreases till it reaches to a relatively stable level. The Pf is higher comparing with the

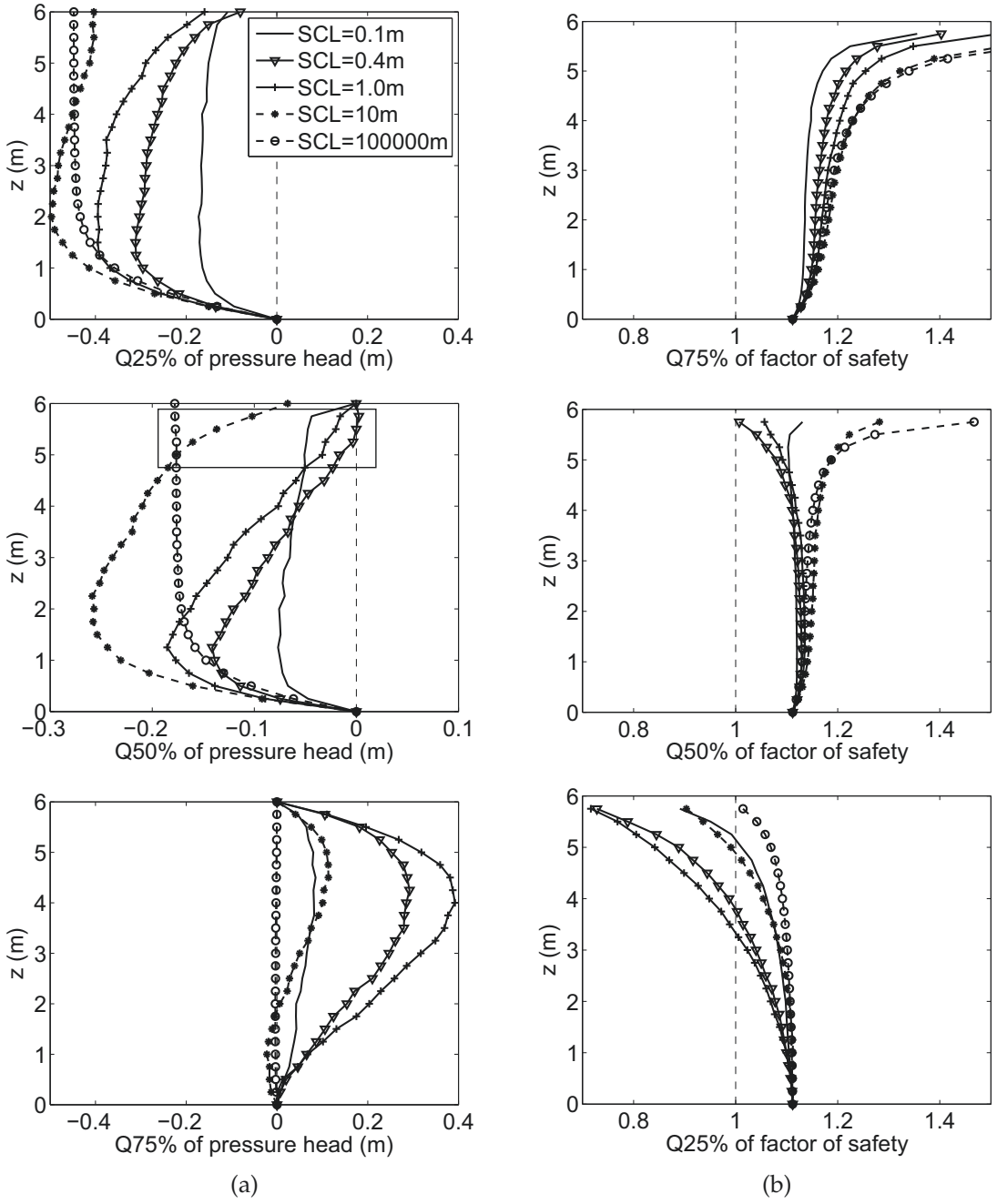

Figure 7.7.: Effect of the spatial correlation length (SCL) of ln(ks) on the pressure head profile of the slope during steady state infiltration

Pf without considering the failure of the top 0.5m. Note that for the case with a very high SCL case, all the failure surface is in the top 0.5m of the slope. This is reasonable, because when the SCL is large enough, the slope approaches to a homogeneous slope without any variation in each realization, so no positive pressure head zone could be generated in the slope, and the slope failure is caused by the reduction of the negative pressure head. Note that, although the Q75% pressure head profile in Figure 7.7a shows the slope with the SCL of 1m has the highest positive pressure head, the highest Pf here is at the case with SCL=0.4m. One reason is that the true flux is the lowest when SCL=1m (see Figure 7.10), and this low true flux can reduce the chance of the positive pressure head generation.

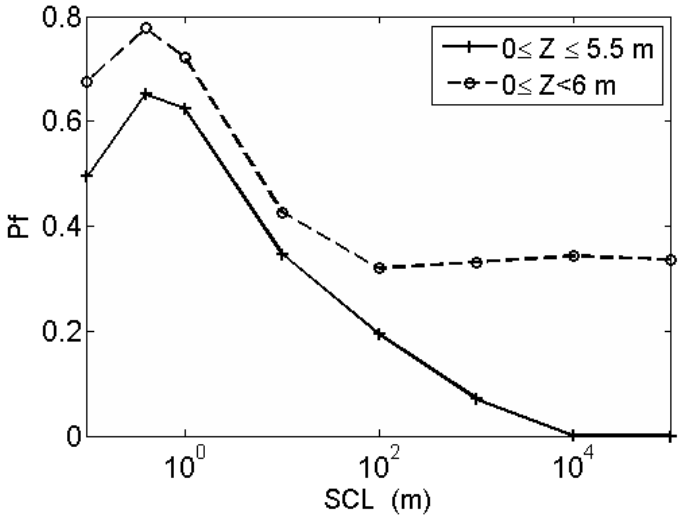

Figure 7.8.: Effect of the spatial correlation length of ln(ks) on the probability of failure during steady state infiltration

Depth of the critical failure surface

Figure 7.9 shows that most of the slope failure happens in the top area of the slope (the failure within the top 0.5m is not considered) under different SCL cases. It can be seen that the slope with a moderate SCL has the largest frequency that the failure happens in the top area of the slope, meanwhile, it also owns the longest failure zone.

True flux

Figure 7.10 shows that the SCL of ln(ks) can significantly influence the true flux. Although the preset negative flux is $5 \cdot 10^{-7}$ m/s, the mean of true negative flux reduces quickly from $4.64 \cdot 10^{-7}$ m/s to $4.04 \cdot 10^{-7}$ m/s when the SCL increases from 0.1m to 1m, then, the mean of true negative flux increases slowly as the SCL keeps increasing. This is because the random field owns the highest fluctuation when the SCL is at the a moderate level.

In summary, the spatial correlation length of ln(ks) has a high effect on the infiltration and the slope stability during the steady state infiltration. A moderate spatial correlation length can cause the greatest fluctuation of the random field of the saturated hydraulic conductivity, so as to results in the greatest variation of both the pressure head profile and the factor of safety profile, the highest probability of failure, and the lowest true negative flux.

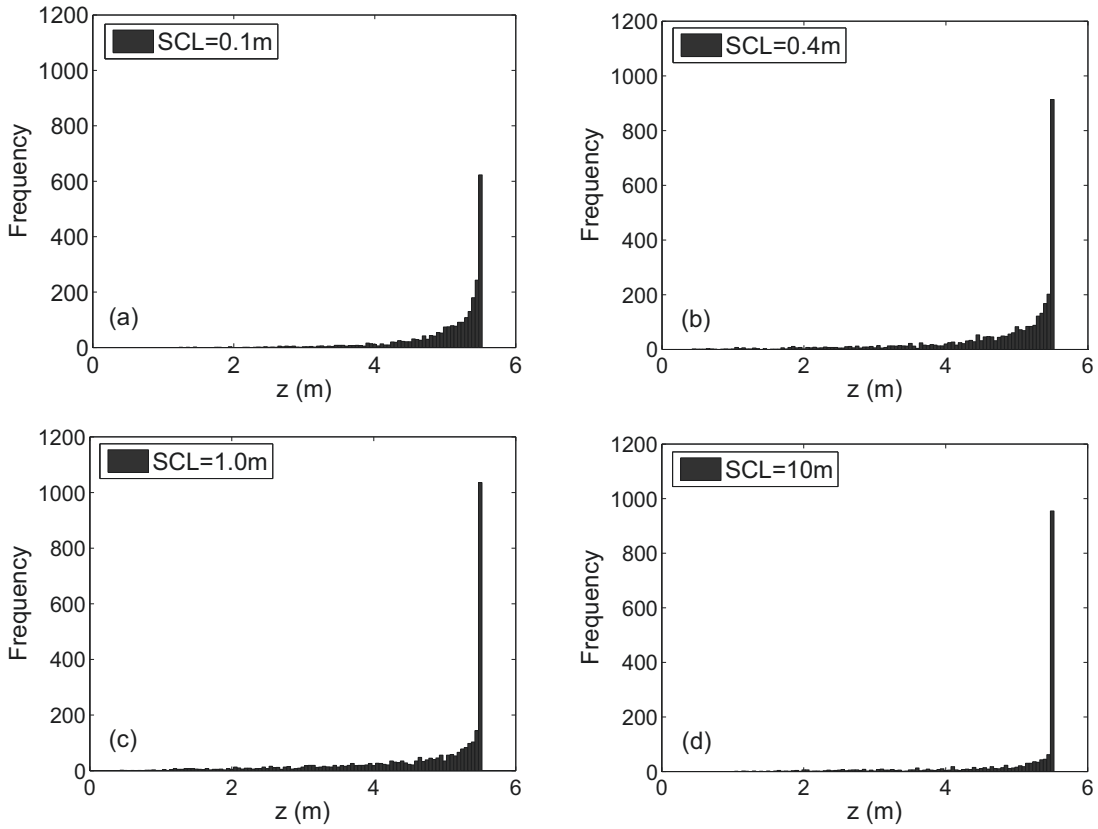

Figure 7.9.: Effect of the SCL of ln(ks) on the elevation of the critical failure surface of the slope during steady state infiltration

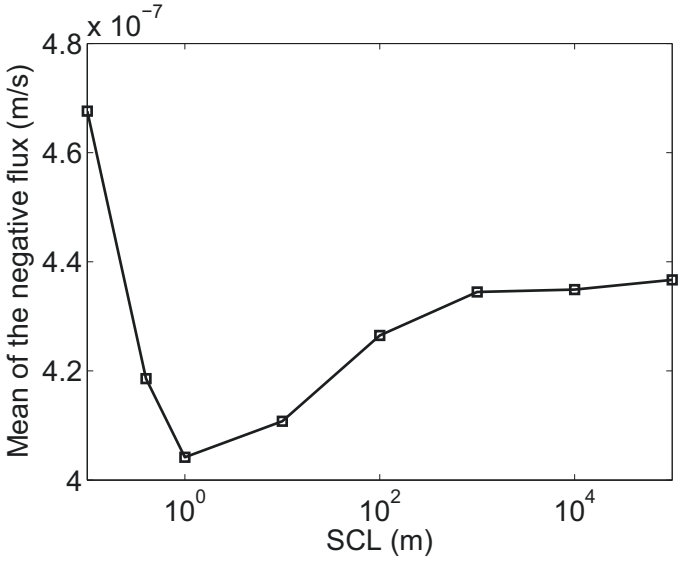

Figure 7.10.: Effect of the spatial correlation length (SCL) of ln(ks) on the true flux

7.3.4. Effect of the variation of ks on the slope stability under transient state infiltration

Steady state infiltration is the final stage of the infiltration. In reality, the rainfall may not last long enough for the infiltration reaching at the steady state, and the slope may fail earlier. Therefore, it is very important to simulate the transient infiltration, and to analyze the slope stability during the transient infiltration.

In this section, the stochastic analysis is carried out to study the effect of the variation of the saturated hydraulic conductivity (ks) on the transient infiltration and the infinite slope stability. In order to have a clear understanding to the transient infiltration and slope stability during the infiltration, the development of the pressure head profile, the factor of safety profile, the probability of failure, and location of the critical failure surface are analyzed during transient infiltration. The coefficient of variation of ks is set to be 1, and the spatial correlation length of ln(ks) is set to be 0.4m.

Pressure head profile and factor of safety profile

Some quantiles of both the pressure head and the factor of safety profiles at several selected time steps are shown in Figure 7.11. A clear difference of the wetting fronts can be found (Figure 7.11a) for the pressure head profile with different quantiles at the same time step, due to the unique structure of each random field. This difference becomes larger and larger as the infiltration duration increases, because as the wetting front goes deeper, there is more chance that the rainwater is blocked by a low permeable layer, which can reduce the true infiltration rate. Figure 7.11b shows the development of the corresponding factor of safety profile. As the infiltration duration increases, the factor of safety of the slope in the wetting zone is reduced. The slope is stable, when the duration is short (t=4 days); however, there is more than 25% probability that the slope fails as the duration reaches to 12 days. Meanwhile, It is interesting to see that the elevation of the minimum factor of safety is different for different quantiles at the same time step in the wetting zone, and the elevation is higher for a lower quantile case.

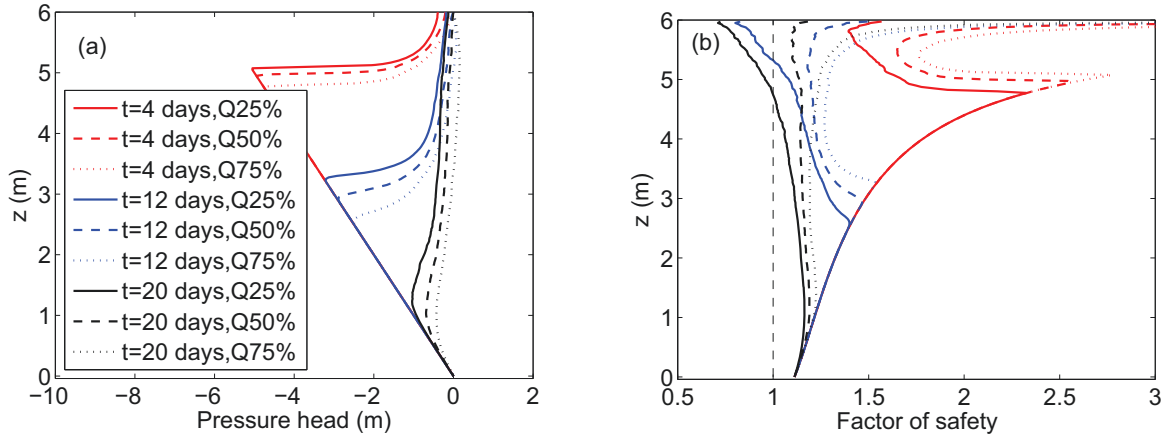

Figure 7.11.: Development of (a) pressure head profile and (b) factor of safety profile during transient infiltration

Probability of failure

The development of the probability of failure during transient infiltration is shown in Figure 7.12. It can be seen that the probability of failure increases dramatically as the infiltration continues. This is because, as the infiltration duration increases, there is more chance that the positive pressure head is generated. Meanwhile, if the failure at the top 0.5m is included, there is 10% to 15% more

chance that the slope failure is induced.

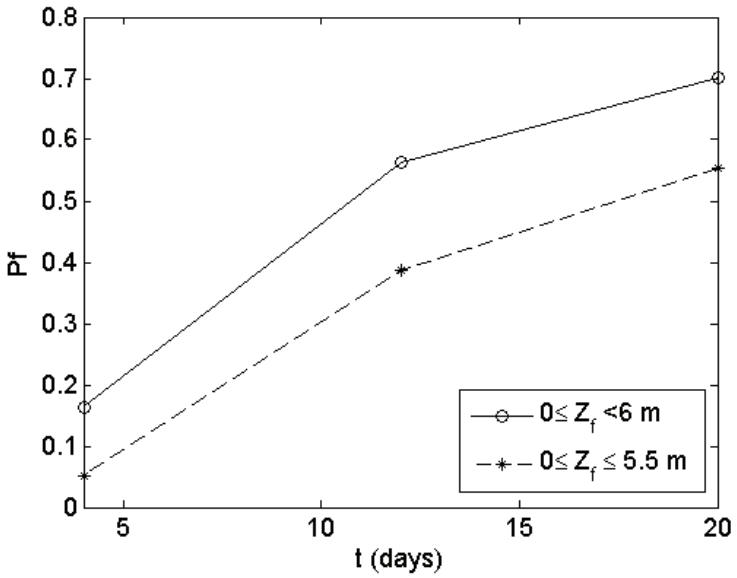

Figure 7.12.: Development of the probability of failure during transient infiltration

Critical failure surface

Figure 7.13 shows the development of the critical failure surface during transient infiltration. When the infiltration duration comes to 4 days, only a small percentage (about 5%) of the slope fails. Most of the slope failure is in the top half of the slope (top 0.5m is not taken into account), and the elevation zone of all the slope failure lies between 5m and 5.5m. As the duration increase, the frequency of the slope failure increases and the failure zone increases.

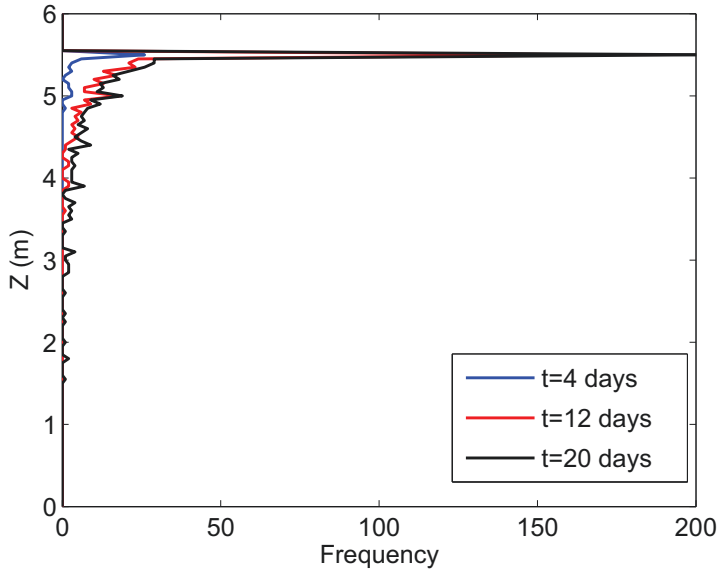

Figure 7.13.: Develop of the elevation of the critical failure surface during transient infiltration

In summary: As the infiltration duration increases, the wetting front goes deeper, the probability of failure increases and the failure zone becomes longer.

7.3.5. Effect of the CV of ks on the slope stability under transient state infiltration

Like in the case with steady state infiltration, three different CVs (0.5, 1.0, 1.5) of ks are used here to analyze the effect of CV on the pressure head profile, the factor of safety profile, the probability of failure, and location of the critical failure surface during transient infiltration. The spatial correlation length of ln(ks) is set to be 0.4m.

Pressure head profile and factor of safety profile

The quantiles of the pressure head profile at several representative time steps are shown in Figure 7.14a. The wetting front is higher for the slope with a higher CV of ks at the same time step. Meanwhile, the elevation difference of the wetting fronts with different CV becomes larger and

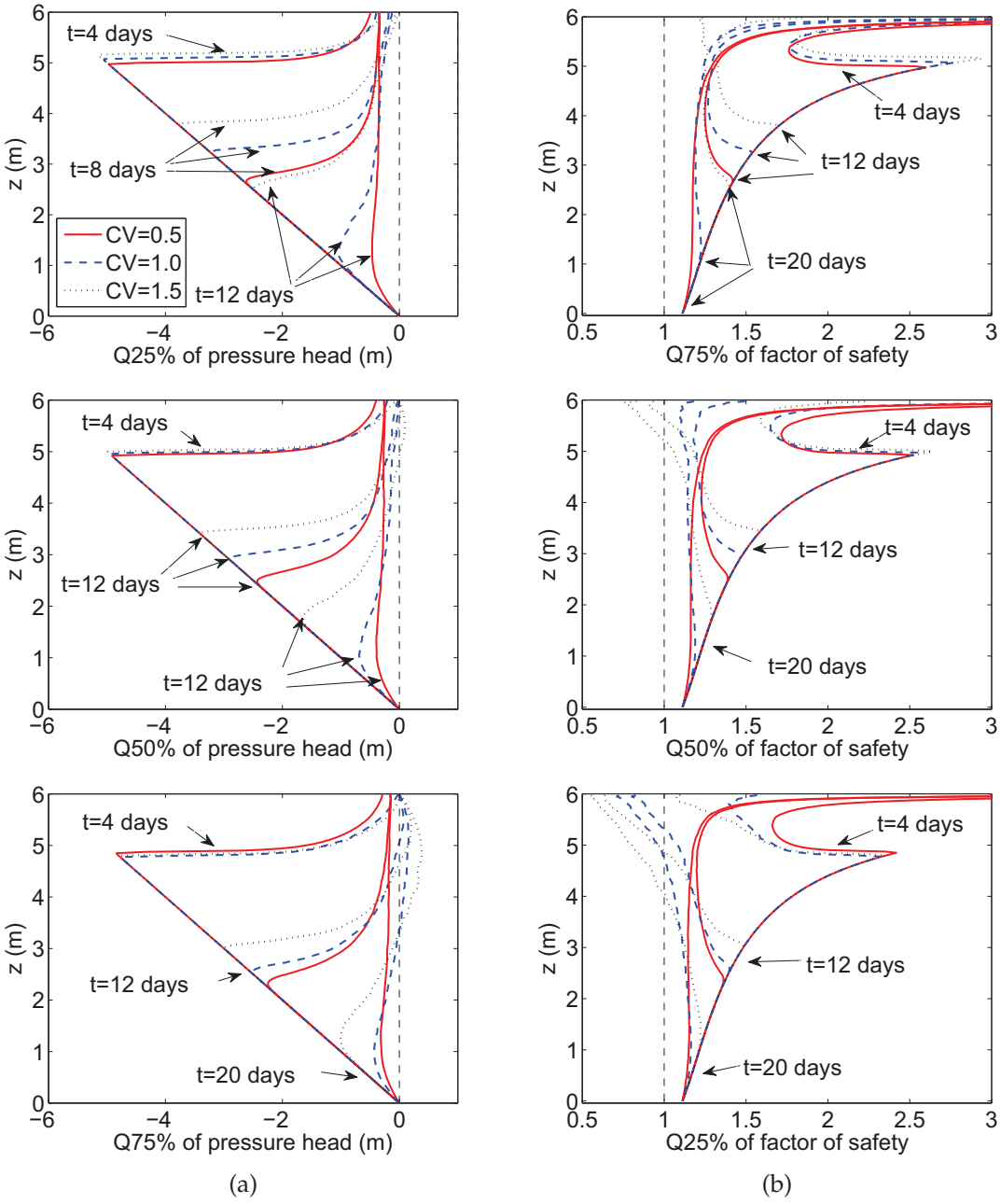

Figure 7.14.: Effect of the CV of ks on the quantiles of (a) pressure head profile and (b) factor of safety profile, during transient infiltration

larger as the infiltration duration increases, and this difference is more dramatic for the small quantile situation. When the CV is small, the ks fluctuates in a small range, so there is a lower probability that a ks lower than the negative flux is generated, which means there is less chance that the rainwater is perched in the wetting zone. Therefore, the wetting front goes deeper for a smaller CV case and the difference becomes more dramatic for small quantile situation. It is worth noting that the positive pressure head in the wetting zone is firstly generated in the slope with the highest CV of ks. Because it is easier that a low permeable layer is generated, and this low permeable layer can cause the generation of a positive pressure head zone.

The effect of the CV of ks on the factor of safety profile during transient infiltration at several selected time steps is shown in Figure 7.14b. It can be seen that the CV of ks can significantly influence the factor of safety profile in the wetting zone, especially in the quantile 25% and quantile 50% situations. The factor of safety of the slope is lower in the wetting zone for the case with a higher CV. It is worth noting that, for the slope with a higher CV of ks, the elevation of the minimum FS in the wetting zone is higher, and the failure zone is larger.

Probability of failure

Figure 7.15 shows the probability of failure at some selected time steps during transient infiltration. It can be seen that the Pf increases as the increase of CV at all time steps. Meanwhile, it can also be seen that the Pf increases as the increase of the infiltration duration, because as the infiltration continues, the wetting front goes deeper, so there is more chance that the positive pressure head is generated in the wetting zone. Moreover, it can be seen that the Pf is very small when the infiltration duration reaches to 4 days because the slope failure of the top 0.5m is not considered, and it increases quickly in the next 8 days. Although the low permeable layer is equally distributed in the slope, the low permeable layer in a high elevation is more important, because while it can cause the generation of the positive pressure head, it can also reduce the negative flux to flowing into a lower layer, and this reduced negative flux can decrease the increasing ratio of Pf from 12 days to 20 days.

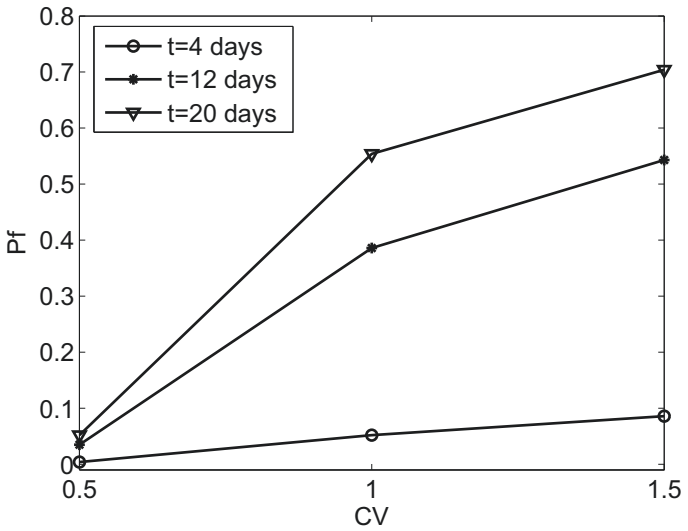

Figure 7.15.: Effect of the CV of ks on the probability of failure during transient infiltration

Critical failure surface

Figure 7.16 shows how the CV affect the location of the critical failure surface during transient infiltration at different time steps. It can be seen that most of the slope failure happens at a shallow location (top 0.5m is not considered). As CV of ks increases, the probability of failure of the slope

is increased and the zone of the critical failure location is longer at the same time step. Meanwhile, as the increase of the transient infiltration duration, the zone of failure location becomes longer.

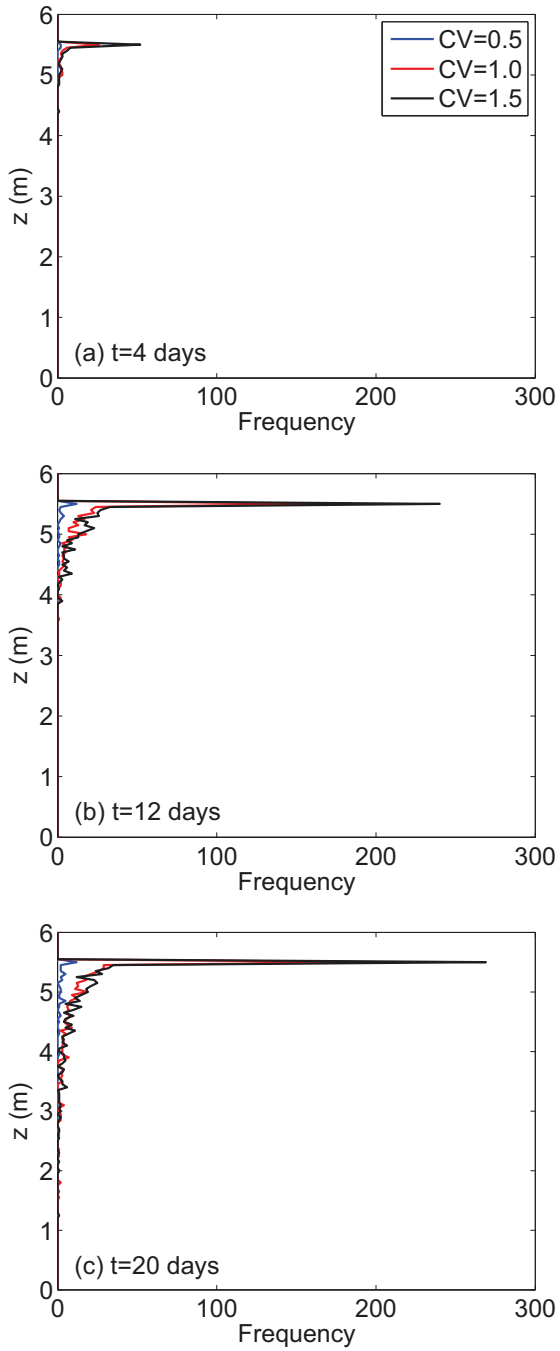

Figure 7.16.: Elevation of the critical failure surface during transient infiltration

In summary, the coefficient of variation of ks has significant influences on both the transient infiltration and the infinite slope stability during transient infiltration. As the increase of the infiltration duration, the differences caused by increasing the coefficient of variation become larger on both the pressure head profile and the factor of safety profile. The probability of failure is increased as the increase of the infiltration duration, especially in the middle stage of the transient infiltration, when the Pf is increased dramatically.

7.3.6. Effect of the SCL on the slope stability analysis under transient state infiltration

Several different SCLs of ln(ks) are used here to analyze its effect on the pressure head profile, the factor of safety profile, and the probability of failure during transient infiltration. The coefficient of variation of ks is set to be 1.

Pressure head profile and factor of safety profile

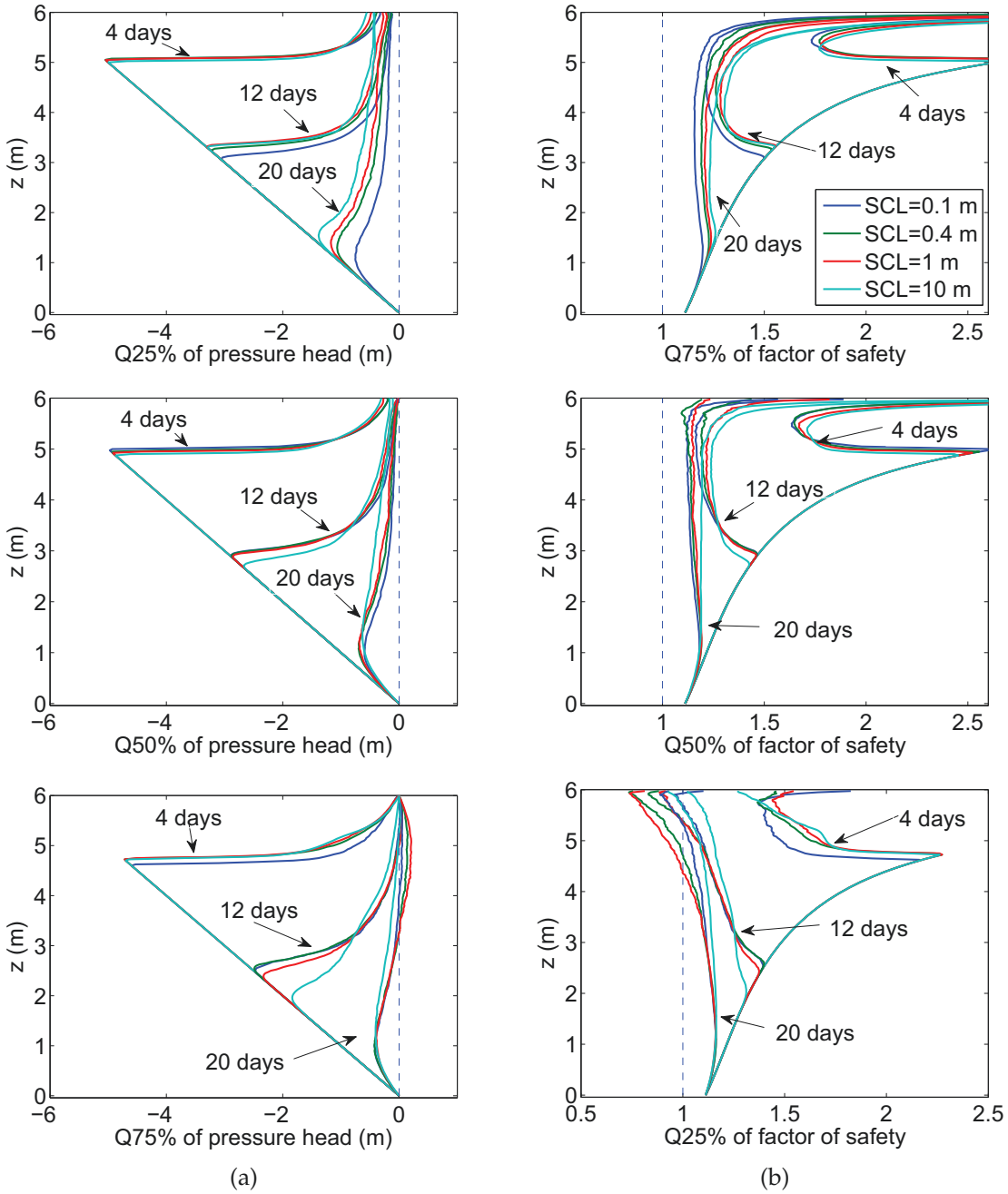

Figure 7.17.: Effect of the spatial correlation length (SCL) of ln(ks) on the quantiles of (a) pressure head profile (b) factor of safety profile, during transient infiltration

Figure 7.17a shows the effect of SCL of ln(ks) on the pressure head profile during the transient infiltration at three different time steps. In the 4 days situation, the location of the wetting fronts

show little difference. The difference becomes larger as the time duration increases. It can be seen that different quantiles have different trends at different time duration, and there is no clear pattern in the effect of SCL on the pressure head profile during transient infiltration. Like on the pressure head profile, Figure 7.17b shows that there is no clear pattern in the effect of the SCL on the factor of safety profile during transient infiltration.

Probability of failure

Figure 7.18 shows that the probability of failure decreases slightly with the increase of SCL at the early stage of the transient infiltration (at t=4 days), and the Pf increases as the infiltration duration increases. Meanwhile, the slope with a moderate SCL (SCL=0.4m here) has the highest probability of failure, and a higher or lower SCL can reduce the probability of failure of the slope when the infiltration duration is over 12 days. Because the variation of ks is related to both the variance reduction and the correlation matrix. A moderate SCL can make a good balance between them, so as to generate the random field with the greatest fluctuation in each random field. At the early stage of the infiltration (t=4 days), this advantage does not appear clearly since the wetting zone is small and the Pf at the top 0.5m is not taken into account. However, as the infiltration continues, this advantage becomes more and more clearly.

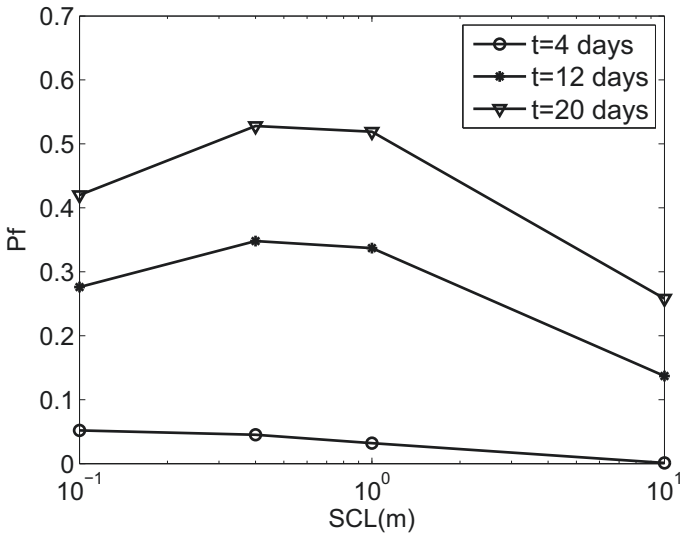

Figure 7.18.: Effect of the SCL of ln(ks) on the Pf during transient infiltration

In summary, the probability of failure is the highest when the SCL of ln(ks) is at a moderate level. A higher or lower SCL can reduce the probability of failure during the transient infiltration, except for the early stage of the infiltration, when the Pf is the highest for the case with the lowest SCL. There is no clear pattern for the effect of the SCL on either the pressure head profile or the factor of safety profile, except that the relative difference of each profile in the wetting zone becomes larger as the infiltration duration increases.

7.4. Probabilistic infinite slope stability analysis during infiltration considering the depth-dependent character

In this section, the depth-dependent character of the stochastic parameters of ks is taken into account, so as to evaluate its effect on the infinite slope stability analysis under both steady state and transient state infiltration.

7.4.1. Effect of the depth-dependent mean of ks on the slope stability under steady state infiltration

In order to evaluate the effect of depth-dependent mean ks on the slope stability analysis during steady state infiltration, the mean of ks is assumed to reduce linearly with soil depth in this section, while the mean ks of the whole slope is the same (10^{-6} m/s). The standard deviation of ks is 10^{-6}, and the spatial correlation length of ln(ks) is 0.4m. The case with constant mean of ks (kk=0) is also used.

Pressure head profile and factor of safety profile

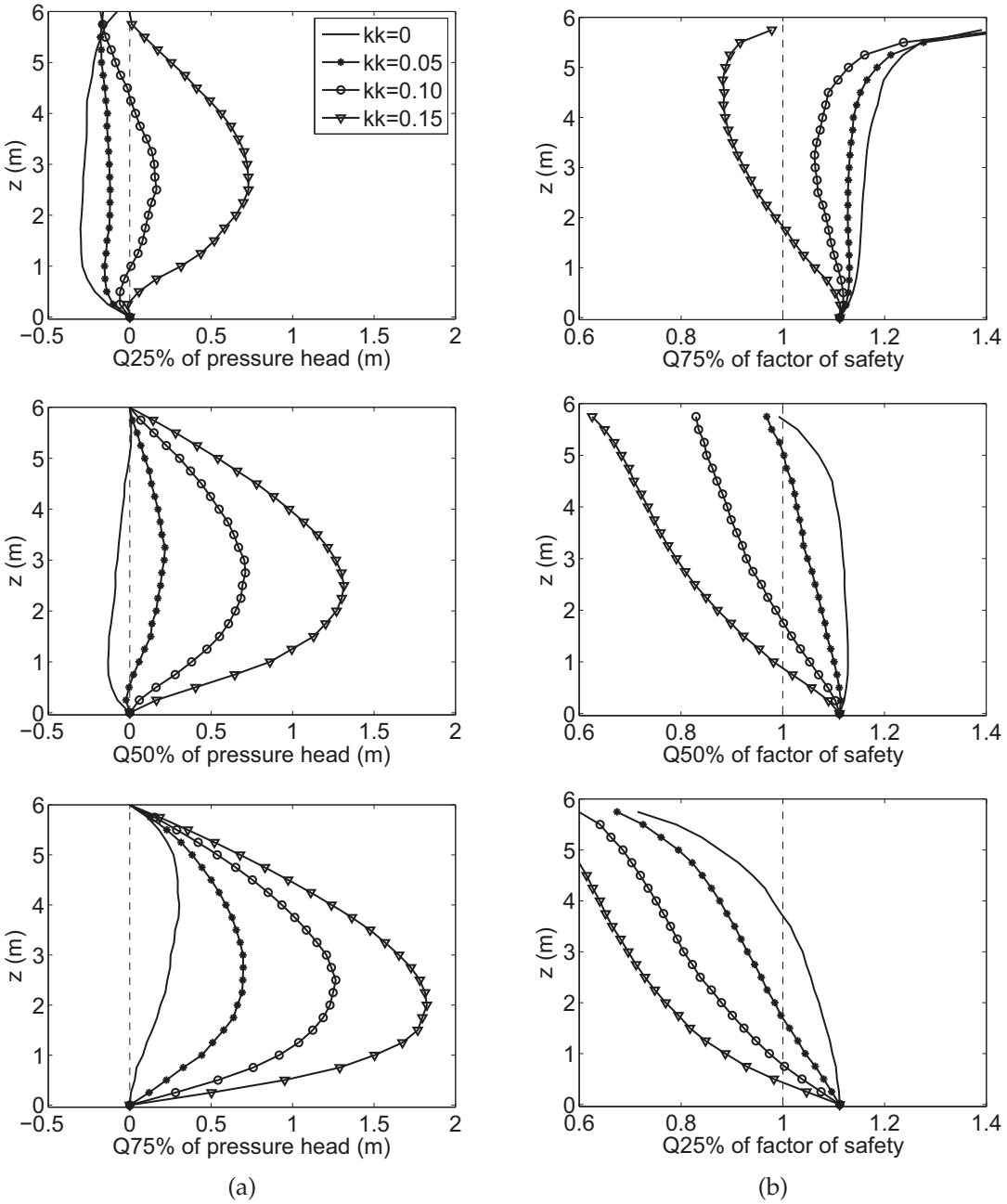

Figure 7.19.: Effect of linearly depth-dependent μ_{ks} on the (a) pressure head profile and (b) factor of safety profile, during steady state infiltration

For the case that the mean of ks reduces linearly with depth, Figure 7.19a shows that the pressure

head profile moves towards right as the increase of kk in almost all Q25%, Q50%, Q75% profiles. Note that the pressure head is positive all over the slope for the case with the highest kk (kk=0.15) in all quantiles, which means the slope is highly possible to be the saturated slope with positive pressure head under steady state infiltration. This is because, for the largest kk case, the mean ks is the smallest at the bottom of the slope, since the standard deviation is constant, there is more chance that the low permeable layers are generated at the bottom. When the wetting front reaches to the bottom, the low permeable layer can stop extra water infiltrating into a lower layer. This perched water is accumulated, and the positive pressure head area becomes larger and larger as the infiltration duration increases, until it covers the whole zone above the low permeable layer.

For the case that the mean of ks reduces linearly with the depth, Figure 7.19b shows that, as the increase of kk, the factor of safety profile moves towards left in all the quantiles, which means the factor of safety above the groundwater table is consistently lower for the slope with a higher kk. Meanwhile, the failure zone is longer for the slope with a higher kk at the same quantile situation. Note that the slope with kk=0.15 fails while the others are still safe in the 75% quantile situation. This means it is very likely that the slope fails during the steady state infiltration when kk is large enough.

Probability of failure

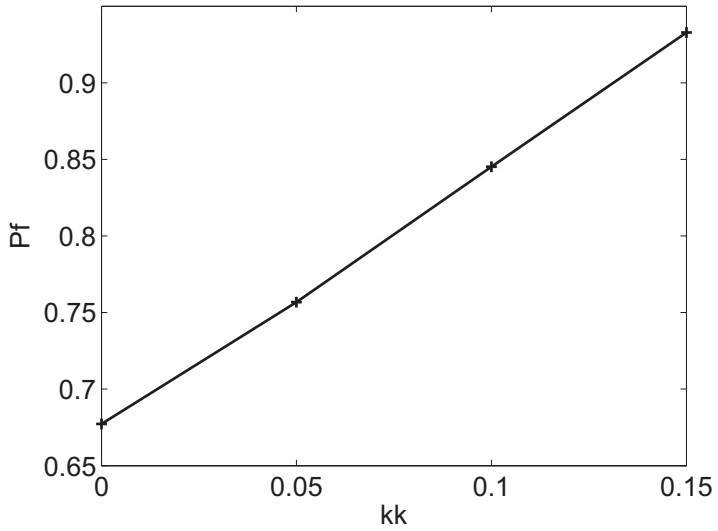

Figure 7.20.: Effect of linearly depth-dependent μ_{ks} on the Pf during steady state infiltration

Figure 7.20 shows the relation between the probability of failure and the depth-dependent character of mean ks. It can be seen that the probability of failure of the slope, without considering the slope failure of the top 0.5m, increases dramatically as the increase of kk. When kk=0 (constant mean ks situation), the Pf is about 0.68. As the kk increases to 0.15, the Pf reaches at 0.93, which means it is almost certain that the slope fails during steady state infiltration when kk is extremely large. This is consistent with the results of the pressure head profile in Figure 7.19a and the factor of safety profile in Figure 7.19b.

Elevation of the critical failure surface

Figure 7.21 shows the effect of the depth-dependent character of mean ks on the frequency of the elevation of the critical failure surface during steady state infiltration. For a lower kk case, the mean ks is smaller in the top half part of the slope, therefore, a lower ks could be generated easier. This low ks layer could reduce the true negative flux. Then the negative flux flowing into a lower part of the slope becomes smaller. Therefore, the frequency of the slope failure happened

at a lower elevation becomes smaller, and most of the slope failure is at the top area of the slope (without considering the top 0.5m). When the kk is larger, the low permeable layers are more likely to be generated in the lower part of the slope, causing a larger area of positive pressure head, which induces more slope failure at the lower part.

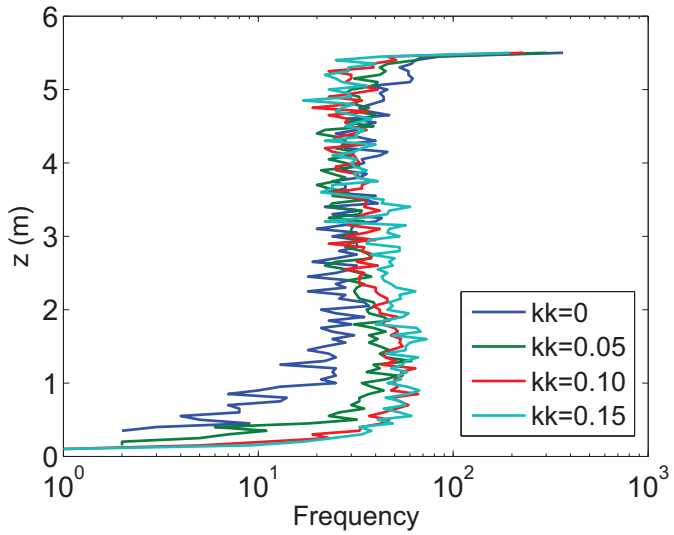

Figure 7.21.: Effect of the linearly depth-dependent μ_{ks} on the elevation of the critical failure surface during steady state infiltration

True flux

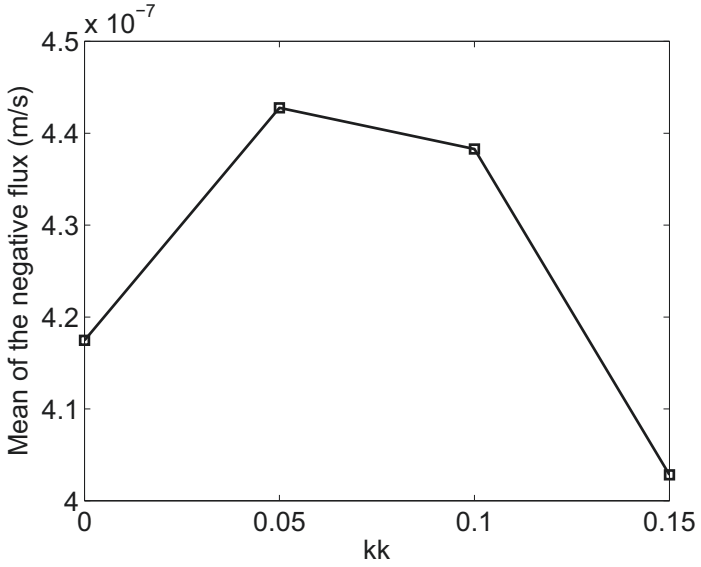

Figure 7.22.: Effect of linearly depth-dependent mean of ks on the real flux infiltrated through the infinite slope during steady state infiltration

Figure 7.22 shows the effect of the depth-dependent character on the mean of true negative flux. Although the preset negative flux is $5 \cdot 10^{-7}$ m/s, the true negative flux is smaller because the variability of ks can cause the generation of low permeable layers, which could reduce the rainwater in infiltrating into a lower layer. It can be seen that, as the increase of kk, the mean of the true negative flux increase at first and then decreases. Comparing to the case with constant mean

ks (kk=0), low permeable layers can be generated harder in the top half of the slope with a higher kk (kk=0.05), allowing more rainwater to infiltrate into a lower location. Although the mean ks is slightly smaller at the bottom part of the slope, the generated positive pressure head can help the negative flux flow towards the groundwater level. Therefore, the mean of the true negative flux becomes larger as kk increases from 0 to 0.05. As kk increases to a higher level (kk=0.1), the mean ks is smaller at the bottom half part, which means the generated ks is smaller in this area. These lower permeable layers can reduce the rainwater infiltrating into the groundwater level, extra water accumulates above the low permeable layer, till it reaches to the slope surface and runs off. This is why the mean of the negative flux is reduced when kk increases from 0.05 to 0.1. The run-off becomes larger when the kk increases to an extremely high level (kk=0.15). Therefore the mean of negative flux is smaller.

In summary, When the depth-dependent character of the mean of ks is considered during steady state infiltration, a higher kk can significantly increase the probability of failure of the slope. Meanwhile, more slope failure happens at a lower elevation. Moreover, as kk increases from zero to an extremely high value, the true negative flux is increased at first, and then it is reduced.

7.4.2. Effect of the depth-dependent mean of ks on the slope stability under transient state infiltration

Pressure head profile and factor of safety profile

Figure 7.23a shows how the depth-dependent mean ks affects the pressure head profiles during transient infiltration at several selected time steps. As the kk increases, the wetting front goes deeper. The difference of the locations of the wetting fronts caused by the linearly depth-dependent mean ks can be divided into 3 stages. (a) The early stage, when the wetting front is in the top half part of the slope (e.g. from the beginning to about 12 days). The difference becomes larger as the infiltration duration increases, because the mean ks in the top half part of the slope is larger for a higher kk case. (b) The middle stage, when the wetting front is in the bottom half part of the slope (e.g. from 12 days to about 20 days). The difference is reduced as the infiltration duration continues. This is because the mean ks of the bottom half part is smaller for a higher kk case. (c) The late stage, when the positive pressure head is accumulated (e.g. 40 days). In this stage, the wetting front is no longer changed. However, the positive pressure head is higher for the slope with a higher kk. This is because its mean ks is smaller at the bottom of the slope, which means there is more chance the low permeable layers are generated. So extra water would be perched and accumulated in the slope, causing an increase of the positive pressure head zone. This is why the positive pressure head is all over the slope in all these three quantiles for the largest kk case at this stage.

Figure 7.23b shows the effect of the depth-dependent mean ks on the factor of safety profiles during transient infiltration. It can be seen that the elevation of the minimum FS in the wetting zone is slightly higher for the slope with a lower kk during transient infiltration, except for the 40 days condition, where the profile can be regarded as in the steady state. For the Q25% factor of safety profile, the slope with a constant mean ks (kk=0) fails at 12 days, while the slopes with the depth-dependent mean ks are still stable; as the infiltration duration increases to 20 days, the slope with a low depth-dependent mean ks (kk=0.05) fails too; when the infiltration duration reaches to 40 days, all slopes fail. However, the failure zone is longer for the slope with a larger kk. This is because, for the slope with a larger kk, the mean ks of the top half of the slope is larger, therefore, the probability that the positive pressure head is generated in this part is lower when the infiltration duration is not long, and the probability of failure is lower. When the wetting front reaches to the lower half part of the slope (t=20 days), where the mean ks is smaller for the slope with a larger kk, the probability of positive pressure head generation is increased. However, the disadvantage of

the smaller Pf it accumulated before, needs some time to be compensated, therefore, the difference of the factor of safety profile is reduced. As the infiltration duration keeps increasing (t=40 days), the advantage of a higher kk in the probability of failure shows up.

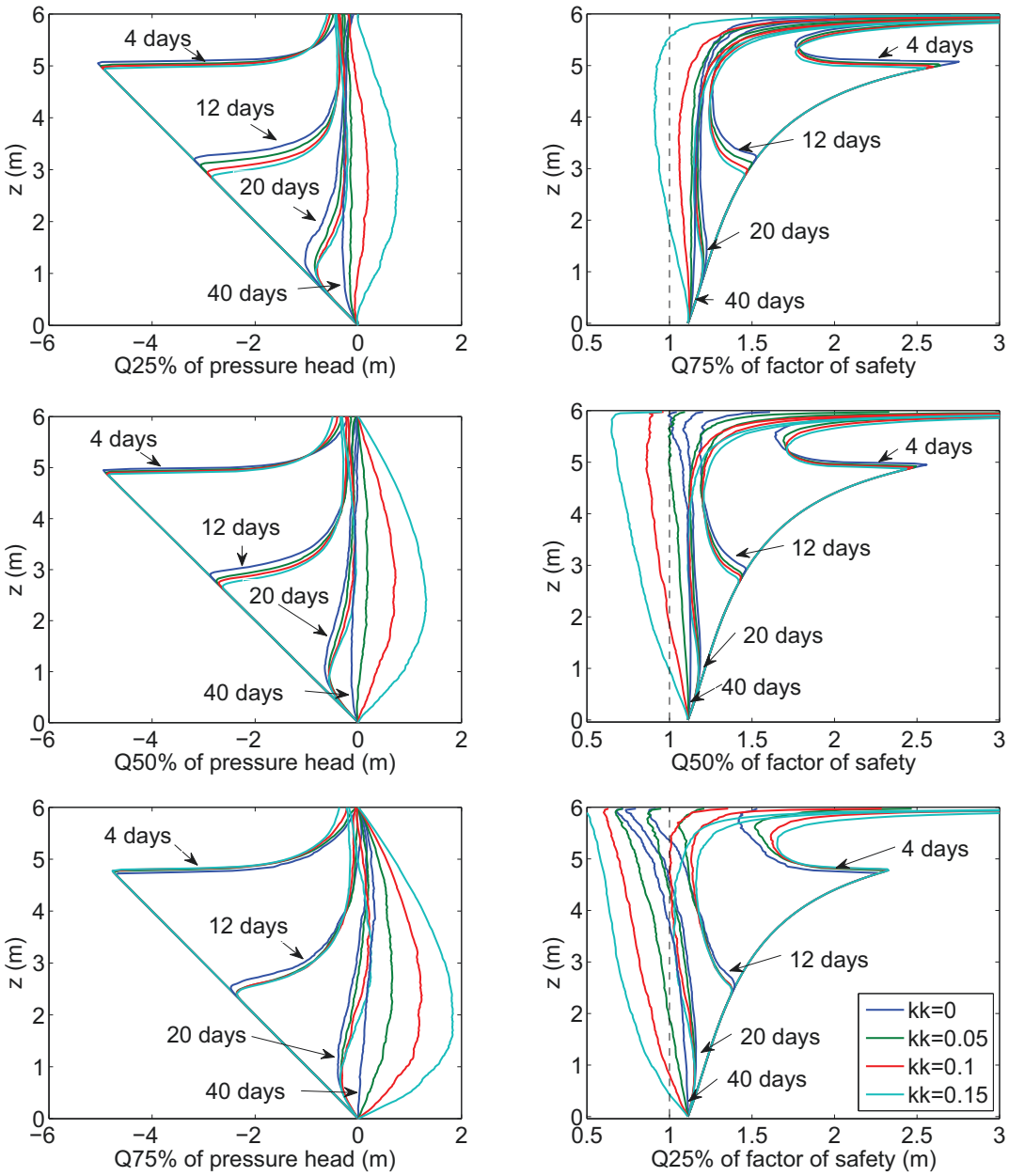

Figure 7.23.: Effect of the depth-dependent mean ks on the (a) pressure head profile and (b) factor of safety profile, during transient infiltration

Probability of failure

Figure 7.24 shows the effect of the depth-dependent mean ks on the probability of failure during transient infiltration at several selected time steps, without considering the slope failure of the top 0.5m. It shows that the effect of the depth-dependent mean ks on the probability of failure can also be divided into three stages: (a) the early stage of the transient infiltration when the wetting front is in the top half of the slope. In this stage, the probability of failure is higher, and the probability of

failure increases quicker for the slope with a lower kk. For instance, when kk=0, the probability of failure equals to 0.05 at t=4 days, and it increase to 0.38 when t=12 days. However, the probability of failure increases from 0.01 to 0.11 for the case with kk=0.15. (b) The middle stage of the transient infiltration when the wetting front is in the bottom half of the slope. In this stage, the probability of failure is higher for the slope with a smaller kk, however, the probability of failure increases quicker for the slope with a higher kk. For instance, when the infiltration duration increase from 12 days to 20 days, the probability of failure increases from 0.38 to 0.55 for the case with kk=0, while it increase from 0.11 to 0.44 for the case with kk=0.15. (c) The late stage of the transient infiltration after the wetting front reaches the bottom the slope. In this stage, the probability of failure is lower for the case with a smaller kk, and the probability of failure increases with the increase of kk. Since the slope with a smaller kk has a smaller mean of ks in the top half part of the slope, the probability of the generation of a low ks is relatively increased. Therefore, the probability of the generation of positive pressure head in this part is relatively increased. This is why the probability of failure is higher when the wetting front is in the top half part of the slope for the case with a lower kk. Meanwhile, some water is blocked by the low permeable layers, therefore, the increase of probability of failure slows down, when the wetting front goes to the bottom half part of the slope. However, for the slope with a higher kk, the mean ks is larger in the top half part of the slope, and less water is blocked. The probability of the generation of a low permeable layer increases with the depth, so the increasing ratio of probability of failure becomes greater as the development of the wetting front. Meanwhile, a smaller ks can cause the accumulation of the positive pressure head area, this is why the probability of failure becomes higher for the slope with a higher kk of mean ks as the infiltration reaches to the late stage.

It is interesting to note that this depth-dependent character can reduce the probability of failure if the infiltration duration is not too long, otherwise, the probability of failure can be significantly increased. Considering the rainfall duration is normally not so long, the probability of failure might be overestimated if the depth-dependent character is not taking into consideration.

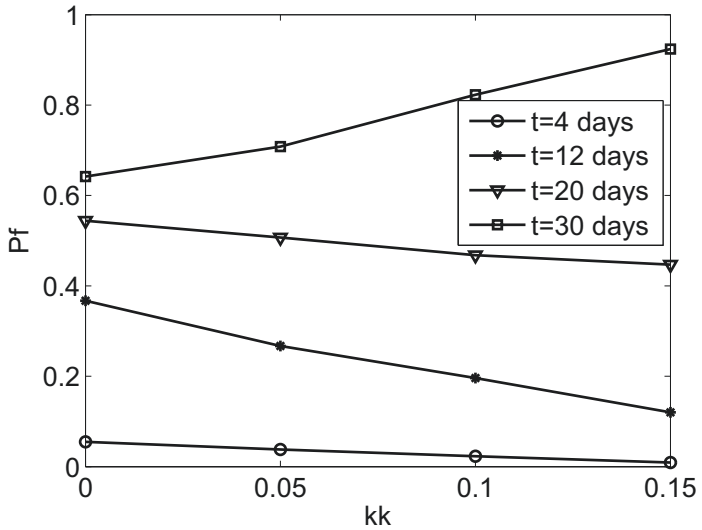

Figure 7.24.: Effect of the depth-dependent mean ks on the probability of failure (Pf) during transient infiltration

In summary, the depth-dependent mean ks can significantly affect the slope stability during transient infiltration. Without considering it, the Pf can be overestimated in the early and middle stage of the infiltration, and it can be underestimated if the infiltration lasts long enough.

7.4.3. Effect of the depth-dependent STD of ks on the slope stability under steady state infiltration

In order to evaluate the effect of depth-dependent standard deviation of ks (STD_{ks}) on the slope stability during steady state infiltration, the standard deviation of ks is assumed to reduce linearly with soil depth in this section, while the mean STD_{ks} of the slope is kept constant. The mean of ks is 10^{-6} m/s, and the spatial correlation length of ln(ks) is 0.4m.

Pressure head profile and factor of safety profile

For the case that the standard deviation of ks reduces linearly with the depth, Figure 7.25a shows that, as the increase of kk, the pressure head profile moves towards left at all quantile situations

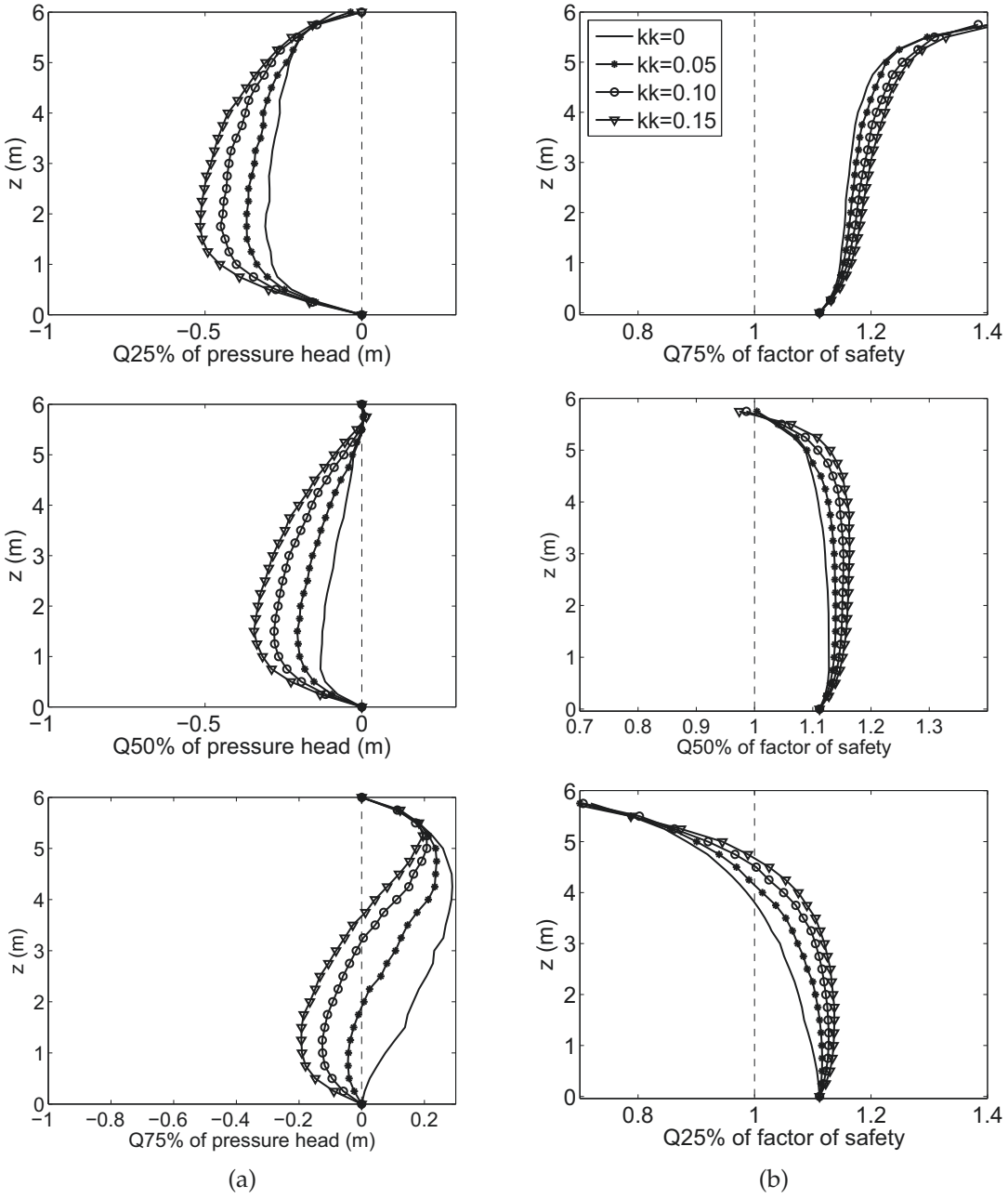

Figure 7.25.: Effect of linearly depth-dependent standard deviation (STD) of ks on the (a) pressure head profile and (b) factor of safety profile, during steady state infiltration

(except for the top 0.5m of the slope). When kk is larger, the standard deviation at the top half part of the slope is higher, which means low permeable layers could be generated easier in this part. These layers can help build positive pressure head and reduce the mean negative flux to infiltrating into a lower layer. Therefore, the slope with a higher kk can consistently produce the lower pressure head in a lower location.

Figure 7.25b shows that the slope with a higher kk consistently has a higher factor of safety above the groundwater table (except for the top 0.5m of the slope). Because the pressure head is lower for the slope with a higher kk in this area. From Q25% factor of safety profile, it can be seen that the slope with a higher kk has a smaller failure zone, which means there is less chance that the slope with a higher kk of STD fails. If the standard deviation is constant (kk=0), the low permeable layers are equally generated in the slope. Therefore, the positive pressure head zone might be easier generated in the lower part of the slope, comparing to the case with a higher kk. This is why the failure zone is longer.

Probability of failure

Figure 7.26 shows that the probability of failure is moderately reduced as the increase of kk. This is because a higher kk means the top half of the slope has a higher standard deviation of ks. Therefore, there is more chance that low permeable layers are generated in the top of the slope. These layers can reduce the mean negative flux, so as to decrease both the positive pressure head generation and probability of failure.

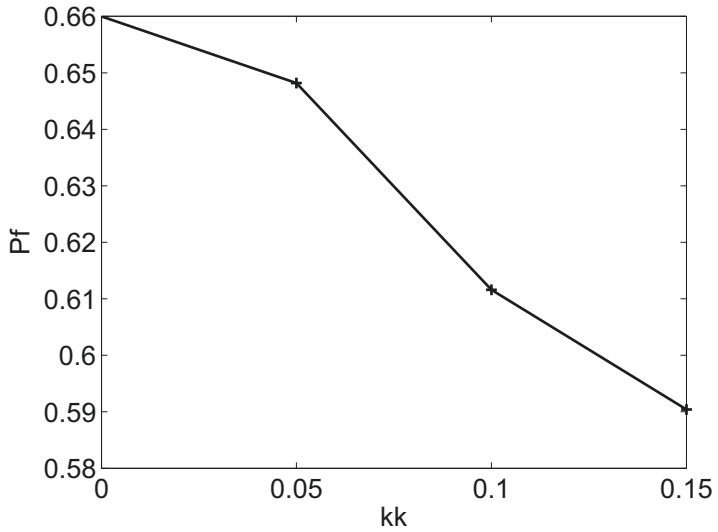

Figure 7.26.: Effect of linearly depth-dependent standard deviation of ks on the Pf during steady state infiltration

Elevation of the critical failure surface

Figure 7.27 shows the frequency of the elevation of the critical failure surface, when the linearly depth-dependent character of STD_{ks} is considered. It can be seen that most of the slope failure is in the top area of the slope (Top 0.5m is not considered). The frequency is slightly higher for the critical failure surface in the top half of the slope with a higher kk. However, the slope with a lower kk has a longer failure zone, and the frequency that the elevation of the critical failure surface at a lower level is relatively higher.

True flux

For the case that the standard deviation of ks reduces linearly with depth, Figure 7.28 shows

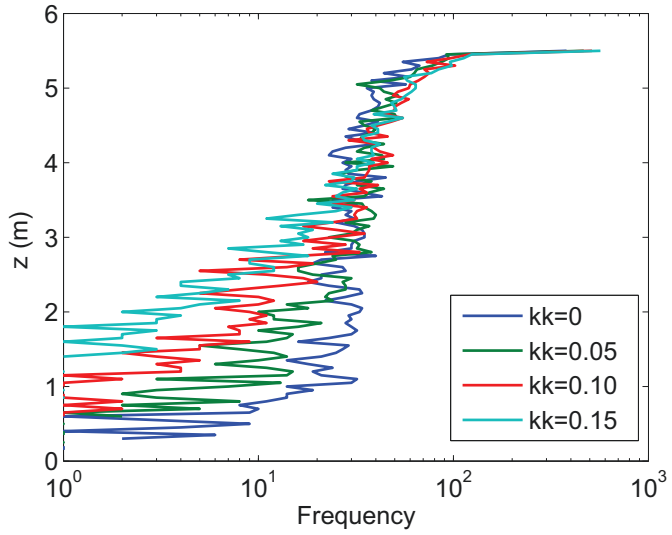

Figure 7.27.: Effect of the linearly depth-dependent standard deviation of ks on the elevation of the critical failure surface during steady state infiltration

that an increase of kk can reduce the mean of negative flux, because the standard deviation of ks is higher in the top half of the slope when kk is higher. The higher standard deviation can cause a more dramatic fluctuation of ks in the top half of the slope, which can reduce the flux to flowing into the slope.

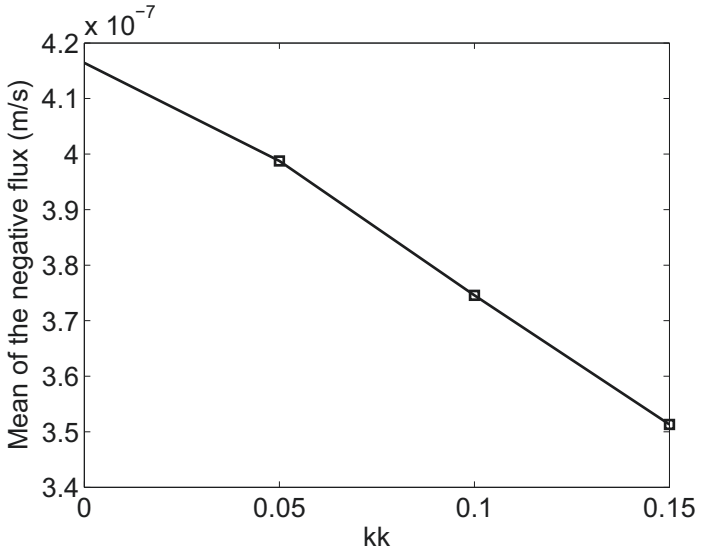

Figure 7.28.: Effect of linearly depth-dependent standard deviation of ks on the true negative flux infiltrated through the infinite slope during steady state infiltration

In summary, for the case that the standard deviation of ks reduces linearly with the depth, an increase of the depth-dependent character of the standard deviation can increase the fluctuation of the ks in the top half area of the slope during steady state infiltration, causing a reduction of the mean negative flux. Therefore, as the depth-dependent character becomes greater, the pressure head is lower, the factor of safety is higher, the probability of failure becomes lower, and the critical failure surface at a lower elevation is decreased.

7.4.4. Effect of the depth-dependent STD of ks on the slope stability under transient state infiltration

Pressure head profile and factor of safety profile

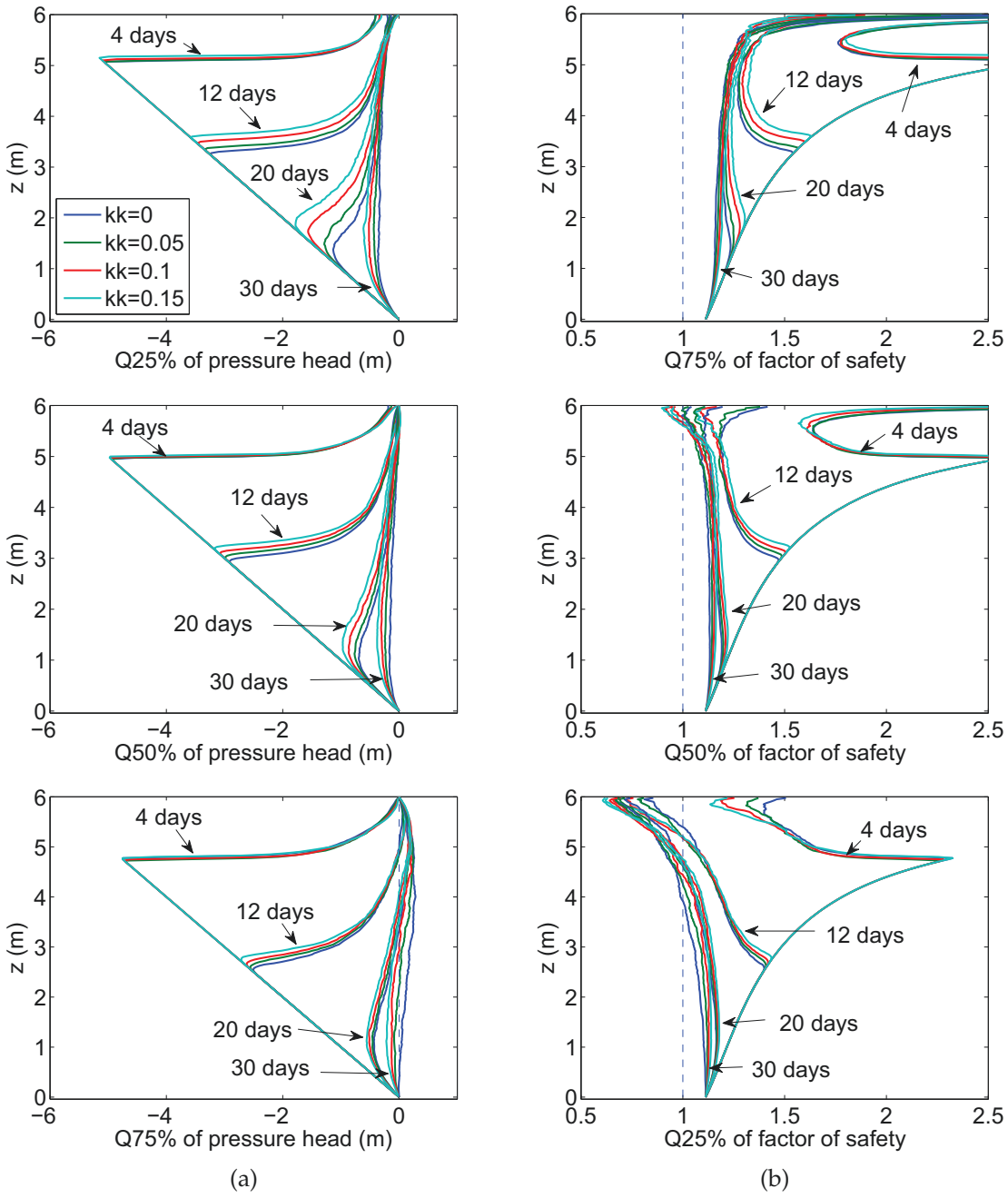

Figure 7.29.: Effect of the depth-dependent standard deviation of ks on the (a) pressure head profiles, (b) factor of safety profile, during transient infiltration

Figure 7.29a shows the effect of the depth-dependent standard deviation of ks on the quantiles of the pressure head profile during transient infiltration at several selected time steps. It can be seen that the location of the wetting front is higher for the slope with a higher kk at all time steps. This is because the standard deviation at the top half part of the slope is larger for a higher kk situation, so there is more chance that the low permeable layer is generated in this area, and this

low permeable layer can reduce the mean negative flux infiltrated into the slope. Therefore, the wetting front is higher.

From Q25% and Q50% factor of safety profiles in Figure 7.29b, it can be seen that the minimum factor of safety is slightly lower in the wetting zone for the slope with a higher kk of the STD_{ks}, which also means the slope fails earlier. Meanwhile, the elevation of its minimum factor of safety is slightly higher in the wetting zone.

Probability of failure

Figure 7.30 shows the effect of the depth-dependent standard deviation of ks on the probability of failure during transient infiltration, without considering the slope failure of the top 0.5m. It can be seen that, for the slope with a higher kk, the Pf is higher if the infiltration duration is less than 20 days, however, the Pf is lower as the infiltration duration reaches to 30 days. The effect of the depth-dependent STD_{ks} on the Pf during transient infiltration can be categorized into 2 stages: (a) the early stage when the wetting front is in the top half part of the slope. In this stage, the Pf is slightly higher for the slope with a higher kk, and the difference of Pf caused by kk becomes larger as the infiltration duration increases. Because the standard deviation is larger for the upper part of the slope with a higher kk, which means there is more chance that the low permeable layers are generated. These layers are the key to generate the positive pressure head which can cause the slope failure. While, they also cause the reduction of the true negative flux. (b) The late stage when the wetting front is in the lower part of the slope. In this stage, the increasing ratio of Pf slows down for the slope with a higher kk, because the standard deviation is smaller. However, for the slope with a smaller kk, the increasing ratio of Pf becomes larger and larger as the infiltration continues, till the total Pf is larger for the slope with a lower kk.

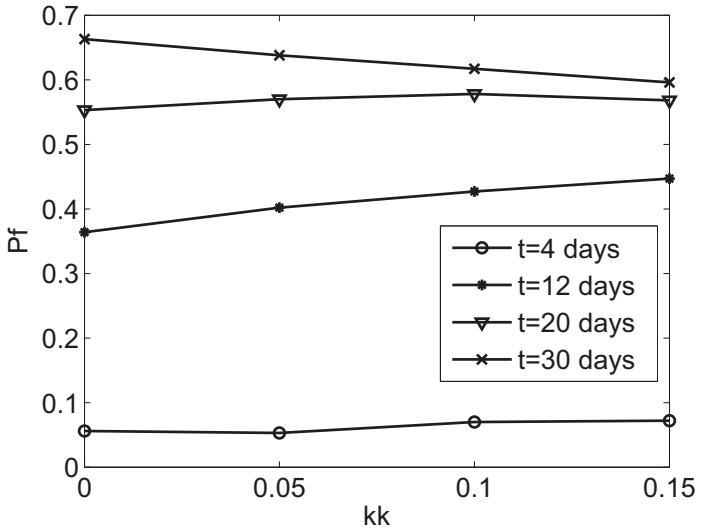

Figure 7.30.: Effect of the depth-dependent standard deviation (STD) of ks on the Pf during transient infiltration

In summary: the depth-dependent standard deviation of ks can moderately affect the infinite slope stability during transient infiltration. A greater depth-dependent character of the standard deviation can make the wetting front at a shallower location, and cause a slightly lower factor of safety in the wetting zone. Without considering it, the Probability of failure can be underestimated in the early stage of the infiltration, and it can be overestimated if the infiltration lasts long enough.

7.4.5. Effect of the depth-dependent mean of ks with CV=1 on the slope stability under steady state infiltration

Normally speaking, both the mean and standard deviation of ks change simultaneously. In this section, the mean of ks is assumed to reduce linearly with soil depth, while its coefficient of variation is kept constant (equals to one in this case). The mean ks of the whole slope above the groundwater table is kept 10^{-6} m/s. The spatial correlation length of ln(ks) is kept 0.4m.

Pressure head profile and factor of safety profile

For the case that both the mean and the standard deviation of ks reduce with soil depth, Figure 7.31a shows that a higher kk can help the slope build a higher pressure head for most cases during

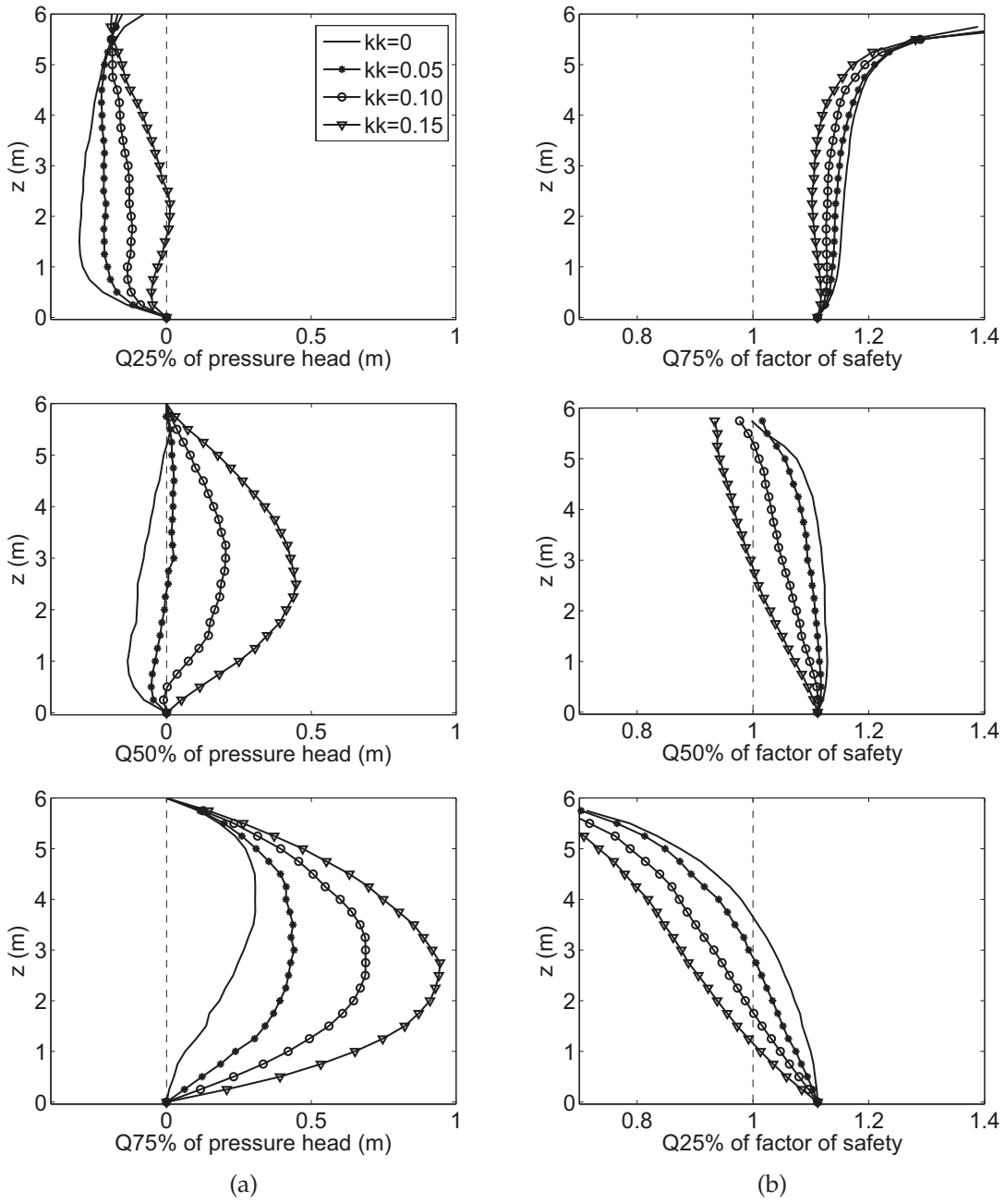

Figure 7.31.: Effect of kk(μ_{ks}) on the (a) pressure head profile, (b) factor of safety profile during steady state infiltration (CV_{ks}=1)

steady state infiltration. It is a combined effect of the depth-dependent character of both the mean and the standard deviation. A higher kk can significantly increase the pressure head for the case with a depth-dependent mean ks (Figure 7.19a), and moderately decrease the pressure head for the case with a depth-dependent standard deviation of ks (Figure 7.25a). When both of them are considered simultaneously, the effect of the depth-dependent mean ks plays a dominant role. Therefore the pressure head is still higher for the slope with a higher kk. The clearly difference of the pressure head profile at the same quantile situation shows the depth-dependent character can significantly affect the pressure head profile during steady state infiltration.

Figure 7.31b shows that the slope with a higher kk has a smaller factor of safety, and its failure zone is longer. This is because the slope with a higher kk has a higher pressure head.

Probability of failure

Figure 7.32 shows that the probability of failure increase quickly with the increase of kk. Therefore, the depth-dependent character can have a significant effect on the probability of failure of the infinite slope during steady state infiltration. However, the Pf is lower in this case, comparing with the Pf in the case considering the depth-dependent mean of ks only (Figure 7.20).

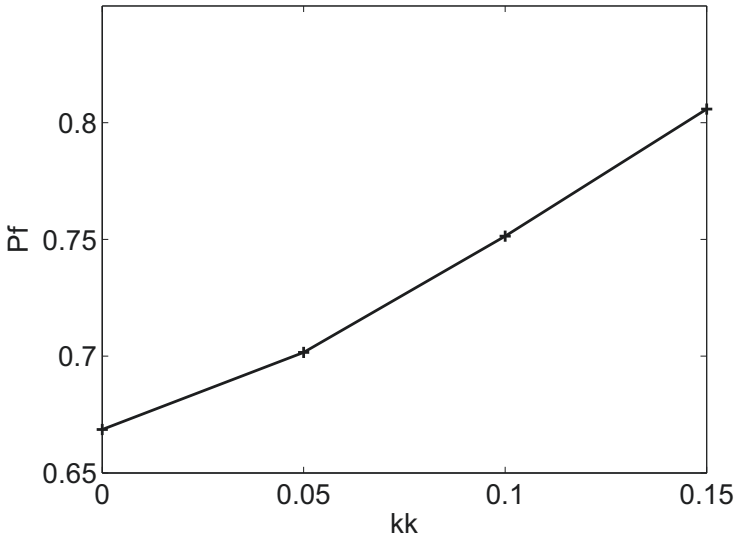

Figure 7.32.: Effect of kk on the Pf during steady state infiltration (CV=1)

Elevation of the critical failure surface

When the depth-dependent character of both the mean and standard deviation are considered, Figure 7.33 shows a similar trend for different kk. However, it can be seen that as the increase of kk, there is a relatively higher chance that the slope fails in a lower elevation of the slope. This result is corresponding to the factor of safety profiles in Figure 7.31b.

True flux

Figure 7.34 shows that the mean of the true negative flux increases as the increase of kk. This is because as kk increases, the mean ks of the top half part of the slope is higher, allowing more flux to infiltrate into the slope. Although a higher standard deviation of the top part of the slope can reduce the negative flux, the quantity is smaller. Because when the effect of both the mean and standard deviation are considered, the effect of the mean ks plays a dominant role. The mean of the negative flux is reduced when kk is increased from 0.05 to 0.15 in Figure 7.22, when only the mean ks is considered to be depth-dependent. This reduction is not found here because the the standard

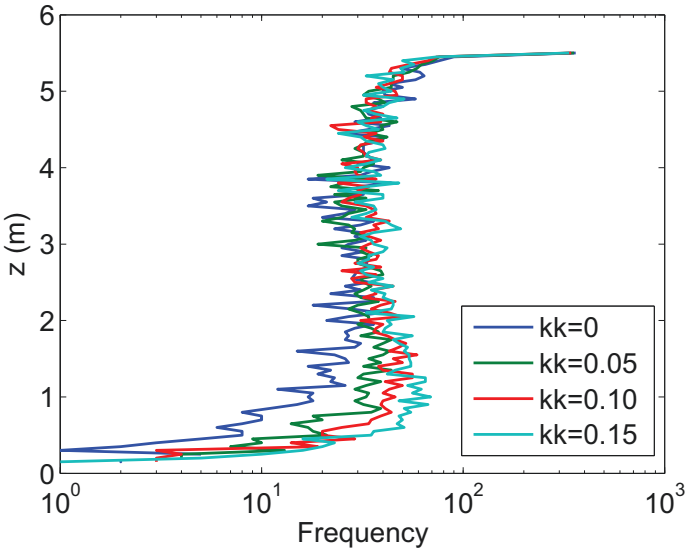

Figure 7.33.: Effect of depth-dependent character of mean ks on the elevation of the critical failure surface during steady state infiltration (CV_{ks}=1)

deviation of ks in the bottom half of the slope is smaller in this case, makes the ks fluctuate in a smaller level in this area. Therefore, there is less chance that the low permeable layer is generated in the bottom half of the slope, comparing with the case that only the depth-dependent mean ks is considered. When the preset negative flux is not so high (e.g. $5{\cdot}10^{-7}$ m/s used here), there is less chance that the perched water reaches to the slope surface and runs off.

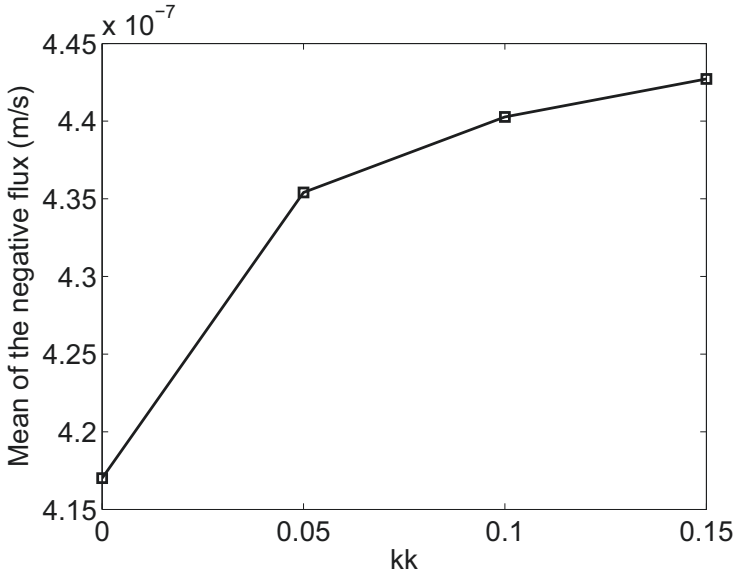

Figure 7.34.: Effect of depth-dependent character of mean ks on the true flux during steady state infiltration (CV_{ks}=1)

In summary, the depth-dependent character of both the mean and standard deviation of ks with constant CV has a significant effect on both the pressure head profile and the factor of safety profile. Meanwhile, as the increase of kk, both the probability of failure and the mean of the true negative flux are increased.

7.4.6. Effect of the depth-dependent mean of ks with CV=1 on the slope stability under transient state infiltration

In this section, the effect of the depth-dependent mean of ks with CV=1 on the slope stability under transient state infiltration is investigated.

Pressure head profile and factor of safety profile

For the case that both the mean and standard deviation reduces with soil depth, Figure 7.35a shows that the slope with a higher kk has a lower wetting front during the transient infiltration. This is reasonable because the top half of the slope have a higher mean value of ks, which means

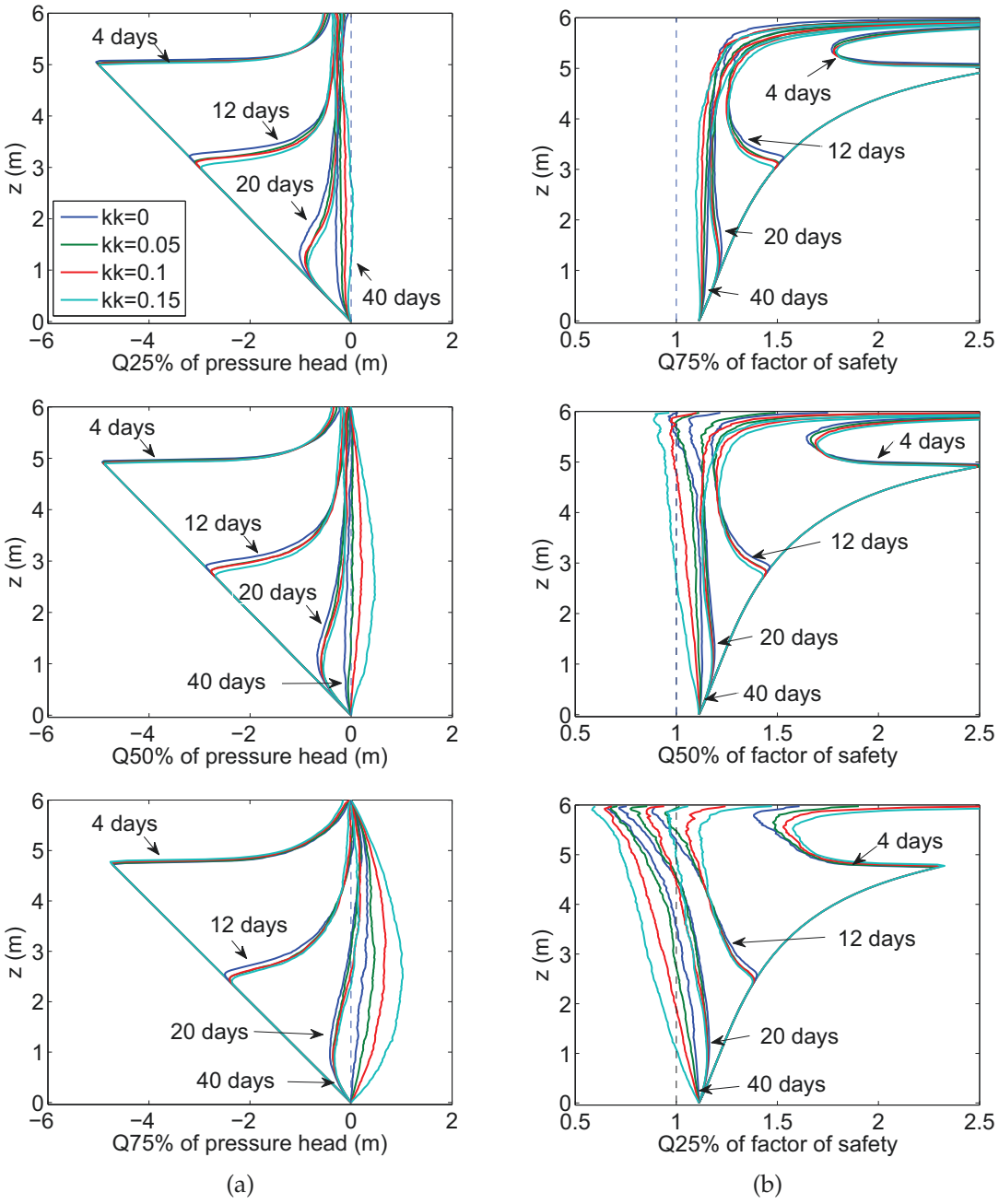

Figure 7.35.: Effect of the depth-dependent mean of ks with CV_{ks}=1 on the (a) pressure head profile, (b) factor of safety profile, during transient infiltration

the water, infiltrated into the slope, is larger at the same quantile situation. As the infiltration duration increases from the beginning till the steady state, the differences of the wetting front becomes larger, smaller, and larger again. This is reasonable because, although the depth-dependent character of both the mean and standard deviation is considered, the depth-dependent character of the mean dominates the effect of the depth-dependent character on the infiltration. This whole transient infiltration can also be categorized into 3 stages, similar to the case in which only the mean value is depth-dependent, and the explanation is similar. However, the difference of the wetting fronts, caused by the depth-dependent character at the same time step, becomes smaller, because the depth-dependent standard deviation can undermine this difference.

From the quantiles of the factor of safety profile in Figure 7.35b, it can be seen that the slope with a lower kk has a lower minimum FS in the wetting zone, and the elevation of this minimum factor of safety is slightly higher, when the infiltration duration is not too long (4-20 days here). However, as the infiltration approaches to the steady state (40 days), the slope with a higher kk has a smaller minimum factor of safety.

Probability of failure

Figure 7.36 shows the probability of failure is lower for the slope with a higher kk at the early and middle stages of transient infiltration. In detail, about 2% of the Pf is reduced at 4 days when kk increases from 0 to 0.15, if the failure of the top 0.5m is excluded. This reduction reaches to 15% at 12 days, and reduces to 8% at 20 days. As the infiltration approaches to the steady state, the probability of failure is higher for the slope with a higher kk. This is because the factor of safety of the slope is smaller in the wetting zone for the slope with a lower kk when the infiltration duration is not too long, however, it is larger when the infiltration approaches the steady state.

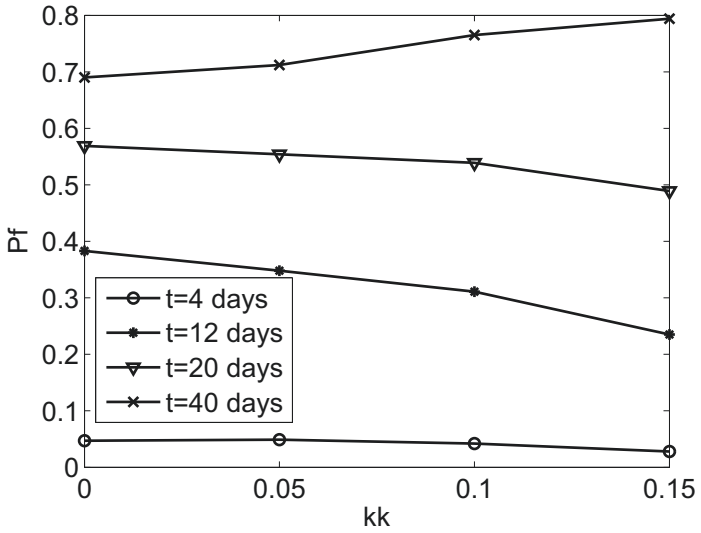

Figure 7.36.: Effect of the depth-dependent character of mean ks with CV_{ks}=1 on the Pf during transient infiltration

In summary: the infinite slope stability during transient infiltration can be significantly affected, if the depth-dependent character of both the mean and the standard deviation of ks are taken into account. Without considering it, the Pf can be overestimated in the early and middle stages of the infiltration, and the Pf can be underestimated if the infiltration approaches to the steady state. Meanwhile, when the depth-dependent character of both the mean and standard deviation is considered, the depth-dependent mean ks plays a dominant role.

7.4.7. Effect of the depth-dependent SCL of ks on the slope stability under steady state infiltration

The slope with depth-dependent spatial correlation lengths (SCL) is simplified as the slope with two layers: the upper and lower layers, with different SCL in each part. This kind of random field is generated by conditional sequential simulation using SGeMS. The situations with and without variance reduction (VR) are also considered. The preset flux, the mean of ks, and the standard deviation of ks is -5·10^{-7} m/s, 10^{-6} m/s, and 10^{-6} respectively in all cases. The SCLs in layered random field are different in different cases: Case A is the stationary random field case with SCL=0.5m all over the slope; Case B and C are slopes with different SCLs in the upper and lower parts, the SCL value and the length of each part in each case are listed in Table 7.2. The kk in the last column of Table 7.2 denotes the deviation of the SCL, it can be expressed as,

$$kk(SCL) = \frac{SCL_{upper} - SCL_{lower}}{SCL_{upper} + SCL_{lower}} \tag{7.2}$$

where the SCL_{upper} and SCL_{lower} are the spatial correlation lengths in the upper and lower layers of the slopes, respectively.

Table 7.2.: Basic information of the slope in each case (layered random field situations)

	Part of the slope	SCL(m)	Length(m)	kk(SCL)
Case A	All	0.5	6	0
Case B	Upper	0.6	3.6	0.2
	Lower	0.4	2.4	
Case C	Upper	0.75	4.5	0.5
	Lower	0.25	1.5	

Pressure head profile and factor of safety profile

Figure 7.37a shows the effect of the depth-dependent SCL on the quantiles of the pressure head profile. For the Q25% and Q50% situations, the pressure head profiles in the upper and lower parts of the slope show opposite trends. As kk increases, the upper part of the pressure head profile moves towards left, while the lower part moves towards right. For the Q75% profile, the pressure head moves towards left as the increase of kk. It can be seen that the difference of the pressure head profile caused by the depth-dependent SCL is not great. Figure 7.37a also shows that the variance reduction has little effect on the quantiles of the pressure head profiles in this case.

Figure 7.37b shows that the factor of safety profile slightly moves towards right, as the increase of kk at the upper part of the slope for Q50% and Q75% situations. Because the pressure head profile moves towards left in the upper part of the slope for Q25% and Q50% situations. The factor of safety profile in the lower part of the slope has little different. For the Q25% situation, the factor of safety profiles have little differences in these three cases. Meanwhile, the variance reduction has little effect on the factor of safety profile here.

Probability of failure

Figure 7.38 shows that the variance reduction can slightly reduce the probability of failure (about 1.5%), because variance reduction decreases the domain variance of ks. For the slope considering the variance reduction, the probability of failure decreases from 0.686 by 0.643 (less than 5%) when the kk increases from 0 to 0.5. In reality, the fluctuation of the SCL in one slope cannot change so sharply, which means the effect of depth-dependent SCL can only slightly reduce the probability

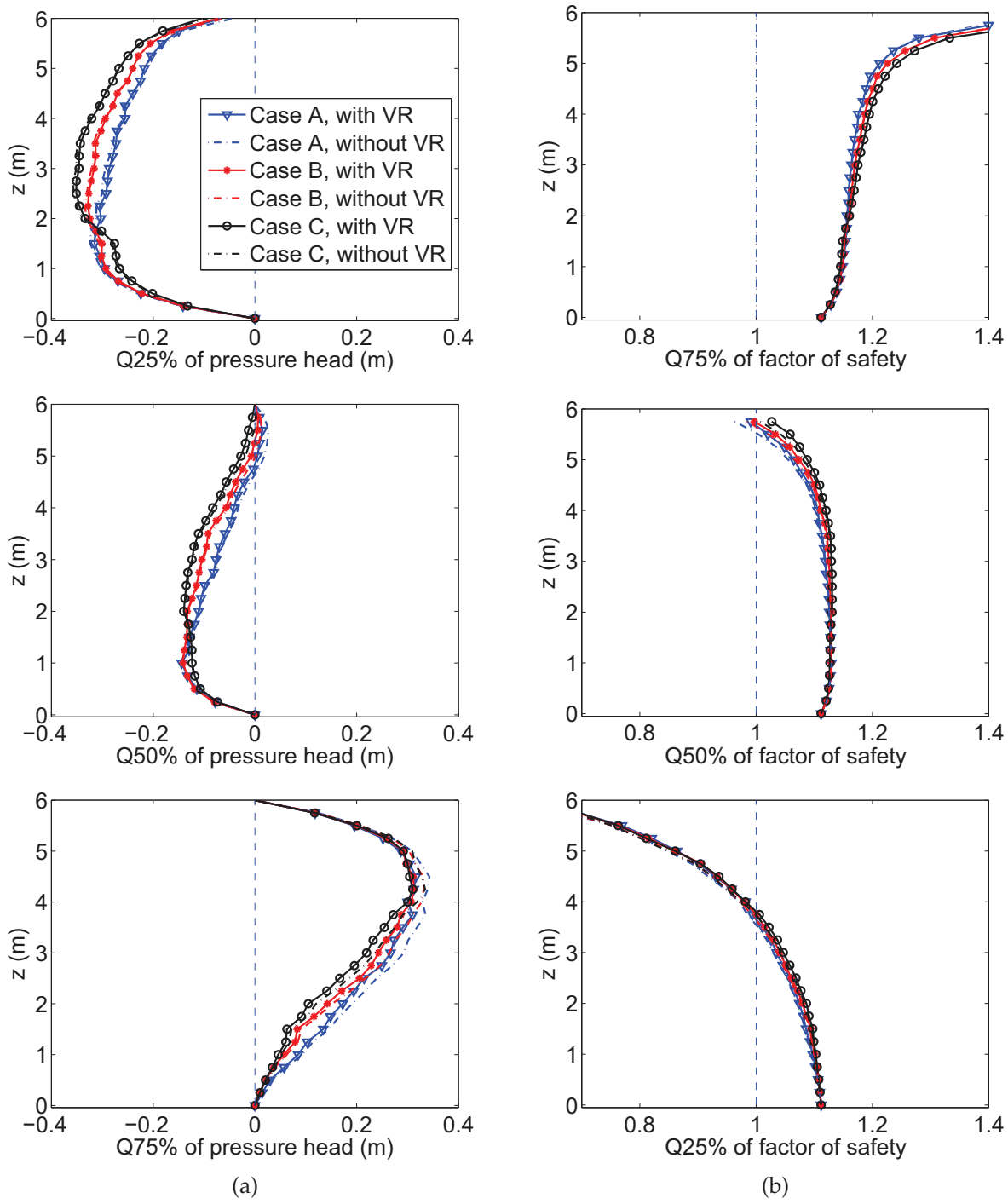

Figure 7.37.: Effect of depth-dependent SCL and VR of ln(ks) on the (a) pressure head profile and (b) factor of safety profile

of failure. Since the probability of failure is slightly higher if the depth-dependent character is neglected, which means the stability of the evaluated slope is a little conservative. It is reasonable to conclude that this depth-dependent character of the SCL can be neglected.

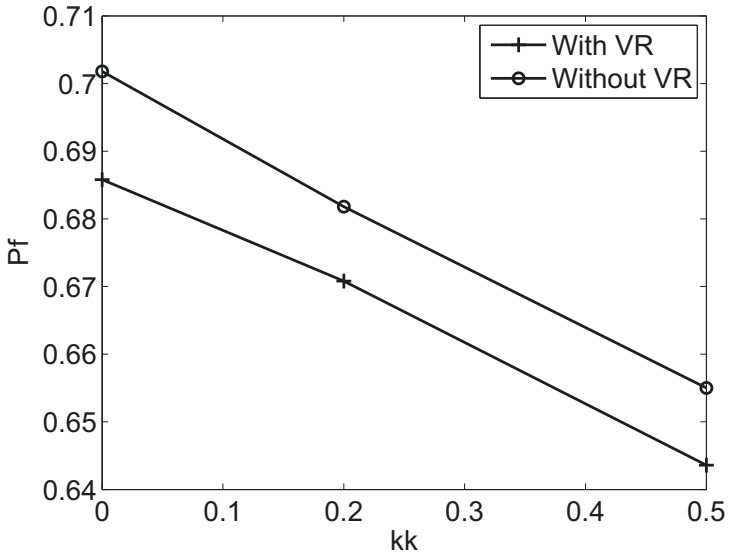

Figure 7.38.: Effect of depth-dependent character of SCL and VR on the probability of failure of the slope

True flux

Figure 7.39 shows that, as kk increases, the mean of true negative flux reduces slightly. Meanwhile, the variance reduction can slightly increase the mean of true negative flux, because the variance reduction reduces the scale of the fluctuation of a random field.

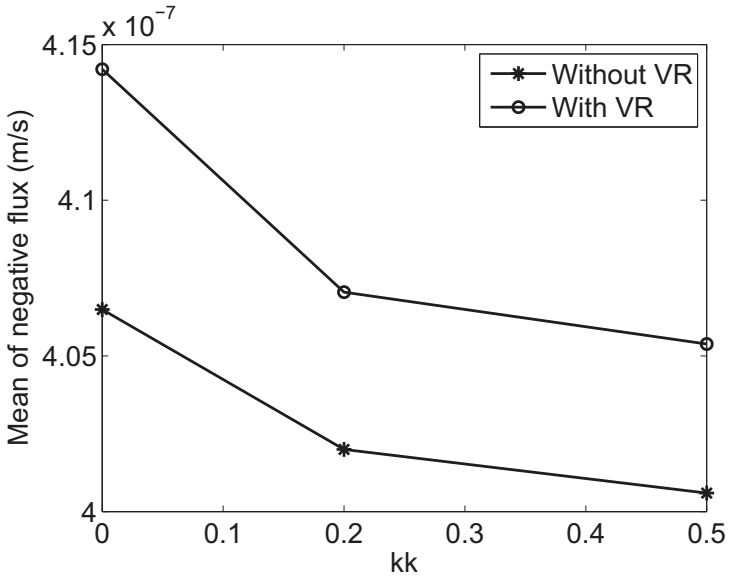

Figure 7.39.: Effect of depth-dependent character of SCL and VR on the mean of true negative flux

In summary, an increase of the depth-dependent character of the spatial correlation length of ln(ks) can slightly reduce both the probability of failure and the mean of true negative flux. This reduction is insignificant. Therefore, the depth-dependent character of the spatial correlation length

can be neglected.

7.5. Synopsis

In this chapter, a stochastic analysis is carried out to study the infinite slope stability during infiltration, taking ks as the only random variable with a lognormal distribution.

Through the study at stationary random field situation, it is found that:

- As the infiltration duration increases, the wetting front goes deeper, the probability of failure increases significantly, and the failure zone becomes longer.
- An increase of coefficient of variation of ks can significantly increase the probability of failure under both transient and steady state infiltration.
- The spatial correlation length of ln(ks) has a significant effect on the probability of failure. When the spatial correlation length is at a moderate level, the probability of failure is the highest. A higher or lower spatial correlation length can reduce the probability of failure during both the steady state infiltration and late stage of the transient state infiltration, while a small spatial correlation length can slightly increase the probability of failure at the early stage of the transient infiltration.

Through the study at non-stationary random field situations, the depth-dependent character of the stochastic parameters of ks is highlighted, it is found that:

- The depth-dependent character of mean ks has a significant effect on the probability of failure. For the case that the mean of ks reduces linearly with depth during steady state infiltration, an increase of the depth-dependent character can significantly increase the probability of failure of the slope. If the transient infiltration is considered, three stages can be categorized according to the infiltration duration. If the depth-dependent character of the mean ks is not considered, the probability of failure is overestimated in the early and middle stages, and it is highly underestimated in the later stage of the infiltration.
- For the case that the standard deviation of ks reduces linearly with depth, the probability of failure is moderately reduced as the increase of the depth-dependent character during steady state infiltration. If the transient infiltration is taken into consideration, the probability of failure is underestimated in the early stage of the infiltration, and it is overestimated if the infiltration lasts long enough, if the depth-dependent character is neglected.
- If the depth-dependent character of both the mean and the standard deviation are considered, the depth-dependent mean value plays the dominate effect on the results.
- The depth-dependent character of the spatial correlation length of ln(ks) can slightly reduce the probability of failure. This reduction is very small and can be neglected.

8. Conclusions and recommendations

The variability of a soil property and its influence can be studied through the quantification of its stochastic parameters (the mean, the standard deviation, and the spatial correlation length), and the evaluation that how these stochastic parameters affects geotechnical practice. Probabilistic simulations have shown that these stochastic parameters of some soil properties can significantly influence geotechnical practice. For all the stochastic studies, the standard deviation and the spatial correlation length are assumed to be constant, while most of the studies are carried out assuming the mean value is constant too. However, these assumptions are not validated. Since these stochastic parameters are very important, the main aim of this thesis is to check whether these assumptions are true, if not, what is the effect?

8.1. Summary and conclusions

Questions were proposed in chapter one as the motivation of this thesis. Some studies are carried out from chapter 3 to chapter 7 based on these questions. In this section, these questions will be answered while the main outcomes are summarized.

1. Does the stress level affect the stochastic parameters of void ratio related properties of sand? How does the stress level affect these parameters? Are the stochastic parameters depth-dependent?

Taking the void ratio as a representative property, the effect of stress level on the stochastic parameters of void ratio related properties of sand, is carried out through the simulation of the one-dimensional compression test, using the VW hypoplastic model. The results show that:

- All the stochastic parameters of void ratio of sand reduce with the increase of the stress level. Since the void ratio is directly related to some of the key properties, such as the saturated hydraulic conductivity, density, unit weight, friction angle, and so on, these parameters should be affected by the stress level too.
- Because soil suffers different self-weight at different soil-depth, the stochastic parameters of the void ratio related parameters of sand should be depth-dependent.

2. Since the stochastic parameters of void ratio related properties of sand are depth-dependent, the following question comes up: How do we generate the random field considering the depth-dependent character of these stochastic parameters? This question is discussed in detail in chapter 4. It is found that:

- The generation of the random field with depth-dependent mean or/and the standard deviation is rather simple, it can be generated through a simple distortion of the stationary random field.
- The generation of the random field with depth-dependent spatial correlation length is relatively complex. Two different methods are proposed: the first one bases on the random field distortion from Hicks (Hicks and Samy, 2002). However, the standard deviation needs to be compensated when it is used. The second method is to layer the random fields with different spatial correlation lengths using conditional random field generation. It is found

that both the length and the spatial correlation length of each individual random field can affect the mean spatial correlation length of the whole random field. The mean spatial correlation length, can be evaluated by the harmonic mean of individual spatial correlation length considering the length of each individual random field.

3. How does the depth-dependent character of the variability of void ratio related properties affect the soil behavior with view to geotechnical practice? Is this effect significantly enough to be considered?

Through the comparison of the strain at different stress level with and without considering the depth-dependent character of the variation of void ratio during the one-dimensional settlement analysis, it is found that:

· The depth-dependent character of these stochastic parameters has low effect on the mean strain.

· If the serviceability limit state is taken as the performance function, the probability of failure can be slightly increased when the mean void ratio is highly depth-dependent in the case. The depth-dependent character of the standard deviation of void ratio can slightly increase the probability of failure. The depth-dependent character of the spatial correlation length has little effect on the probability of failure.

· In reality, the settlement is far smaller than the results simulated in chapter 3, because the real hs is far larger. Therefore, the depth-dependent character has little effect on both the strain and the probability of failure. This might be caused by the limitation of the hypoplastic model. It is known that one of the tails of the distribution is the key to generate the week path, however, the void ratio of hypoplasticity in this study follows a truncated Gaussian distribution, and there is no tail.

The saturated hydraulic conductivity (ks) is positively related to the void ratio. Therefore, the stochastic parameters of ks should be depth-dependent. Through the deterministic infinite slope stability analysis, the effect of the depth-dependent mean trend of ks on both the infiltration of rainwater and slope stability are analyzed. The results show that:

· During the steady state infiltration of rainwater, the depth-dependent ks has significant influences on both the pressure head profile and the slope stability when the negative flux is high (near to the mean of ks). This is because the positive pressure head can be generated in the slope with depth-dependent ks. This positive pressure head can cause the slope failure in a lower critical failure surface. Neglecting the depth-dependent character of mean ks, the positive pressure head can not be generated, and the factor of safety can be overestimated during steady state infiltration, when the negative flux is high.

· During the transient state infiltration, the positive pressure head is generated earlier, and the slope fails earlier in the soil with a greater depth-dependent ks, in the case that the negative flux is high. The considered slope is always stable if the depth-dependent character is not regarded.

· If the negative flux is not so high, the depth-dependent character can only moderately affect the pressure head profile and slightly influence the factor of safety profile, during both the steady state and transient state infiltration.

Some parametric studies are carried out. It is found that the SWCC parameter n controls the shape of the degree of saturation profile, the pressure head profile, and the factor of safety profile, while the empirical fitting parameter α controls the magnitude of these profiles. Moreover, when

the flux is taken into consideration, it is found that, a small negative flux can help stabilize the slope above the groundwater table in the case with a large n, which is surprising since rainwater is responsible for the slope failure.

The stochastic infinite slope stability analysis during infiltration is also carried out considering the variability of the saturated hydraulic conductivity. The depth-dependent character of these stochastic parameters of ks can affect the slope stability. It can be summarized:

- The depth-dependent character of mean ks has a significant effect on the slope stability analysis. For the case that the mean of ks reduces linearly with depth during steady state infiltration, increasing the depth-dependent character can significantly increase the probability of failure of the slope. If the transient infiltration is considered, three stages can be categorized to describe the transient infiltration process. If the depth-dependent character of the mean ks is not considered, the probability of failure is overestimated in the early and middle stages, and it is highly underestimated in the late stage of the infiltration. This is because the mean ks reduces with depth, which means there is more chance that the low permeable layer is generated at a lower location of the slope. These low permeable layers are the key to the positive pressure head generation, when the wetting front reaches at this area. The positive pressure head is essential to the slope failure.
- In the case that the standard deviation of ks reduces linearly with depth, the probability of failure is moderately reduced as the increase of the depth-dependent character, during steady state infiltration. If a transient infiltration is taken into consideration, the probability of failure is underestimated in the early stage of the infiltration, and it is overestimated when the infiltration lasts long enough, if the depth-dependent character is neglected. This is because, when the linearly depth-dependent character of the standard deviation is taken into consideration, the standard deviation of the top half of the slope is higher, which means the low permeable layer in this area can be generated in a higher chance. These low permeable layers can reduce the true negative flux infiltrated into a lower area, so as to reduce the chance of positive pressure head generation in the late stage of the infiltration.
- If the depth-dependent character of both the mean and the standard deviation of ks is considered, the depth-dependent mean value plays a dominate effect on the results.
- The depth-dependent character of the spatial correlation length of ln(ks) can slightly reduce the probability of failure. This reduction is very small and can be neglected.
- Besides the probability of failure, the effect of the depth-dependent character on the pressure head profile, the factor of safety profile, the elevation of the critical failure surface, and the flux are also discussed.

An increase of the coefficient of variation of ks can significantly increase the probability of failure in both transient and steady state infiltration.

Moreover, it is found that the spatial correlation length of ln(ks) has a significant effect on the probability of failure. The probability of failure is the highest when the spatial correlation length of ln(ks) is at a moderate level. A higher or lower spatial correlation length can reduce the probability of failure during the infiltration. This is because the moderate spatial correlation length can make the random field of ks has the greatest fluctuation.

It can be shown that the effect of the depth-dependent character is different for different cases of geotechnical practice, since the depth-dependent character has little effect on the one-dimensional settlement, while it has significant effects on both the infiltration and infinite slope stability analysis.

8.2. Recommendations for future study

To give a closure to this thesis, the following recommendations for future researches can be given:

- The effect of stress level on the properties of cohesive soil. This study focuses on the effect of stress level on the stochastic parameters of void ratio related properties of sand. Since there is a big difference between the sandy soil and cohesive soil, it is necessary to change the material from sand into a cohesive soil and then to analyze the results. It can be expected that the variability of water content and cohesion have a strong effect to all kinds of stability-problems.
- How does the depth-dependent character of the stochastic parameters of the other void ratio related parameters affect geotechnical practice? In this thesis, only the variation of void ratio and saturated hydraulic conductivity are regarded to be depth-dependent. The effect of the variability of other void ratio related parameters might be worthy of study.
- Only the settlement analysis and infinite slope stability analysis are carried out considering the depth-dependent character. Since the effect of the depth-dependent character is different for different geotechnical applications, it is necessary to find out the effect of this depth-dependent character on the other geotechnical applications. Meanwhile, only one-dimensional simulations are carried out in this thesis, it is necessary to carry out the two-dimensional and three-dimensional simulations, and to compare the results.
- The depth-dependent character of both the void ratio and the ks is assumed to reduce linearly with soil depth in this thesis. However, the trend is non-linear in reality. It is necessary to find the real trends of these stochastic parameters through experiments, and then to carry out some simulations based on the real trends.
- In this thesis, only one variable is considered, the cross-correlation between void ratio related variables of sand is neglected. Therefore, it might be a good topic to study the effect of the depth-dependent character on geotechnical practice considering the cross-correlation of variables.

Bibliography

Ahmed, A. A. (2009), 'Stochastic analysis of free surface flow through earth dams', *Computers and Geotechnics* **36**(7), 1186–1190.

Akaike, H. (1998), A bayesian analysis of the minimum aic procedure, *in* 'Selected Papers of Hirotugu Akaike', Springer, pp. 275–280.

Al-Bittar, T. and Soubra, A.-H. (2013), 'Bearing capacity of strip footings on spatially random soils using sparse polynomial chaos expansion', *International Journal for Numerical and Analytical Methods in Geomechanics* **37**(13), 2039–2060.

Alonso, E. E. (1976), 'Risk analysis of slopes and its application to slopes in canadian sensitive clays', *Geotechnique* **26**(3), 453–472.

Armstrong, M. (1998), *Basic linear geostatistics*, Springer Science & Business Media.

Assimaki, D., Pecker, A., Popescu, R. and Prevost, J. (2003), 'Effects of spatial variability of soil properties on surface ground motion', *Journal of earthquake engineering* **7**(spec01), 1–44.

Baecher, G. B. and Christian, J. T. (2005), *Reliability and statistics in geotechnical engineering*, John Wiley & Sons.

Baecher, G. B. and Keeney, R. L. (1982), 'Statistical examination of reservoir-induced seismicity', *Bulletin of the Seismological Society of America* **72**(2), 553–569.

Baker, J. W. and Faber, M. H. (2008), 'Liquefaction risk assessment using geostatistics to account for soil spatial variability', *Journal of geotechnical and geoenvironmental engineering* **134**(1), 14–23.

Bakhtiari, S. (2011), Stochastic finite element slope stability analysis, PhD thesis, University of Manchester.

Bakr, A. A., Gelhar, L. W., Gutjahr, A. L. and MacMillan, J. R. (1978), 'Stochastic analysis of spatial variability in subsurface flows: 1. comparison of one-and three-dimensional flows', *Water Resources Research* **14**(2), 263–271.

Barnes, R. J. (1991), 'The variogram sill and the sample variance', *Mathematical geology* **23**(4), 673–678.

Beacher, G. B. and Ingra, T. S. (1981), 'Stochastic fem in settlement predictions', *Journal of Geotechnical and Geoenvironmental Engineering* **107**(ASCE 16179).

Bergado, D. T. and Anderson, L. R. (1985), 'Stochastic analysis of pore pressure uncertainty for the probabilistic assessment of the safety of earth slopes.', *Soils and Foundations* **25**(2), 87–105.

Box, G. E., Jenkins, G. M., Reinsel, G. C. and Ljung, G. M. (2015), *Time series analysis: forecasting and control*, John Wiley & Sons.

Burkardt, J. (2014), 'The truncated normal distribution', *Department of Scientific Computing Website, Florida State University* .

Calamak, M., Kentel, E. and Yanmaz, A. (2012), Seepage analysis through earth-fill dams having random fields, *in* '10th International Congress on Advances in Civil Engineering, Ankara, Turkey', p. 97.

Calamak, M., Yanmaz, A. et al. (2014), Probabilistic assessment of slope stability for earth-fill dams having random soil parameters, *in* '11th National Conference on Hydraulics in Civil Engineering & 5th International Symposium on Hydraulic Structures: Hydraulic Structures and Society-Engineering Challenges and Extremes', Engineers Australia, p. 34.

Carrier III, W. D. (2003), 'Goodbye, hazen; hello, kozeny-carman', *Journal of geotechnical and geoenvironmental engineering* **129**(11), 1054–1056.

Carroll, R. J., Ruppert, D. and Welsh, A. H. (1998), 'Local estimating equations', *Journal of the American Statistical Association* **93**(441), 214–227.

Cavoundis, S. (1987), 'On the ratio of factors of safety in slope stability analyses', *Geotechnique* **37**(2).

Chen, R. and Chameau, J.-L. (1983), 'Three-dimensional limit equilibrium analysis of slopes', *Geotechnique* **33**(1), 31–40.

Cheng, Y. (2008), 'Numerical simulation of unsaturated flow using modified transformation methods', *Civil Engineering. National University of Singapore* p. 259.

Cherubini, C. (2000), 'Reliability evaluation of shallow foundation bearing capacity on c'φ'soils', *Canadian Geotechnical Journal* **37**(1), 264–269.

Cherubini, C., Giasi, C. and Rethati, L. (1995), The coefficients of variation of some geotechnical parameters, *in* 'Conference on Probabilistic Methods in Geotecnhical Engineering', Balkema.

Chiasson, P., Lafleur, J., Soulié, M. and Law, K. T. (1995), 'Characterizing spatial variability of a clay by geostatistics', *Canadian Geotechnical Journal* **32**(1), 1–10.

Chiles, J.-P. and Delfiner, P. (2009), *Geostatistics: modeling spatial uncertainty*, Vol. 497, John Wiley & Sons.

Cho, S. E. (2007), 'Effects of spatial variability of soil properties on slope stability', *Engineering Geology* **92**(3), 97–109.

Cho, S. E. (2009), 'Probabilistic assessment of slope stability that considers the spatial variability of soil properties', *Journal of geotechnical and geoenvironmental engineering* **136**(7), 975–984.

Cho, S. E. (2012), 'Probabilistic analysis of seepage that considers the spatial variability of permeability for an embankment on soil foundation', *Engineering Geology* **133**, 30–39.

Cho, S. E. (2014), 'Probabilistic stability analysis of rainfall-induced landslides considering spatial variability of permeability', *Engineering Geology* **171**, 11–20.

Cho, S. E. and Park, H. C. (2010), 'Effect of spatial variability of cross-correlated soil properties on bearing capacity of strip footing', *International journal for numerical and analytical methods in geomechanics* **34**(1), 1–26.

Chowdhury, R. and Xu, D. (1995), 'Geotechnical system reliability of slopes', *Reliability Engineering & System Safety* **47**(3), 141–151.

Christian, J. T., Ladd, C. C. and Baecher, G. B. (1994), 'Reliability applied to slope stability analysis', *Journal of Geotechnical Engineering* **120**(12), 2180–2207.

Collins, B. D. and Znidarcic, D. (2004), 'Stability analyses of rainfall induced landslides', *Journal of Geotechnical and Geoenvironmental Engineering* **130**(4), 362–372.

Cornforth, D. (1973), Prediction of drained strength of sands from relative density measurements, *in* 'Evaluation of relative density and its role in geotechnical projects involving cohesionless soils', ASTM International.

Cornforth, D. (2005), *Landslides in practice: investigation, analysis, and remedial/preventative options in soils*, Wiley.

Cressie, N. (2015), *Statistics for spatial data*, John Wiley & Sons.

Dasaka, S. M. (2005), Probabilistic site characterization and reliability analysis of shallow foundations and slopes, PhD thesis, Indian Institute of Science Bangalore.

Dasaka, S. and Zhang, L. (2012), 'Spatial variability of in situ weathered soil', *Géotechnique* **62**(5), 375.

David, M. (2012), *Geostatistical ore reserve estimation*, Elsevier.

De Campos, T., Andrade, M. and Vargas, E. (1991), Unsaturated colluvium over rock slide in a forested site in rio de janeiro, brazil, *in* 'Proc. 6th Int. Symp. on Landslides, Christchurch New Zealand, Balkema, Rotterdam, Netherlands', pp. 1357–1364.

DeGroot, D. J. (1996), Analyzing spatial variability of in situ soil properties, *in* 'Uncertainty in the geologic environment: From theory to practice', ASCE, pp. 210–238.

DeGroot, D. J. and Baecher, G. B. (1993), 'Estimating autocovariance of in-situ soil properties', *Journal of Geotechnical Engineering* **119**(1), 147–166.

Deodatis, G., Ellingwood, B. R. and Frangopol, D. M. (2014), *Safety, reliability, risk and life-cycle performance of structures and infrastructures*, CRC Press.

Duncan, J. M. (1996), 'State of the art: limit equilibrium and finite-element analysis of slopes', *Journal of Geotechnical engineering* **122**(7), 577–596.

Duncan, J. M. (2000), 'Factors of safety and reliability in geotechnical engineering', *Journal of geotechnical and geoenvironmental engineering* **126**(4), 307–316.

Easa, S. M. (1992), 'Exact probabilistic solution of two-parameter bearing capacity for shallow foundations', *Canadian Geotechnical Journal* **29**(5), 867–870.

Ejezie, S. and Harrop-Williams, K. (1984), 'Probabilistic characterization of nigerian soils', *Probabilistic characterization of soil properties: bridge between theory and practice/edited by David S. Bowles and Hon-Yim Ko* .

El-Ramly, H., Morgenstern, N. and Cruden, D. (2002), 'Probabilistic slope stability analysis for practice', *Canadian Geotechnical Journal* **39**(3), 665–683.

El-Ramly, H., Morgenstern, N. and Cruden, D. (2003), 'Probabilistic stability analysis of a tailings dyke on presheared clay shale', *Canadian Geotechnical Journal* **40**(1), 192–208.

El-Ramly, H., Morgenstern, N. and Cruden, D. (2005), 'Probabilistic assessment of stability of a cut slope in residual soil', *Geotechnique* **55**(1), 77–84.

El-Ramly, H., Morgenstern, N. and Cruden, D. (2006), 'Lodalen slide: a probabilistic assessment', *Canadian Geotechnical Journal* **43**(9), 956–968.

Elachachi, S., Breysse, D. and Denis, A. (2012), 'The effects of soil spatial variability on the reliability of rigid buried pipes', *Computers and Geotechnics* **43**, 61–71.

Elkateb, T. M. (2003), Quantification of soil heterogeneity, PhD thesis, Ph. D. thesis, University of Alberta, Edmonton, Alta.

Fayer, M. J. (2000), 'Unsat-h version 3.0: Unsaturated soil water and heat flow model. theory, user manual, and examples', *Pacific Northwest National Laboratory* **13249**.

Fenton, G. A. (1999*a*), 'Estimation for stochastic soil models', *Journal of Geotechnical and Geoenvironmental Engineering* **125**(6), 470–485.

Fenton, G. A. (1999*b*), 'Random field modeling of cpt data', *Journal of Geotechnical and Geoenvironmental Engineering* **125**(6), 486–498.

Fenton, G. A. and Griffiths, D. (1994), *Flow through earth dams with spatially random permeability*, Geomechanics Research Center, Colorado School of Mines.

Fenton, G. A. and Griffiths, D. (1996), 'Statistics of free surface flow through stochastic earth dam', *Journal of geotechnical engineering* **122**(6), 427–436.

Fenton, G. A. and Griffiths, D. (2002), 'Probabilistic foundation settlement on spatially random soil', *Journal of Geotechnical and Geoenvironmental Engineering* **128**(5), 381–390.

Fenton, G. A. and Griffiths, D. (2003), 'Bearing-capacity prediction of spatially random c φ soils', *Canadian geotechnical journal* **40**(1), 54–65.

Fenton, G. A. and Griffiths, D. (2005), 'Three-dimensional probabilistic foundation settlement', *Journal of Geotechnical and Geoenvironmental Engineering* **131**(2), 232–239.

Fenton, G. A. and Griffiths, D. V. (2008), *Risk assessment in geotechnical engineering*, Wiley.

Fenton, G. A. and Vanmarcke, E. H. (1991), Spatial variation in liquefaction risk assessment, *in* 'Geotechnical Engineering Congress?1991:', ASCE, pp. 594–607.

Fredlund, D. and Dahlman, A. (1972), 'Statistical geotechnical properties of glacial lake edmonton sediments', *Statistics and Probability in Civil Engineering* .

Fredlund, D. G. and Rahardjo, H. (1993), *Soil mechanics for unsaturated soils*, John Wiley & Sons.

Freeze, R. A. (1975), 'A stochastic-conceptual analysis of one-dimensional groundwater flow in nonuniform homogeneous media', *Water Resources Research* **11**(5), 725–741.

Gardner, W. (1958), 'Some steady-state solutions of the unsaturated moisture flow equation with application to evaporation from a water table.', *Soil science* **85**(4), 228–232.

Gasmo, J., Rahardjo, H. and Leong, E. C. (2000), 'Infiltration effects on stability of a residual soil slope', *Computers and Geotechnics* **26**(2), 145–165.

Godt, J. W., Baum, R. L. and Mckenna, J. P. (2007), Vadose-zone response to rainfall leading to shallow landslide initiation on the puget sound bluffs, washington, *in* '2007 GSA Denver Annual Meeting'.

Goovaerts, P. (1997), *Geostatistics for natural resources evaluation*, Oxford University Press on Demand.

Griffiths, D. and Fenton, G. A. (2001), 'Bearing capacity of spatially random soil: the undrained clay prandtl problem revisited', *Geotechnique* **51**(4), 351–360.

Griffiths, D. and Fenton, G. A. (2004), 'Probabilistic slope stability analysis by finite elements', *Journal of Geotechnical and Geoenvironmental Engineering* **130**(5), 507–518.

Griffiths, D. and Fenton, G. A. (2009), 'Probabilistic settlement analysis by stochastic and random finite-element methods', *Journal of geotechnical and geoenvironmental engineering* **135**(11), 1629–1637.

Griffiths, D., Fenton, G. A. and Manoharan, N. (2002), 'Bearing capacity of rough rigid strip footing on cohesive soil: probabilistic study', *Journal of Geotechnical and Geoenvironmental Engineering* **128**(9), 743–755.

Griffiths, D., Fenton, G. A. and Manoharan, N. (2006), 'Undrained bearing capacity of two-strip footings on spatially random soil', *International Journal of Geomechanics* **6**(6), 421–427.

Griffiths, D., Huang, J. and Fenton, G. A. (2009*a*), 'Influence of spatial variability on slope reliability using 2-d random fields', *Journal of Geotechnical and Geoenvironmental Engineering* **135**(10), 1367–1378.

Griffiths, D., Huang, J. and Fenton, G. A. (2009*b*), On the reliability of earth slopes in three dimensions, *in* 'Proceedings of the Royal Society of London A: Mathematical, Physical and Engineering Sciences', The Royal Society, p. rspa20090165.

Griffiths, D., Huang, J. and Fenton, G. A. (2011), 'Probabilistic infinite slope analysis', *Computers and Geotechnics* **38**(4), 577–584.

Gui, S., Zhang, R., Turner, J. P. and Xue, X. (2000), 'Probabilistic slope stability analysis with stochastic soil hydraulic conductivity', *Journal of Geotechnical and Geoenvironmental Engineering* **126**(1), 1–9.

Harr, M. E. (1977), *Mechanics of particulate media*, McGraw-Hill.

Hicks, M. A., Nuttall, J. D. and Chen, J. (2014), 'Influence of heterogeneity on 3d slope reliability and failure consequence', *Computers and Geotechnics* **61**, 198–208.

Hicks, M. A. and Onisiphorou, C. (2005), 'Stochastic evaluation of static liquefaction in a predominantly dilative sand fill', *Géotechnique* **55**(2), 123–133.

Hicks, M. A. and Samy, K. (2002), 'Influence of heterogeneity on undrained clay slope stability', *Quarterly Journal of Engineering Geology and Hydrogeology* **35**(1), 41–49.

Hicks, M. A. and Samy, K. (2004), 'Stochastic evaluation of heterogeneous slope stability', *Italian Geotechnical Journal* **38**(2), 54–66.

Hicks, M. A. and Spencer, W. A. (2010), 'Influence of heterogeneity on the reliability and failure of a long 3d slope', *Computers and Geotechnics* **37**(7), 948–955.

Hoeksema, R. J. and Kitanidis, P. K. (1985), 'Analysis of the spatial structure of properties of selected aquifers', *Water Resources Research* **21**(4), 563–572.

Huber, M. (2013), Soil variability and its consequences in geotechnical engineering, PhD thesis.

Hungr, O. (1987), 'An extension of bishop's simplified method of slope stability analysis to three dimensions', *Geotechnique* **37**(1), 113–117.

Hydraulic, S. (2008), 'Standard guideline for fitting saturated hydraulic conductivity using probability density functions'.

Jaksa, M. B. (1995), The influence of spatial variability on the geotechnical design properties of a stiff, overconsolidated clay., PhD thesis.

Jaksa, M., Kaggwa, W. and Brooker, P. (1999), Experimental evaluation of the scale of fluctuation of a stiff clay, *in* 'Proc. 8th Int. conf. on the application of statistics and probability, Sydney', Vol. 1, pp. 415–422.

Jamshidi Chenari, R. and Mahigir, A. (2014), 'The effect of spatial variability and anisotropy of soils on bearing capacity of shallow foundations', *Civil Engineering Infrastructures Journal* **47**(2), 199–213.

Jardine, R., Potts, D., Higgins, K., Bromhead, E. and Martin, P. (2004), Three-dimensional limit equilibrium analysis of the taren landslide, *in* 'Advances in Geotechnical Engineering-The Skempton Conference. A Three Day Conference on Advances in Engineering, Organised By The Institution of Civil Engineers, Held at The Royal Geographical Society, London, 29-31 March 2004', Vol. 2.

Ji, J. and Low, B. K. (2012), 'Stratified response surfaces for system probabilistic evaluation of slopes', *Journal of Geotechnical and Geoenvironmental Engineering* **138**(11), 1398–1406.

Jimenez, R. and Sitar, N. (2009), 'The importance of distribution types on finite element analyses of foundation settlement', *Computers and Geotechnics* **36**(3), 474–483.

Journel, A. G. and Huijbregts, C. J. (1978), *Mining geostatistics*, Academic press.

Kasama, K. and Whittle, A. J. (2011), 'Bearing capacity of spatially random cohesive soil using numerical limit analyses', *Journal of Geotechnical and Geoenvironmental Engineering* **137**(11), 989–996.

Kasama, K., Whittle, A. J. and Zen, K. (2012), 'Effect of spatial variability on the bearing capacity of cement-treated ground', *Soils and Foundations* **52**(4), 600–619.

Kim, H.-S., Major, G., Ross-Brown, D. et al. (1978), Application of monte carlo techniques to slope stability analyses, *in* '19th US Symposium on Rock Mechanics (USRMS)', American Rock Mechanics Association.

Kim, J. M. and Sitar, N. (2013), 'Reliability approach to slope stability analysis with spatially correlated soilproperties', *Soils and Foundations* **53**(1), 1–10.

Koltermann, C. E. and Gorelick, S. M. (1996), 'Heterogeneity in sedimentary deposits: A review of structure-imitating, process-imitating, and descriptive approaches', *Water Resources Research* **32**(9), 2617–2658.

Kulhawy, F. H. (1993), On the evaluation of static soil properties, *in* 'Stability and performance of slopes and Embankments II', ASCE, pp. 95–115.

Kuo, Y., Jaksa, M., Kaggwa, G., Fenton, G., Griffiths, D. and Goldsworthy, J. (2004), 'Probabilistic analysis of multi-layered soil effects on shallow foundation settlement'.

Kwak, K., Kim, K. J., Huh, J., Lee, J. H. and Park, J. H. (2010), 'Reliability-based calibration of resistance factors for static bearing capacity of driven steel pipe piles', *Canadian Geotechnical Journal* **47**(5), 528–538.

Lacasse, S. and Nadim, F. (1997), 'Uncertainties in characterising soil properties', *Publikasjon-Norges Geotekniske Institutt* **201**, 49–75.

Le, T. M. H., Gallipoli, D., Sánchez, M. and Wheeler, S. (2015), 'Stability and failure mass of unsaturated heterogeneous slopes', *Canadian Geotechnical Journal* **52**(11), 1747–1761.

Li, D.-Q., Qi, X.-H., Phoon, K.-K., Zhang, L.-M. and Zhou, C.-B. (2014), 'Effect of spatially variable shear strength parameters with linearly increasing mean trend on reliability of infinite slopes', *Structural safety* **49**, 45–55.

Li, K. and Lee, I. (1991), 'The assessment of geotechnical safety', *Selected Topics in Geotechnical Engineering-Lumb Volume* **195**, 229.

Li, K. and Lumb, P. (1987), 'Probabilistic design of slopes', *Canadian Geotechnical Journal* **24**(4), 520–535.

Lim, T., Rahardjo, H., Chang, M. and Fredlund, D. G. (1996), 'Effect of rainfall on matric suctions in a residual soil slope', *Canadian Geotechnical Journal* **33**(4), 618–628.

Lloret-Cabot, M., Fenton, G. A. and Hicks, M. A. (2014), 'On the estimation of scale of fluctuation in geostatistics', *Georisk: Assessment and Management of Risk for Engineered Systems and Geohazards* **8**(2), 129–140.

Lu, N. and Godt, J. (2008), 'Infinite slope stability under steady unsaturated seepage conditions', *Water Resources Research* **44**(11).

Lu, N. and Griffiths, D. (2004), 'Profiles of steady-state suction stress in unsaturated soils', *Journal of Geotechnical and Geoenvironmental Engineering* **130**(10), 1063–1076.

Lumb, P. (1966), 'The variability of natural soils', *Canadian Geotechnical Journal* **3**(2), 74–97.

Lumb, P. (1971), Precision and accuracy of soil tests, *in* 'Proceedings, First International Conference on Applications of Statistics & Probability to Soil & Structural Engineering, Hong Kong', pp. 329–345.

Lumb, P. (1975), Spatial variability of soil properties, *in* 'Proceedings of the second international conference on application of statistics and probability in soil and structural engineering, Aachen, Germany', pp. 397–421.

Madsen, H. (1992), 'Probability-based fatigue inspection planning. mtd publication 92/100', *The Marine Technology Directorate Limited, UK* **2**, 897–913.

Marachi, N. D. (1969), *Strength and deformation characteristics of rockfill materials*, Department of Civil Engineering, University of California.

Marachi, N. D., Chan, C. K. and Seed, H. B. (1900), 'Evaluation of properties of rockfill materials', *Journal of Soil Mechanics & Foundations Div* **97**(SM1).

Matsuo, M. and Kuroda, K. (1974), 'Probabilistic approach to design of embankments', *Soils and Foundations* **14**(2), 1–17.

Meyerhof, G. G. (1995), 'Development of geotechnical limit state design', *Canadian Geotechnical Journal* **32**(1), 128–136.

Morgan, C. J. (2005), Analysing spatial data via geostatistical methods, PhD thesis, Faculty of Science, University of the Witwatersrand, Johannesburg.

Morse, R. (1971), Importance of proper soil units for statistical analysis, *in* 'Proccedings of the 1st International Conference On applications of Statistics and Probability to Soil and Structural Engineering, Hong Kong'.

Nie, X., Zhanga, J., Huanga, H., Liu, Z. and Lacasse, S. (2015), 'Scale of fluctuation for geotechnical probabilistic analysis', *Proceedings of ISGSR2015, Rotterdam, The Netherlands, October* .

Nishimura, S.-i., Shimada, K. and Fujii, H. (2002), 'Consolidation inverse analysis considering spatial variability and non-linearity of soil parameters.', *Soils and Foundations* **42**(3), 45–61.

Nobahar, A. (2003), Effects of soil spatial variability on soil-structure interaction, PhD thesis, Memorial University of Newfoundland.

Nobahar, A. and Popescu, R. (2000), Spatial variability of soil properties?effects on foundation design, *in* 'Proceedings of 53rd Canadian geotechnical conference, Montreal, Quebec'.

Nobahar, A. and Popescu, R. (2001), Some effects of soil heterogeneity on bearing capacity of shallow foundations, *in* 'Foundations and Ground Improvement', ASCE, pp. 788–798.

Nobahar, A. and Popescu, R. (2002), Bearing capacity of shallow foundations on heterogeneous soils, *in* 'Proc. 2nd Canadian spec. conf. on computer applications in geotechnique, Winnipeg, MA'.

Nour, A., Slimani, A. and Laouami, N. (2002), 'Foundation settlement statistics via finite element analysis', *Computers and Geotechnics* **29**(8), 641–672.

Nowak, A. S. and Collins, K. R. (2012), *Reliability of structures*, CRC Press.

Paice, G., Griffiths, D. and Fenton, G. (1994), Influence of spatially random soil stiffness on foundation settlements, *in* 'Vertical and Horizontal Deformations of Foundations and Embankments', pp. 628–639.

Pebesma, E. J. (2001), 'Gstat user's manual', *Dept. of Physical Geography, Utrecht University, Utrecht, The Netherlands* .

Phoon, K. K. and Kulhawy, F. H. (1996), On quantifying inherent soil variability, *in* 'Uncertainty in the geologic environment: From theory to practice', ASCE, pp. 326–340.

Phoon, K.-K. and Kulhawy, F. H. (1999*a*), 'Characterization of geotechnical variability', *Canadian Geotechnical Journal* **36**(4), 612–624.

Phoon, K.-K. and Kulhawy, F. H. (1999*b*), 'Evaluation of geotechnical property variability', *Canadian Geotechnical Journal* **36**(4), 625–639.

Phoon, K.-K., Quek, S.-T. and An, P. (2003), 'Identification of statistically homogeneous soil layers using modified bartlett statistics', *Journal of Geotechnical and Geoenvironmental Engineering* **129**(7), 649–659.

Phoon, K. and Kulhawy, F. (2005), 'Characterisation of model uncertainties for laterally loaded rigid drilled shafts', *Geotechnique* **55**(1), 45–54.

Phoon, K., Quek, S., Chow, Y. and Lee, S. (1990), 'Reliability analysis of pile settlement', *Journal of Geotechnical Engineering* **116**(11), 1717–1734.

Popescu, R. (1995), *Stochastic variability of soil properties: data analysis, digital simulation, effects on system behavior*, Princeton University.

Popescu, R., Deodatis, G. and Nobahar, A. (2002), Bearing capacity of heterogeneous soils?a probabilistic approach, *in* 'Proceedings of 55th Canadian geotechnical conference, Niagara Falls, ON', pp. 1021–1028.

Popescu, R., Deodatis, G. and Nobahar, A. (2005), 'Effects of random heterogeneity of soil properties on bearing capacity', *Probabilistic Engineering Mechanics* **20**(4), 324–341.

Popescu, R., Prevost, J. and Deodatis, G. (2004), '3d effects in seismic liquefaction of stochastically variable soil deposits'.

Popescu, R., Prevost, J. H. and Deodatis, G. (1996), Influence of spatial variability of soil properties on seismically induced soil liquefaction, *in* 'Uncertainty in the Geologic Environment: from Theory to Practice', ASCE, pp. 1098–1112.

Popescu, R., Prévost, J. H. and Deodatis, G. (1997), 'Effects of spatial variability on soil liquefaction: some design recommendations', *Geotechnique* **47**(5), 1019–1036.

Popescu, R., Prevost, J. H. and Deodatis, G. (1998*a*), Characteristic percentile of soil strength for dynamic analyses, *in* 'Geotechnical Earthquake Engineering and Soil Dynamics III', ASCE, pp. 1461–1471.

Popescu, R., Prevost, J. H. and Deodatis, G. (1998*b*), Spatial variability of soil properties: two case studies, *in* 'Geotechnical Earthquake Engineering and Soil Dynamics III', ASCE, pp. 568–579.

Poulos, H. G. and Davis, E. H. (1974), *Elastic solutions for soil and rock mechanics*, John Wiley.

PrzewLócki, J. (2000), 'Two-dimensional random field of mechanical soil properties', *Journal of geotechnical and geoenvironmental engineering* **126**(4), 373–377.

Przewłócki, J. (2005), 'A stochastic approach to the problem of bearing capacity by the method of characteristics', *Computers and Geotechnics* **32**(5), 370–376.

Pyrcz, M. J. and Deutsch, C. V. (2014), *Geostatistical reservoir modeling*, Oxford university press.

Rahardjo, H., Ong, T., Rezaur, R. and Leong, E. C. (2007), 'Factors controlling instability of homogeneous soil slopes under rainfall', *Journal of Geotechnical and Geoenvironmental Engineering* **133**(12), 1532–1543.

Remson, I., Hornberger, G. M. and Molz, F. J. (1971), *Numerical methods in subsurface hydrology*, Wiley-Interscience.

Remy, N., Boucher, A. and Wu, J. (2009), *Applied geostatistics with SGeMS: A user's guide*, Cambridge University Press.

Robert, Y. (1997), 'A few comments on pile design', *Canadian Geotechnical Journal* **34**(4), 560–567.

Roddeman, D. (2016), 'Tochnog professional user's manual', *Heerlen: FEAT* .

Rowe, P. (1969), 'The relation between the shear strength of sands in triaxial compression, plane strain and direct', *Geotechnique* **19**(1), 75–86.

Santoso, A. M., Phoon, K. and Quek, S. (2011), Role of uncertainty in soil hydraulic properties in rainfall-induced landslides, *in* 'Proceedings of the 3rd International Conference on Geotechnical Engineering for Disaster Mitigation and Rehabilitation 2011: Combined With, the 5th International Conference on Geotechnical and Highway Engineering: Practical Applications, Challenges and Opportunities', World Scientific, p. 172.

Schiffman, R. L. and Gibson, R. E. (1963), The consolidation of non-homogeneous clay layers. part ii. analytical solutions, Technical report, DTIC Document.

Schweiger, H., Thurner, R. and Pöttler, R. (2001), 'Reliability analysis in geotechnics with deterministic finite elements-theoretical concepts and practical application', *International Journal of Geomechanics* **1**(4), 389–413.

Seed, R. B., Mitchell, J. K. and Seed, H. B. (1990), 'Kettleman hills waste landfill slope failure. ii: stability analyses', *Journal of Geotechnical Engineering* **116**(4), 669–690.

Shen, H. and Fu, H. (2011), 'Spatial variability and slope reliability analysis', *Electronic Journal of Geotechnical Engineering* **16**, 1261–1276.

Sivakumar Babu, G. and Murthy, D. (2005), 'Reliability analysis of unsaturated soil slopes', *Journal of geotechnical and geoenvironmental engineering* **131**(11), 1423–1428.

Sivakumar Babu, G., Srivastava, A. and Murthy, D. S. (2006), 'Reliability analysis of the bearing capacity of a shallow foundation resting on cohesive soil', *Canadian Geotechnical Journal* **43**(2), 217–223.

Smith, L. and Freeze, R. A. (1979), 'Stochastic analysis of steady state groundwater flow in a bounded domain: 2. two-dimensional simulations', *Water Resources Research* **15**(6), 1543–1559.

Soga, K. and Mitchell, J. (2005), 'Fundamentals of soil behavior', *John Wiley & Sons, Hoboken, New Jersey, USA* .

Somerton, W. H., Söylemezoglu, I. and Dudley, R. (1975), Effect of stress on permeability of coal, *in* 'International journal of rock mechanics and mining sciences & geomechanics abstracts', Vol. 12, Elsevier, pp. 129–145.

Soubra, A.-H., Massih, D. S. Y. A. and Kalfa, M. (2008), 'Bearing capacity of foundations resting on a spatially random soil', *GeoCongress 2008: Geosustainability and Geohazard Mitigation* **178**, 66.

Soulie, M., Montes, P. and Silvestri, V. (1990), 'Modelling spatial variability of soil parameters', *Canadian Geotechnical Journal* **27**(5), 617–630.

Spencer, W. A. and Hicks, M. A. (2007), *Parallel Stochastic and Finite Element Modelling of Clay Slope Stability in 3D*, University of Manchester.

Srivastava, A. and Babu, G. S. (2009), 'Effect of soil variability on the bearing capacity of clay and in slope stability problems', *Engineering Geology* **108**(1), 142–152.

Srivastava, A., Babu, G. S. and Haldar, S. (2010), 'Influence of spatial variability of permeability property on steady state seepage flow and slope stability analysis', *Engineering Geology* **110**(3), 93–101.

Srivastava, R. and Yeh, T.-C. J. (1991), 'Analytical solutions for one-dimensional, transient infiltration toward the water table in homogeneous and layered soils', *Water Resources Research* **27**(5), 753–762.

Stark, T. D. and Eid, H. T. (1998), 'Performance of three-dimensional slope stability methods in practice', *Journal of Geotechnical and Geoenvironmental engineering* **124**(11), 1049–1060.

Sudicky, E. A. (1986), 'A natural gradient experiment on solute transport in a sand aquifer: Spatial variability of hydraulic conductivity and its role in the dispersion process', *Water Resources Research* **22**(13), 2069–2082.

Tang, W. H. (1984), Principles of probabilistic characterizations of soil properties, *in* 'Probabilistic characterization of soil properties: Bridge between theory and practice', ASCE, pp. 74–89.

Tantalla, J., Prevost, J.-H. and Deodatis, G. (2001), 'Spatial variability of soil properties in slope stability analysis: Fragility curve generation', *Structural Safety and Reliability: ICOSSAR'01* p. 2001.

Taylor, D. W. (1948), *Fundamentals of soil mechanics*, Vol. 66, LWW.

Terzaghi, K., Peck, R. B. and Mesri, G. (1996), *Soil mechanics in engineering practice*, John Wiley & Sons.

Uzielli, M., Lacasse, S., Nadim, F. and Phoon, K. (2006), 'Soil variability analysis for geotechnical practice', *Characterization and engineering properties of natural soils* **3**, 1653–1752.

Uzielli, M., Vannucchi, G. and Phoon, K. (2005), 'Random field characterisation of stress-normalised cone penetration testing parameters', *Geotechnique* **55**(1), 3–20.

Van Genuchten, M. T. (1980), 'A closed-form equation for predicting the hydraulic conductivity of unsaturated soils', *Soil science society of America journal* **44**(5), 892–898.

Vanmarcke, E. (2010), *Random fields: analysis and synthesis*, World Scientific.

Vanmarcke, E. H. (1977), 'Probabilistic modeling of soil profiles', *Journal of the geotechnical engineering division* **103**(11), 1227–1246.

Venables, W. N., Smith, D. M., Team, R. D. C. et al. (2004), 'An introduction to r'.

von Wolffersdorff, P.-A. (1996), 'A hypoplastic relation for granular materials with a predefined limit state surface', *Mechanics of Cohesive-frictional Materials* **1**(3), 251–271.

Warren, J., Price, H. et al. (1961), 'Flow in heterogeneous porous media', *Society of Petroleum Engineers Journal* **1**(03), 153–169.

Webster, R. and Oliver, M. A. (2007), *Geostatistics for environmental scientists*, John Wiley & Sons.

Wolle, C. and Hachich, W. (1989), Rain-induced landslides in southeastern brazil, *in* 'The 12 th International Conference on Soil Mechanics and Foundation Engineering, Rio de Janeiro, Br, 08/13-18/89', pp. 1639–1642.

Wu, T. and Kraft, L. (1967), 'The probability of foundation safety', *Journal of Soil Mechanics & Foundations Div* **93**, 213–231.

Yegian, M. K. and Whitman, R. V. (1978), 'Risk analysis for ground failure by liquefaction', *Journal of Geotechnical and Geoenvironmental Engineering* **104**(GT7), 921–938.

Yeh, T.-C. J. (1989), 'One-dimensional steady state infiltration in heterogeneous soils', *Water Resour. Res* **25**(10), 2149–2158.

Youssef Abdel Massih, D. S. and Soubra, A.-H. (2008), 'Reliability-based analysis of strip footings using response surface methodology', *International Journal of Geomechanics* **8**(2), 134–143.

Zeitoun, D. and Baker, R. (1992), 'A stochastic approach for settlement predictions of shallow foundations', *Geotechnique* **42**(4), 617–629.

Zekkos, D., Bray, J. and Der Kiureghian, A. (2004), 'Reliability of shallow foundation design using the standard penetration test', *Proceedings ISC-2 on Geotechnical and Geophysical Site Characterization* pp. 1575–1582.

Zhang, L. and Chen, J.-J. (2012), 'Effect of spatial correlation of standard penetration test (spt) data on bearing capacity of driven piles in sand', *Canadian Geotechnical Journal* **49**(4), 394–402.

Zhang, L., Zhang, L. and Tang, W. (2005), 'Rainfall-induced slope failure considering variability of soil properties', *Geotechnique* **55**(2), 183–188.

A. Appendix - Method of isotropic RF generation, its validation and limitation

A.1. Isotropic RF generation

Hicks and Samy (2002) provided a way to generate an anisotropic random field with both δ_v and δ_h constant, and $\delta_v \neq \delta_h$. The basic steps are:

Step 1. Generate an isotropic normalized spatial correlated random field based on δ=δ_h (step 1 in Figure A.1). Detail steps are already explained in chapter 4 (Step 2 - Step 3, stationary random field generation).

Step 2. Distort the random field in the vertical direction by compressing the cells by a distortion ratio $\xi = \delta_h/\delta_v$, as is shown in step 2 of Figure A.1. ξ is an integer here. After distortion, the element size in the vertical direction is ξ times shorter, and the original element contains ξ elements.

Step 3. Average cell values in the vertical direction so that new square cells are produced, as is shown in step 3 of Figure A.1.

Step 4. Transfer the cell values directly onto the sampling points in the problem domain.

Step 5. Transform the sampling point values into the true value using the mean and variance.

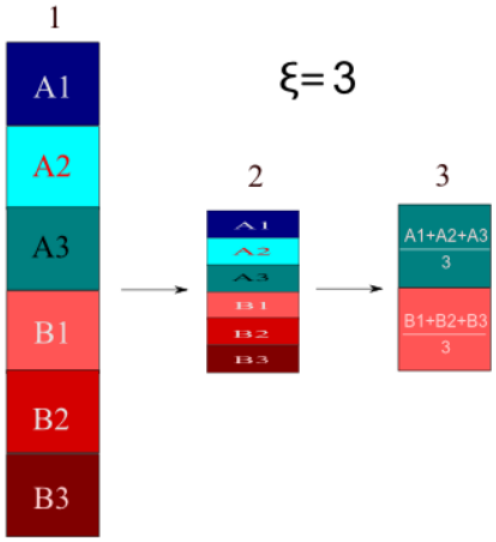

Figure A.1.: Schematic diagram of the first 3 steps

For instance: as is shown in Figure A.2a, the isotropic normalized spatial correlated Gaussian random field is generated, it contains 256*256 elements with both horizontal and vertical spatial correlation length are 32. When the $\delta_h \neq \delta_v$, the random field needs to be distorted, as is shown in Figure A.2b-d where the δ_v = 16, 8, 4, respectively. Then the distorted random field can be transferred to the final random field base on its true mean, variance, and distribution.

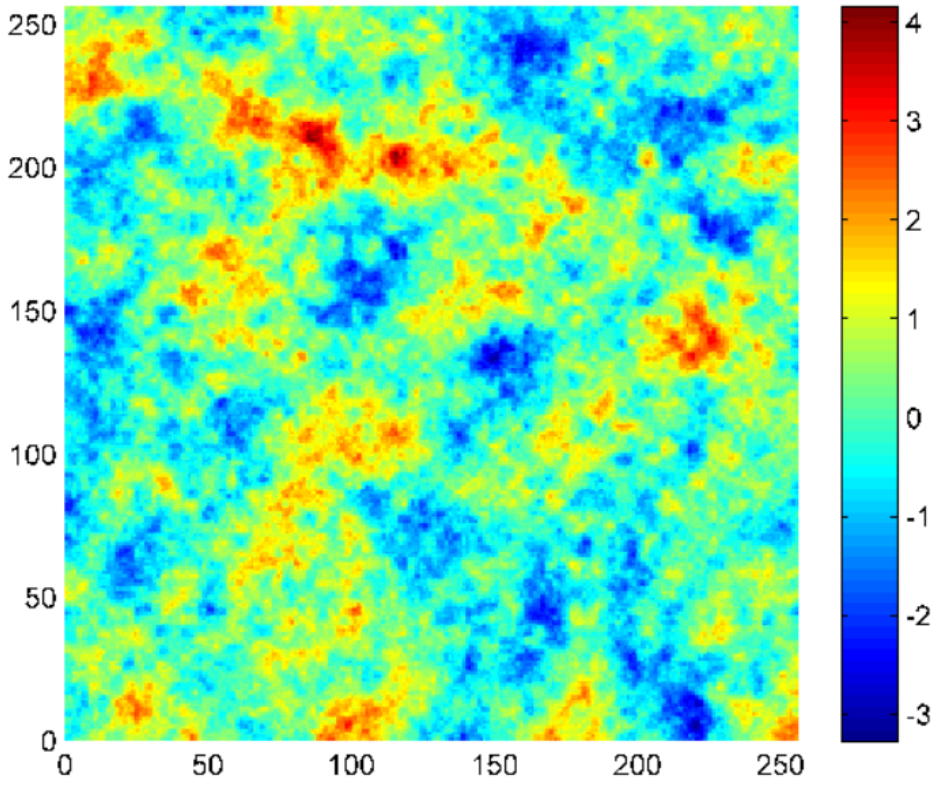

(a) δ_v=32

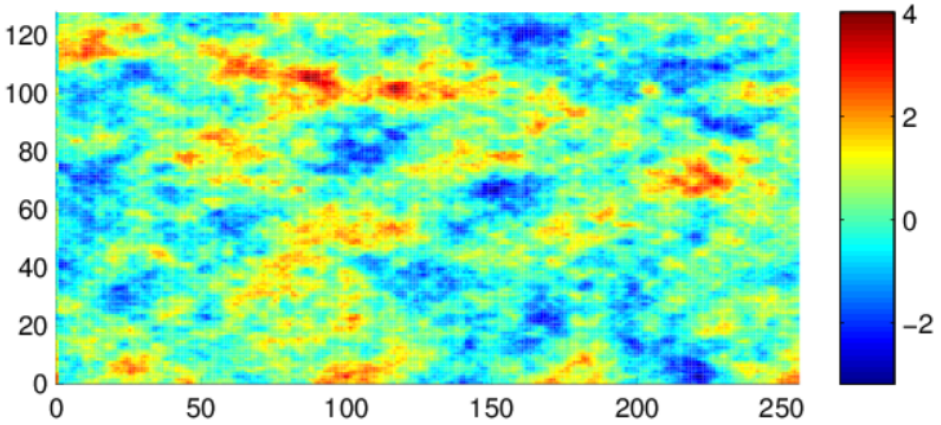

(b) δ_v=16

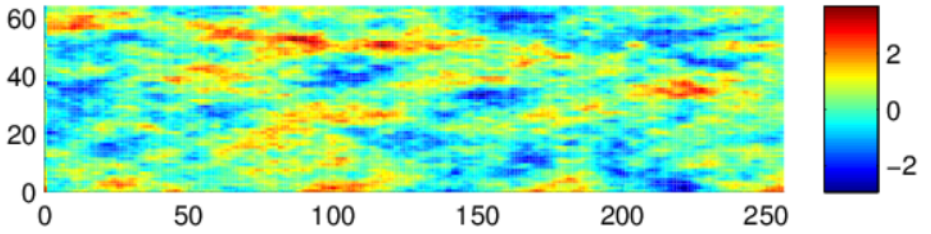

(c) δ_v=8

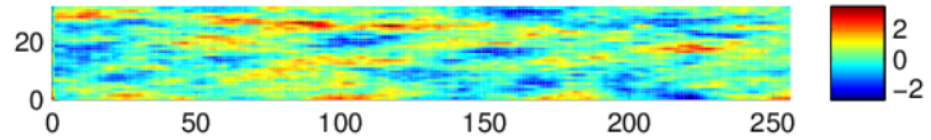

(d) δ_v=4

Figure A.2.: Anisotropic random field generation through distortion of an isotropic random field

A.2. Validation and limitation

3000 one-dimensional random fields are generated so as to validate this method. The length of a random field is 200m with each element 1m, and the original spatial correlation length of the random field is 20m, with its mean and standard deviation zero and unit, respectively. Then these random fields are distorted with ξ=2 using this method. The frequencies of the spatial correlation length of the 3000 random fields before and after distortion are shown in Figure A.3. Figure A.3a shows that, before the distortion, the mean spatial correlation length of each random field is about 20m. After distortion, most of the spatial correlation lengths are around 10m (Figure A.3b). So the distortion can be used to reduce the spatial correlation length or to generate the anisotropic random field.

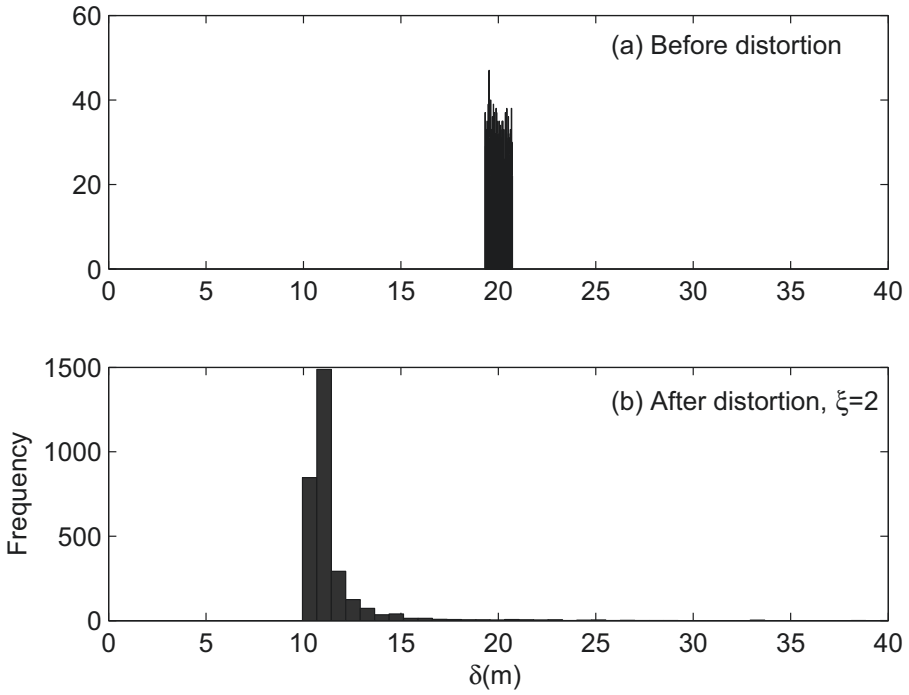

Figure A.3.: Spatial correlation length comparison (a) before and (b) after distortion

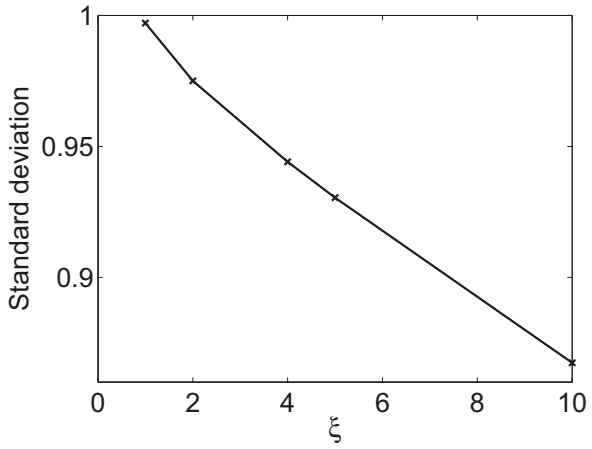

Figure A.4.: Distortion ratio (ξ) VS the standard deviation

However, the standard deviation reduces linearly with the increase of the distortion ratio, as is shown in Figure A.4. This reduction can be regarded as one part of the variance reduction. Therefore, it is necessary to check the true standard deviation after the distortion. If the true standard deviation is not correct, some compensation should be made.

In summary, the method used by Prof. Hicks can be used to reduce the spatial correlation length through a distortion of the isotropic stationary random field. However, it should be noted that the standard deviation can also be reduced during the distortion.